NASA TECHNICAL TRANSLATION NASA TT F-12,382

NASA TT F-12,382

AUTOMOTIVE TIRES, CONSTRUCTION, DESIGN, TESTING AND OPERATION

V. L. BIDERMAN, R. L. GUSLITSER, S. P. SAKHAROV, B. V. NENAKHOV, I. I. SELEZNEV AND S. M. TSUKERBERG

Translation of: "Avtomobil'nyye shiny (konstruktsiya, raschet, ispytaniye, ekspluatatsiya)" Moscow, State Scientific and Technical Press for Chemical Literature, pp. 1-171, 291-383, 1963.

N70-16410
(ACCESSION NUMBER) (THRU)
246 1
(PAGES) (CODE)
✓ 15
(NASA CR OR TMX OR AD NUMBER) (CATEGORY)
FACILITY FORM 602

NATIONAL AERONAUTICS AND SPACE ADMINISTRATION
WASHINGTON, D.C. 20546 SEPTEMBER 1969

TABLE OF CONTENTS

CHAPTER I. GENERAL REMARKS ON AUTOMOTIVE TIRES

The Construction of Automotive Tires and the Basic Stages in Their Development..... 1

Contemporary Trends in Pneumatic Tire Development..... 8

Classification of Automotive Tires and Rims..... 15

Types of Automotive Wheel Rims..... 18

A Brief Outline of the Technology of Automotive Tire Production..... 21

Preliminary Processes..... 21

Cord Rubberization..... 24

Cord Cutting and the Positioning of the Cord Plies..... 26

Production of Tread..... 28

Wing Production..... 29

The Assembly of Outer Covers and Tubeless Tires..... 30

Molding and Vulcanization of Outer Covers..... 32

The Production of Tubes and Rim Bands..... 34

CHAPTER II. FUNDAMENTALS OF THE THEORY OF PNEUMATIC TIRES

Rubberized Cord Construction Grids and Their Properties..... 36

The Geometry of Cord Fibers in the Carcass of the Tire... 36

Elastic Properties of an Element of Rubberized Cord Construction..... 47

Internal Pressurization..... 61

The Equilibrium Configuration of a Tire..... 61

Determination of the Equilibrium Configuration of a Tire According to a Known Profile of the Vulcanization Mold..... 70

Determining Forces in the Cord Fibers..... 72

Radial Compression and Free-Rolling of the Tire..... 89

Tire Contact with the Road..... 89

Load Characteristics of a Tire..... 93

Stresses and Deformations Arising in Elements of a Rolling Tire..... 105

Rolling Losses..... 118

The Effects of Traction, Braking, and Lateral Forces on a Tire..... 121

Traction and Braking Forces..... 121

Lateral Force..... 123

Operating Characteristics of Tires at High Rolling Velocities..... 126

Stresses in Tire Elements Caused by Centrifugal Forces... 126

Critical Rolling Velocity of a Tire..... 130

Deformation Regimes of Tire Materials..... 142

Similarity Relationships and the Choice of Basic Tire Dimensions..... 149

Tube Deformations in Pneumatic Tires..... 154

CHAPTER VI. METHODS OF TESTING TIRES

Types of Tire Tests..... 156

Determining the Operating Characteristics of Tires..... 157

The Pliability of a Tire and the Contact Surface..... 157

Pressure in the Contact Surface..... 159

Traction..... 160

Sideslip..... 164

Rolling Resistance..... 166

Investigation of the Characteristics Which Determine the Lifetime of a Tire..... 174

Bench Rolling Tests..... 174

Evaluation of Carcass Resistance to Concentrated Stresses..... 179

Estimate of the Wear Resistance of Tires..... 185

Operational Tire Tests..... 189

Accelerated Road Tests..... 197

CHAPTER VII. THE OPERATION OF AUTOMOBILE TIRES

Basic Reasons for Tire Failure During Operation..... 198

The Influence of Road Conditions and Climate on Tire Operation. 199

Operating Regime of the Tire..... 200

Tire Servicing..... 205

Observing the Norms of Weight and Internal Pressure..... 208

Operating the Automobile..... 208

Care of the Automobile..... 209

Rotating the Tires..... 210

Tire Repair..... 210

Keeping Track of Tire Operation..... 211

REFERENCES..... 213

APPENDICES..... 217

CHAPTER 1

/8*

GENERAL REMARKS ON AUTOMOTIVE TIRES

The Construction of Automotive Tires and the Basic Stages in Their Development

The invention of pneumatic tires was a most important factor in the development of non-rail land transportation. Steam engines, developed in the 18th century, and then internal combustion engines provided an opportunity to develop quite powerful and fast-moving self-propelled vehicles. However, this opportunity could not be realized due to the absence of means for absorbing the shocks undergone by the vehicle.

In the 1820's, sheets of rubber were fastened to the wheel rims of the huge steam engines to absorb the shocks. The discovery of vulcanization made it possible to convert to a rubber shock-absorbing strip attached to the wheel rim by means of grooves in the shape of swallowtails.

In the 1880's, massive tires were developed, vulcanized to the wheel rim. Hollow tires and tires with porous cores were also developed. However, all these tires, lacking the necessary shock-absorbing ability, were unable to meet the needs of automotive transportation.

Therefore, the development of the pneumatic tire by Dunlop in 1888 had enormous importance.

In the following several years, improvements were made in the method of attaching the Dunlop tire to the rim, originally done using strips of fabric, and later (1890-1892) using wire rings attached to the beads of the tire. Inner tubes were first used at this time (1891).

All aspects of tire construction were improved during this period.

A particularly significant role in the improvement of tire efficiency was played by the development of nonwoven fabric (cord). The first outer cover made using cord appeared in 1893.

*Numbers in the margin indicate pagination in the foreign text.

Up to 1925 clincher tires were used which had annular flanges on the sides that fit in the corresponding notches in the edge of the wheel rim. This method of fastening was unreliable when the vehicle was moving at high speeds. In addition, there were other deficiencies in clincher tires, such as the possibility of damage /9
to the side part of the edge of the wheel rim and also the difficulties of mounting.

After the clincher tire, straight-bead tires became popular and have remained in use up to the present time.

Tread design, an important aspect of tire construction, was in wide use on bicycle tires in the 1890's. At that time it was discovered that smooth rubber tires are prone to skidding on dirt roads. At first the rolling part was slightly grooved, and subsequently (1891) various tread designs apppeared. Tread design appeared on automobile tires about twelve years later. The first tread designs were simple alternations of ridges and grooves located across the rolling part.

Subsequently more widely separated tread designs came into use to improve traction, decrease wear on the tread and also to decrease noise while the automobile was in motion.

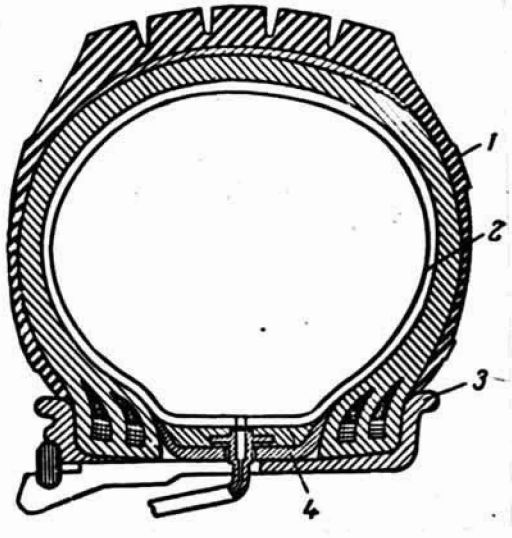

Fig. 1: A Single-Tube Pneumatic Tire on an Expanded Rim with Beveled Bead Seats (Cross Section): (1) The Outer Cover; (2) The Tube; (3) The Wheel Rim; (4) The Rim Band.

We may assume that contemporary automobile tires, in their fundamental aspects, were developed around the 1930's and their subsequent development consisted in a gradual change in construction proportions, the use of new materials and the development of tires for special conditions.

We will examine now the basic types of automobile tires.

The single tube pneumatic tire, whose cross section is shown in Figure 1, is designed for mounting on a flat-base or expanded rim with beveled bead seats. This tire consists of an outer cover, comprising the major part of the tire, a tube which holds the air in the internal cavity of the tire, and a rim band which protects the tube from being pinched between the bead of the outer cover and the rim and from damage by roughness of the rim.

Up to 1925 clincher tires were used which had annular flanges on the sides that fit in the corresponding notches in the edge of the wheel rim. This method of fastening was unreliable when the vehicle was moving at high speeds. In addition, there were other deficiencies in clincher tires, such as the possibility of damage /9 to the side part of the edge of the wheel rim and also the difficulties of mounting.

After the clincher tire, straight-bead tires became popular and have remained in use up to the present time.

Tread design, an important aspect of tire construction, was in wide use on bicycle tires in the 1890's. At that time it was discovered that smooth rubber tires are prone to skidding on dirt roads. At first the rolling part was slightly grooved, and subsequently (1891) various tread designs apppeared. Tread design appeared on automobile tires about twelve years later. The first tread designs were simple alternations of ridges and grooves located across the rolling part.

Subsequently more widely separated tread designs came into use to improve traction, decrease wear on the tread and also to decrease noise while the automobile was in motion.

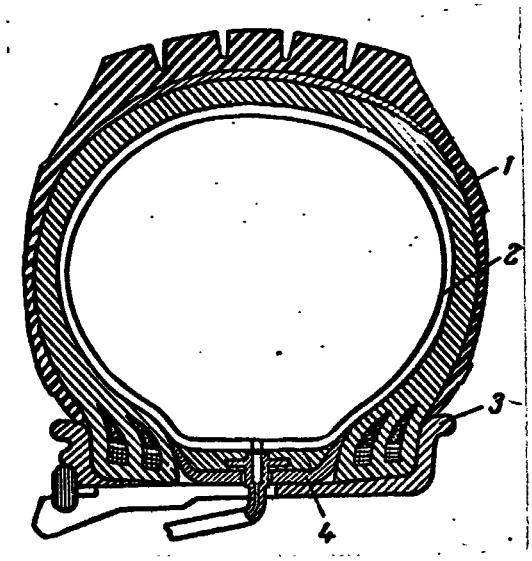

Fig. 1: A Single-Tube Pneumatic Tire on an Expanded Rim with Beveled Bead Seats (Cross Section): (1) The Outer Cover; (2) The Tube; (3) The Wheel Rim; (4) The Rim Band.

We may assume that contemporary automobile tires, in their fundamental aspects, were developed around the 1930's and their subsequent development consisted in a gradual change in construction proportions, the use of new materials and the development of tires for special conditions.

We will examine now the basic types of automobile tires.

The single tube pneumatic tire, whose cross section is shown in Figure 1, is designed for mounting on a flat-base or expanded rim with beveled bead seats. This tire consists of an outer cover, comprising the major part of the tire, a tube which holds the air in the internal cavity of the tire, and a rim band which protects the tube from being pinched between the bead of the outer cover and the rim and from damage by roughness of the rim.

Tires designed for use on well-base rims (Fig. 2) do not have a rim band.

Figure 3 shows a cross section of the outer cover of a heavy duty tire. The carcass of the outer cover is the basic force-absorbing part of the tire. The carcass bears the force of the internal air pressure and the force caused by the transfer to the tire of radial force, tractive force, braking force and lateral force. The carcass consists of several plies of rubberized cord, arranged in a criss-cross fashion. The cord plies of the carcass are fastened to the wire rings of the bead. /10

Cord is a fabric composed of a base of strong fibers and a weave of widely spaced fine fibers[1]. This type of fabric structure provides the opportunity to have gaps filled with rubber between the fibers. This provides a high degree of flexibility and an extended lifetime of the carcass when the tire is used.

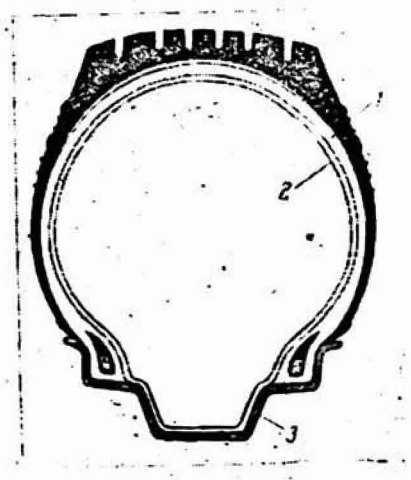

Fig. 2: A Single-Tube Pneumatic Tire on a Well-Base Rim (Cross Section): (1) The Outer Cover; (2) The Tube; (3) The Rim.

Cord is made of natural (cotton), artificial (rayon) or synthetic (Kapron, Nylon) fibers.

The number of cord plies in the body (usually from 2 to 12 and sometimes more) depends on the dimensions and construction of the tire, the degree of internal pressure and the conditions of usage. In multiply truck tires, rubber seams (squeegees) are placed between certain plies to increase the elasticity of the outer cover. The seams are located for the most part between the outer plies of the body (near the tread), where the greatest stress occurs. These seams are also used in tires operating with high radial distortions; for example, tires with variable internal pressure.

Above the basic cord plies of the body there is a breaker, several (usually 2-4) layers of widely-spaced cord, located in the rolling part of the tire and not attached to the bead rings. Above

---

[1]The weave has a purely technological value: it strengthens the fibers of the base during rubberization. Later in the formation process the fibers of the weave are torn away. Nonwoven cord is also used.

and below the breaker plies and also between them are rubber interlayers. The breaker increases the body resistance to mechanical damage when the tire hits a bump in the road and also increases the strength of the seal between the tread and the body. /11

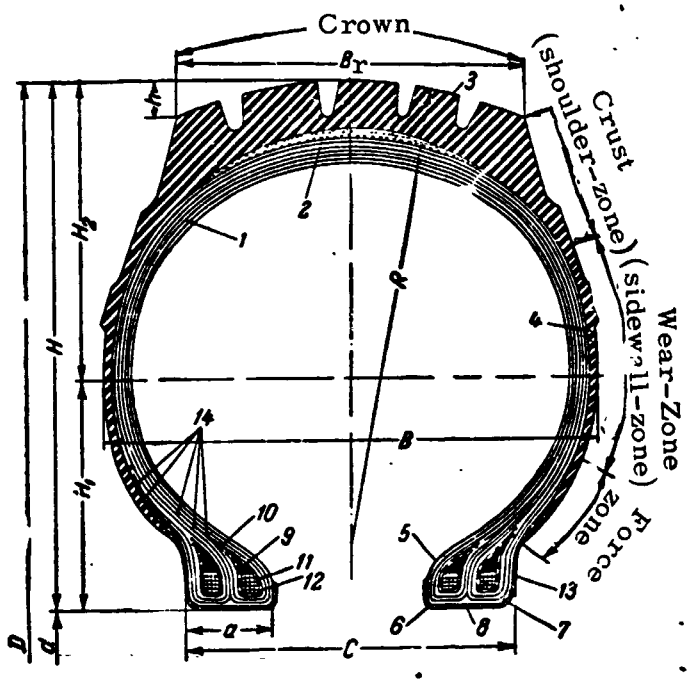

Fig. 3: The Basic Construction Aspects and Dimensions of the Outer Cover: (1) The Body; (2) The Cushioning Layer (Breaker); (3) The Tread; (4) The Sidewall; (5) The Bead; (6) The Nose of the Bead; (7) The Heel of the Bead; (8) The Base of the Bead; (9) Filler; (10) The Flipper; (11) The Envelope; (12) The Bead Wires; (13) The Chafer Strip; (14) The Cord Loops. H Is the Height of the Outer Cover Profile; H_1 Is the Distance from the Base of the Bead of the Outer Cover to the Horizontal Axial Line of the Profile; H_2 is the Distance From the Horizontal Axial Line of the Profile of the Outer Cover to the Equators; B Is the Width of the Outer Cover Profile; B_r Is the Width of the Rolling Part of the Tread Along the Cord; R Is the Radius of Curvature of the Tread; C Is the Span of the Beads; D Is the External Diameter of the Tire; d Is the Internal (Landing) Diameter of the Tire; h Is the Rise of the Tread Arc; a Is the Width of a Bead.

In recent years tires have been developed using metallic cord in the breakers to increase resistance to punctures and blowouts.

The tread of the outer cover is a massive rubber covering layer, located on the rolling part of the tire; the ridges and grooves of this layer form the tread design. The tread protects the carcass of the tire from mechanical damage and its design insures traction. The large number of different patterns is explained by the fact that there are many different road conditions and uses of tires. /12 The rubber of the tread must have high durability and be highly resistant to mechanical damage and wear as the tire vibrates along the road.

Since the rubber of the tread ridges and the rubber of the ply beneath the tread operate under many drastically different conditions, the tread is sometimes made of two kinds of rubber: an upper layer (rolling part), made of hard, wear-resistant rubber to resist wear, and a lower ply (subtread layer) made of elastic rubber.

Toward the sidewalls of the outer cover, the tread becomes finer rubber plies; i.e., the sidewalls which cover the side areas of the body and protect them from external factors. The sidewalls are thin (up to 3-4 mm); sometimes on passenger car tires they are white or colored.

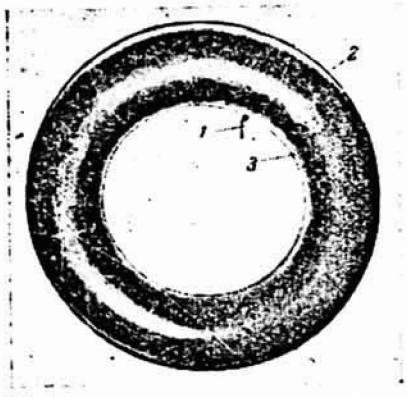

Fig. 4: An Overall View of an Inner Tube: (1) The Valve; (2) The Rolling Part; (3) The Belt

The bead rings are strips of interwoven steel wires or several parallel rows of individual steel wires. The rubberized wire ring, wrapped in rubberized fabric, forms the wing. The wing provides rigidity and durability of the outer cover beads. With a large number of cord plies in the body the bead can have two or even three wings. In this case a filler is usually wrapped around the outer surf of the wire rings, along entire circumference. Th fillers are usually made of hard rubber which is fastened by wrapping the bead ring with thin fabric strips. The filler allows us to obtain a smooth outline of the bead. To strengthen the bead during installation, the wing is wrapped in a wide rubberized strip called the wing strip or flipper.

The beads of the outer covering are wrapped from the outside by a chafer strip made of rubberized fabric in a square weave, to protect against wear and damage against the edge and bead seat of the rim.

The tube (Fig. 4) is a closed rubber tube and holds the compressed air inside the tire. The tube is inflated through a valve attached to it with a stem which acts as a check valve. The rolling part of the tube corresponds to the rolling part of the tire, and the belt corresponds to the rim. The thickness of the walls /13
of the tube is usually uniform in cross section (about 2-4 mm). In certain constructions, the thickness of the belt is greater, and in others, the thickness of the rolling part is greater. The dimensions of the tube are somewhat less than the dimensions of the internal cavity of the cover. Therefore, in an inflated tire, expanding but not contracting forces act on the walls of the tube. This is done to prevent wrinkles in the tire when it is mounted on the rim.

Two types of valves are used for automobile tubes: rubber-metal valves for the tubes of light automotive tires, and metallic valves for the tubes of heavy duty tires (Fig. 5). The difference in the construction of these two types of valves lies only in the shape and dimensions of the body of the valve and the means of fastening the valve to the walls of the tube. Rubber-metal valves are designed for tires used on well-base rims; metal valves are designed for use on tires on other types of rims.

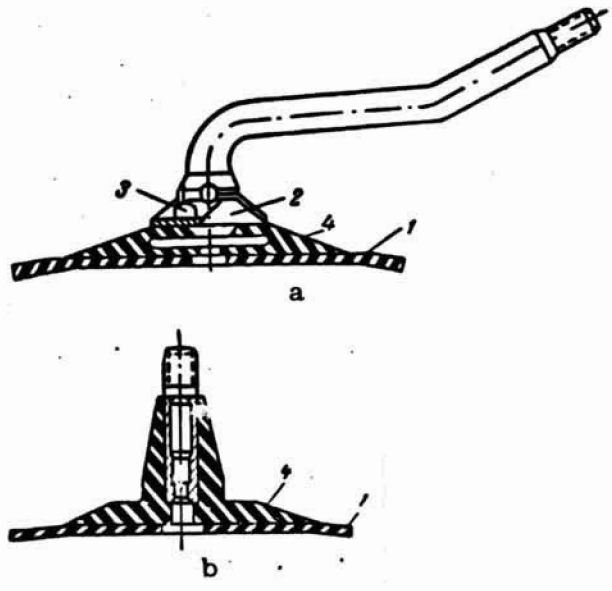

Fig. 5: Automotive Inner Tube Valves: (a) Metal; (b) Rubber-Metal. (1) The Wall of the Tube; (2) The Bridge; (3) The Nut; (4) The Rubber Heel of the Valve.

From the outside, the aperture of the valve is closed by a cap-key, which protects the channel of the valve from dirt, helps prevent leakage of air from the tube and also acts as a key for screwing and unscrewing the stem. The body of the valve is vulcanized to the wall of the tube when the tube is made.

Valves with metal bodies sometimes have other mounting details: a bridge and a nut (Fig. 5a). Metal valves without these details are also used.

Tubeless tires [4-6] have several advantages over tube /14
tires, namely increased travelling safety, simplified mounting and unmounting and ease of repairs while en route.

When a tube tire is punctured, in certain cases the tire may rupture over a large area and the pressure will decrease rapidly with the ensuing danger of an accident.

When a tubeless tire is punctured, the hole does not enlarge and the internal pressure decreases slowly, which decreases the danger of an accident. Tubeless tires also remove from the mounting-unmounting operations the need to remove (or insert) the inner tube into the tire. Therefore, repairs can be made en route without unmounting the tire.

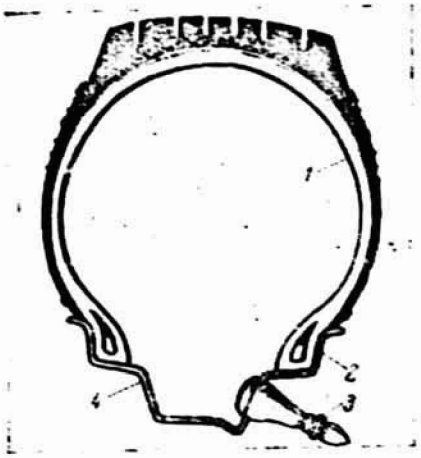

Fig. 6: A Tubeless Tire on a Rim (Cross Section): (1) The Inner Sealing Ply; (2) The Sealing Layer of the Bead; (3) The Valve; (4) The Rim.

In addition, a tubeless tire will operate under greater stresses, since it fulfills the functions of the outer cover and the tube at the same time. This determines the construction characteristics of tubeless tires. The cavity between the tubeless tire and the rim must be hermetically sealed, which is accomplished by a hermetically-sealing ply (usually about 2 mm) and a sealing layer on the bead, special construction of the beads and hermetic sealing of the rim and the place where the valve is attached to the rim. For a tight fit of the beads, sometimes their surfaces which are fitted to the edges are ribbed, but more often the air-tight seal is secured by an increase of up to 2-4 mm in the diameter of the stretch of the heel of the bead.

To insure the stability of the stretch and the hermetic seal for the entire lifetime of the tire, the bead wire rings are made of high strength wire. To do this, the beads of tubeless tires are packed with an envelope made of viscose or kapron monofiliment.

In a tubeless tire, the air permeates from the internal cavity through the body of the tire, which contributes to the loosening of the carcass plies and the peeling of the tread[2]. To prevent this, the sealing layer is made o rubber having minimum gas permeability: /15 butyl rubber, nyrite, etc. Tubeless tires are made of viscose or kapron cords whose fibers are significantly less permeable to gas than the fibers of cotton cords. The latter are not used in tubeless tires.

[2]In a tube tire, the air diffusing through the tube escapes under the beads of the outer cover and into the valve aperture.

Tubeless tires are inflated through a valve attached to the rim. Metal valves with reinforced rubber washers or special rubber-metal valves (Fig. 7) are used for tubeless tires. The internal construction of these valves is the same as that of the valves of tube tires.

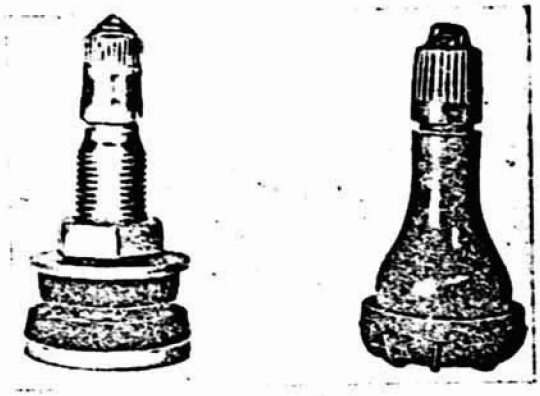

a b

Fig. 7: The Two Types of Valves for Tubeless Tires: (a) the Metal; (b) The Rubber-Metal

Contemporary Trends in Pneumatic Tire Development

After the basic construction of contemporary pneumatic tires was developed in the 1920's, improvements consisted to a significant degree of a gradual change in a number of construction ratios between the basic dimensions of the tire (cf. Fig. 3).

This change was continuously related to the improvements in motor vehicles, namely their increased speeds and the corresponding increase in demand for comfort and stability.

To provide stability of the vehicle at high speeds, a decrease in the height of the vehicle was required. This was accomplished by a decrease in the external diameter of the wheels. The increased construction of improved roads also provided an opportunity to decrease the height of the vehicle above the road.

The demand for increased cushioning ability of tires led to /16 the need for a decrease in their internal pressure and the corresponding increase in the dimensions of the tire profile.

The decrease in the external diameter of the wheel with a simultaneous increase in the tire profile could be accomplished only by a decrease in the diameter of the rims.

During the last thirty years, the standard diameters of the rims[3] of light tires have decreased from 18-19 inches to 13-14 inches.

For heavy-duty tires, the necessity of providing a rather high degree of roadability for trucks did not allow as much of a decrease in rim diameters as for light tires.

---

[3]According to international custom, the external diameters and widths of wheel rims are expressed in inches (1 inch = 25.4 mm).

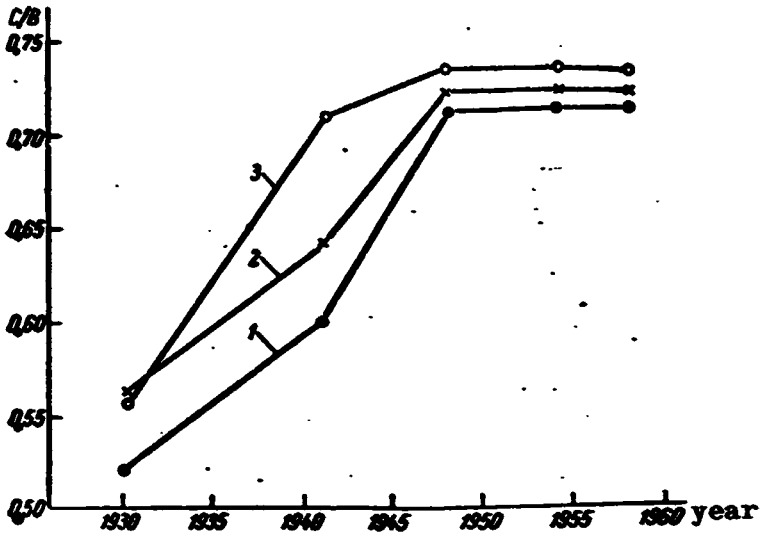

Fig. 8: The Change in the Ratio of Rim Width to the Width of the Tire Profile: (1) 7.00 - 20; (2) 7.50 - 20; (3) 6.00 - 16.

At the present time, standard rims for heavy duty tires generally have an internal diameter of 20 inches, and rims of the same diameters as for passenger automobiles are used only for light trucks of less than one ton capacity.

The demand for providing sufficient lateral stability of motor vehicles with lower pressure in the tires and also the necessity of increasing the efficiency of tires called for an increase in rim width.

The trend of widening rims is shown graphically in Figure 8, which shows the change in the ratio of rim width C to the width of the tire profile B by years fcr three tire sizes.

The present stage in the development of automotive tires is /17 characterized by a high degree of specialization according to the purpose of the motor vehicle. In addition, a number of major improvements are being applied to the construction of pneumatic tires, and new materials are being used. Previously there were two separate types of tires, high pressure tires and low pressure tires.

Low pressure tires were designed for an internal pressure of from 2 to 5 kg/cm^2. High pressure tires had a normal pressure of 5-7 kg/cm^2 and were distinguished from low pressure tires by less distortion under normal load, a lower width of the rolling part and an increased number of cord plies in the carcass.

At the present time, high pressure tires are not used for new motor vehicles, and there is a trend toward decreasing the internal pressure in both light and heavy duty tires.

The specialization of tires depending on their usage leads to the appearance of a number of new types of tires.

Included in the first apecialized tire constructions were balloon tires with a lower air pressure and greater overall dimensions. These tires were developed in 1930. Balloon tires (Fig. 9) provided

a b

Fig. 9: Automobiles with Ordinary Tires and with Balloon Tires When Moving Through Sand: (a) Balloon Tires; (b) Ordinary Tires

much higher roadability of the vehicle on soft ground, but did not gain wide popularity due to the poor handling of vehicles using these tires and the short lifetimes of the tires themselves.

The Second World War provided a great impetus to the development of tires with variable pressure. These tires allowed a vehicle to travel under conditions impossible with low pressure. Variable pressure tires are all-purpose. With normal pressure, a vehicle using variable pressure tires /18 can travel on hard roads with no problem. These tires differ from ordinary tires in their higher roadability, lower carcass thickness and lower load carrying capacity.

In the decade 1950-1960, specialized tires appeared which were capable of sharply increasing the roadability of motor vehicles on soft ground: ground-grip tires (Fig. 10), wide-profile tires (Figs. 11, 12) and rollers (Fig. 13).

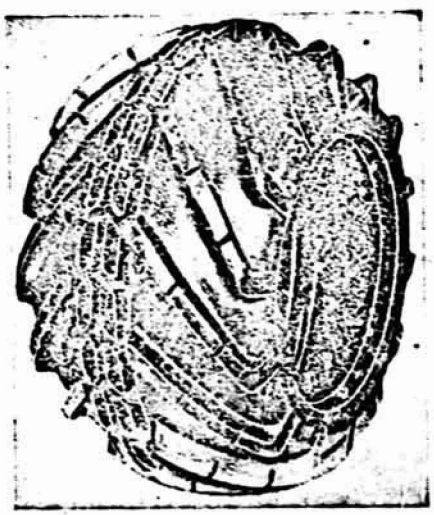

Fig. 10: A Ground-Grip Tire.

Fig. 11: A Wide-Profile Tire With Ordinary Tread.

If for ordinary tires the ratio of profile height to width $\frac{H}{B}$ lies within the limits 0.9 - 1.1, then for wide-profile tires this

ratio is 0.40 - 0.90, for ground-grip tires the ratio is 0.3 - 0.4 and for rollers the ratio is 0.2 to 0.35.

Wide-profile and ground-grip tires were designed to replace four ordinary tires on the rear axle of a truck with two tires, which improves the roadability of the vehicle and decreases the weight of the tires.

Rollers are used on special transport machines designed for traveling off roads. The construction of high roadability tires is examined in detail in Chapter 5.

Since the advent of pneumatic tires, attempts have been made to increase the safety of travel by motor vehicle, i.e., to prevent the possibility of an accident if the tire is suddenly punctured. /19 Innovations concerning traveling safety on pneumatic tires came in the area of the construction of puncture-proof tires and tires whose construction allows the tire to continue to function after a puncture. However, despite the numerous innovations and patents, practical value was found on a very limited scale, only for double-tube "safety" tires (Fig. 14).

A further development in the construction of "safety" tires was the tubeless tire. Tubeless tires became very popular, especially on passenger automobiles. Thus in 1961, a high proportion of passenger automobile tires manufactured in the Soviet Union were tubeless.

Fig. 12: A Wide-Profile Tire with Double Tread.

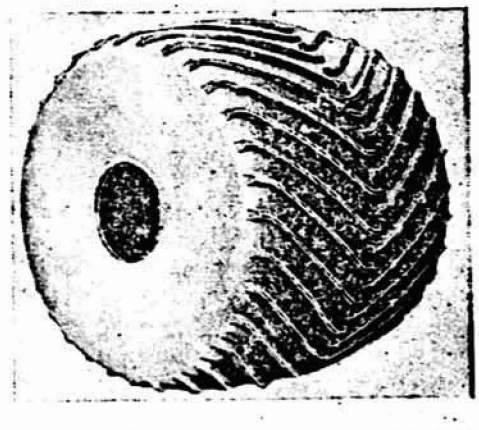

Fig. 13: A Roller.

As an additional safety measure, tubeless tires were sometimes used with a diaphragm. The construction of such a tire is shown in Figure 15.

New opportunities in the construction of automotive tires were opened by the use of metal cord. [7]. The first tires made of metal cord were manufactured by the French Company, Michelin, which in 1939 showed these tires at a Paris exhibit. The tires were intended for use by heavy duty trucks and were designed for twice the load of ordinary tires of the same dimensions. The tires cost 60% more than ordinary tires.

After the Second World War, metalic cord tires began to be manufactured by prominent American and English firms.

In connection with the high durability of metal cord, tires /20
made with metal cord require a small number of plies. Thus heavy duty truck tires are 2- or 4-ply (instead of 10- to 14-ply for fabric cord). The breakers, usually two-ply, were also made of rubberized metal cord. The construction of a four-ply metal cord tire is shown in Fig. 16.

In metal cord tires with more than two plies, interlayers of soft rubber are placed between the plies of the carcass to alleviate the problem of the plies shifting when the tire was distorted. The fibers of adjacent plies run at the same angle as in ordinary outer covers. The density of the positioning of the fibers is 1.5 - 2 times less than for tires with fabric cord.

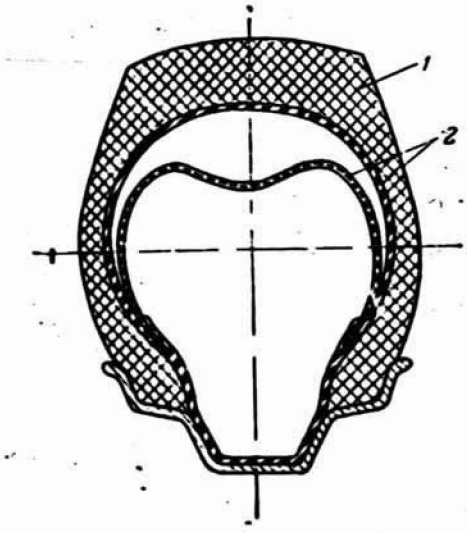

Fig. 14: A Double-Tube Tire: (1) The Outer Cover; (2) The Double Inner Tube.

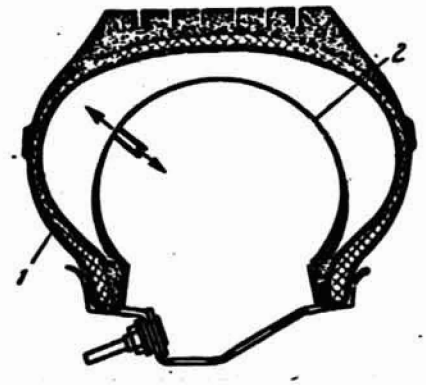

Fig. 15: A Tubeless Tire with a Diaphragm: (1) The Outer Cover; (2) The Diaphragm.

The overall weight of an outer cover made of metal cord is about equal to the weight of an ordinary outer cover. In this case, the weight of the metal cord is somewhat greater than the weight of the fabric cord, but the weight of the rubber is less. Thus in a 9.00-20 outer cover the fabric (viscose) cord weighs 12.8 kg.

Outer covers made of metal cord differ from ordinary outer covers by their greater strength of the carcass (by about a factor of 2); the pressure in metal cord tires are recommended for heavy loads and high velocities if used under good road conditions.

Along with tires made entirely of metal cord, there are tires with a fabric carcass and metal cord breakers. Metal cord breakers increase the tire's resistance to punctures and blowouts. In addition, the presence of a strong breaker leads to a decrease in tire slippage in the plane of contact with the road and to a decrease in wear. /21

A major new type of tire was a tire with the cord fibers in the carcass running in a radial direction [8], type R tires. These tires were first introduced by the Michelin Company in 1951 under the brand-name "Michelin X Tires". These tires (Fig. 17) had a fabric carcass with the fibers running in a radial direction (from bead to bead) and a breaker made of three plies of metal cord. The first ply of metal cord also ran radially and the others criss-crossed, forming an angle with the meridian of about 70°.

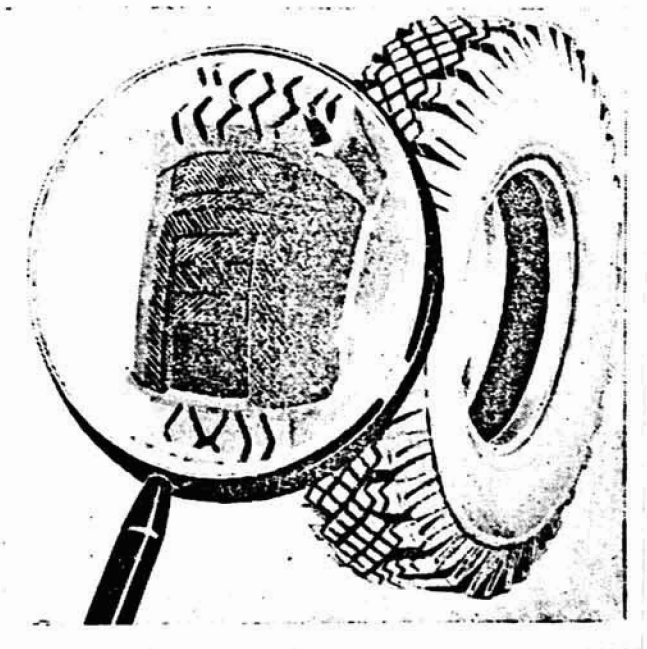

Fig. 16: A Tire Made of Metal Cord.

Subsequently type R tires were made both entirely of metal cord and entirely of fabric cord. This type of tire made from fabric cord (by the Pirelli Co.) is shown in Figure 18.

Type R tires have substantial economic advantages over ordinary tires since their carcasses require about half as many plies.

The combination in type R tires of a carcass with its fibers running almost circumferentially accounts for their unique features. Thus these tires have a substantially higher radial pliability and a higher wear resistance than ordinary tires. /22

The construction and design of type R tires is examined in detail in Chapter 4. Based on the construction of type R tires, tires with removable tread called type RS tires came into production. These tires decrease the necessity of replacing the tire when the tread wears out. These tires consist of individual parts (Fig. 19): a body which has a fabric carcass with the cord fibers

running radially and rigid tread bands reinforced by metal cord placed around the circumference of the tire.

Fig. 17: A Tire With Cord Fibers Running in a Radial Direction in the Carcass and a Breaker Made of Metal Cord.

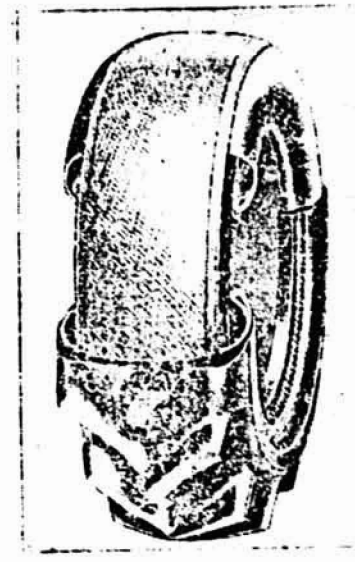

Fig. 18: A Tire With the Cord Fibers Running in a Radial Direction in the Carcass and Made Entirely of Fabric Cord.

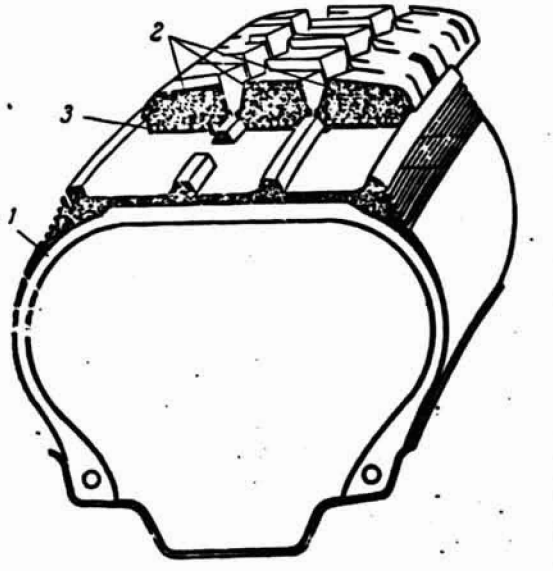

Fig. 19: An RS Tire with Removable Tread (Cross Section): (1) The Carcass with the Fibers Running Radially; (2) Removable Tread Bands; (3) Metal Cord.

Mounting and unmounting of the tread bands are done with the tire deflated. When the tire is inflated, the bands tightly grip the rolling part of the body.

Attempts at developing a carcassless tire have been of great interest.

There have been several announcements of progress in this area. There are several different construction variations of these tires with partial or total elimination of the carcass. The absence of a carcass is compensated by an increase in the thickness of the walls and a greater elasticity modulus of the rubber. Some variants of this type of construction call for the presence of cord reinforcing inser-

tions placed in various parts of the tire.

In the remaining sections of the tire, nylon, metal cord or other materials may be used. In all these cases the breaker is maintained.

Research on the development of carcassless tires is, as far as we know, being conducted in a number of countries. Positive results have been obtained for bicycles and hand-carts. Research is also being done on the development of carcassless tractor and automotive tires. /23

The first carcassless tires were developed in the USA and Europe. These tires were made of polyurethane with a spongy polyurethane filler.

However, at the present time the feasability of developing automotive tires without a carcass has not been established.

Classification of Automotive Tires and Rims

Automotive tires are divided into two basic types: light and heavy duty.

Light tires are used on passenger cars and small capacity trucks.

Heavy duty tires are used on trucks, buses, trailers and trolleys.

Light tires have few plies (no more than 6), are used on a well base rim with a small diameter (16 inches or less), have a low internal pressure (no more than 2.5 kg/cm^2) and a low load capacity. /24

In the construction of contemporary light tires there is a tendency to increase the comfort of the automobile by decreasing the internal pressure in the tires and simultaneously decreasing the overall height of the automobile by decreasing the diameter of the wheel rim.

In connection with this great popularity was enjoyed by low pressure tires (about 1.7 kg/cm^2 with a decreased rim diameter (the domestic constructions are 5.60-15 for Moskvich models and 6.70-15 for the Volga and other models.

In contrast to light tires, heavy duty tires have more plies, are designed for a rim with a larger diameter (usually 20 inches), have a higher internal pressure (usually from 3 to 5 kg/cm^2) and a greater load capacity.

The basic dimensions of each tire are given on the tire.

There are several different notation systems: in the most widely used system the first number represents a rounded-off (nominal) value of the profile width and the second represents the internal diameter of the wheel rim (for example 6.70-15).

In another system the first number represents the external diameter of the tire and the second number represents the rounded-off profile width (for example, 1140 X 700). In certain cases the notation consists of three numbers: the first is the external diameter, the second is the profile width and the third is the internal diameter of the rim (for example, 1200 X 500-508). Sometimes tires of special type are denoted by letters (for example, R or RS). The tire notations are carried on the sidewalls and are printed by the tire mold.

Usually each tire has a serial number carried on the sidewall. The manufacturer and the date the tire was issued are abbreviated before the serial number.

Tubes and rim bands are denoted in most cases in the same way as the outer covers for which they are designed.

Automotive tires are classified as follows by construction and usage characteristics:

(a) Tires with road tread;
(b) Tires with all-purpose tread;
(c) Tires with high roadability tread;
(d) Tires designed for use in quarries, logging, etc.;
(e) Tires with variable internal pressure;
(f) Ground-grip tires;
(g) Wide-profile tires (all-purpose, economy, high roadability);
(h) Rollers;
(i) Tires for road construction machines; /25
(j) Tires for sports cars and racing cars.

Tires with road tread are designed for use on roads with a hard surface (Fig. 20). These tires have good wear resistance but do not have sufficient traction on roads covered with mud or snow or on soft ground. The tread design of this type of tire usually consists of shallow zig-zag ribs and grooves.

Tires with all-purpose tread (Fig. 21) are designed for use under varying road conditions (on roads with a hard surface and on dirt roads). These tires have a satisfactory wear resistance on hard roads and have good traction on a road covered with mud or snow.

The tread designs of these tires usually are a combination of longitudinal ribs or checks in the central part of the tire surface and heavy massive ridges divided by wide grooves along the edge of the tire. The wide grooves rid themselves easily of mud and snow.

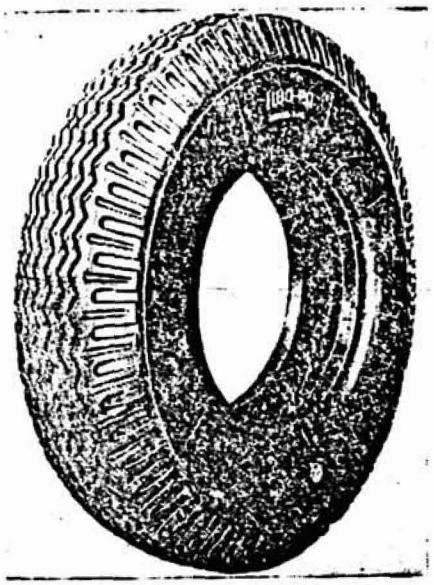

Fig. 20. A Tire with Road Tread.

Fig. 21. A Tire with All-Purpose Tread.

Tires with high roadability tread (Fig. 22) are designed for use on hard-to-travel dirt roads and roads covered with mud or snow. /26 These tires can provide a significant increase in the roadability of the vehicle on soft ground since the internal pressure in these tires is the same as in tires operating on roads with hard surfaces. Tires with high roadability tread do not have a long life span on roads with hard surfaces since the tire quickly becomes inoperative due to wear on the tread. The tread design of high roadability tires consists of wide grooves running laterally across the surface of the tire or at an angle to the circumference of the tire and strong massive ridges for gripping the ground.

Fig. 22. A Tire with High Roadability Tread.

Tires for quarries and logging are somewhat similar in terms of tread design to high roadability tires but, in contrast to the latter, have narrower grooves and wider ridges. The tires are designed for use under conditions of unimproved roads covered with sharp-edged debris or large rocks.

The massive tread design, its greater thickness and also its reinforced carcass provide a high degree of resistance to mechanical damage and wear.

The remaining types of tires are examined in detail in their respective sections.

Types of Automotive Wheel Rims

The rim of an automotive wheel is that part of the wheel to which the pneumatic tire is fastened. Rim construction is determined mainly by the construction of the pneumatic tire. Rims are categorized as follows:

(1) For ordinary tires:
  (a) flat base;
  (b) well base;
  (c) expanded rims with conical bead seats.

(2) For special tire constructions: /27
  (a) for tires with variable internal pressure;
  (b) for ground-grip tires;
  (c) for wide-profile tires;
  (d) for rollers.

Flat base rims (Fig. 23a) are widely used for heavy duty tires. The rim has a detachable flange and a cylindrical internal section.

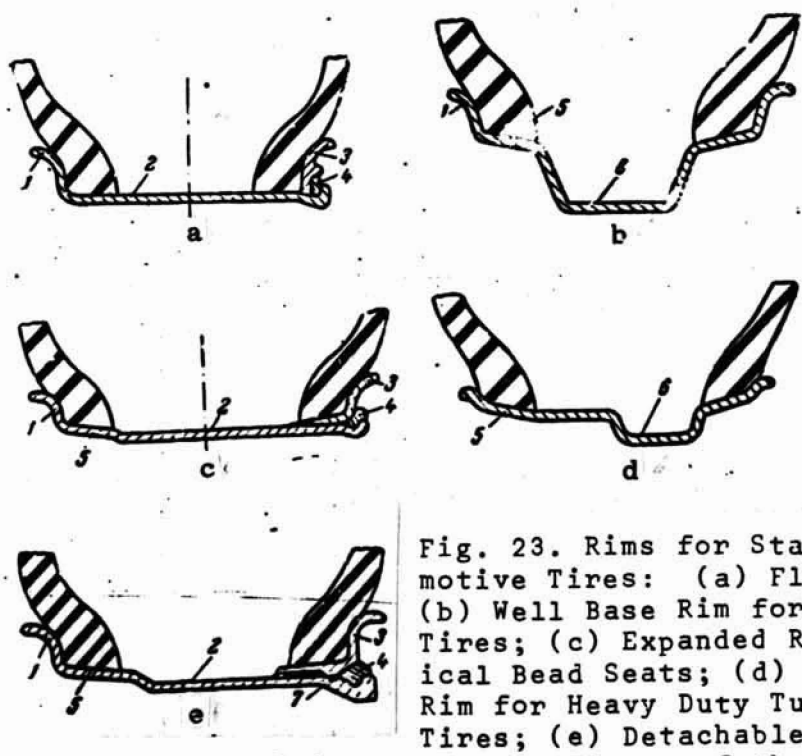

Fig. 23. Rims for Standard Automotive Tires: (a) Flat Base Rim; (b) Well Base Rim for Light Tires; (c) Expanded Rim with Conical Bead Seats; (d) Well Base Rim for Heavy Duty Tubeless Tires; (e) Detachable Rim for Heavy Duty Tubeless Tires. (1) The Edge or Flange of the Rim; (2) The Cylindrical Part of the Rim; (3) Detachable Flange; (4) Air Sealing Rings; (5) Conical Bead Seat; (6) Rim Saddle; (7) Rubber Packing Cord.

This type of rim is obsolete; it does not provide a satisfactory seal of the tire on the rim. Well base rims (Fig. 23b) are single unit, i.e. they do not have removable parts. So that the tire can be mounted, the rim has a saddle. Well base rims are used mainly for light tires and also for heavy duty tubeless tires.

Expanded rims with beveled bead seats for heavy duty tubeless tires (Fig. 23c) have widely replaced flat base rims; in terms of construction they differ from flat base rims by a greater width and the presence of beveled bead seats (usually at an angle of 5°), insuring a tight seal between the beads of the outer cover and the rim. Expanded rims provide greater operating reliability, longer life spans and a greater load capacity of the tire.

Rims for tubeless tires differ in that they are hermetically /28
sealed, which is accomplished by sealing the detachable parts and by the absence of holes in the body of the rim.

Heavy duty well base rims for tubeless tires (Fig. 23d) have more beveled bead seats (15°) and a lower height of the drop center rim in comparison to the well base rims of passenger cars. This type of rim is designed for tires with a profile width of less than 11" (279 mm) inclusive. For tubeless tires of greater dimension detachable rims are used (Fig. 23e) in view of the difficulty of mounting on a single-unit rim. These detachable rims are hermetically sealed at the place where the detachable flange is joined to the rim using a rubber cord ring.

For tires with variable internal pressure detachable rims with spacer rings are used (Fig. 24a). The spacer ring is placed between the beads of the outer cover: the tire beads are pressed between the internal spacer ring and the rim flanges. This method of installing the beads for tires with variable air pressure insures that the tires will hold at low air pressure.

Rims for ground-grip tires (Fig. 24b) have various constructions, but they all provide for pressing the beads between the flanges of the rim and the spacer ring or a similar device replacing the spacer ring.

The major difference in rims for ground-grip tires is their greater width, more than two times greater than the width of rims for ordinary tires.

Rims for wide profile tires (Fig. 24c) have beveled bead seats (inclined at an angle of 5°) and the same flanges as ordinary tires. The width of these rims is greater than for ordinary tires because of the larger profile of the tire and also the greater ratio of rim width to tire profile width. Rims with spacer rings are used for wide profile tires with variable internal pressure.

For rollers, wheels and rims are used which are similar to

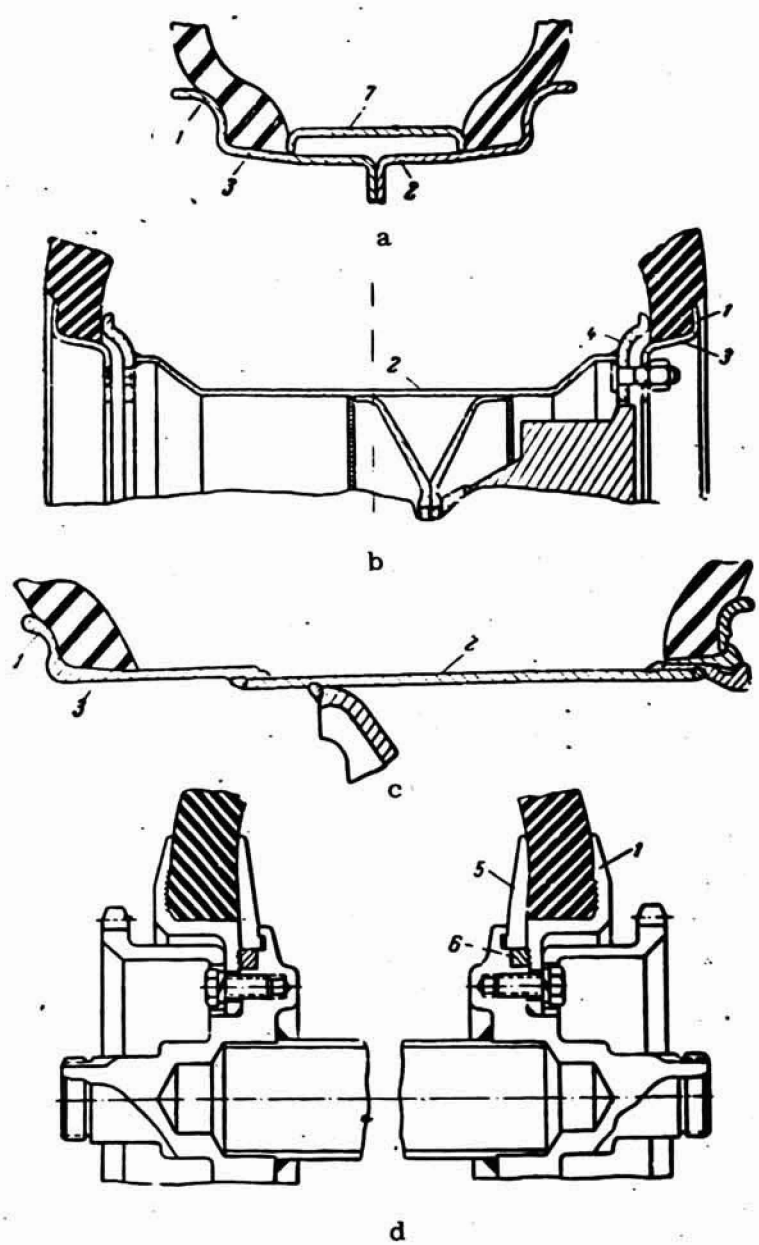

Fig. 24. Rims for Special Automotive Tires: (a) Detachable Rim with a Spacer Ring; (b) Rim for Ground-Grip Tires; (c) Rim for Wide Profile Tires; (d) Wheel with Rim for Rollers. (1) Edge or Flange of the Rim; (2) Cylindrical Part of the Rim; (3) Beveled Bead Seat; (4) Internal Part of the Rim; (5) Slot Ring; (6) Rubber Filling Ring; (7) Spacer Ring.

those of ground-grip tires in terms of the means used to fasten the beads. The major difference is the small internal diameter of rollers. /29

Rim Notation. As a rule, rims are designated according to their width and the shape of the flange; for example, 4.00E; 6.00T. In this notation the number refers to the rim width in inches, the letter shows the type of rim flange. In the notations for expanded rims with beveled bead seats letters are not used since a particular rim width corresponds to a particular type of flange. Examples of expanded rim notations are: 6.0; 8.5.

Rims for tires with variable pressure are designated by a number and two letters. For example, 10.00RG: the number shows the rim width; the letter R stands for variable pressure; G is the flange type. /30

Rims for ground-grip tires are designated by two numbers (1000 X 600) in the same way as ordinary tires. The first number shows the diameter of the tire and the second shows the width of the tire profile; the rim width is usually about 3-3.5% less than the width of the tire profile. Rims for wide profile all-purpose tires are designated by two numbers (for example, 380-508).

The first number shows the rim width and the second number shows the internal diameter expressed in millimeters.

Rims for rollers are designated by three numbers (in inches): for example, 24 X 36 X 6, in the same way as tire notation. The first number shows the diameter of the roller, the second shows the profile width (the rim width is about 5% less than the profile width) and the third shows the internal diameter of the roller.

A Brief Outline of the Technology of Automotive Tire Production

The purpose of this section is to present an overall view of the fundamental processes of tire construction to the extent necessary for an understanding of the characteristics of tire construction.

Detailed presentations of the technology of tire production and descriptions of the corresponding equipment are given in a number of special references [9-11].

The most complex process is the production of the outer covers of tube tires and the very similar production of tubeless tires.

The manufacture of tubes and rim bands is a separate and relatively simple process.

Let us examine now briefly the process of manufacturing outer covers, which consists basically of the preparation of the rubber, the preparation of the rubber mix, rubberization of the cord, construction of the components of the outer cover, assembly of the crude outer cover, its molding and vulcanization.

Preliminary Processes

The rubber is prepared so that it will have characteristics which facilitate subsequent technological processes. To do this the natural rubber is plasticated. During this process a partial mechanical and oxidizing decomposition of the rubber molecules takes place. As a result we obtain a product with a high degree of plasticity and homogeneity.

Plastication on rollers consists in passing the rubber between rollers a small distance apart (3-8 mm) and rotating in opposite directions at low circular velocities. The intense and frequent intermixing of the rubber in the gap between the rollers, together with heating of the rubber to 40-50°C causes plastication. Plastication on rollers is not very efficient and requires a great expenditure of electrical energy. /31

At the present time more efficient methods are used to plasticate rubber: rubber-mixing tanks and special plasticators (worm presses).

Synthetic rubber, i.e. soft butadiene-styrene and butyl rubber, are plasticated in the same way as natural rubber. As a preliminary, strong butadiene-styrene rubber undergoes thermal plastication by hot air in thermoplasticators (boilers) or hot mechanical plastication in continuous action machines in the presence of an antiager.

At the present time synthetic rubber factories produce mostly soft butadiene-styrene rubber which does not require thermal plastication.

Rubber of one or another kind forms the basis of the *rubber mix* or *"crude" rubber*.

Included in the composition of the rubber mix are, in addition to rubber, fillers, vulcanizing compounds, vulcanization accelerators and activators, softeners and antiage ingredients. Sometimes in the rubber mix (primarily for the less important components of the tire) reclaimed rubber is used together with new rubber.

The fillers, mainly carbon black of various kinds, are used to obtain rubber with the necessary characteristics.

Carbon black increases the durability of the rubber, its strength and wear resistance. Especially important is the role of carbon black in the preparation of rubber mixes based on synthetic rubber. Rubber mixes with various characteristics can be obtained depending on the type and quantity of carbon black used.

To produce white and colored rubber mixes used for decorative sidewalls on light tires, special white fillers (so-called "white carbon") are used instead of carbon black.

The vulcanizing agent, in the overwhelming majority of rubber mixes for tires, is sulfer. In the vulcanization process the sulfur molecules are bonded to the linear rubber molecules forming a kind of bridge between them. As a result one obtains vulcanized rubber, i.e. an elastic material which, in contrast to crude rubber at ordinary temperatures, is not susceptible to plastic flow.

Vulcanization accelerators, contained in the rubber mix in small quantities, accelerate the vulcanization process and improve the physical and mechanical characteristics of the vulcanized rubber.

In contemporary practice, organic accelerators are used almost exclusively (altax, captax, thiuram, sulfenamide BT, etc.). To increase the activity of the accelerators special agents called *vulcanization activators* are introduced into the rubber mix. These agents allow a decrease in the duration of the vulcanization process. Two such agents are zinc oxide and magnesium oxide. /32

Softeners serve mainly to improve the technological characteristics of the crude rubber. They also affect the physical and mech-

anical properties of the vulcanized rubber. Liquid or solid petroleum products are usually used as softeners.

Antiagers are included in the composition of the rubber mix to protect it from aging and to increase its durability with repeated distortions.

Changes in the properties of the rubber with aging and repeated distortion are related basically to oxidation of the rubber by oxygen in the air and ozone. Therefore special chemical substances (antioxidants) are used as antiagers. These substances capture the oxygen which penetrates the rubber.

The most active antiagers are phenyl-betanaphthylamine D and santoflex A.

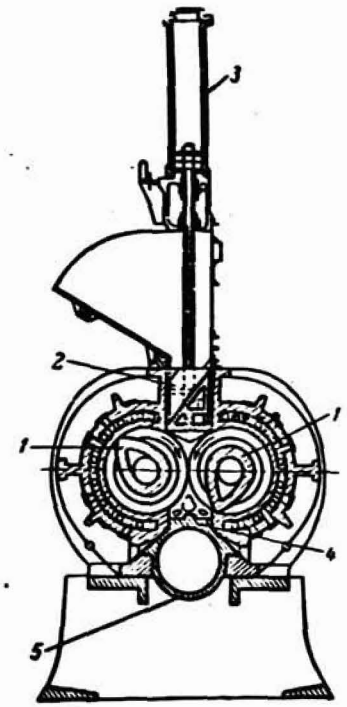

Fig. 25. Diagram of a Rubber Mixer (Lateral Cross Section): (1) The Rotor; (2) The Feed Aperture; (3) The Pneumatic Cylinder of the Upper Gate; (4) The Discharge Aperture; (5) The Lower Gate.

Mixing is a technological process whose goal is a complete and uniform distribution in the rubber of all materials included in the composition of the crude rubber. The physical and mechanical indicators and homogeneity of the rubber depend to a significant degree on the quality of the mixing process and on the degree of dispersion in the rubber of all ingredients in the mix.

Mixing is done in a rubber mixer. A diagram of one type of rubber mixer is shown in Figure 25. The rotors (1) rotating in opposite directions provide intense mixing of the mix. Rubber and the other ingredients are fed into the mixture through a feed aperture (2) which is opened and closed by a pneumatic cylinder (3). The prepared mix is released through a discharge aperture (4) in the lower section of the mixer, closed by a gate (5).

Cooling water is fed through the housing of the rubber mixer to maintain the proper temperature regime for the mixing process. /33

The operations of the rubber mixer and all related equipment for batching and loading the ingredients are carried out automatically.

In the majority of cases a mix without sulfer is prepared in the rubber mixers. Sulfur is introduced into the mixture later on sheet rollers. This mixing sequence is designated to prevent partial prevulcanization of the rubber during mixing.

In recent years a two-stage mixing method has become popular. In this case an auxilliary mixture is first prepared without sulfur and accelerators, and then in the second mixing stage the sulfur and accelerators are added to the auxilliary mixture.

Using this process the quality of the rubber mix is improved because of better mixing.

The mixing process is usually controlled by recording the temperature of the mix during mixing. Each rubber mix has its own characteristic curve of temperature increase during mixing.

The quality of the rubber mix is regulated according to the physical-mechanical indices of samples from each batch. Usually the plasticity and density are determined for each batch produced by the rubber mixer. In addition, the modulus [4] and hardness are determined for the vulcanized samples taken from a given rubber mix. In recent years so-called "rapid analysis" has become popular. In this method the samples of the mix are vulcanized in a small press at temperatures of 180 - 250° C for 1 - 2 min., after which the annular modulus is determined.

The prepared rubber mixes are then used to produce the rubber parts of the tire (tread, sidewalls, rubber layers) and to rubberize the cord.

Cord Rubberization

A high strength of the seal between the cord and the rubber coating must be reached during rubberization. It is first necessary to give the cord a preliminary soaking in special latexes and resins to increase the strength of the seal between the cord and the rubber.

The production of rubberized cord takes place on an assembly line with automatic controls so that the processes of soaking, drying and rubberizing take place continuously.

A diagram of such an assembly line is shown in Figure 26. The unbleached fabric cord passes from a roll into the tank (6) which contains the soaking agent. The excess soaking agent is squeezed /34 out of the cord by the rollers (8). Then the cord enters the drying tank (9) where, passing along a drum lattice, it is dried. The dried cord then enters a calender (15) for rubberizing, and after rubberization the cord is wound on the rolling equipment (19). In this case to prevent sticking, the cord is wound with a fabric packing.

---

[4] Usually the so-called annular modulus is determined by stretching a vulcanized sample in the shape of a ring. Tests are made according to All-Union State Standard 412-453.

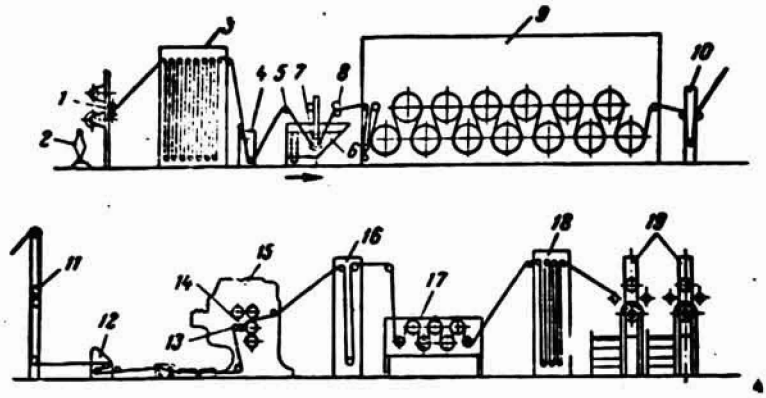

Fig. 26: Diagram of the Assembly Line for Rubberizing Cord: (1) The Unrolling Rack; (2) Sewing Machine for Batching the Cord Linen; (3) Compensator; (4) Vacuum Cleaner; (5) Stretching Roller; (6) Soaking Tank; (7) Guide Roller; (8) Squeeze Roller; (9) Intake Chamber; (10) Compensator; (11) Centralizing Device; (12) Stretching Device; (13) Guide Rollers; (14) Mold Roller; (15) Calender; (16) Compensator; (17) Cooling Drums; (18) Compensator; (19) Winding Device.

Figure 27 shows a diagram of the coating of the cord in the calender (four-roller, Z-shaped).

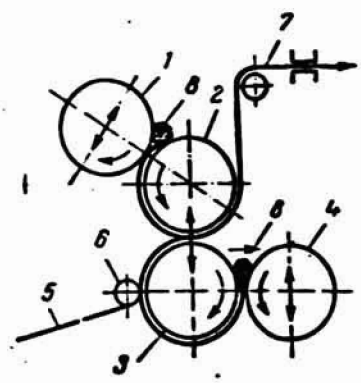

Fig. 27. A Diagram of the Two-Sided Coating of the Cord by Rubber Mix in a Four-Roller, Z-Shaped Calender: (1,2,3,4) Calender Rollers; (5) Cord Linen (Unbleached Cord); (6) Press Roller; (7) Rubberized Cord Linen; (8) The Rubber Mix.

The cord linen (5) enters the space between rollers (2) and (3) of the calender where it is coated from two sides with a thin layer of the rubber mix. Since in the space between the rollers the rubber is under high pressure, it completely fills the spaces between the fibers of the cord.

The rubber mix (8) continuously and uniformly flows onto the

calender to the space between the rollers from the heating rollers. A cord calender is a very efficient piece of equipment; the speed of the cord in the calender reaches 90 m/min. In connection with /35 this fact, the constant measurement and automatic regulation of the thickness of the rubberized cord is of great importance. For the continuous measurement of the thickness of the cord, instruments using radiation have recently come into use.

Nonwoven cord is used in tire production in addition to woven cord. Nonwoven cord has significant advantages over woven cord since it provides a more uniform distribution of fibers in the finished tire. Metal cord is used only as nonwoven cord.

The system for rubberizing nonwoven cord is the same as for woven cord but the cord linen enters the assembly not from a roller but from a spool. The spool is a special device where each fiber is wound on an individual bobbin provided by the tightening device. Uniform distribution of the cord fibers and the obtaining of a prescribed interval are guaranteed by a guide comb.

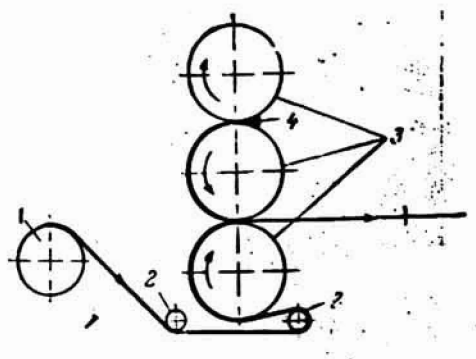

Fig. 28. A Diagram of the Fabric Coating Process on a Three-Roller Calender: (1) Roller; (2) Guide Rollers; (3) Calender Rollers; (4) The Rubber Mix.

Square weave fabrics, used in tire production (wing casing, bead casing), are coated with rubber (frictionated).

A diagram of fabric coating on a three-roller calender is shown in Figure 28. From a roller (1) the fabric passes through the guide rollers (2) to the space between the lower and middle rollers of the calender. The rubber mix flows into the space between the middle and upper rollers and coats the middle roller. The middle roller rotates at a higher speed than the lower roller and the rubber mix is pressed into the spaces between the fabric fibers coating them on one side. To coat the fabric on the other side, it passes again through the space between the rollers of the calender. Then the fabric, coated on both sides, is wound up in packing.

Cord Cutting and the Positioning of the Cord Plies

To prepare the cord plies of the tire the rubberized cord canvas must be cut into strips of a prescribed width at a particular angle α, called the cut angle. A diagram of the system for cutting cord is shown in Figure 29a.

In this way strips of cord are obtained in the form of parallel- /36 ograms. These strips are then joined along the fibers forming con-

tinuous bands (Fig. 29b).

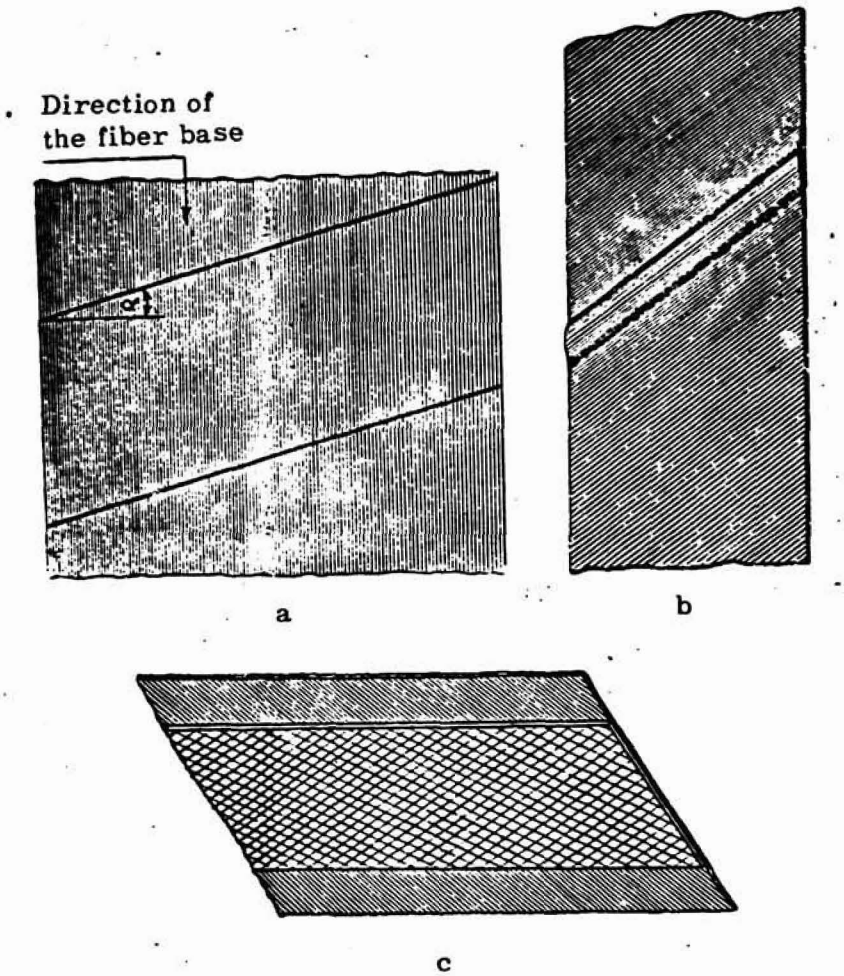

Fig. 29. A Diagram of the Process of Cutting Cord Canvas: (a) Cutting the Canvas into Strips; (b) The Strips, Bonded into a Continuous Band; (c) The Band of Cord with a Rubber Layer Attached.

The rolls of cord are cut on diagonal cutting machines (horizontal or vertical). On these machines the cord linen moves along a conveyer stopping periodially. When the canvas stops the cut is made by a revolving blade moving at the necessary angle. From the conveyer of the diagonal cutting machine the strips of cord are relayed to a /37
bonding conveyer where they are bonded. Then the cord band is wound on a reel.

Where necessary, rubber interlayers (squeegees) are superimposed on the cord bands (cf. Fig. 29c).

Figure 30 shows a diagram of the production of rubber interlayers on a three-roller calender and its bonding onto the cut rubberized cord. The mix flows into the space between rollers (1) and (2) of the calender, from there it passes through the space between rollers (2) and (3). On the lower roller are the blades with which the rubber strips are cut to the proper width. The rubber strip passes onto a conveyer where the bonding of the rubber to the rubberized cord takes place using double rollers. The cord with the bonded rubber interlayers (Fig. 29c) then passes onto a conveyer where it is wound on rollers with canvas packing.

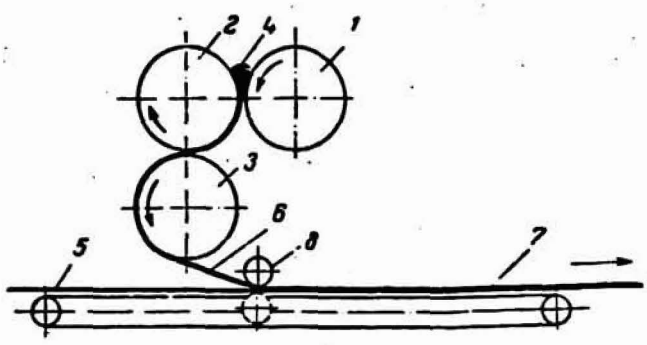

Fig. 30. A Diagram of the Production of Rubber Interlayers on a Three-Roller Calender and Their Bonding onto the Rubberized Cord: (1,2,3) Calender Rollers; (4) The Rubber Mix; (5) Rubberized Cord; (6) Rubber Interlayers; (7) The Rubberized Cord with the Rubber Interlayers Bonded to It; (8) The Double Roller.

Square weave fabrics (cafer, calico) used for the wing casing and the bead casing, are cut as is cord, on diagonal cutting machines into wide bands, then each band is cut into narrow bands (strips). To cut wide bands of fabric into narrow strips lateral cutting machines are used. Square weave fabric is usually cut at an angle of 45°

Production of Tread

The pretread of a tire (crude tread) is a band of crude rubber with a figured cross section (Fig. 31).

As a rule, tread is produced by extrusion (molding) on worm presses.

A diagram of a worm press (extrusion machine) is shown on Figure 32. /38

Crude rubber, passing from the rollers to the press, is supplied by an auger (worm) (1) of the press to the head (2), where it is pressed through an aperture in the shaping slat (3) in the form of a continuous strip having the cross section of the crude tread.

In tire factories all operations in the process of producing tread are made on a single tread-producing unit. On this unit, which is a series of consecutive machines linked by a conveyer, the following operations are performed: cooling (with water), air blowing, roughing and the application of adhesive (in the case of tread made of synthetic rubber), drying, cutting of the pretread into the proper length.

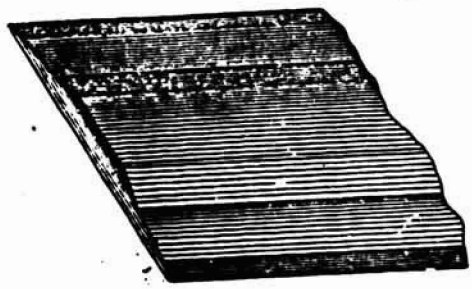

Fig. 31. The Profile of the Crude Tread.

In some cases the tread is made of two kinds of rubber: the tread-base ply and the sidewalls are made of relatively soft rubber and the rolling part is made of stronger more wear-resistant rubber. Two-ply treads are made on tread-producing machines with /39 two worm presses. On one of the presses the lower part of the tread is made (the tread-base ply and the sidewalls) and on the other press the rolling part is made. Doubling is done by a special roller on the conveyer. In wide use also are tread-producing machines with two opposing worm presses operating with a common T-shaped head. In this case doubling of the rubber takes place during the actual process of extrusion.

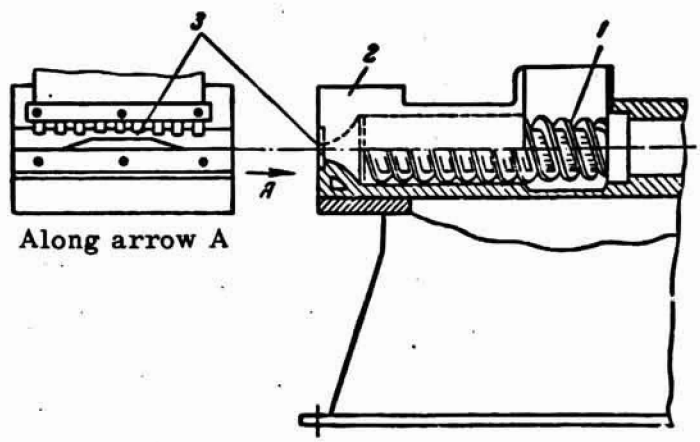

Fig. 32. Diagram of an Extrusion Machine: (1) Auger; (2) Head; (3) Shaping Slat.

Wing Production

The wing (Fig. 33) consists of a wire ring (1), a filler (2), a wing casing (3) and a flipper (4).

The wire rings are made of woven wire or a single wire [5].

The wire weave is a series of parallel wires interconnected by a weave of finer wire.

---

[5] In most configurations a steel wire 1 mm in diameter having an ultimate resistance of 140 - 200 kg/mm^2 is used.

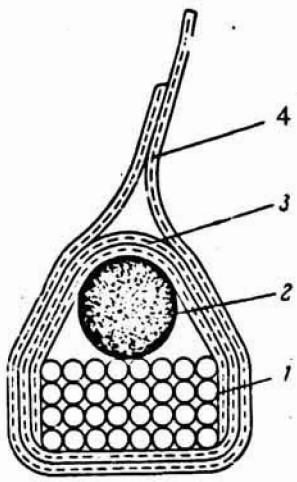

Fig. 33. An Outer Cover Wing (Crude):
(1) Steel Wire Ring;
(2) Rubber Filler;
(3) Wing Casing;
(4) Flipper.

The woven wire is rubberized on the ring-producing equipment by passing it through the head of a special worm press, and then the ring is wound on a special mold while the ends of the woven wire are bound by a strip of fabric. At the present time woven wire is used very little; single wires are used for the most part. The distinguishing feature in the production of wings made of single wire is that a number of wires, each unrolling from a separate bobbin, are rubberized rather than woven wire. For greatest density the ring made from single wires is wrapped spirally by a thin band of rubberized fabric. Special wrapping machines are used for this operation.

In certain cases to increase the strength of the ring the rubberized, single wire rings undergo preliminary vulcanization during the assembly of the tire.

The Assembly of Outer Covers and Tubeless Tires [6]

/40

The assembly of an outer cover consists in the cementing together of pre-prepared components on special assembling machines.

The basic part of the assembling machine is a drum to which, naturally, the outer cover is fitted. The drum can have various profiles depending on the method of assembly.

At the present time semiplane and collapsible drum methods are used to assemble outer covers. The various profiles can be seen in Figures 34 and 35.

In the collapsible drum method the outer cover is assembled from bands.

The band is a ring made of several (2, 4 or 6) plies of cord fitted together so that the fibers of adjacent plies intersect. The bands are made on special band-making machines equipped with elastic rollers. The pressure of these rollers provides a tight seal of the plies.

---

[6] Tubeless tires are assembled in the same way as outer covers. The only difference is in the operations related to the use of sealing and tightening bead plies. These operations are conducted with special care to prevent defects which could cause air permeation from the internal cavity of the tire to its body and lead to the separation of the carcass plies and the separation of the tread during usage.

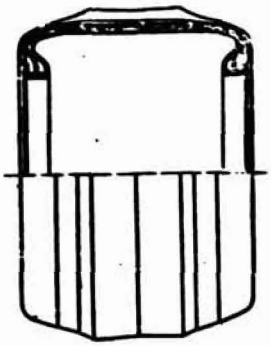

Fig. 34. A Crude Outer Cover, Made by the Collapsible Drum Method.

Fig. 35. A Schematic Cross Section of a Semiplane Drum with an Outer Cover Fitted to It.

The prepared bands are fed onto a collapsible drum attached to the assembling machine (Fig. 36).

In this case, since the length of the band is 5 - 10% less than the circumference of the drum, the band adheres tightly along the cylindrical surface of the drum.

In the bead section the band is pressed along the surface of the drum by rollers.

After one or two (depending on the construction of the outer cover) bands [7] are placed on the drum, the wings with bead rings are added, centered using special guages. The edges of the bands are folded up onto the wing and rolled. Then depending on the construction of the outer cover the remaining bands are added and the second /41
wing is fitted (for tires with two wings in the bead).

The operations of feeding the bands onto the drum and folding their edges up are done alternately with a roller.

After the process of mounting the carcass on the drum is completed, the breaker and tread usually in the form of bands, are added and also the chafer strip and the bead casing.

Then the drum is collapsed, the outer cover is removed and the edges of the bead are tucked inside the bead.

The semi-plane assembly differs from collapsible assembly by /42
its different profile of the assembly drum and also by the fact that individual plies of cord are fed onto the drum rather than pre-prepared rubber bands.

The layer-by-layer assembly of outer covers on a semiplane drum is more efficient than assembly by the collabsible drum method.

---

[7] In a number of cases the first band is fed onto an additional drum and assumes the proper position when the drum is expanded.

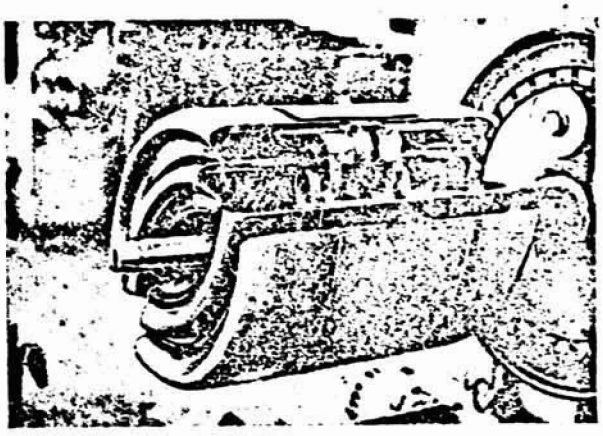

a

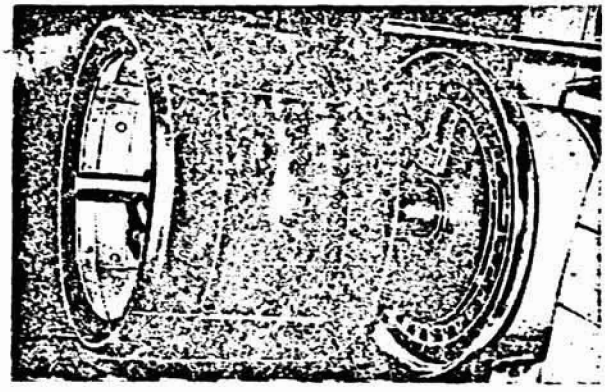

b

Fig. 36. A Collapsible Drum (a) Collapsed; (b) Expanded.

Since in the molding process of outer covers made by the semi-plane method, the bead is folded with respect to the wire ring, this assembly method can be used only for the outer covers with a single wire ring in the bead, i.e., for outer covers for passenger cars and light trucks.

Molding and Vulcanization of Outer Covers

Before molding the outer covers are coated ("painted") with lubricant. The external surface is covered with a water emulsion of silicon which facilitates the flow of rubber in the mold and prevents the rubber from sticking to the mold. The internal surface is covered with a special lubricant (with mica and other materials), which facilitates the proper fitting inside the outer cover of the heating chamber and prevents welding.

The prepared outer covers are then molded. Figure 37 shows the process of molding outer covers on an air press.

The outer cover is placed on /43 the platform of the press, after which a vertical plunger descends until it comes in contact with the bead of the outer cover. The internal cavity of the outer cover is pressurized (1.2-2.5 kg/cm^2) and, simultaneously, due to the descent of the vertical plunger the beads of the outer cover are brought close together. The outer cover now takes the shape of a torus, and the heating chamber, which was placed in the aperture of the vertical plunger of the press, is inserted into the outer cover. An overall view of an air press is shown in Figure 38.

The crude outer covers with the heating chambers inserted in them are then transfered to the vulcanization presses.

For vulcanization the outer cover is placed in a vulcanization mold which has been heated with steam. Superheated steam is then injected into the heating chamber at a pressure of 20-25 kg/cm^2 and a temperature of 165-185°C. Using water pressure in the heating chamber

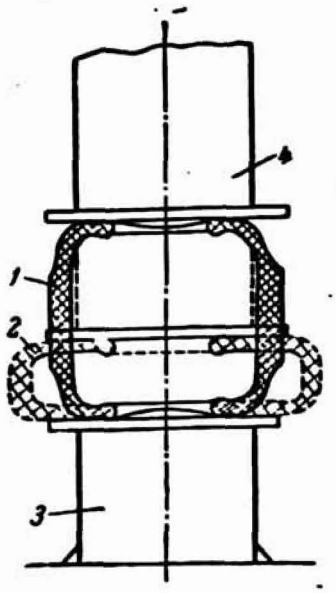

Fig. 37. The Molding Process for Outer Covers on an Air Press: (1) The Crude Outer Cover Before Molding; (2) The Crude Outer Cover After Molding; (3) The Platform of the Press; (4) The Cylinder with Plunger.

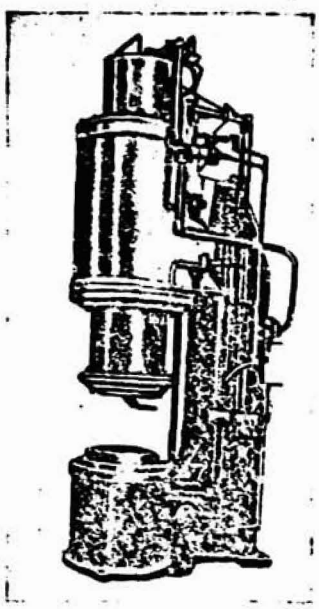

Fig. 38. An Overall View of an All-Purpose Air Press.

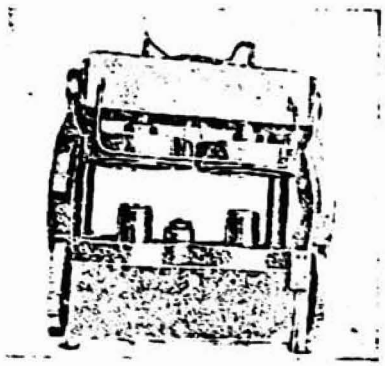

Fig. 39. An Overall View of a Press-Vulcanizer with Crude Outer Covers Placed on the Diaphragms.

the outer cover is pressed tightly against the mold, while at the same time the tread is molded onto the outer cover.

Vulcanization takes place in autoclave type presses or in individual vulcanizers. Due to a number of advantages (increase in the quality of the tire, increased operating efficiency and improvement of its conditions) individual vulcanizers have become very popular.

In recent years press-vulcanizers (Fig. 39) have been used for simultaneous molding and vulcanizing.

The diagrams in Figure 40 show the operating principles of press-vulcanizers. In Figure 40, a shows the position of the crude outer cover and the diaphragms in the open press. When the upper half of the press is lowered (Fig. 40b), the diaphragm simultaneously ascends and straightens out inside the outer cover; the diaphragm is lifted by injecting steam into it. Under the pressure created inside the diaphragm, the outer cover is molded (Fig. 40c) and pressed against the mold. For the vulcanization process, a heat transfer agent (steam or super-heated water) is injected into the diaphragm. Toward the end of the vulcanization process, the diaphragm resumes its initial position (cf. Fig. 40a) and the press is opened. The outer cover and the upper half of the press move upward before the press has opened completely, after which the bead ring of the upper half of the press ejects the finished outer cover (Fig. 40d).

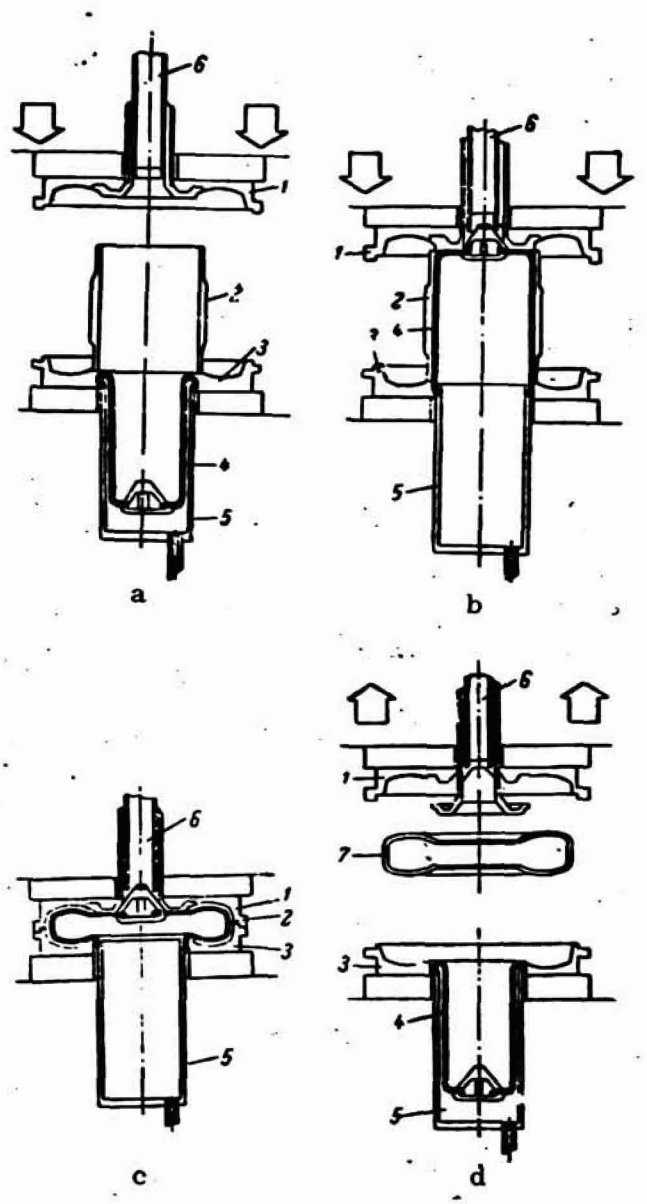

Fig. 40. Operating Principles of a Press-Vulcanizer: (a) Position of the Crude Outer Cover and the Diaphragms in the Open Press; (b) Position of the Diaphragm When the Upper Half of the Mold Descends; (c) Position of the Outer Cover and Diaphragms in the Closed Press; (d) Position of the Press After Vulcanization. (1) Upper Half of the Mold; (2) Crude Outer Cover; (3) Lower Half of the Mold; (4) Diaphragm; (5) Cylinder; (6) Shaft; (7) Vulcanized Outer Cover.

The operation of a press-vulcanizer can be fully automated. /44

After the outer covers are vulcanized and the heating chambers removed, the excess is trimmed off and the outer covers are waxed, i.e., coated with special agents to prevent ozone and light aging.

The final technical operations are the removal of the outer covers and, if necessary, balancing.

The Production of Tubes and Rim Bands

Tubes are prepared by extrusion on a worm press. /45 Figure 41 shows the construction of the head of a worm press which serves as the outlet for the sleeve. By varying the position of the fissure (1) of the relative calibration ring (2) one can vary the thickness of the walls of the obtained sleeve. The fissure has a device which covers the inner cavity of the sleeve with talc to prevent slippage.

Tubes are produced on an assembly line. From the worm press the sleeve is fed onto a conveyer belt where it is cut into segments of the desired length. Halves are then installed on these segments. The ends of these segments are bonded on special machines. In certain cases in order to increase the strength of the bond a strip of cord is fastened to it. After air blowing the tube segments are placed in

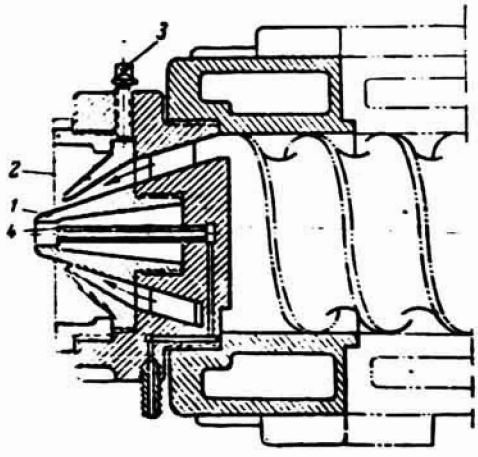

Fig. 41. The Head of a Worm Press (for Producing the Tube Sleeve): (1) Fissure; (2) Calibrated Ring; (3) Regulating Screw; (4) A Conduit for Blowing the Inner Cavity of the Tube.

a mold and vulcanized in individual vulcanizers.

Segments of rim bands are also extruded. After cutting and bonding the rim bands are vulcanized in special presses.

CHAPTER II

FUNDAMENTALS OF THE THEORY OF PNEUMATIC TIRES

Rubberized Cord Construction Grids and Their Properties

The Geometry of Cord Fibers in the Carcass of the Tire

The carcass of a pneumatic tire which is the force-base is /46
formed by a series of intersecting plies of rubberized cord (cf. Ch. I). In the tire production process the cord fibers of each ply occupy a particular position on the surface of rotation which is itself a ply. This position is characterized by an angle β formed by the fiber with the meridian of the surface at each point (Fig. 42). The angle β, which we will call the cord fiber angle, varies from point to point along the meridian but is identical at all points lying on parallel circles.

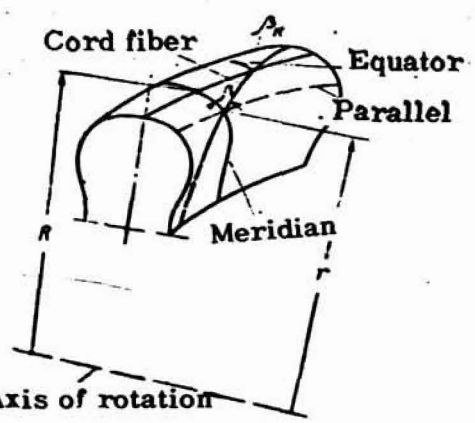

Fig. 42. The Position of the Cord Fibers on the Surface of the Ply in a Tire.

We will examine the change in the cord fiber angle with the meridian during the tire production process. We will assume that initially the cord plies are prepared in the form of bands. (With a collapsible drum assembly the bands are made on special machines, and with semiplane assembly the bands are made directly on the assembling drum). We will assume also that the intersecting plies in the band do not shift relative to one another during the molding of the tire and that the cord fibers along the entire length are stretched uniformly by a factor of $(1 + \delta_1)$. [1]

It follows from the hypothesis concerning the absence of inde- /47
pendent shifting of the plies that in view of complete axial symmetry any point on the band lying in a certain radial plane remains in that plane even after the tire has been molded and vulcanized. Thus the central angle between the radial planes passing through any two

[1] The coefficient δ_1 is called the relative stretch of the fiber.

points on the band does not change during the tire production process.

We will now examine a unit section of fiber $AB = dl$ (Fig. 43a) which in the band corresponds to a central angle $d\phi$ and consequently has a projection on the circular direction equal to $r_b d\phi$, where r_b is the radius of the band.

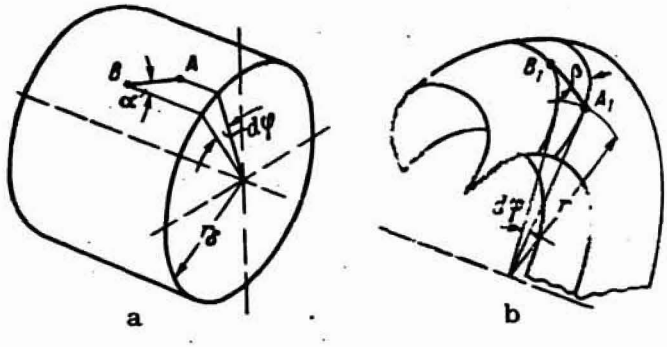

Fig. 43. The Determination of Cord Fiber Geometry in the Tire: (a) Band; (b) Molded Outer Cover.

In the tire (Fig. 43b) this section will have a length

$$A_1B_1 = dl_1 = dl(1 + \delta_1). \tag{1}$$

Since the ends of the section even in the finished tire lie in radial planes forming an angle $d\phi$, the projection of the section on the circular direction will now be equal to $rd\phi$, where r is the distance of the section from the axis of rotation in the finished tire.

Since the sine of the angle of inclination of the fibers to the meridian is equal to the ratio of the projection of a unit section on the circular direction to the length of the section itself, then we can write

$$\sin\alpha = \frac{r_b d\varphi}{dl} \tag{2}$$

and analogously

$$\sin\beta = \frac{rd\varphi}{dl_1} = \frac{rd\varphi}{dl(1+\delta_1)} \tag{3}$$

where α and β are angles formed by the fiber with the meridian in

the band and in the finished tire.

Dividing equation (3) by equation (2) term by term, we obtain /48

$$\sin\beta = \frac{r}{r_6(1+\delta_1)}\sin\alpha \qquad (4)$$

Formula (4) is basic in our theory. Using this formula we can obtain equations to determine the frequency of cord fibers in the tire, the width of separation of the assembly drum, etc. The validity of (4) can be easily substantiated experimentally.

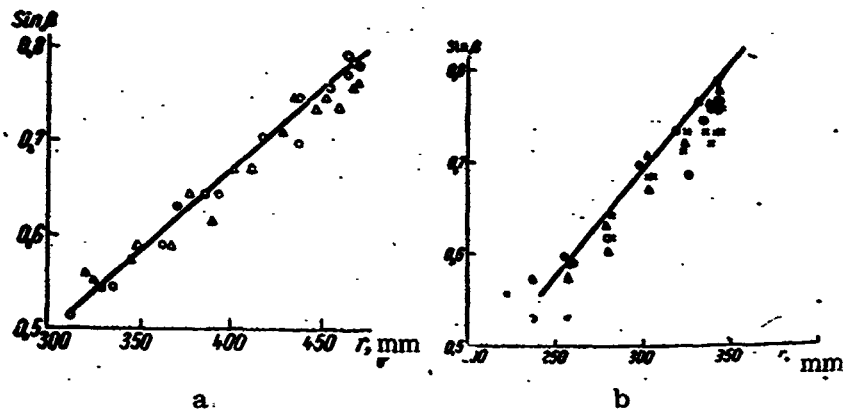

Fig. 44. Comparison of Computed and Experimental Values of the Angles Formed by the Cord Fibers With the Meridian: (a) For 9.00 - 20 Outer Covers Made Completely of Synthetic Rubber; (b) For 6.00 - 16 Outer Covers Made Completely of Synthetic Rubber; For 6.00 - 16 Outer Covers Made Completely of Natural Rubber.

We note that for the given cord ply in the values of r_b, δ_1 and α are constant. Thus it follows from (4) that the sine of the angle of inclination of the cord fiber to the meridian in the finished tire is directly proportional to the distance of the given point from the axis of rotation.

By constructing according to the data of graphic measurements the relationship between the sine of the angle of inclination of the cord fiber and the value of r for a number of tires we can determine to what extent formula (4) is valid.

Figure 44 a shows these graphs for two 9.00 - 20 outer covers, /49

and Figure 44b shows these graphs for three 6.00 - 16 outer covers with carcasses made of synthetic rubber. The graph in Figure 44b is constructed for 6.00 - 16 outer covers with carcasses made of natural rubber.

As can be seen from the graphs, the points obtained by measurement lie with satisfactory accuracy on the computed lines corresponding to equation (4). The values for the relative stretch of the fiber δ_1 which we used in constructing these lines were obtained by analysis of the specifications of these tires.

Thus the experiment confirms the hypotheses proposed on the basis of the derivation of (4).

Formula (4) shows that the angle of the cord fiber at any point on a tire of given profile is completely determined by the value of this angle along the equator (crown) of the tire (cf. Fig. 42).

In fact, after finding from this formula the angle of the cord fiber along the equator β_c, we obtained

$$\sin\beta_c = \frac{R}{r_b(1+\delta_1)}\sin\alpha$$

where R is the radius of the ply along the equator.

Combining the obtained function with formula (4) we can find the sine of the angle at any point on the tire:

$$\sin\beta = \frac{r}{R}\sin\beta_c \qquad (5)$$

From this it follows that the angle of the cord fiber along the equator completely determines the entire geometry of the fibers in the tire and is therefore one of the most important construction characteristics.

The same position of the fibers in the finished tire can be obtained with various values of the angle of the cord fiber in the band α if

$$\frac{R}{r_b(1+\delta_1)}\sin\alpha$$

has a constant value.

Thus the choice of the angle in the band α and the radius of the band r_b with a constant ratio $\frac{\sin\alpha}{r_b}$ is determined not by construction but by technological considerations. The same applies to the coefficient of relative stretch of the fiber δ_1, whose value is determined in such a way that the cord fiber during vulcanization would be taut and not crooked. Choosing too great a value for the coefficient δ_1 usually leads to a stretching of the cord plies from the twists

(withdrawal), but it is also possible that there will be a certain increase in the strength of the overstretched fibers. Too small a value of δ_1 leads to the appearance of convolutions in the fibers in the finished tire. The necessary relative stretch of the fibers is attained by taking this problem into account when establishing the separation width of the assembly drum (cf. Ch. III, p. 33*). /50

Along with the formulas in (4) and (5), which determine the angle of the cord fibers to the meridian at each point, there is an important relationship which allows us to compute the frequency of the cord fibers in a ply and the length of the fibers.

The frequency of the fibers i means the number of fibers in a ply per unit length of a cross section perpendicular to the fibers. Usually, frequency is expressed in fibers per centimeter or fibers per decimeter.

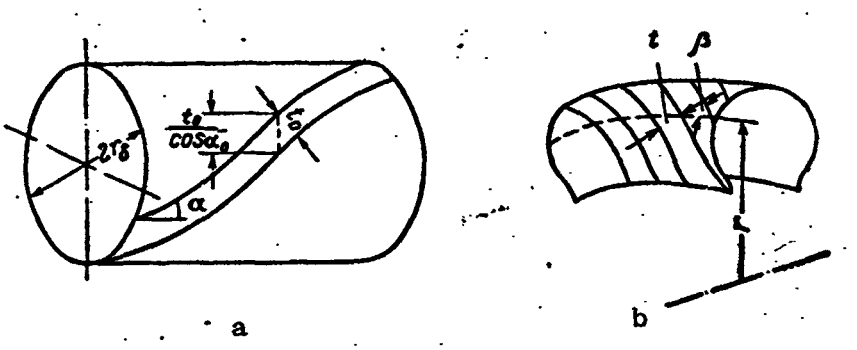

Fig. 45. Determination of the Frequency of Cord Fibers in the Tire: (a) Band; (b) Tire.

The frequency i is related to the fiber step t, i.e., to the distance between the axes of two adjacent fibers by the function

$$i=\frac{1}{t}.$$

The relationship between the frequency of rubberized cord in the band and its frequency in the finished tire can be found in the following way.

The total number of fibers in a cord ply (Fig. 45a) is equal to

$$\nu=2\pi r_b\frac{\cos\alpha}{t_0}$$

where $2\pi r_b$ is the circumference of the band and t_0 is the fiber step in the band. This number of fibers in the ply is also true, obviously, in the finished tire.

We will now examine a section of ply in a tire with circumference

*of previous translation

of radius r (Fig. 45b) and we will express the total number of fibers ν across their interval t:

$$\nu = 2\pi r \frac{\cos\beta}{t}$$

where β is the angle of the cord fiber with the meridian at a given point on the profile.

By comparing the obtained expression for ν, we can find the relationship between the fiber interval in the band and in the tire /51

$$t = t_0 \frac{r}{r_b} \cdot \frac{\cos\beta}{\cos\alpha}. \qquad (6)$$

Since the frequency of fibers is in the inverse of the interval then, respectively,

$$i = i_0 \frac{r_b}{r} \cdot \frac{\cos\alpha}{\cos\beta} \qquad (7)$$

where i is the frequency of fibers in the tire and i_0 is the frequency of fibers in the band.

In particular, we obtain for the frequency of cord fibers along the equator of the tire:

$$i_c = i_0 \frac{r_b}{R} \cdot \frac{\cos\alpha}{\cos\beta_c}$$

Deleting from the obtained formula and formula (7) the values referring to the band, we obtain

$$i = i_c \frac{R}{r} \cdot \frac{\cos\beta_c}{\cos\beta}$$

Substituting according to formula (5) $\frac{r}{R} = \frac{\sin\beta}{\sin\beta_c}$ we find

$$i = i_c \frac{\sin\beta_c}{\sin\beta} \cdot \frac{\cos\beta_c}{\cos\beta} = i_c \frac{\sin 2\beta_c}{\sin 2\beta}. \qquad (8)$$

Since for a given tire the frequency of cord along the equator i_c and the angle β_c are constant, then it follows from (8) that the frequency of cord fibers at an arbitrary point on the tire profile is inversely proportional to the sine of twice the angle of inclination of the fiber to the meridian at the same point. The value of sine 2β reaches a maximum, equal to unity, when $\beta = 45°$. Thus the lowest frequency of fibers corresponds to that point of the carcass at which the angle of inclination of the fibers is equal to 45°, in ordinary tires β_c is greater than 45° and the frequency increases both toward the bead of the tire and toward its equator. An approximate graph of the change in the cord frequency along the tire pro-

file is shown in Figure 46.

The length of cord fiber in the tire, for which it is necessary to compute specifications (cf. Ch. III, p. 31*) and to compute the configuration of the inflated tire, can be determined without difficulty if we know the tire profile and the angle of the cord fiber along the equator.

We can see from Figure 47 that the length dl of a unit section of fiber in the tire is related to the projection ds of this section on the profile (meridian) section by the function:

$$ds = dl\cos\beta$$

Consequently the length of the fiber l corresponding to an arbitrary section s of the tire profile is determined by the integral: /52

$$l = \int_s \frac{ds}{\cos\beta} \qquad (9)$$

As a rule integral (9) cannot be reduced to tabulated functions and must be computed by numerical integration.

One of these methods [12] involves the fact that the length of the profile is divided into small sections Δs, so that within each section the angle β may be assumed to be approximately constant. Then integral (9) can be replaced by the summation

$$l = \Sigma \frac{\Delta s_i}{\cos\beta_i} \qquad (10)$$

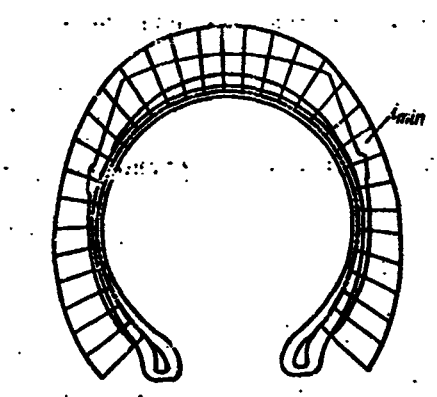

Fig. 46. Change in the Frequency of Fibers Along the Tire Profile.

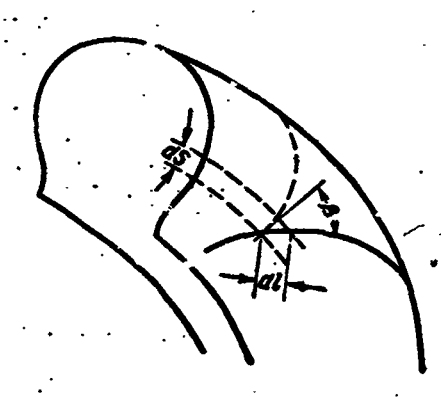

Fig. 47. Determination of the Length of Cord Fibers in a Ply.

*of previous translation

where the length of each section Δs_i is divided by the cosine of the angle of inclination to the meridian of the fiber at the midpoint of the same section.

If all sections Δs_i are chosen with identical lengths Δs, then

$$l = \Delta s \Sigma \frac{1}{\cos \beta_i}$$

where the angle β_i at the midpoint of each section is determined as a function of the distance from the axis of rotation according to formulas (4) or (5).

This method for computing the length of the fiber is used when, in addition to the total length of the fiber, we must determine the length of the fiber in each section Δs individually; for example, /53 when dealing with diagrams of the outer cover in the press (cf. Ch. III, p. 24). If it is necessary to determine only the total length of the fiber (for example when computing the configurations of the inflated tire; cf p. 80) then it would be better to use the Simpson parabola formula for our integration. As experiment will show in this case, to obtain high accuracy it is sufficient to divide the tire profile into only four different sections.

Examples of computing the length of cord fibers will be examined later.

Of significant interest is the change in thickness of the carcass in the outer cover during its preparation. This change is characterized by the ratio of the thickness of a ply of fiberized cord h_0 to the thickness h of the same ply in the finished outer cover. The ratio h/h_0 (called the molding coefficient) can be found approximately from the condition that the volume of the material is constant.

Let us now examine the volume of material of a section of the band in the limits of one interval of fibers t_0 per unit length of fiber dl_0:

$$dv_0 = h_0 t_0 dl_0$$

The volume of the same material in the outer cover is:

$$dv = h t dl$$

By setting $dv = dv_0$, we obtain

$$\frac{h}{h_0} = \frac{t_0}{t} \cdot \frac{dl_0}{dl}$$

Using formulas (1) and (6), we obtain finally:

$$\frac{h}{h_0} = \frac{r_0 \cos \alpha}{(1 + \varepsilon_y) r \cos \beta} \qquad (11)$$

Formula (11) is valid (a) if the crude rubber does not contain gases, and (b) for those zones of the outer cover where there is no intense overflow of rubber. The molding coefficient in the bead section of the outer cover where there is no intense overflow of rubber is determined according to experimental data.

/54

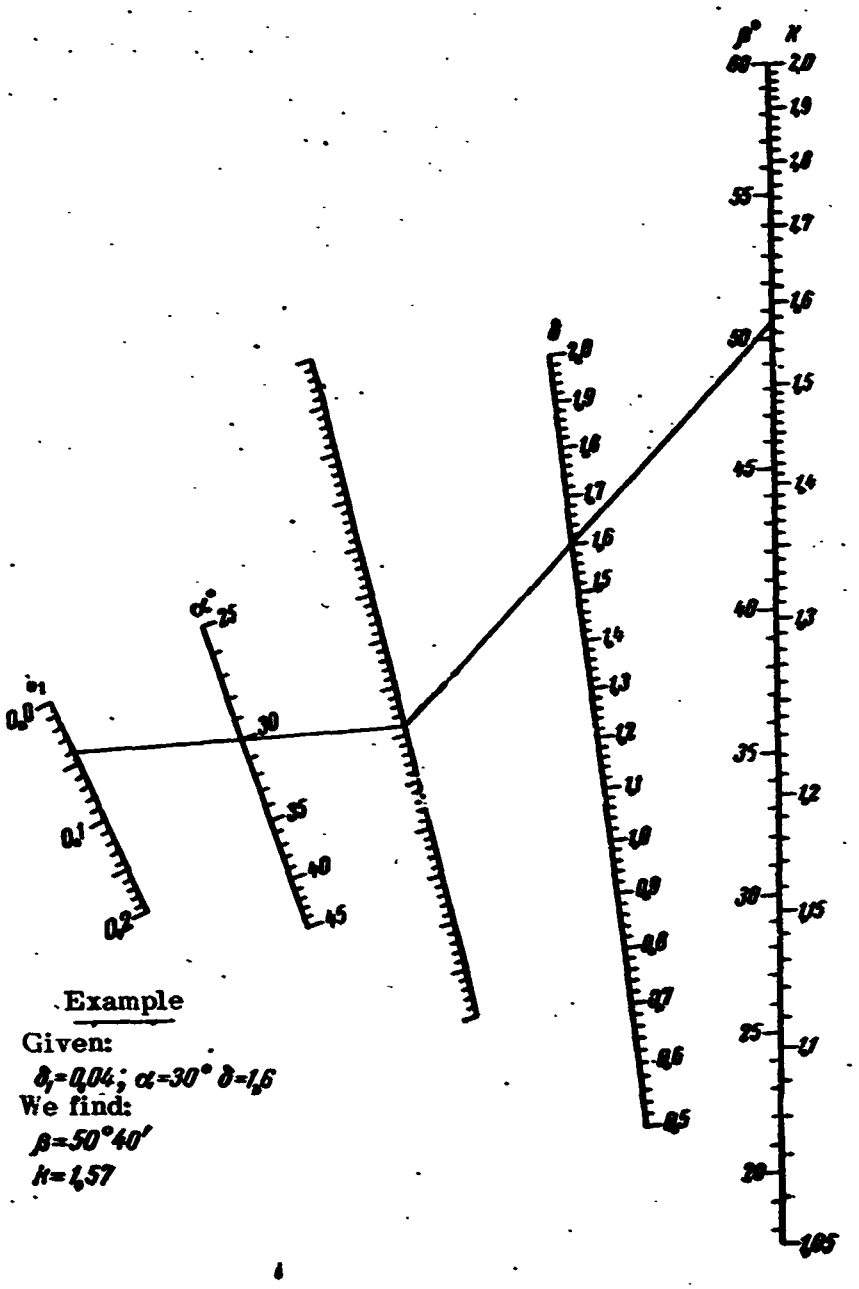

Fig. 48. The Nomogram for Calculating the Geometry of Cord Fibers in a Tire.

When calculating the geometry of cord fibers it is convenient to use the nomogram shown in Figure 48. For convenience in calculation this nomogram is also given in the Appendix. This nomogram [13] illustrates formula (4), which may also be written in the form

$$\sin\beta = \frac{\delta}{1+\delta_1}\sin\alpha \qquad (12)$$

where $\delta = \frac{r}{r_b}$ is the ratio of the distance of a given section from the axis of rotation in the tire to the radius of the band (this ratio is usually called the stretch). The nomogram allows us to de- /55
termine any of the values included in formula (12) if the remaining three values are known.

Since the value $k = \frac{1}{\cos\beta}$ (the value k is introduced to reduce the notation) which is necessary to compute the length of the fiber by formula (10) varies only with angle β; these values are placed on the β scale of the nomogram in the form of a functional scale.

We will now examine certain typical calculations using the nomogram.

The determination of the angle and frequency of cord fibers in the outer cover according to a prescribed cord angle (α), band length (l) [2], relative stretch of the fiber (δ_1) and frequency of cord fibers in the band (i_0).

(a) The stretch from the band to the given point of the ply in the outer cover should be determined as follows:

$$\delta = \frac{r}{r_b} = \frac{2\pi r}{l}$$

(b) Joining the corresponding points on the α scales and the δ_1 scales by a straight line, we obtain the intersection on the auxiliary (third) scale.

(c) Joining the obtained intersection with the value of δ on the fourth scale and extending the straight line, we find on the fifth scale the value of the unknown angle of cord fiber β in the outer cover and the value of the coefficient $k = \frac{1}{\cos\beta}$.

---

[2] For semiplane assembly the length of the first band is equal to the circumference of the assembly drum; for collapsible assembly the length of the band is determined by technological requirements. In order to guarantee that the band will cover the drum and at the same time have sufficient tension, the ratio of the circumference of the collapsible drum to the length of the first band must lie within the limits $\frac{\pi D_b}{l} = 1.06 - 1.12$.

(d) The frequency of cord fibers at a given point is determined by formula (7):

$$i = i_0 \frac{r_b}{r} \cdot \frac{\cos\alpha}{\cos\beta} = i_0 \frac{\cos\alpha}{\delta} k.$$

(e) The theoretical value of the molding coefficient of a ply at the same point can be determined by formula (11):

$$\frac{k}{k_0} = \frac{r_b \cos\alpha}{(1+\delta_1) r \cos\beta} = \frac{\cos\alpha}{(1+\delta_1)\delta} k.$$

A Numerical Example

Tc find the angle, frequency, and theoretical molding value of a rubberized cord along the equator of the outer cover, for which the following are given: the diameter of the outer cover along the first ply (along the equator) D_C = 955 mm; the cut angle $\alpha = 30°$; the band length l = 1880 mm; the relative fibe stretch $\delta_1 = 0.04$; the initial frequency of rubberized cord is 94 fibers/dm. /56

We compute:

$$\delta = \frac{\pi D_C}{l} = \frac{3{,}14 \cdot 955}{1880} = 1{,}60.$$

According to the nomogram (cf. the example in Fig. 48) we find the angle along the equator of the outer cover

$$\beta_C = 50°40'; \qquad k = \frac{1}{\cos\beta} = 1{,}57.$$

The frequency of cord fibers in the outer cover is:

$$i = i_0 \frac{\cos\alpha}{\delta} k = 94 \cdot \frac{\cos 30°}{1{,}60} \cdot 1{,}57 = 80 \text{ fibers/dm}.$$

The theoretical molding value of the ply is:

$$\frac{k}{k_0} = \frac{\cos\alpha}{(1+\delta_1)\delta} k = \frac{\cos 30°}{1{,}04 \cdot 1{,}60} \cdot 1{,}57 = 0{,}82.$$

Let us determine the cut angle with a given angle β_C of the cord along the equator of the outer cover and with a given relative stretch δ_1 of the fiber. With a given band length l we first compute the stretch:

$$\delta = \frac{\pi D_C}{l}.$$

Joining the point corresponding to the given angle β_C on the scale of the nomogram which is to the far right with the point on the δ scale, we obtain the intersection on the auxiliary scale. Now joining this intersection with the value of the relative stretch of the fiber δ_1 on the first scale, we find on the second scale the required value of the cut angle.

Determination of the angle of the cord fiber on the drum. For semiplane assembly the cord angle on the drum is equal to the cut angle, but for collapsible drum assembly they are somewhat different. The angle of cord fiber on the drum α_b for collapsible drum assembly can be found as a function of the cut angle or of the angle in the finished outer cover.

In the first case, since the cord fiber is not stretched when the band is fitted to the drum, we plot on the first scale the values of $\delta_1 = 0$, and on the second scale the cut angle. We join the intersection obtained on the auxiliary scale with the value $\delta = \frac{\pi D_b}{l}$, where D_b is the diameter of the drum, l is the length of the first band and we find on the scale to the far right the angle of the drum.

In the second case when the angle β_c is given in the finished outer cover we plot the value of this angle on the scale to the far right, and on the δ scale, we plot $\delta = \frac{D_c}{D_b}$, i.e., the stretch from the drum to the outer cover. Joining the intersection obtained on /57 the auxiliary scale with the value of δ_1 on the first scale we find the angle on the drum on the second scale.

Elastic Properties of an Element of Rubberized Cord Construction

The tire carcass which consists of criss-crossing plies of rubberized cord has unique mechanical characteristics.

This is explained by the sharp difference in rigidity between rubber and cord. Thus the elasticity modulus of rubber lies in the range of 10 - 80 kg/cm^2, while the longitudinal elasticity modulus of textile cord is 10,000 - 20,000 kg/cm^2 and the longitudinal elasticity modulus for metal cord is on the order of 10^6 kg/cm^2.

The mechanical properties of the tire wall depend to a great degree on the angle formed by the fibers of the intersecting plies of cord. A change in this angle leads to significant changes in the properties of the tire as a whole. Thus, for example, tires with radial cord fibers in the carcass (Type R, cf. Ch. IV) differ fundamentally in terms of their characteristics from ordinary tires. Therefore, a study of the mechanical properties of an element of rubberized cord construction is very important and provides the basis for the entire theory of pneumatic tires.

Let us now examine deformation of an element of the tire wall shown in Figure 49a in its own plane. In view of the high rigidity of cord fiber, deformations of the elements related to expansion of the fibers are difficult. In addition, deformations arising without a change in the length of the fibers and related only to a change in the angle of the rhombi formed by the fibers of adjacent plies (Fig. 49b) are comparatively easy.

Let us now examine in more detail this type of deformation of the element. Let a small rectangular element of the wall *ABCD* (Fig. 50) correspond to the rhombus *OMNP* formed by the fibers with a length of the side $OM = dl$. The sides of the rectangle are equal, respectively, to $ON = dx = 2dl \sin\beta$ and $MP = dy = 2dl \cos\beta$, where β is the angle formed by the cord fibers with the y axis. With deformations of the type we are considering the cord fibers, retaining their length, shift by an angle θ and after deformation form the angle $\beta + \theta$ with the y axis. In connection with this the dimensions of the rectangular elements also change and become equal to

$$dx_1 = ON_1 = 2dl \sin(\beta + \theta); \quad dy_1 = M_1P_1 = 2dl \cos(\beta + \theta).$$

Assuming the shift angle θ is small and assuming $\sin\theta = \theta$, $\cos\theta = 1$, we find

$$dx_1 = 2dl(\sin\beta\cos\theta + \cos\beta\sin\theta) \approx 2dl(\sin\beta + \theta\cos\beta)$$
$$dy_1 = 2dl(\cos\beta\cos\theta - \sin\beta\sin\theta) \approx 2dl(\cos\beta - \theta\sin\beta).$$

We may now compute the relative deformations of the element in the /58
x and y directions:

$$\left.\begin{aligned} \varepsilon_{0x} &= \frac{dx_1 - dx}{dx} = \frac{2dl(\sin\beta + \theta\cos\beta) - 2dl\sin\beta}{2dl\sin\beta} = \theta\cot\beta \\ \varepsilon_{0y} &= \frac{dy_1 - dy}{dy} = \frac{2dl(\cos\beta - \theta\sin\beta) - 2dl\cos\beta}{2dl\cos\beta} = -\theta\tan\beta \end{aligned}\right\} \qquad (13)$$

It follows from this that in the given deformation case ε_{0x} and ε_{0y} are not independent but are related by the equation

$$\varepsilon_{0x} = -\varepsilon_{0y}\cot^2\beta. \qquad (14)$$

Equation (14) is one of the conditions of nonexpandability of the cord fibers. On the other hand, it is clear from Figure 50 that the diagonals of the rhombus remain perpendicular to one another with deformation. Consequently the x and y axes are, in this case, the directions of the major deformations and there is no relative shift in these directions.

$$\gamma_{0xy} = 0.$$

This equation is the second condition of nonexpandability of the cord fibers.

Let us now calculate the potential energy stored by an element of the wall during a deformation of the type being examined. This energy is the sum of the deformation energy of the rubberized plies and the interlayers and the deformation energy of the rubber which fills the spaces between fibers in the cord plies. Since we assume

that the cord fibers themselves are not deformed, the energy is stored only in the rubber.

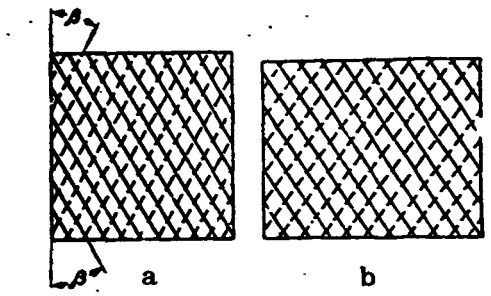

Fig. 49. Deformations of an Element of Rubberized Cord of the Tire Wall Without a Change in the Length of the Figers: (a) Element Before Deformation; (b) Element After Deformation.

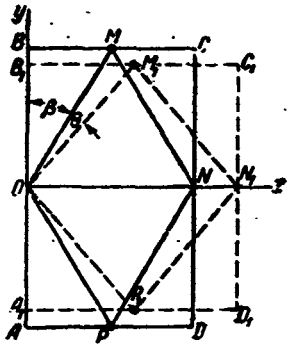

Fig. 50. Change in the Dimensions of the Rhombus Formed by the Cord Fibers While Retaining Their Length.

The deformation energy of the rubber interlayers which undergo /59 deformations of ε_{0x} and ε_{0y} relative to one square centimeter of the surface is determined by the expression [14]

$$W_p = 2G(h - nd)(\varepsilon_{0x}^2 + \varepsilon_{0y}^2 + \varepsilon_{0x}\varepsilon_{0y}) \qquad (15)$$

where G is the shift modulus of the rubber; h is the total thickness of the wall; n is the number of cord plies; d is the caliber of the cord fiber.

The value $(h - nd)$ is the total thickness of the rubber plies.

Formula (15) refers to that case where all the rubber interlayers have identical rigidity; in the opposite case, the product $G(h - nd)$ should be replaced by the summation $\Sigma G_i h_i$ of the products of the shift modulus of each rubber ply and its thickness.

Computing the deformation energies of rubber in the cord ply is a more complex process. This is related to the fact that between the fibers, rubber deformations are greater than in the rubber plies since they are constrained by undeformed fibers. As calculation shows [14], the deformation energy of rubber in the cord plies can be determined by a formula analogous to (15):

$$W_{rc} = 2GKnd(\varepsilon_{0x}^2 + \varepsilon_{0y}^2 + \varepsilon_{0x}\varepsilon_{0y}) \qquad (16)$$

where K is a correction factor depending on the ratio of the fiber diameter d to the fiber interval t:

$$K=\frac{t}{d}\left[\frac{2}{\sqrt{1-\left(\frac{d}{t}\right)^2}}\arctan\sqrt{\frac{t+d}{t-d}}-\frac{\pi}{2}\right]. \tag{17}$$

A graph of the relationship between the coefficient K and the ratio d/t is shown in Figure 51.

The total energy stored in one cm^2 of the tire walls during deformation without expansion of the fibers is equal to

$$W=W_p+W_{rc}=2Gh_{red}(\varepsilon_{0x}^2+\varepsilon_{0y}^2+\varepsilon_{0x}\varepsilon_{0y}) \tag{18}$$

where h_{red} denotes the value

$$h_{red}=h+nd(K-1) \tag{19}$$

which should be viewed as the reduced wall thickness.

The values of ε_{0x} and ε_{0y} in formula (18) are related by function (14) and are expressed by the shift angle θ based on (13).

Therefore the energy W may be expressed in terms of θ: /60

$$W_\theta=2Gh_{red}(\tan^2\beta+\cot^2\beta-1)\theta^2. \tag{20}$$

We will now examine deformations of an element of the tire wall related to a change in the length of the fibers without a change in the angle between the fibers.

Let us assume that fibers going in one direction (for example, fibers running from the left upwards to the right in Fig. 52) undergo an expansion ε_1, and fibers going in the opposite direction undergo an expansion ε_2. In this case the rhombus with side dl becomes a parallelogram with sides $dl(1+\varepsilon_1)$ and $dl(1+\varepsilon_2)$. Using simple geometric construction we can find the corresponding components of deformation along the x and y axes:

$$\left.\begin{aligned}\varepsilon_x'&=\frac{1}{2}(\varepsilon_1+\varepsilon_2)\\ \varepsilon_y'&=\frac{1}{2}(\varepsilon_1+\varepsilon_2)\\ \gamma_{xy}&=\frac{\varepsilon_1-\varepsilon_2}{\sin 2\beta}\end{aligned}\right\} \tag{21}$$

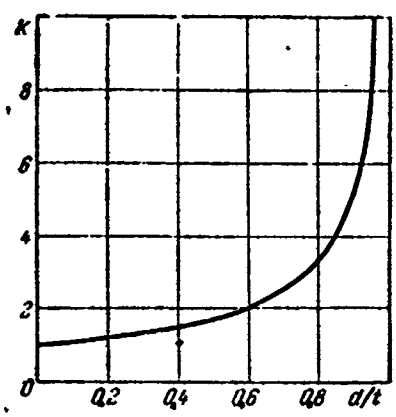

Fig. 51. The Relationships Between the Coefficient K and the Ratio d/t of the Cord Fiber Thickness to Their Interval.

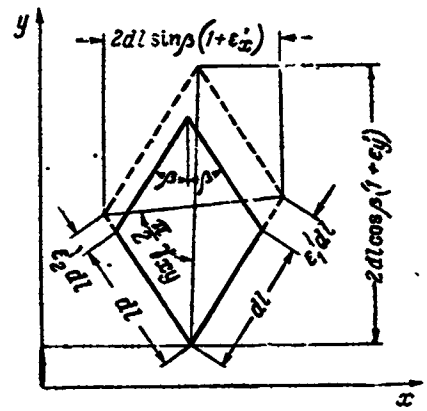

Fig. 52. Deformations of a Rhombus Element in Relation to Expansions of the Cord Fibers.

When computing the potential energy stored during this type of deformation we can ignore the energy of the rubber in comparison with the energy of the significantly more rigid cord fibers. Assuming that the stretch characteristic of the fiber is linear, so that the force /61 in the fiber is determined by the equation

$$N = E_C \varepsilon \tag{22}$$

where E_C [kg/fiber] is the "elasticity modulus" of the fiber, we arrive at the following expression for the deformation energy of the fibers:

$$W_1 = \frac{ni}{2} E_C \cdot \frac{1}{2}(\varepsilon_1^2 + \varepsilon_2^2) \tag{23}$$

where $ni/2$ is the total length of the fibers of each direction per unit area of the element; n is the total number of cord plies; i is the frequency of fibers in a ply.

If simultaneously there are deformations accompanied by a change in angles of the cord fibers and their stretching, then the total deformations along the x and y axes are:

$$\left.\begin{aligned} \varepsilon_x &= \varepsilon_{0x} + \varepsilon_{1x} = \delta\cot\beta + \frac{1}{2}(\varepsilon_1 + \varepsilon_2) \\ \varepsilon_y &= \varepsilon_{0y} + \varepsilon_{1y} = -\delta\tan\beta + \frac{1}{2}(\varepsilon_1 + \varepsilon_2) \\ \gamma_{xy} &= \frac{\varepsilon_1 - \varepsilon_2}{\sin 2\beta} \end{aligned}\right\} \tag{24}$$

Equation (24) may be solved relative to the deformations ε_1 and ε_2 and the fiber shift angle θ:

$$\left.\begin{aligned} \varepsilon_{1,2} &= \varepsilon_x \sin^2\beta + \varepsilon_y \cos^2\beta \pm \frac{1}{2}\gamma_{xy}\sin 2\beta \\ \theta &= \frac{1}{2}(\varepsilon_x - \varepsilon_y)\sin 2\beta \end{aligned}\right\} \qquad (25)$$

The total deformation energy W relative to a unit area of the element is equal to the sum of the energy of the rubber W_0 and the energy of the fiber W_1. Substituting for the corresponding expressions ε_1, ε_2 and θ their values according to (25), we find:

$$\begin{aligned} W = 2Gh_{red}(\sin^4\beta + \cos^4\beta - \sin^2\beta\cos^2\beta)(\varepsilon_x - \varepsilon_y)^2 + \\ + \frac{ni E_c}{2}[(\varepsilon_x \sin^2\beta + \varepsilon_y \cos^2\beta)^2 + \gamma_{xy}^2 \sin^2\beta\cos^2\beta]. \end{aligned} \qquad (26)$$

If we know the specific potential energy we can determine the mean values of the forces T_x, T_y and S_{xy} in the cross sections of the tire wall (Fig. 53). These forces can be determined as the partial derivatives of energy with respect to the corresponding deformations: /62

$$\left.\begin{aligned} T_x &= \frac{\partial W}{\partial \varepsilon_x} = 4Gh_{red}(\sin^4\beta + \cos^4\beta - \sin^2\beta\cos^2\beta)(\varepsilon_x - \varepsilon_y) + \\ &\quad + ni E_c(\varepsilon_x \sin^2\beta + \varepsilon_y \cos^2\beta)\sin^2\beta \\ T_y &= \frac{\partial W}{\partial \varepsilon_y} = 4Gh_{red}(\sin^4\beta + \cos^4\beta - \sin^2\beta\cos^2\beta)(\varepsilon_y - \varepsilon_x) + \\ &\quad + ni E_c(\varepsilon_x \sin^2\beta + \varepsilon_y \cos^2\beta)\cos^2\beta \\ S_{xy} &= ni E_c \sin^2\beta\cos^2\beta\gamma_{xy} \end{aligned}\right\} \qquad (27)$$

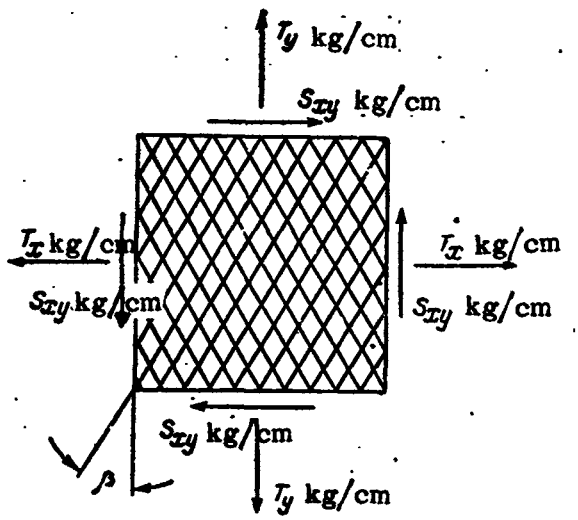

Fig. 53. The Intensity of the Internal Forces in a Cross Section of Rubberized Cord Constructic.

The validity of the obtained formulas can be established experimentally [14]. To do this we took two-ply rubberized cord layers prepared at various angles β, and we also cut samples at various angles ϕ (Fig. 54). These samples were tested for stretch and we established their pliability, i.e., the ratio of the relative expansion to the intensity of the stretching force. We can also compute pliability using the formulas in (27); to do this we must determine

the following forces as a function of the intensity of longitudinal load capacity of sample q:

$$T_x = q\cos^2\varphi;\quad T_y = q\sin^2\varphi;\quad S_{xy} = q\sin\varphi\cos\varphi.$$

Then according to (27) we can find deformations ε_x, ε_y and γ_{xy} and, finally, using the deformation theory [14] we can find longitudinal expansion of the sample. /63

The results of calculations (pliability as a function of the angle ϕ) for various angles β are shown in polar coordinates in Figure 55. In the same graphs we show the points obtained experimentally.

The curves of Figure 55 show that rubberized cord construction is sharply anisotropic; its pliability in different directions varies by a factor of 10. This is an established fact in all aspects of the behavior of pneumatic tires. Therefore, by varying the angle of the cord fibers we can significantly alter the properties of the tire.

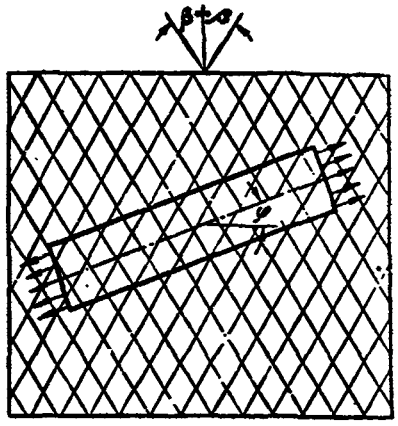

Fig. 54. A Sample Cut From a Two-Ply Rubberized Cord Layer.

Of great practical value are formulas for calculating rubberized cord grid constructions without taking into account those forces pertaining to the rubber.

Let us now examine an element of rubberized cord construction $\Delta x \times \Delta y$ (Fig. 56a). We will indicate the forces in the cord fibers running from the left upward to the right by N_1 and the forces in the fibers of intersecting plies by N_2. Then the total vertical force exerted on cross section Δx of the element, shown in Figure 56a, can be computed as

$$(N_1 + N_2)\cos\beta\Delta x\cos\beta\, i\frac{n}{2}$$

where $N_1\cos\beta$ and $N_2\cos\beta$ are projections on the vertical axis of force N_1 and N_2; $\Delta x\cos\beta\, i$ is the number of fibers of each ply, intersecting section Δx; $i = 1/t$ is the frequency of cord fibers in the ply; n is the total number of plies, $n/2$ is the number of cord plies in a given direction.

On the other hand, the same force may be expressed in terms of the force intensity T_y as the product $T_y\Delta x$ (Fig. 56b).

Comparing the two expressions for the same force we find

$$T_y = \frac{1}{2}ni(N_1 + N_2)\cos^2\beta. \qquad (28)$$

By an analogous method, examining the horizontal forces exerted /64
on cross section Δy, we obtain:

$$T_x = \frac{1}{2} ni (N_1 + N_2) \sin^2 \beta. \qquad (29)$$

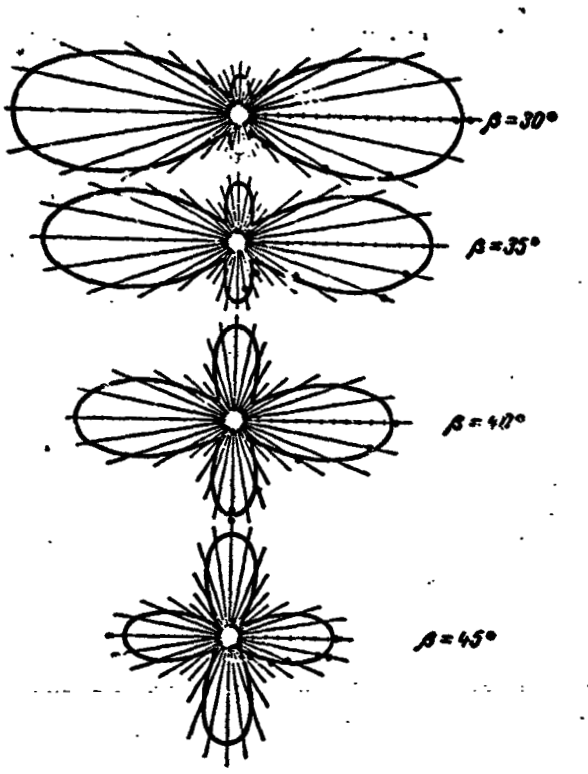

Fig. 55. The Pliability of Rubberized Cord Layer Samples Cut in Various Directions and Prepared at Various Angles β. The Solid Lines Indicate the Calculations; the Dots Indicate the Experiment.

The shift force S_{xy} is determined by the formula

$$S_{xy} = \frac{1}{2} ni (N_1 - N_2) \sin \beta \cos \beta. \qquad (30)$$

The functions (28) - (30) can also be obtained from the general formulas in (27) if we ignore those terms containing the factor Gh_{red} in comparison to those terms containing the factor niE_C [4], and if we bear

[4] In view of the high rigidity of fibers in comparison to the rubber Gh_{red} is usually 500 - 1000 times less than niE_C.

in mind that

/65

$$E_C(\varepsilon_x \sin^2\beta + \varepsilon_y \cos^2\beta + \gamma_{xy} \sin\beta\cos\beta) = E_C\varepsilon_1 = N_1$$
$$E_C(\varepsilon_x \sin^2\beta + \varepsilon_y \cos^2\beta - \gamma_{xy} \sin\beta\cos\beta) = E_C\varepsilon_2 = N_2.$$

We obtain from expressions (28) and (29) an important function relating the intensities of forces T_x and T_y in the case where we can ignore the tensions in the rubber:

$$T_x = T_y \tan^2\beta. \qquad (31)$$

Formula (31) is used to calculate the equilibrium configuration of the tire.

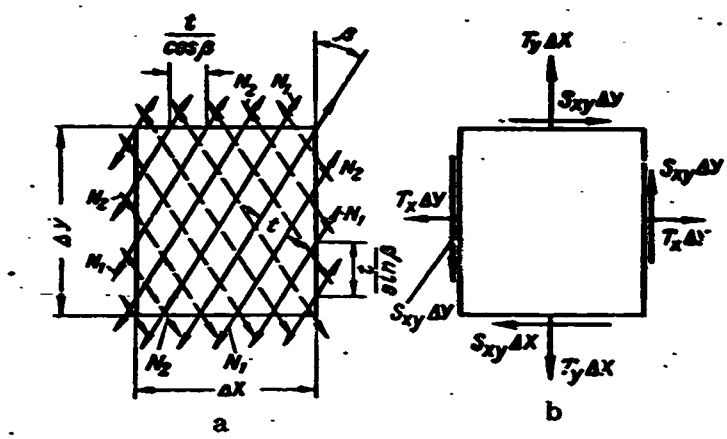

Fig. 56. The Determination of the Forces in Cross Sections of Rubberized Cord Construction.

Let us now examine curvature of rubberized cord wall of a tire. Due to the presence of comparatively rigid cord plies and soft rubber interlayers between them, the curvature of the wall is characterized by certain important properties, the most important of which are shift deformation in the interply rubber.

For a qualitative analysis of the operation of this construction, let us examine now, with curvature, its most simple variant (Fig. 57), i.e., a three-ply layer whose outer plies are made of significantly more rigid material than the inner ply. We will assume that the thickness of the external ply is small in comparison to the total thickness of the construction.

With cylindrical curvature of this layer the external plies will undergo stretch deformations (compression) and the internal layer

will undergo primarily shift deformations.

Now let us consider an element of length ds (Fig. 58a) cut from the layer. With cylindrical curvature of the layer, the normal to its median surface shifts by an angle ϕ, and the cross section of the layer shifts relative to the normal by a shift angle γ. In this case the upper external layer will undergo compression deformation equal to /66

$$\varepsilon = \frac{h}{2} \cdot \frac{d\gamma + d\gamma}{ds} \qquad (32)$$

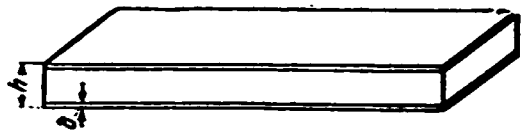

Fig. 57. A Three-Ply Layer Made of Materials of Varying Rigidity.

and the lower layer will undergo the same stretch deformation. In these plies forces arise whose intensities per unit width of the layer are equal to

$$P = E\delta\varepsilon$$

where E is the elasticity modulus of the material and δ is the thickness of the external plies.

These forces correspond to the moment (Fig. 58b)

$$M = Ph = \frac{E\delta h^2}{2}\left(\frac{d\gamma}{ds} + \frac{d\gamma}{ds}\right). \qquad (33)$$

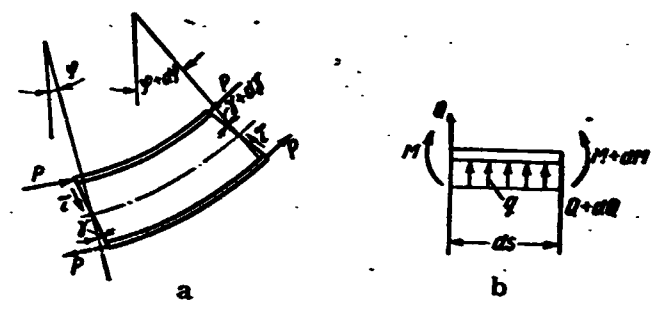

a b

Fig. 58. The Deformations of a Layer Element ds and the Forces Affecting It.

In the middle ply the tangential stress is equal to $\tau = G\gamma$, and the intensity of the lateral force Q is

$$Q = \tau h = Gh\gamma. \qquad (34)$$

Examining the equilibrium state of the element shown in Figure 58b, we obtain an equation of moments: /67

$$Q = \frac{dM}{ds} \tag{35}$$

and a projection equation:

$$\frac{dQ}{ds} = q. \tag{36}$$

Substituting the expressions for M and Q into the equilibrium equation (35) we find:

$$Gh\gamma = \frac{Eh^3}{2}\left(\frac{d^2\varphi}{ds^2} + \frac{d^2\gamma}{ds^2}\right). \tag{37}$$

On the other hand, with small deformations the rotation angle ϕ is related to the buckling of the layer v by the function

$$\varphi = \frac{dv}{ds}.$$

Let us now examine those stresses arising in the compound layer during deformation along a given surface.

Fig. 59. Deformations of the Layer When it is Compressed so that it Assumes the Form of a Wave Surface.

For example, let the layer be compressed so that it becomes a sinusoidal wave surface (Fig. 59), so that

$$v = A\cos\frac{\pi s}{l}$$

where l is the half-wavelength of the sinusoidal curve.

Then,

$$\varphi = \frac{dv}{ds} = -A\frac{\pi}{l}\sin\frac{\pi s}{l}$$

and (37) assumes the following form:

$$\frac{d^2\gamma}{ds^2} - k^2\gamma = -A\frac{\pi^2}{l^2}\sin\frac{\pi s}{l} \tag{38}$$

where

$$k^2 = \frac{Gk}{\frac{Eh^3}{2}}$$

is the ratio of shift rigidity to rigidity with ideal curvature.

The periodic solution to equation (38) has the form

$$\gamma = \frac{A\frac{\pi}{l}}{1+\frac{k^2l^2}{\pi^2}} \sin\frac{\pi s}{l}. \qquad (39)$$

/68

The obtained formula shows that with given deformations of the plate, the values of the shift deformation in the middle ply generally depend to a significant degree on the product k^2l^2 and decrease as this product increases.

According to (32) the deformations of the external layers of the plate are:

$$\varepsilon = \frac{h}{2}\left(\frac{d\varphi}{ds} + \frac{d\gamma}{ds}\right) = -A\frac{\pi^2}{l^2}\cdot\frac{h}{2}\cdot\frac{\frac{k^2l^2}{\pi^2}}{1+\frac{k^2l^2}{\pi^2}}\cos\frac{\pi s}{l}. \qquad (40)$$

The value

$$\frac{k^2l^2}{\pi^2} = \frac{Gh}{E\delta}\cdot\frac{2l^2}{\pi^2h^2}$$

included in (39) and (40) is dimensionless; it varies with the relationship between the elasticity of the middle and outer plies of the layer and with the ratio of the half-wavelength of the sinusoidal curve to the thickness of the layer. If these ratios are small (soft middle layer and short wavelengths), the second term in the elemental formula (39) will be small in comparison with unity and with $\gamma \approx -\phi$.

In this case, during curvature the cross sections of the layer remain vertical, the external plies do not undergo longitudinal deformation ($\varepsilon = 0$) and the curvature is brought about only by a shift in the middle ply.

As the value of $\frac{k^2l^2}{\pi^2}$ increases (a rigid middle ply), deformations in the uppermost and lowermost plies increase and shift deformation in the middle ply decreases. In this case the layer will be curved in the same way as a uniform layer.

Figure 60 shows the relationships between the maximum shift and stretch deformations and the value of $\frac{k^2l^2}{\pi^2}$. Along the horizontal axis we have plotted the value of $\frac{k^2l^2}{\pi^2}$, and along the vertical axis the values of $\frac{\gamma}{\gamma_0}$ and $\frac{\varepsilon}{\varepsilon_0}$, where $\gamma_0 = \frac{A\pi}{l}$ is the maximum possible shift with a pliable middle ply; $\varepsilon_0 = A\frac{\pi^2}{l^2}\cdot\frac{h}{2}$ is the linear deformation with a rigid middle ply, when the law of plane cross sections holds.

We can see from these formulas that despite the fact that the /69
bucklings of the layer are generally prescribed, shift deformations in the middle ply and linear deformations in the uppermost and lowermost plies depend to a significant degree on the relationship between the elastic characteristics and the geometric dimensions of the plies, as well as on the relationship between the half wavelength of deformation l and the layer thickness h.

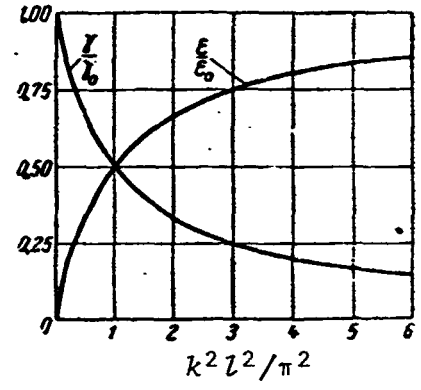

Fig. 60. The Relationship Between the Maximum Shift and Stretch Deformations and the Value of $\frac{k^2l^2}{\pi^2} = \frac{2}{\pi^2}\frac{G}{E}\frac{l^2}{\delta h}$.

The conclusions we obtained for the simplest three-ply layer are also valid for multi-ply constructions of the same type, if we mean by k^2 the ratio of the rigidity to shift of this construction to the rigidity to curvature:

$$k^2 = \frac{C_{\text{shift}}}{C_{\text{curv}}}.$$

For example, let us examine a band of unit width cut from the wall of a tire in two cross sections running along the fibers (Fig. 61a). The lateral cross section of this band (Fig. 61b) will be perpendicular to the fibers of even or odd cord plies; the fibers of other plies will be approximately parallel to this cross section.

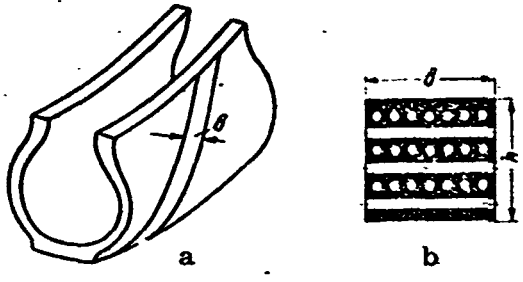

Fig. 61. A Band Cut From a Tire Carcass Along the Direction of the Fibers (a), and a Lateral Cross Section of This Band (b).

The rigidity of this band during shift can be found approximately by the formula

$$C_{\text{shift}} = Gh\frac{h}{h-nd}$$

where G is the shift modulus of the rubber; h is the cord carcass thickness; d is the fiber thickness; n /70
is the number of cord plies. The factor $\frac{h}{h-nd}$ accounts for the increase in rigidity to shift due to the presence of cord.

The rigidity during curvature is determined by the formula

$$C_{\text{curv}} = E_C\Sigma iy^2$$

where E_C is the modulus of the cord fibers; Σiy^2 is the sum of products of the frequencies of ply fibers contained in that cross section[5]

[5] i.e., only even or only odd plys.

and the squares of their distances from a neutral axis.

With a sufficiently large number of plies we find approximately that

$$C_{curv} \approx \frac{E_C n i h^3}{24}$$

where i is the mean frequency of fibers.

We can estimate the order of magnitude of C_{shift} and C_{curv} and the coefficient k^2 for heavy-duty automotive tires.

Let us assume that the number of plies is n = 8, the fiber frequency is i = 8 fibers/cm, the thickness of the fiber is d = 0.8 mm, the cord is rayon with a modulus E_C = 100 kg/fiber, the carcass thickness is h = 12 mm, the shift modulus of the rubber is G = 10 kg/cm^2.

We now obtain:

$$C_{shift} = Gh\frac{h}{h-nd} = 10 \cdot 1{,}2 \cdot \frac{1{,}2}{1{,}2 - 8 \cdot 0{,}09} = 30 \text{ kg/cm}$$

$$C_{shift} = E_C \Sigma i y^2 = 100 \cdot 8 \cdot 2 (0{,}15^2 + 0{,}45^2) = 360 \text{ kg} \cdot \text{cm}$$

where 0.15 cm and 0.45 cm are the distances of the plies from the neutral axis.

According to the approximate formula we obtain

$$C_{curv} = \frac{E_C n i h^3}{24} = \frac{100 \cdot 8 \cdot 8 \cdot 1{,}2^3}{24} = 385 \text{ kg} \cdot \text{cm}$$

Thus, for an eight-ply carcass the approximate formula is sufficiently accurate.

For the coefficient k^2 we find:

$$k^2 = \frac{C_{shift}}{C_{curv}} = \frac{30}{360} = 0{,}083 \frac{1}{cm^2}.$$

If the half-wavelength of these formations is l = 10 cm, which corresponds, for example, to the curvature of the rolling part of a tire on cobblestones, then the value of $\frac{k^2 l^2}{\pi^2}$ is 0.85.

We can see from Figure 60 that in this case shift deformations are very substantial and linear deformation comprises less than half of that deformation which would arise in a uniform band if the law of plane cross section held. /71

An analogous calculation for four-ply passenger car tires shows that the value of k^2 is approximately 4-5 times greater than that for

heavy duty tires. In this case the role of shift deformations between plies is negligible.

This investigation of the curvature of multi-ply construction made of various materials allows us to determine the relationship between the stresses arising from rubber and cord of the tire and the properties of these materials and the construction parameters.

The results of this investigation will be used later in our examination of the operating regimes of tire materials.

INTERNAL PRESSURIZATION

The Equilibrium Configuration of a Tire

The determination of the forces arising in a tire carcass under the action of internal pressure has been a subject of much research.

A tire was examined as a torus-shaped rotation shell with a thin wall, and the intensities of the forces in circumferential and radial directions were determined. However, the obtained mean values of the forces in the cross section did not allow us to determine the forces in the cord fibers.

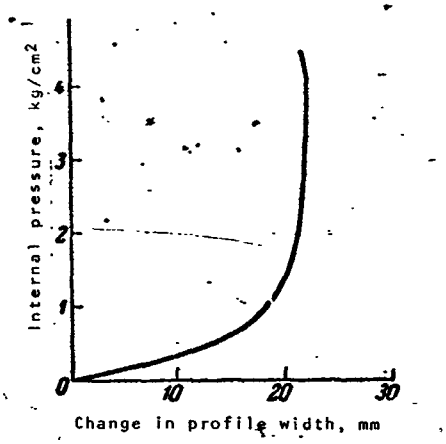

Fig. 62. The Decrease in the Profile of a 9.00-20 Tire as a Function of Internal Pressure.

The references we have cited did not take into account the basic anisotropic properties of a tire carcass made of comparatively rigid cord fibers and elastic rubber. These properties, which we have already examined in detail, provide the unique behavior of a tire when it is pressurized.

By observing the change in the dimensions of a tire when it is inflated, we can establish that at first the dimensions change substantially; then, after pressure has reached a low value (on the order of 0.5-1 kg/cm^2), the change in dimensions decelerates. This can be seen, for example, in Figure 62 which shows the change in profile width of a 9.00-20 tire as a function of internal pressure.

This phenomenon can be explained by the fact that at low pressure, due to deformations related to a change in the angles between cord fibers, the tire carcass takes a shape in which the forces are exerted only on the fibers. Subsequent change in the shape of the tire takes place due to changes in the length of the fibers and, in view of the rigidity of the latter, is more difficult.

The carcass configuration in which the load from internal pressure is absorbed only by the forces in the fibers (equilibrium configuration) can be computed theoretically.[6] The solution to this problem is examined in detail in reference [13].

We assume that the cord fibers are nonexpandable and that the forces in the rubber are small in comparison to the forces in the fibers.

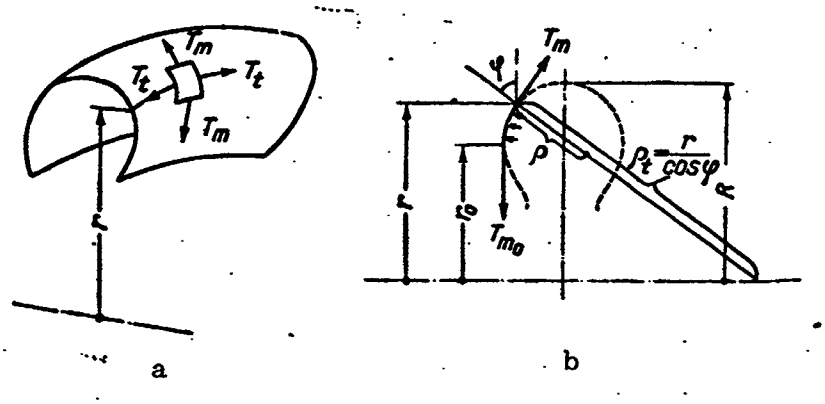

Fig. 63. The Derivation of the Equilibrium Equation: (a) For an Infinitely Small Element of the Wall; (b) For a Finite Part of the Shell.

In this case the forces in the fibers and the average intensities of the forces in the wall of the tire will be related by the formulas in (28)-(31).

Viewing the tire as a thin walled shell with internal pressure p, we can find from the equilibrium conditions the intensities of forces in its wall. Thus, the equilibrium conditions of an infinitely small element shown in Figure 63a leads to the known Laplace equation:

$$\frac{T_m}{\rho} + \frac{T_t}{\rho_t} = p \qquad (41)$$

where T_m and T_t are the intensities of the radial and circumferential forces (i.e., forces acting on a unit length of the cross section); ρ is the radius of curvature of the profile at the examined point; $\rho_t = \frac{r}{\cos\phi}$ is the radius of curvature of a cross section normal to the meridian; r is the distance of the point from the axis of rotation of the tire; ϕ is the angle formed between the normal to the surface and the axis of symmetry of the profile. /73

[6] The equilibrium configuration corresponds to the maximum possible internal volume of a tire with a given cord fiber length [14].

The equilibrium conditions of the shell part defined by the cylindrical surface with radius r_0 and a conical surface passing through the given point normally to the meridian (Fig. 63b) has the following form:

$$T_m \cdot 2\pi r \cos\varphi = p\pi (r^2 - r_0^2). \tag{42}$$

The radius r_0 is the distance from the axis of rotation of the tire to the place on the profile where the width is the lowest, and where the normal to it is parallel to the axis of rotation.

As we have already shown, in addition to the equilibrium equations (41) and (42), equation (31) expressing the hypothesis that only cord fibers absorb the load also holds. In this case the equation has the form

$$\frac{T_t}{T_m} = \tan^2\beta \tag{43}$$

where β is the angle formed by the cord fiber with the meridian.

Excluding from (41), (42) and (43) the forces T_m and T_t, we arrive at the relationship

$$\frac{1}{\rho} + \frac{\tan^2\beta\cos\varphi}{r} = \frac{2r\cos\varphi}{r^2 - r_0^2} \tag{44}$$

which includes only geometric parameters. Equation (44) also determines the equilibrium configuration of the tire profile.

Considering that the angle β of the cord fiber with the meridian at any point on the tire is related to the angle along the equator β_c by equation (5) and that

$$\frac{1}{\rho} = -\frac{d\varphi}{dr}\sin\varphi$$

we can reduce (44) to the following form:

$$\frac{1}{\cos\varphi}\cdot\frac{d}{dr}(\cos\varphi) = \frac{2r}{r^2 - r_0^2} - \frac{r}{\frac{R^2}{\sin^2\beta_{c1}} - r^2}.$$

Integrating the attained differential equation and determining the integration constant given that $r = R$ and $\phi = 0$, we obtain:

$$\cos\varphi = \frac{(r^2 - r_0^2)\sqrt{1 - \frac{\sin^2\beta_{c1}}{R^2}r^2}}{(R^2 - r_0^2)\cos\beta_{c1}} = \frac{(r^2 - r_0^2)\cos\beta}{(R^2 - r_0^2)\cos\beta_{c1}}. \tag{45}$$

Equation (45) determines the angle formed by the normal to the /74

profile and the axis symmetry of the latter as a function of the distance between the points on the profile and the axis of rotation.

By graphic integration according to expression (45) we can construct an equilibrium tire profile if we know the parameters R, r_0 and β_c.[7]

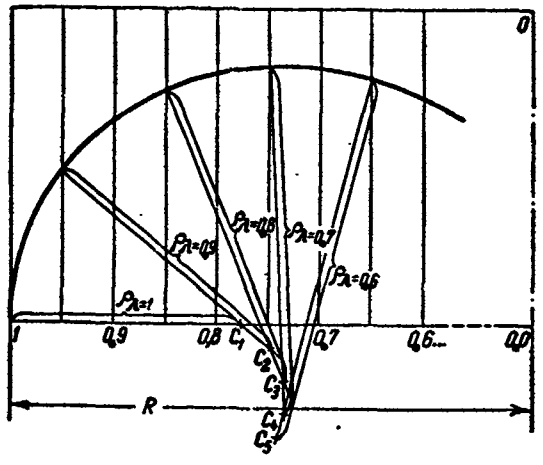

Fig. 64. Construction of the Equilibrium Tire Profile Using Circular Arcs.

However, it is more convenient for our purposes to use the values for the radius of profile curvature ρ, which we can obtain by substituting expression (45) into formula (44):

$$\rho = R\frac{1-\lambda_0^2}{\lambda}\cdot\frac{\cos\beta_c\sqrt{1-\lambda^2\sin^2\beta_c}}{2-(3\lambda^2-\lambda_0^2)\sin^2\beta_c} \qquad (46)$$

where

$$\lambda = \frac{r}{R}; \qquad \lambda_0 = \frac{r_0}{R}.$$

From (46) we can construct an equilibrium profile for the tire by replacing it at each small section by an arc of radius ρ calculated for the midpoint of the section (Fig. 64).

The equilbrium profiles thus constructed are given in the Appendix for a number of angles along the equator β_c in the form of nomograms.

In each of the nomograms compiled for a particular angle along the equator β_c, we have constructed a number of equilibrium profiles corresponding to various values of the parameter $\lambda_0 = \frac{r_0}{R}$. In addition, the nomograms show a curve corresponding to constant ratios $\frac{L}{R}$, where L is the length of a section of cord fiber in the tire from the equator to the given point. /75

Using these nomograms we can solve the following problems:

(1) Determining the profile of an inflated outer cover with a given external diameter mounted on a particular type of rim.

(2) Finding the dimensions of the rim on which an outer cover

---

[7] An analytic determination of the profile shape can be made only by numerical methods, since the corresponding integrals cannot be reduced to tabulated functions.

with a particular outer diameter must be mounted so that its profile will have a particular width.

(3) According to a given rim dimension and outer cover profile width, constructing a profile and determining the external diameter of the inflated tire.

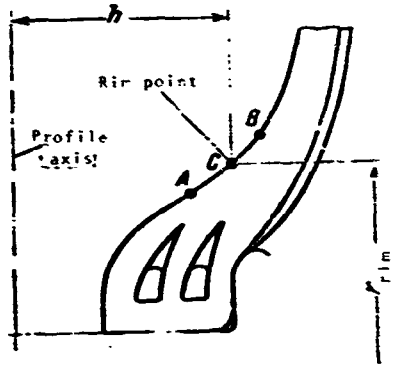

Fig. 65.

When solving these problems we should bear in mind that we have calculated the dimensions along the internal contour of the outer cover carcass.[8] To obtain the external dimensions of the outer cover we should add to these dimensions the carcass thickness and, respectively, the thickness of the tread or the sidewall of the outer cover.

As the point at which outer cover profile is attached to the rim (in short, the rim point) let us take a certain point on the internal contour of the carcass *C* located near the rim edge (Fig. 65). We assume that outside this point on the rim the tire is freely deformed and will take an equilibrium shape, and the tire bead inside this point will not be deformed at all. The choice of the position of this point on the rim is to a certain degree arbitrary. Thus, for example, in Figure 65 we could take as the rim point any point on segment *AB*.

We can determine the profile of an outer cover mounted on a given rim with a known external diameter in the following way.

First of all we should find the radius *R* of the carcass of the outer cover along the equator. To do this we subtract from its external radius the thickness of the tread, breaker and carcass. Then, depicting the outer cover bead in our diagram of the rim (cf. Fig. 65) we determine r_{rim}, which is the distance between the point at which the profile of the outer cover is attached to the rim and the axis of rotation. We then determine the scale of the unknown profile on the nomogram (Fig. 66) which is equal to the ratio of the actual radius *R* to the radius of the equator *AO* on the nomogram

/76

$$m = \frac{R}{AO}.$$

The nomogram shows the point at which the profile is attached to the rim *C* in terms of the known dimension r_{rim} and the distance of

[8] Using the midline of the carcass for our calculations is more justifiable, but calculation along the internal contour is, practically speaking, much more convenient and, as practice will show, provides a sufficient degree of accuracy.

this point h from the axis of symmetry of the profile. To do this we plot on the nomogram the segments $OD = \frac{r_{rim}}{m}$ and $DC = \frac{h}{m}$.

If one of the curves of the nomogram passes through point C, then this curve also expresses the internal contour of the carcass of the outer cover (in the m scale). In the opposite case we can resort to interpolation between the two curves lying closest to point C (line ABD in Fig. 66).

The width of the equilibrium tire profile along the internal contour of the carcass is determined by multiplying twice the dimension of BE, taken from the nomogram, by the m scale.

In order to find the overall width of the profile we must add to the attained dimension twice the thickness of the carcass and the sidewall.

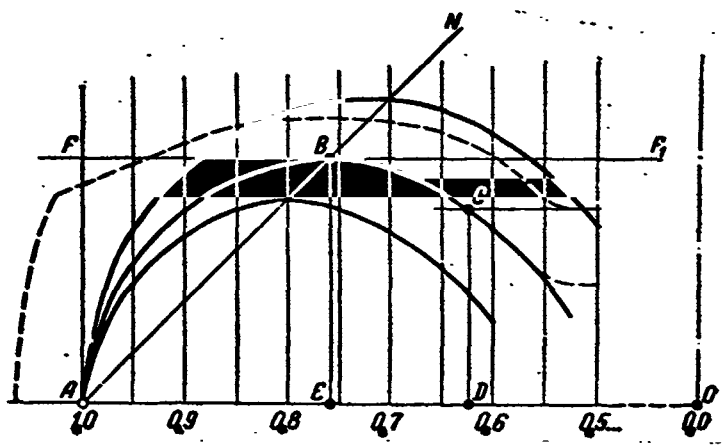

Fig. 66. Determining the Diameter of a Tire of Given Width Mounted on a Given Rim.

To solve the second problem (determining the dimensions of the rim on which a tire with given dimensions must be mounted) we use the following method. We should determine according to a given R the nomogram m scale and plot on it the line FF_1 at a distance AF equal to the halfwidth of the profile of the outer cover along the internal contour of the carcass divided by the m scale (Fig. 66). The profile of the outer cover is represented on the nomogram by that curve which is tangent to FF_1. If none of the curves is tangent to the line we can turn to interpolation. Interpolation is easier since the highest points of several adjacent curves on the nomogram lie roughly in one straight line (AN). /77

Any point C on curve ABC can now be used for the point at which the outer cover profile is joined to the rim. Thus according to a given rim diameter we can find the necessary width or vice versa given the width we can find the diameter.

The third of these problems which we can solve using the nomograms (the construction of the profile from a given rim dimension and profile width) is different, since in this case the nomogram scale is not known beforehand, since the radius of the equator R

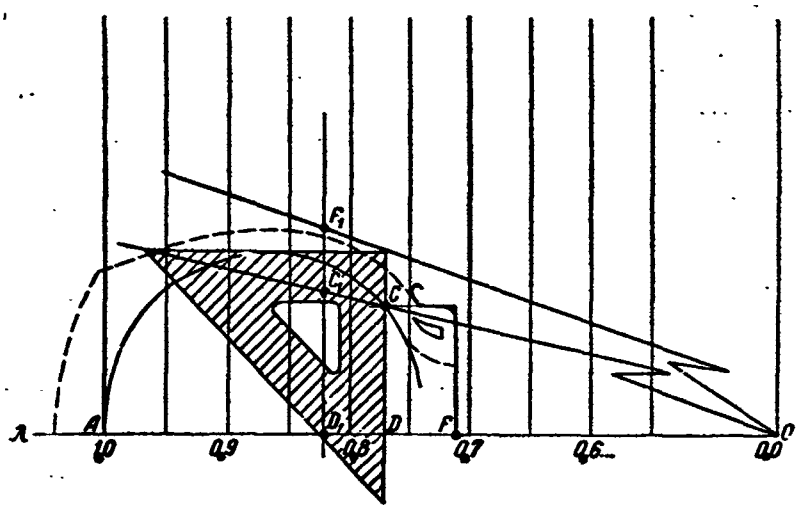

Fig. 67. Determining the Diameter of a Tire of Given Width Mounted on a Given Rim.

requires determination. The solution to this problem for this case is given in Figure 67. We plot on the λ axis from point O an arbitrary scale r_{rim}; i.e., the distance of the rim point to the axis of rotation (OD_1 in Fig. 67). On the perpendicular drawn from point D_1 we plot in the same scale the distance of the rim point from the axis of symmetry of the profile (D_1C_1) and half the profile width along the internal contour E_1F_1. We now draw rays from point O through points C_1 and F_1. If having made a right triangle we now shift it so that the vertex of the right angle always remains on ray OF_1 and one of the legs is parallel to the horizontal axis, then the unknown profile is determined by that position of the triangle in /78
which one of its legs is tangent to the curve and the other passes through point C of the intersection of this curve with ray OC_1. The scale in which the unknown profile is represented in the nomogram is determined by dividing the distance h from the axis of symmetry of the profile to the rim point by the length of segment DC on the nomogram of $m = \frac{h}{DC}$. The radius R of the equator of the internal contour of the carcass is determined by multiplying the dimension OA of the nomogram by the m scale.

The nomograms we have examined allow us to solve a number of problems related to the projection of a tire having given dimensions after inflation. However these nomograms are inconvenient for determining the dimension of an inflated tire as a function of the dimensions of the vulcanization mold. In this case, a calculation can be made only by several trial calculations. The nomograms do not allow us to estimate the change in tire dimensions related to cord fiber expension by internal pressure.

The reason for these difficulties is that the nomograms were constructed for particular values of the cord fiber angles β_c along the equator of the outer cover, while when the tire is inflated the value of this angle changes.

The enumerated problems can be solved if we use nomograms in which the initial parameters are those tire dimensions which do not change when the tire is inflated or whose change is known. These dimensions are the length of the cord fiber in the tire from the rim point to the equator, the values r_{rim} and h which determine the position of the rim point and the angle of α_{rim} of the cord fiber with the meridian at the rim point.

The new nomograms in which the initial parameters are the enumerated values can be obtained by constructing nomograms of equilibrium profile.

Given the value of the angle α_{rim}, we can find the corresponding vertical lines on the nomogram. Actually, distance between this line and the axis of rotation of the tire can be determined easily according to the formula:

$$r_{rim} = \frac{\sin \alpha_{rim}}{\sin \beta_c} R$$

where β_c is the angle along the equator for which the nomogram was constructed. The construction is shown in Figure 68. For intersection points of a given vertical with the lines of the nomogram we determine the distance from the axis of symmetry h, the half-width of corresponding profile b, the ratio $\frac{r_0}{R} = \lambda_0$ and the fiber length L from the equator to the rim point.

The obtained values of $\frac{L}{r_{rim}}$; $\frac{h}{r_{rim}}$ are plotted on the coordinate axis (Fig. 69), while each of the intersection points of the vertical $\beta = \alpha_{rim}$ with the profiles (cf. Fig. 68) correspond to a particular point in the coordinate $\frac{L}{r_{rim}}$; $\frac{h}{r_{rim}}$. /79

Joining these points we obtain in these coordinates a curve corresponding to a given cord angle at the rim point and a given angle along the crown β_c.

On this curve we can note points corresponding to particular values of $\frac{b}{r_{rim}}$ and λ_0.

Repeating this construction for various angles along the equator β_c (using different nomograms), we obtain in the coordinates $\frac{L}{r_{rim}}$; $\frac{h}{r_{rim}}$, a series of curves for a given angle α_{rim} and various values of β_c.

Joining on these curves points with identical values of $\frac{b}{r_{rim}}$ and λ_0, we obtain two more series of curves (cf. Fig. 69). Thus we have obtained the reconstructed nomograms shown in the Appendix.

In the following sections we will examine the application of these nomograms to the solution of a number of practical problems. /80

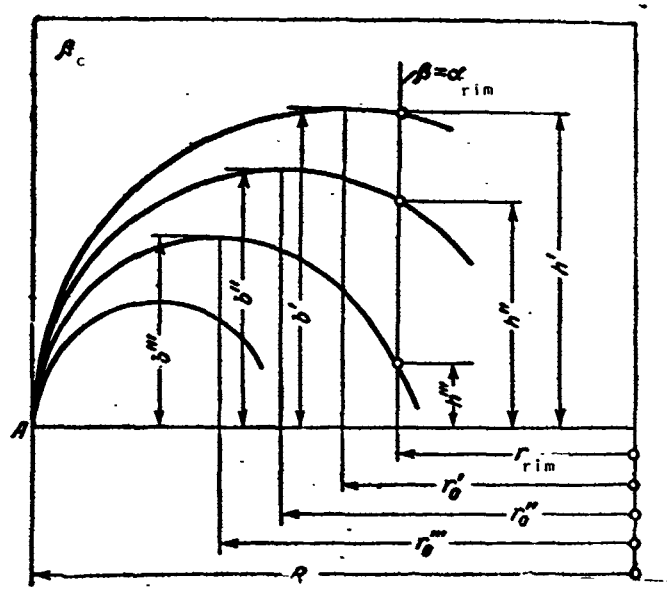

Fig. 68. Determination of the Characteristic Dimensions of Equilibrium Profiles Having a Given Cord Fiber Angle on the Equator and at the Rim Point.

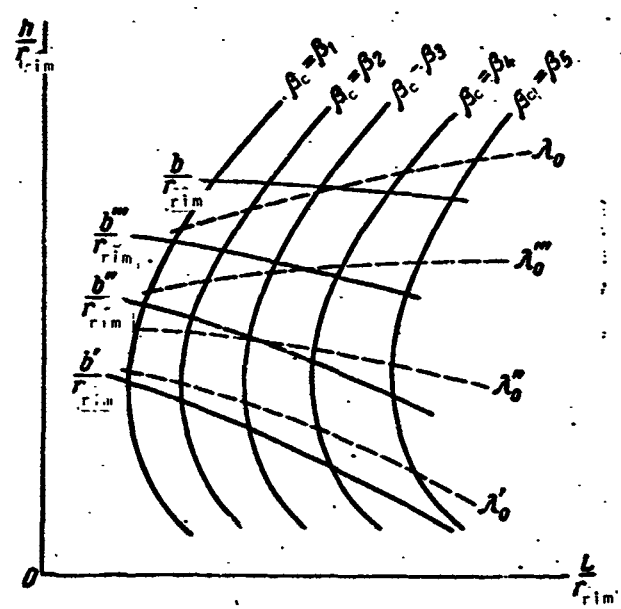

Fig. 69. The Construction of Nomograms for a Given Value of the Cord Fiber Angle at the Rim Point.

Determination of the Equilibrium Configuration of a Tire According to a Known Profile of the Vulcanization Mold.

If we are given the outer cover profile in the vulcanization mold and if we know the cord fiber angle in the mold along the equator β'_c, then we can determine the equilibrium configuration of the tire in the following ways.

(1) On the internal contour of the carcass we choose a point on the rim so that the cord angle at this point is equal to one of the angles α_{rim} for which we have constructed a nomogram. The distance of this rim point from the axis of rotation is determined according to the formula

$$r_{rim} = R' \frac{\sin \alpha_{rim}}{\sin \beta'_c}$$

where R' is the radius of the equator along the internal contour of the carcass of the outer cover in the vulcanization mold. From all the values of α_{rim} for which we have constructed nomograms we choose the one for which the rim point falls in the segment AB (cf. Fig. 65) of the internal contour of the carcass.

(2) We determine the length of the cord fiber from the equator to the rim point in the tire found in the vulcanization mold: /81

$$L = \int_s \frac{ds}{\cos \beta}$$

while we use for integration one of the approximate methods (cf. the calculation example).

(3) For a given value of α_{rim} we plot on the nomogram (Fig. 69) points corresponding to the ratio $\frac{L}{r_{rim}}$ (plotted along the abscissa) and to the ratio $\frac{h}{r_{rim}}$ (plotted along the ordinate).

The value of h is the distance of the rim point from the axis of symmetry of profile when the outer cover is mounted on the corresponding rim.

(4) For the obtained point on the nomogram we determine: the angle along the equator of the inflated outer cover β_c, the ratio $\frac{b}{r_{rim}}$ and λ_0.

In the case where the points on the nomogram do not lie on the curves, the corresponding values can be determined by interpolation.

(5) We determine the radius R of the inflated outer cover along the internal contour of the carcass along the equator:

$$R = R' \frac{\sin \beta_c}{\sin \beta_c'}. \tag{47}$$

Since the angles β_c and β_c' are usually close to one another, instead of formula (47) it is more convenient to use the formula

$$R = R' + R' \cot \beta_c' \frac{\beta_c - \beta_c'}{57.3} \tag{48}$$

where the angles are expressed in degrees.

It is clear from (48) that the increase in the radius of the outer cover when it is inflated in comparison to the dimension along the vulcanization mold is:

$$\Delta R = R' \cot \beta_c' \frac{\beta_c - \beta_c'}{57.3}. \tag{49}$$

If the angle in the inflated outer cover β_c is found to be greater than the cord angle along the equator of the outer cover in the vulcanization mold, then ΔR is positive and the outer cover increases in diameter due to internal pressure. In the opposite case the outer cover shrinks.

(6) We determine the width $2b$ of the outer cover profile along the internal contour:

$$2b = 2r_{rim}\left(\frac{b}{r_{rim}}\right).$$

(7) We determine the distance from the axis of rotation to the widest point on the profile of the inflated outer cover: /82

$$r_0 = \lambda_0 R_0$$

(8) We determine the external dimensions of the deflated tire (Fig. 70).

The external diameter is:

$$D = D' + 2\Delta R$$

where D' is the external diameter of the outer covering along the mold, and ΔR is determined by formula (49).

The width of the profile is:

$$B = 2b + 2t$$

where t is the thickness of the wall of the outer cover along the sidewall.

The obtained dimensions fully define the dimensions of the outer cover. They also allow us to determine the forces in the cord fibers arising under the effect of internal pressure. The calculation will be valid if cord fiber expansion due to internal pressure differs little from elastic expansion when the outer cover is in the vulcanization mold. In practice, this condition holds under normal internal pressure for tires made of cotton or viscose cord.

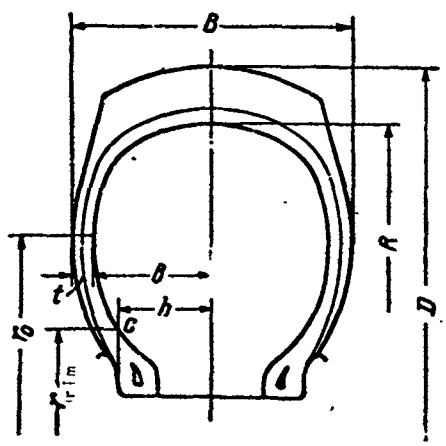

Fig. 70. Determining the Dimensions of the Inflated Tire.

As experience from using this method in tire industry shows, the calculated width of the inflated tire corresponds to reality with an accuracy of 2-3 mm, and the calculated change in the tire diameter when it is inflated is somewhat greater than the actual change. An important factor in this case is the significant rigidity of the rubber in the tread part of the tire, which prevents attaining equilibrium configuration. In the vulcanization process for tires made of polyamide cord, the elastic elongations of the cord fibers are completely relaxed and when the tire is inflated the length of the fibers increases in comparison to the length of the fibers in the vulcanization mold.

Therefore, to determine the dimensions of outer covers made of polyamide cord and also to determine the dimensions of outer covers at the moment of blowout by hydrostatic pressure we must take into account cord fiber expansion. Methods for taking these expansions into account are examined below. /83

Determining Forces in the Cord Fibers

Using the results obtained in the section "Rubberized Cord Grid Constructions and Their Properties", we can determine the forces arising in tire elements by action of internal pressure.

By substituting the value cos ϕ according to formula (45) into equation (42) we can find the intensity of the meridian force:

$$T_m = \frac{p(R^2 - r_1^2)\cos\beta_{c1}}{2r\cos\beta}. \qquad (50)$$

On the other hand, the intensity of the force T_m is related to the forces in the cord fibers by (28). Taking into account that with action of internal pressure the cord fibers of even and odd plies undergo identical stresses ($N_1 = N_2 = N$), we may write formula (28) in the form

$$T_m = Nni\cos^2\beta$$

and from this we can find the force in the cord fibers

$$N = \frac{p(R^2 - r_0^2)\cos\beta_c}{2rni\cos^2\beta}$$

where the fiber frequency i and the fiber angle β are taken at the point at a distance r from the axis of rotation at which the force is calculated. Replacing i according to formula (8):

$$i = i_c \frac{R}{r} \cdot \frac{\cos\beta_c}{\cos\beta}$$

we obtain:

$$N = p\frac{R^2 - r_0^2}{2Rni_c} \cdot \frac{1}{\cos^3\beta}. \qquad (51)$$

Formula (51) determines the force in the cord fibers at an arbitrary point on the profile. We include in this formula the dimensions R, r_0 of the equilibrium configuration of the tire which we computed by methods shown above.

The value ni_c is the product of the cord fiber frequency along the equator and the number of plies.

If the densities of the various plies are different, then this product must be replaced by the summation of the cord fiber frequencies in all plies along the equator Σi_c. In this case /84

$$N = p\frac{R^2 - r_0^2}{2R\Sigma i_c} \cdot \frac{1}{\cos^3\beta}. \qquad (52)$$

For tires without fabric breakers the number of plies is identical at any point on the profile. In this case all values included in (52) except the factor $\frac{1}{\cos^2\beta}$ will be constant and the force in the fibers will vary with this factor. It reaches the maximum at the points of the equator of the outer cover while

$$N_{max} = p\frac{R^2 - r_0^2}{2R\Sigma i_c} \cdot \frac{1}{\cos^3\beta_c} \qquad (53)$$

and decreases toward the beads. A diagram of the change in forces in the fiber along the profile of the outer cover is shown in Figure 71a.

When using formula (52) to calculate an outer cover with a fabric breaker we should take the summation of the fiber frequencies of all plies including the breaker when calculating the stresses from the equator to the end of the breaker, and the sum of frequencies of the basic plies of the carcass when calculating stresses at the remaining points of profile.

In this case the diagram of the change in forces in the fibers along the profile of the outer cover will have the form shown in Figure 71b. The maximum forces will exist either along the equator (they are determined by (53) while in the expression Σi_c the breaker is also taken into account) or at the point where the breaker ends (the calculation is made according to (52) into which we have substituted the value of the cord angle at the corresponding point and the summation of fiber frequencies along the equator of only the basic plies). /85

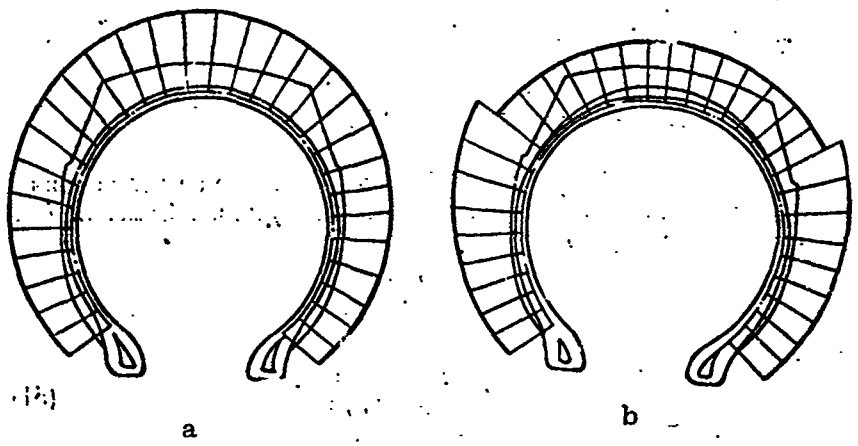

Fig. 71. The Change in Forces in the Cord Fiber Along the Profile of the Tire. (a) Without Cord Breaker; (b) With Cord Breaker.

The value of the force in the fibers for the point where the breaker ends is significant only when calculating the hydrostatic pressure which causes blowout; with a calculation made in order to choose the necessary number of cord plies, we should use only the force along the equator determined according to formula (53).

The ratio of the static blowout force for the cord fiber N_{blo} to the force N_{max} arising in the fibers with normal pressure is usually called the safety factor. We should note that this ratio $\frac{N_{blo}}{N_{max}}$ is not, strictly speaking, the safety factor since pressurization never puts the tire out of service during usage.

This ratio should be viewed as a coefficient characterizing the similarity between tires (cf. p. 148). With projection of new tires the number of cord plies is chosen so that the ratio $\frac{N_{blo}}{N_{max}}$ lies within particular practically determined limits (cf. Ch. III, p. 20).

Forces in the Bead Rings

Forces are transmitted from the cord plies of the carcass to the bead rings. We can show that in the absence of friction between

the bead and the rim edge, the intensity of the meridian force in the carcass near the bead ring is determined from formula (50), in which β denotes the angle of cord fiber with the meridian on a circle of radius $r = r_c$ (Fig. 72a). Thus, by examining the equilibrium of the half-ring (Fig. 72b), we find that the force in the bead is:

$$P_0 = T_m r_c = p \frac{R^2 - r_c^2}{2\cos\beta_c} \cos\beta_c. \qquad (54)$$

This formula determines the force in the bead without taking into account forces arising due to tightness on the rim or friction between the rim and the bead.

Friction somewhat decreases the force in the bead.[9] This decrease can be calculated from the formula

$$\Delta P = kp \frac{r_0^2 - r_c^2}{2}$$

where k = 0.2-0.4 is the coefficient of friction. However, when making calculations for the bead rings we should ignore the value ΔP /86 since when the tire is rolling, due to small shifts in the bead part of the tire, the friction forces decrease and the load on the rings increases.

Additional forces arise when the tire is mounted on the rim and the rings are tightened. With a high degree of tightness these forces can be very significant. In the case of improper construction, these forces may cause the beads to break when the tire is mounted.

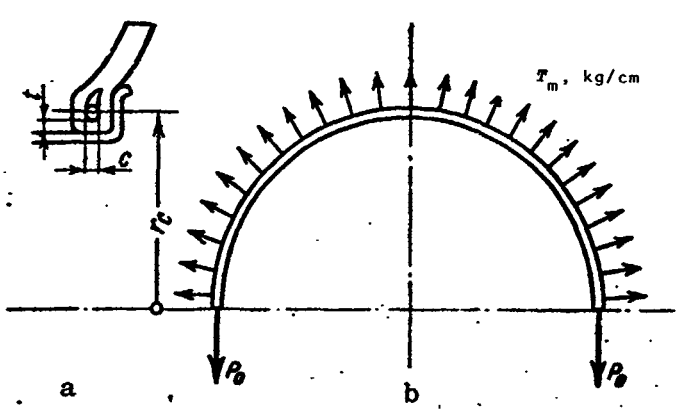

Fig. 72. Determining the Forces in the Bead Rings: (a) Tire Bead; (b) Equilibrium of the Half-ring.

We will now examine those forces arising in the bead when the tire is mounted on the rim and tightened. In the mounted and inflated tire, forces act on the bead along the entire circumference in the carcass with intensity T_m, determined by formula (50), and the pressure from the rim q (in kg/cm^2), which we will consider to be distributed along the base of the bead on the width of the ring.

If we ignore rim defor-

[9] The influence of friction explains the discrepancy between the calculated forces in the rings and the forces measured experimentally [15].

mations, then under the action of forces T_m and q the external diameter of the tire varies with the value of tension δ.[10] The change in the internal diameter is related to the stretch Δr_c of the wire ring with compression Δt of the material under the ring.

$$\delta = 2\Delta r_c + 2\Delta t. \tag{55}$$

The total force stretching the ring is:

$$P = P_0 + qbr_c \tag{56}$$

where P_0 is the force in the ring caused by cord fiber tension which is determined according to formula (54). /87

The change in the ring radius in relation to its stretch can be found from the formula

$$\Delta r_c = \frac{P}{EF} r_c$$

where F is the total cross sectional area of the wires in the ring and E is their elasticity modulus.

The change in the thickness of the material under the ring can be determined according to the formula

$$\Delta t = \frac{qt}{E_1}.$$

where t is the thickness of the material under the bead, E_1 is the mean compression modulus of this material.

Substituting the values Δr_c and Δt into (55), we find the pressure intensity of the tire on the bead seat:

$$q = \frac{E_1}{t}\left(\frac{\delta}{2} - \Delta r_c\right) = \frac{E_1}{t}\left(\frac{\delta}{2} - \frac{P}{EF} r_c\right).$$

Substituting this value into formula (56) we obtain:

$$P = P_0 + \frac{E_1 b r_c}{t}\left(\frac{\delta}{2} - \frac{P}{EF} r_c\right)$$

from which the total force in the bead is:

---

[10] δ means the difference between the rim diameter and the internal diameter of the outer cover under the ring in the vulcanization mold at the corresponding point.

$$P=\frac{P_0+\frac{E_1 b r_c}{2t}\delta}{1+\frac{E_1 b r_c^2}{Eft}}.$$

As calculations show, the value $\frac{E_1 b r_c^2}{Ert}$ is usually small in comparison to unity, and within a certain margin of error the force in the bead can be approximately computed using the more simple formula:

$$P=P_0+\frac{E_1 b r_c}{2t}\delta. \qquad (57)$$

The mean elasticity modulus of the material under the bead E_1 varies with the rigidity of the rubber and cord, the ratio of the total thickness t to the total thickness of the cord plies under the ring and with the ratio $\frac{b}{t}$.

The value of E_1 increases as the ratio $\frac{b}{t}$ increases and the rubber content decreases.

We can determine the value of E_1 experimentally by compressing /88
a layer of material cut from under the ring. We may take the tentative value

$$E_1=300\text{--}500\ \text{kg/cm}^2.$$

After the force in the bead P is determined according to (57) we can find the stress in the wire according to the formula

$$\sigma=\frac{P}{n_1 f} \qquad (58)$$

where n_1 is the number of wires in the bead[11] and f is the cross sectional area of one ring in mm^2.

The safety factor k_s of the wire is defined as the ratio

$$k_s=\frac{\sigma_u}{\sigma}$$

where σ_u is the ultimate strength of the wire when it is broken.

The recommended values for the safety factor are shown in Chapter III, p. 21.

---

[11] We usually introduce into our calculation the number of revolutions of the wire strip reduced to unity in order to account for weakening of the rings due to bonding.

Determining the Configuration of the Inflated Tire and the Forces in Its Elements Taking into Account Cord Fiber Expansion

The above-mentioned methods for calculating the dimensions of the inflated tire according to the configuration of the vulcanization mold are based on the hypothesis that the cord fibers undergo identical expansion during vulcanization and inflation.

As we have already shown, these methods are sufficiently accurate to determine the dimensions of outer covers made of cotton or viscose cord under normal pressure.

To calculate the dimensions of these outer covers when they are inflated with hydrostatic pressure to the blowout point, and also to calculate outer covers made of polyamide cord, we must take cord fiber expansion into account.

The change in the force along the length of the cord fiber is determined according to formula (52) and shown graphically in Figure 71 (p. 74). If we know this stress we can determine the corresponding expansion according to the characteristics of cord stretch.

Since the force is unevenly distributed along the length of the fibers, the deformation of the fibers is also different at different points. It is at a maximum along the equator and decreases with distance from the equator; at the point where the breaker ends, deformations increase and then gradually decrease toward the bead.

If fiber expansion were uniform, then for our calculations we could use the method proposed above; we would only have to take into account that the length of the fibers in the inflated outer cover is greater than in an outer cover located in the vulcanization mold and that the angle at the rim point is smaller in relation to the value of fiber expansion. /89

The fact that the expansion value is variable along the length of the fiber drastically complicates the problems.

However, considering that fiber expansions exert little influence on the shape of the outer cover, we may use an approximate method to determine this influence.

We assume that deformation is constant and corresponds to a force averaged along the length of the fiber:

$$\overline{N} = \frac{1}{L}\int_{L} N dl$$

where we integrate along the length of the fiber from the rim to the

equator, and $L=\int_s \frac{ds}{\cos\beta}$ is the length of the cord fiber. Substituting into the formula for the mean force of the values $N = N_{max} \frac{\cos^2\beta_c}{\cos^2\beta}$ [cf. formulas (51) and (52)] and changing to integration along the profile $s(dl = \frac{ds}{\cos\beta})$, we obtain

$$\bar{N}_s = N_{max} \frac{\cos^2\beta_c}{L} \int_s \frac{ds}{\cos^3\beta} \qquad (59)$$

where N_{max} is the force in the fiber along the equator and the integral is taken along the profile of the outer cover from the rim point to the equator. Formula (59) holds if the outer cover does not have a cord breaker. In the presence of the latter we should use the formula

$$N = N_{max} \frac{\cos^2\beta_c}{L} \left[\frac{\Sigma i_c}{\Sigma i'_c} \int_s \frac{ds}{\cos^3\beta} - \frac{\Sigma i_c - \Sigma i'_c}{\Sigma i'_c} \int_{s_1} \frac{ds}{\cos^3\beta} \right] \qquad (59a)$$

where $\Sigma i'_c$ is the summation of cord fiber frequencies along the equator of only the basic plies of the carcass and Σi_c is the summation including the breaker; the first integral in brackets is taken along the entire contour of the carcass from the equator to the rim point and the second is taken along the sub-breaker part of the carcass.

After we compute the mean force $\bar{N}$ according to (59) we can determine the corresponding relative expansion according to the characteristics of fiber stretch. The stretch characteristics of certain cords are shown in Figure 73.

The length of the fiber from the rim point to the equator in the inflated tire is taken to be equal to /90

$$L_1 = L(1+\bar{\varepsilon})$$

where L is the length of the fiber without taking expansion into account.

The cord fiber angle at the rim point of an inflated tire is found from the equation

$$\sin\alpha_{rim.1} = \frac{\sin\alpha_{rim}}{1+\bar{\varepsilon}}$$

where α_{rim_1} is the angle at the same point computed without taking into account fiber expansion.

If the value of α_{rim_1} is found to be such that there is no nomogram for it, then the rim point shifts somewhat so that α_{rim_1} is equal to 26°, 28°, 30° etc.

When calculating $\overline{N}$ and $\overline{\varepsilon}$, formula (59) should include the force N_{max} determined for the equilibrium configuration of a tire without taking into account cord fiber expansion. If the configuration taking into account fiber expansion differs significantly from its configuration without considering this expansion, then the value of the force in the fibers must be determined more accurately and the calculation must be repeated (practically speaking, there is usually no need to repeat such a calculation). To calculate the hydrostatic pressure necessary to cause a tire blowout we must first determine its configuration at the blowout point. In this case, when calculating the mean expansion the maximum force (along the equator or at the point where the breaker ends) is assumed to be equal to the blowout force for the cord fiber.

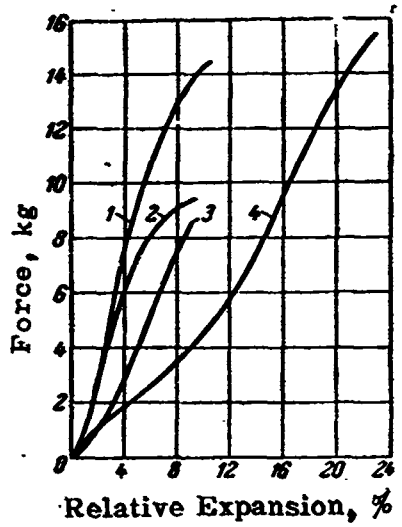

Fig. 73. Stretch Characteristics of Tire Cords: (1) Cord 14V; (2) 10V; (3) 9T; (4) 14K.

After determining the tire configuration taking into account fiber expansion we can compute the forces in its elements. In this case we should substitute all dimensions for an inflated tire into the respective formulas.

Numerical Example

Determine the dimensions of an inflated 9.00-20 outer cover on 9T cord with a cord angle along the equator of 52° (in the vulcanization mold).

Determine the forces in the cord fibers and in the bead rings.

Find the value of the hydrostatic pressure necessary to cause tire blowout. /91

The tire profile along the vulcanization mold is shown in Figure 74; the external diameter is 1022 mm. The tire diameter along the internal contour $2R' = 953$ mm.

Choose a rim point. As a preliminary point let us take point A in Figure 74 located at a distance of 312 mm from the axis of rotation. The sine of the cord fiber angle at this point is equal to

$$\sin\beta_A = \frac{r_A}{R'}\sin\beta_c = \frac{312 \cdot 0{,}787}{476{,}5} = 0{,}515$$

from which we find that $\beta_A = 31°$.

Since there is no nomogram for this value of the angle at the rim point, then as a calculated angle let us take $\alpha_{rim} = 30°$.

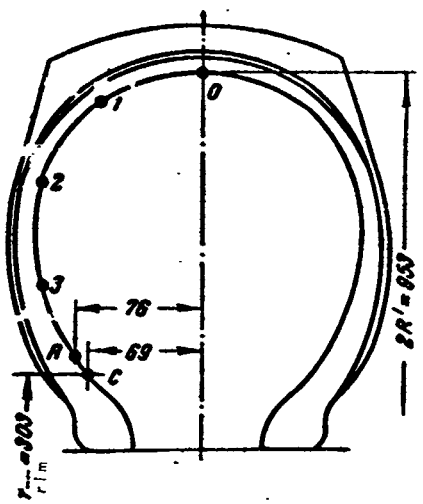

Fig. 74. The Profile of a 9.00-20 Outer Cover.

Find the distance of the rim point from the axis of rotation:

$$r_{rim} = \frac{\sin\alpha_{rim}}{\sin\beta_c}R' = \frac{\sin 30°}{\sin 52°} \cdot 476{,}5 = 303 \text{ mm}.$$

Find the rim point on the diagram of the tire profile (point C in Fig. 74).

Measure the distance of the rim point from the axis of symmetry of the profile: h = 69 mm.

Determine the length of the cord fiber from the rim point to the equator according to the formula

$$L = \int \frac{ds}{\cos\beta}$$

using the Simpson formula with four intervals.

To do this after establishing the measurement on a span of 10 mm, measure the contour length from the equator to the rim point. We obtain s = 240 mm.

Plot on the diagram those points corresponding to the division of the arc into four equal sections with Δs = 60 mm (points 1, 2 and 3 in Fig. 74). Measure the distance of each point of the division from the axis of rotation and determine for each point the value $\frac{1}{\cos\beta_i}$, taking into account that $\sin\beta_1 = \frac{r_i}{R}\sin\beta_c$.

When calculating $\frac{1}{\cos\beta}$ it is convenient to use the nomogram (Fig. 48) described earlier (cf. p. 44). To do this compute the ratio δ of the distance of each point from the axis of rotation to a certain arbitrary value R_0 (taken to equal R_0 = 300 mm). Then join the value of the cord angle along the equator $\beta_c = 52°$ on the extreme right scale of the nomogram to the value δ = 1.59 for the equator, taken on the second scale from the right, and obtain the intersection on the auxiliary scale. Passing straight lines through this intersection and the values of δ for each point, obtain on the far right scale

/92

the respective values of $k_i = \frac{1}{\cos\beta_i}$. These values are given in Table 1. In this table we show the values $k_i^3 = \frac{1}{\cos^3\beta_i}$, necessary to take into account cord fiber expansion.

TABLE 1. DETERMINATION OF CORD FIBER LENGTH

Point	r, mm	$\delta = \frac{r}{300}$	$k_i = \frac{1}{\cos\beta_i}$	$k_i^3 = \frac{1}{\cos^3\beta_i}$
Equator	476.5	1.59	1.62	4.25
1	461	1.54	1.55	3.74
2	416	1.39	1.38	2.63
3	356	1.19	1.24	1.90
Rim Point C	303	1.01	1.16	1.56

The fiber length is determined according to the Simpson formula:

$$L = \frac{\Delta s}{3}(k_c + 4k_1 + 2k_2 + 4k_3 + k_{rim} =$$

$$= \frac{60}{3}(1.62 + 4 \cdot 1.55 + 2 \cdot 1.38 + 4 \cdot 1.24 + 1.16) = 334 \text{ mm}.$$

Compute the ratios:

$$\frac{L}{r_{rim}} = \frac{334}{303} = 1.10; \quad \frac{b}{r_{rim}} = \frac{69}{303} = 0.228.$$

Plot the corresponding points on the nomogram of the equilibrium configuration for $\alpha_{rim} = 30°$ (Fig. 75, point A).

Find on the nomogram by interpolation the values of the cord angle for this point along the equator in the inflated outer cover, the value of $\frac{b}{r_{rim}}$ and λ_0:

$$\beta_c = 51.2°; \quad \frac{b}{r_{rim}} = 0.356; \quad \lambda_0 = 0.796.$$

Determine the dimensions of the inflated outer cover:
the change in radius of the equator is

$$\Delta R = R' \cot\beta_c' \frac{\beta_c - \beta_c'}{57.3} = 476.5 \cot 52° \frac{51.2 - 52}{57.3} = -5.2 \text{ mm};$$

the radius of the equator along the internal contour of the carcass is

$$R = R' + \Delta R = 476.5 - 5.2 = 471.3 \text{ mm}$$

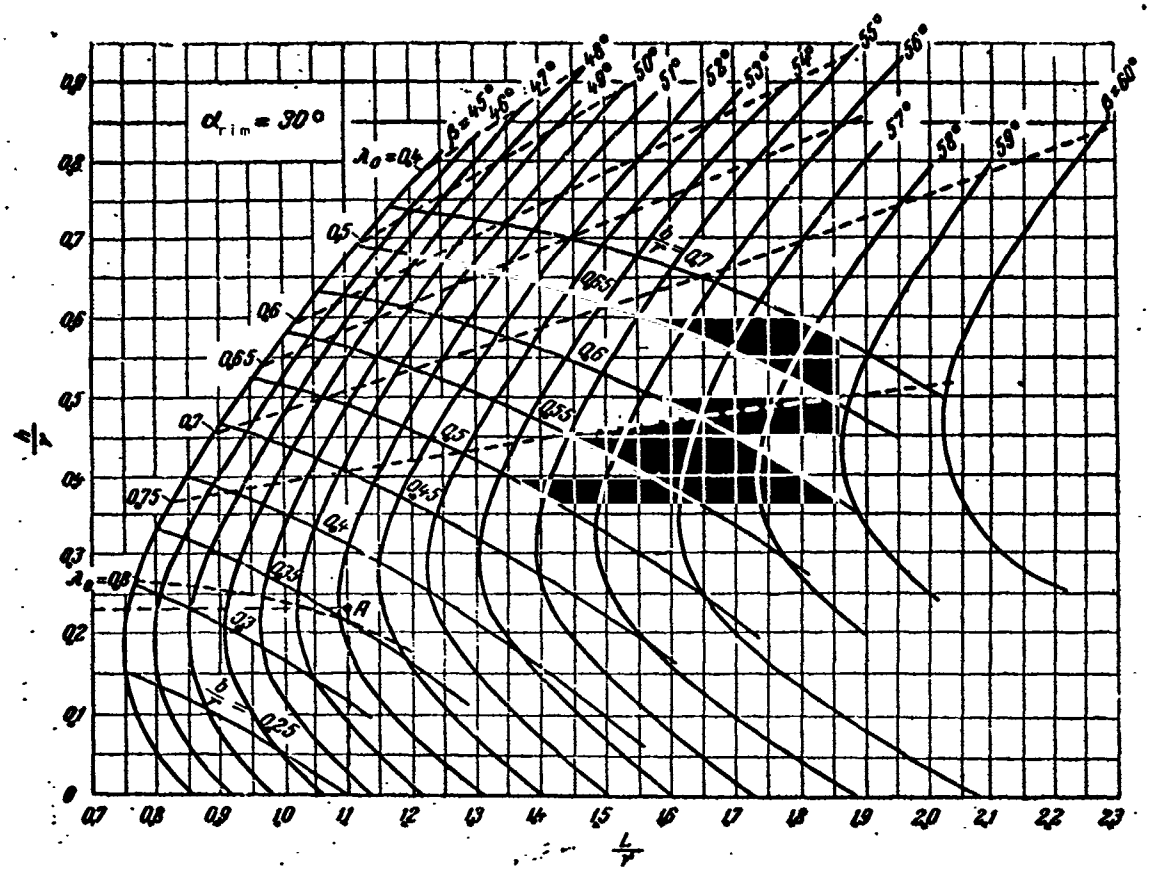

/93

Fig. 75. Determining the Parameters of an Inflated Tire Using Nomograms (for the Calculation Example).

the external diameter of the inflated tire is /94

$$D = D' + 2\Delta R = 1022 - 2 \cdot 5{,}2 = 1012 \text{ mm}$$

The distance from the widest point on the profile to the axis of rotations:

$$r_0 = \lambda_0 R = 0{,}796 \cdot 471{,}3 \doteq 376 \text{ mm}$$

The width of the profile along the internal contour of the carcass is:

$$2b = 2r_{rim}\left(\frac{b}{r}_{rim}\right) = 2 \cdot 303 \cdot 0{,}356 = 216 \text{ mm}.$$

The width of the profile along the external contour is:

$$B = 2b + 2t = 216 + 2 \cdot 14{,}5 = 245 \text{ mm}.$$

Determine the forces in the cord fibers along the equator according to formula (53). All dimensions included in this formula have already been determined, and we should substitute into this formula only the values of pressure and Σi_c; i.e., the summation of the fiber frequencies in all plies along the equator.

Taking into account both the cord plies and the breaker we obtain for a 9.00-20 outer cover:

$$\Sigma i_c = 8i'_c + 2i''_c + 2i'''_c$$

where i'_c is the fiber frequency along the equator of plies made of 9T cord (8 ply);

i''_c is the fiber frequency along the equator of plies made of widely spaced 94T cord (2 ply);

i'''_c is the fiber frequency of a 923T cord breaker (2 ply).

The cord fiber frequency along the equator can be determined as a function of the initial frequency i_0 and the cut angle α according to (7):

$$i_c = i_0 \frac{D_{bl.}}{2R} \cdot \frac{\cos\alpha}{\cos\beta_c}$$

where D_b is the band diameter.

For 1-8 ply 9T cord, i_0 = 9.4 fibers/cm, the band diameter is D_b = 630 mm (on the average) and the cut angle is α = 33°

$$i'_c = 9{,}4 \cdot \frac{630}{2 \cdot 471{,}3} \cdot \frac{\cos 33°}{\cos 51{,}2°} = 8{,}4 \text{ fibers/cm}$$

analogously we attain for 9 and 10-ply 94T cord

$$i_0 = 7{,}0 \text{ fibers/cm} \quad i''_c = 6{,}3 \text{ fibers/cm}$$

and for the breaker cord

$$i_0 = 4{,}6 \text{ fibers/cm} \quad i'''_c = 4{,}1 \text{ fibers/cm}$$

Thus

$$\Sigma i_c = 8 \cdot 8{,}4 + 2 \cdot 6{,}3 + 2 \cdot 4{,}6 = 87{,}7 \text{ fibers/cm}$$

The force in the fiber along the equator is: /95

$$N_{max} = \frac{4{,}5(47{,}13^2 - 37{,}6^2)}{2 \cdot 47{,}13 \cdot 87{,}8 \cos^2 51{,}2°} = 1{,}14 \text{ kg}.$$

It follows from the stretch diagram for 9T cord (cf. Fig. 73), that a force of 1.14 kg corresponds to fiber expansion of approximately 3%.

Since this value is rather small and almost coincides with the value for elastic expansion of fibers in the outer cover located in a vulcanization mold, the calculation we have made without taking into account cord fiber expansion is sufficiently valid.

The ratio of the blowout force for fibers (9 kg) to the force arising under normal internal pressure is:

$$\frac{N_{\text{fib}}}{N_{\max}} = \frac{9}{1.14} = 8.0.$$

The force P_0 in the bead ring is determined according to (54):

$$P_0 = p\frac{R^2 - r_0^2}{2\cos\beta_c}\cos\beta = 4.5\cdot\frac{47.13^2 - 37.6^2}{2\cos 28^\circ}\cos 51.2^\circ = 1300 \text{ kg}.$$

In the bead there are 72 wires 1 mm in diameter. The cross sectional area of the wire is equal to:

$$f = 0.785 \text{ mm}^2.$$

The stress in the wire is:

$$\sigma = \frac{P_0}{n_1 f} = \frac{1300}{72\cdot 0.785} = 23.3 \text{ kg/cm}^2.$$

The safety factor of the wire is:

$$\frac{\sigma_b}{\sigma} = \frac{140}{23.3} = 6.0.$$

To determine the blowout pressure we must first find the tire configuration before blowout, taking into account cord fiber expansions.

Since the tire has a breaker, we will use formula (59a) to compute the mean force in a fiber. Let us substitute the blowout force for 9T cord (9 kg) for $N_{\max}$.

The summation of the densities along the equator of all plies and the breaker was computed above: Σi_c = 87.8 fibers/cm. The summation of only the carcass ply densities is $\Sigma i'_c$ = 79.6 fibers/cm. Formula (59a) yields in this case

$$\bar{N} = \frac{N_{\max}\cos^2 52^\circ}{L}\left[1.1\int_s \frac{ds}{\cos^2\beta} - 0.1\int_{s_k} \frac{ds}{\cos^2\beta}\right].$$

The first integral in brackets can be computed using Simpson's formula by taking advantage of the data in Table 1:

$$\int_0 \frac{ds}{\cos^3\beta} = \frac{\Delta s}{3}\left[k_c^3 + 4k_1^3 + 2k_2^3 + 4k_3^3 + k_{rim}^3\right] =$$

$$= \frac{60}{3}\left[4{,}25 + 4 \cdot 3{,}74 + 2 \cdot 2{,}63 + 4 \cdot 1{,}90 + 1{,}56\right] = 673 \text{ mm}.$$

The length of the sub-breaker section of the carcass s_1 is 90 mm. In this section the value of $\frac{1}{\cos^3\beta}$ varies insignificantly and on the average we can assume that $k^3 = \frac{k_c^3 + k_1^3}{2} = 4.0$; thus /96

$$\int_{s_1} \frac{ds}{\cos^3\beta} = 90 \cdot 4 = 360 \text{ mm}.$$

As a result we obtain:

$$N = \frac{9 \cdot 0{,}615^2}{334}\left(1{,}1 \cdot 673 - 0{,}1 \cdot 360\right) = 7{,}2 \text{ kg}.$$

The relative cord fiber expansion with a force of $\bar{\varepsilon}$, found according to the stretch characteristic, is about 10%.

Now find the cord fiber angle with the meridian at the rim point C taking into account fiber stretch:

$$\sin\alpha_c = \frac{\sin 30^\circ}{1+\bar{\varepsilon}} = \frac{0{,}5}{1{,}1} = 0{,}455$$

from which we find that $\alpha_c = 27^\circ$.

Since there is no nomogram for $\alpha_{rim} = 27^\circ$, we will use in our calculations $\alpha_{rim_1} = 28^\circ$ and find on the tire profile that point which has such an angle taking into account fiber stretch

$$r_{rim_1} = \frac{R'(1+\bar{\varepsilon})\sin\alpha_{rim_1}}{\sin\beta'_{cd}} = \frac{476{,}5 \cdot 1{,}1 \sin 28^\circ}{\sin 52^\circ} = 312 \text{ mm}$$

The corresponding point on Figure 74 coincides with point A. This point is at a distance $h_1 = 76$ mm from the axis of symmetry of the profile.

We will now determine the length of the cord fiber from the equator to point A. If we do not take expansion into account, this length is less than the length we have already calculated (334 mm) to point C by the value $\frac{AB}{\cos\beta}$.

The segment AC is equal to 10 mm, and we may assume that the cord fiber angle in this segment β is equal to the angle at point C, i.e., 30°.

Thus without taking into account expansion, the cord fiber from the equator to point A has a length

$$L = 334 - \frac{10}{\cos 30^\circ} = 322{,}5 \text{ mm}$$

Taking expansion into account we have

$$L_1' = L(1+\bar{\varepsilon}) = 322{,}5 \cdot 1{,}1 = 355 \text{ mm}$$

We can now find the ratios:

$$\frac{L_1}{r_{\text{rim}_1}} = \frac{355}{312} = 1{,}14; \qquad \frac{h_1}{r_{\text{rim}_1}} = \frac{76}{312} = 0{,}243$$

We will now plot the corresponding point on the nomogram for the angle $\alpha_{\text{rim}} = 28°$ (point A on Fig. 76).

We can find by interpolation of the nomogram that:

$$\beta_{c_1} = 48°50'; \qquad \lambda_0 = 0{,}79$$

Thus at the moment of blowout the outer cover will have an angle along the equator $\beta_{c_1} = 48°50'$ and the radius along the equator (along the internal contour of the carcass) will be:

$$R_1 = r_{\text{rim}_1} \frac{\sin \beta_{c_1}}{\sin \alpha_{\text{rim}_1}} = 312 \frac{\sin 48°50'}{\sin 28°} = 500 \text{ mm}$$

The zenith radius of the tire (distance from the axis of rotation to the widest point on the tire profile) is:

$$r_{0_1} = \lambda_0 R_1 = 0{,}79 \cdot 500 = 395 \text{ mm}$$

We can now determine the pressure p_b required to cause tire blowouts according to formula (53). We should substitute into the left-hand side of this equation the blowout force in the cord fibers N_{blo} and we should substitute into the right-hand side the tire dimensions found above.

Thus, we obtain:

$$p_b = \frac{2R_1 (\Sigma i_c)_1 \cos^2 \beta_{c_1}}{R_1^2 - r_{0_1}^2} N_{\text{blo}}$$

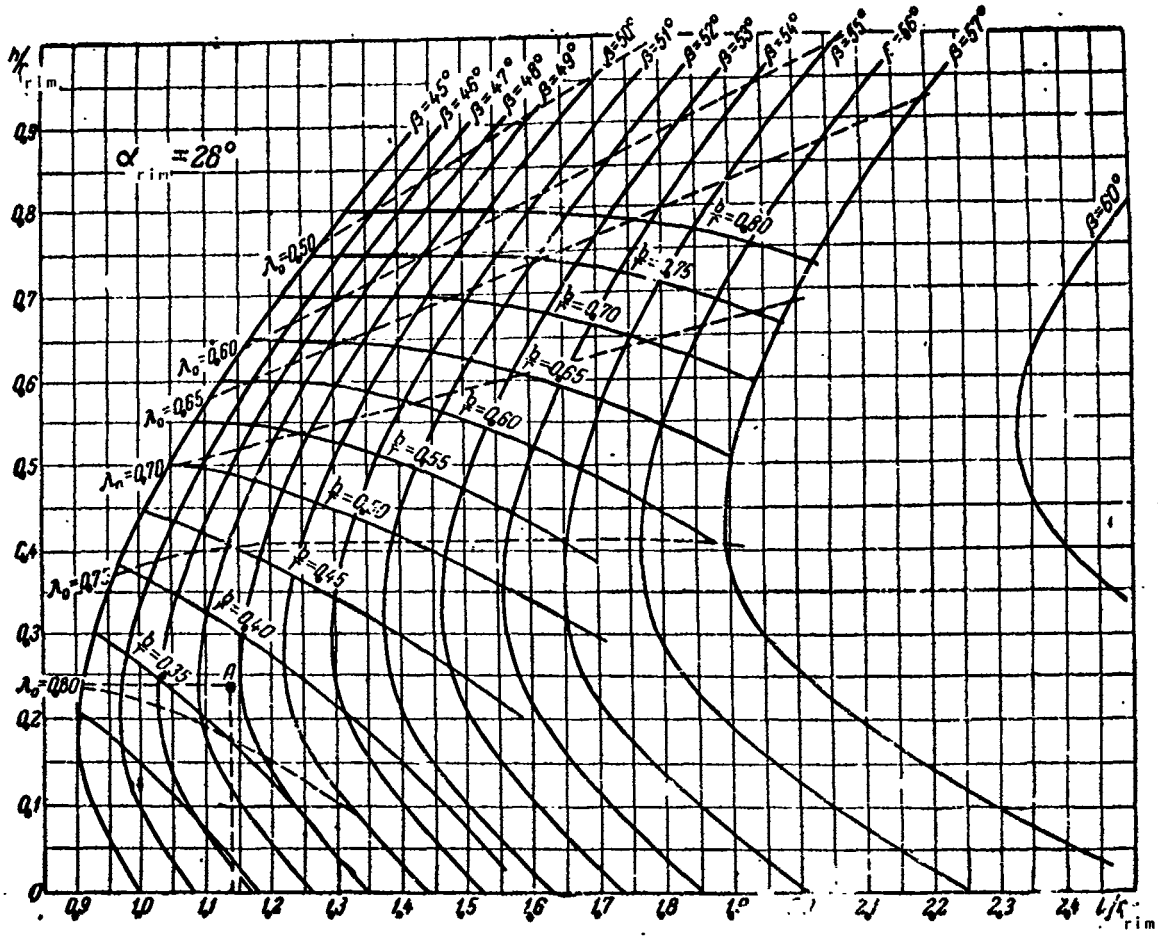

Fig. 76. Determining the Tire Configuration Taking Cord Fiber Expansion into Account.

When using this formula we must take into account that due to fiber expansion, the fiber frequency along the equator varies and the value (Σi_{c_1}) for a tire at the moment of blowout is related to Σi_c for a tire in the mold by the function

$$(\Sigma i_c)_1 = \Sigma i_c \frac{R}{R_1} \cdot \frac{\cos\beta_{1c}}{\cos\beta_{c1}}$$

In this case

$$(\Sigma i_c)_1 = 87{,}8 \cdot \frac{471{,}3}{500} \cdot \frac{\cos 51°12'}{\cos 48°50'} = 79 \text{ Fibers/cm}$$

Substituting this and other values into the formula for p_b we find the pressure required to cause a blowout in the tire carcass[12]:

$$p_b = \frac{2 \cdot 50 \cdot 79 \cos^2 48°50'}{50^2 - 34{,}5^2} \cdot 9 = 33 \text{ kg}$$

The ratio of hydrostatic blowout pressure to normal pressure is:

$$\frac{p_b}{p} = \frac{33}{4{,}5} = 7{,}35$$

This figure is 8% lower than the ratio of the blowout force in the fiber to the force arising under normal internal pressure. The difference between these figures is caused by a change in the tire dimensions due to cord fiber expansion.

Radial Compression and Free-Rolling of the Tire

In the previous section we examined the axisymmetrical deformation of a tire under the effect of internal pressure. This problem found a comprehensive solution due to the application of the theory of the equilibrium configuration of rubberized cord shells.

The calculated determination of tire element deformations /99
under radial compression and rolling is accompanied by significantly greater difficulties. Although the differential equations describing arbitrary deformations of a rubberized cord shell were compiled in [16-18], their solutions for the real aspects of tire pressurization are very complicated.

Therefore when discussing tire rolling we should use a different type of approximate method for our calculation. Under these conditions an experimental investigation of tire operation is of particularly great importance.

Tire Contact With the Road

With the action of vertical load on a tire, the tire is deformed and part of its surface comes into contact with the road surface, as is shown systematically in Figure 77.

The depression of the tire f and the dimensions of the contact surface with the road surface are functions of the load Q and the

---

[12]The actual blowout pressure is somewhat lower than the computed value due to nonuniform load distribution among the cord fibers.

internal pressure p. The height of the axis of a deformed tire above the road surface R_s is called the static radius of the tire:

$$R_s = R_0 - f$$

where R_0 is the external radius of an undeformed tire.

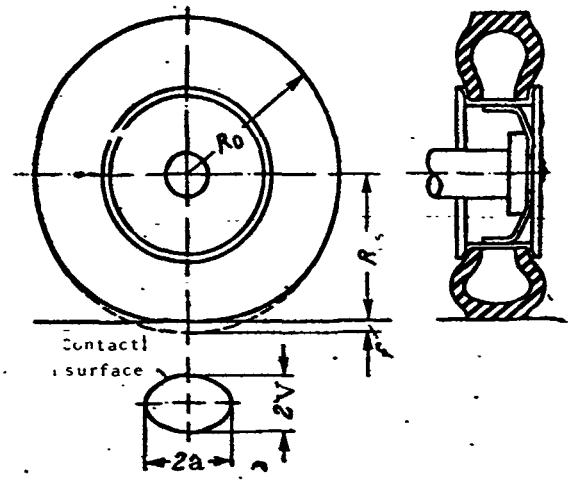

Fig. 77. Tire Contact with the Road.

When the wheel is rolling at a certain velocity the distance of its axis from the road surface increases somewhat and becomes equal to $R_d > R_s$. The value R_d is called the dynamic radius of the tire. The increase in the dynamic radius in comparison to the static radius is explained both by an increase in the rigidity of the tire materials during dynamic deformation and the corresponding decrease in depression f, and also by the increase in the external radius of the tire R_0 in relation to the action of centrifugal forces. As a rule, at ordinary velocities the difference between R_d and R_s is significant, and we can assume roughly that $R_d = R_s$. /100

An important tire characteristic is its rolling radius R_{rl}, by which we mean a certain value equal to the ratio of the linear rolling velocity of the wheel v to the angular velocity ω of its rotation.

$$R_{rl} = \frac{v}{\omega}$$

By multiplying the numerator and denominator of this formula by the time of motion t we can define the rolling radius as the ratio of the distance $s = vt$ traversed by the wheel to its angle of revolution $\phi = \omega t$ expressed in radians:

$$R_{rl} = \frac{s}{\varphi} \qquad (60)$$

Let us now examine free rolling of a tire along a plane. For simplicity we will assume that the tire axis is stationary in space and the road surface moves with velocity v. In the middle part of the contact surface where there is no slip, the tire tread moves with the same velocity as the road surface and for one revolution of the tire travels a distance s_1.

It is obvious that for one revolution of the wheel the entire

tire tread passes across the road surface, the initial length of which is $2\pi R_0$.

However, since in the contact zone the tread undergoes compression deformation ε in the circular direction (cf. below), its deformed length s_1 is:

$$s_1 = 2\pi R_0(1-\varepsilon)$$

Substituting this value into formula (60) and taking into account that one revolution of the wheel corresponds to an angle of revolution $\phi = 2\pi$, we find that

$$R_{\text{rl}} = R_0(1-\varepsilon) \tag{61}$$

Thus the ratio of the rolling radius to the external radius of the tire varies with the value of circular deformation of the tire tread in contact. This value in turn varies with the depression of the tire and its construction (cord fiber angle, type and depth of tread).

The contact surface of a tire with the road surface usually has an elliptical shape (cf. Fig. 77). Due to the presence of tread, /101 contact is attained not along the entire surface of the ellipse but only under the ridges of the tread. Figure 78 shows the prints of the contact surface of tires with road tread (Fig. 78a) and high roadability tread (78b).

The intensity of the forces of interaction between the tire and the road surface can be described by the mean pressure in the contact surface:

$$q_{\text{mn}} = \frac{Q}{F_{\text{gr}}} \tag{62}$$

where F_{gr} is the total area of the contact ellipse.

A more precise characteristic is the mean pressure relative to the actual area of the imprint F_{sat}:

$$q'_{\text{mn}} = \frac{Q}{F_{\text{sat}}}$$

The value q'_{mn} is greater than q_{mn}, while the relationship between them depends on the saturation of the tread; i.e., on the relationship between the surface of the ridges and the surface of the grooves.

The most highly perfected method of experimentally determining the pressure in tire contact with the road surface using tensometric

sensors is described in [19] (cf. Chapter VI, p. 158). Figure 79 shows the pressure distribution with slow rolling of a 7.50-16 tire with smooth tread along a drum (the distribution was taken from the above-mentioned reference). The internal pressure in the tire was 2.5 kg/cm^2; the load was 785 kg.

As we can see from the figure, in the given case the pressure at the edges of the rolling part is significantly higher than in the remaining part of the contact surface.

The character of the pressure distribution over the contact surface varies with tire depression. The tire construction (primarily the tread curvature) also exerts a significant influence on the pressure distribution. With a high degree of tread curvature

/102

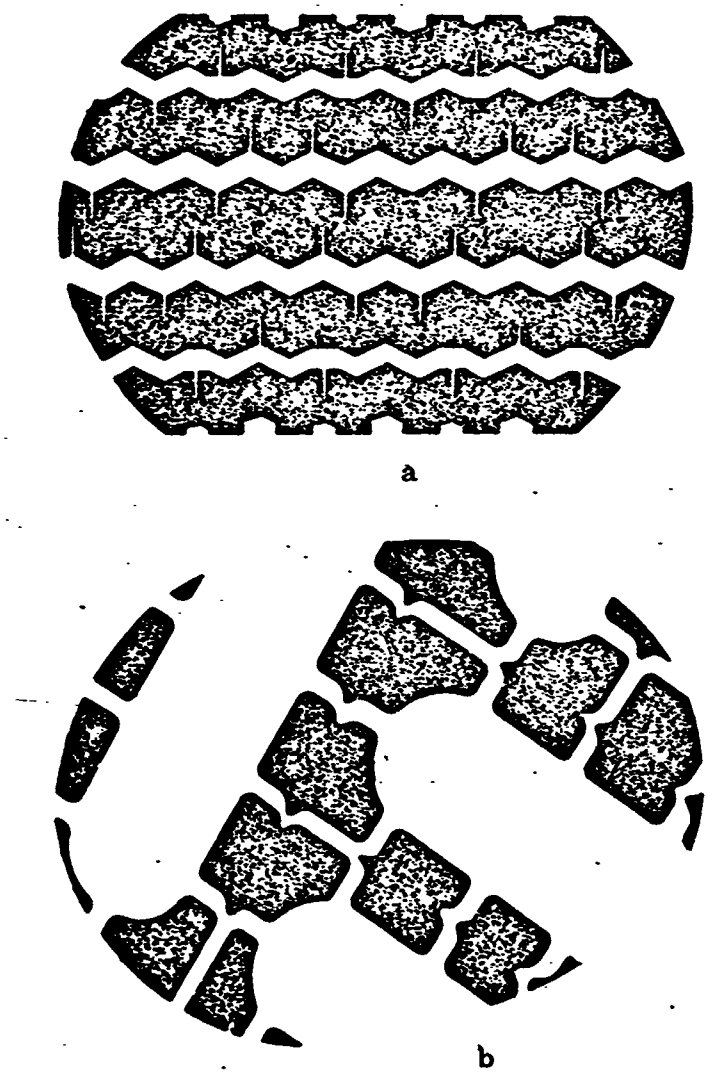

Fig. 78. Imprints of the Contact Surface of a Tire with the Road: (a) Tire With Road Tread; (b) Tire with High Roadability Tread.

the pressure in the center of the rolling part is greater than at the edges; as the curvature of the tread decreases, the pressure increases toward the edges of the rolling part and decreases along the center.

In the presence of tread, along with the overall nonuniformity of pressure distribution over the contact surface, its distribution is also nonuniform at the limits of each tread element. In the center of an element (Fig. 80) the pressure is higher than at its edges. This is explained by the fact that at the edges of the element the /103 rubber has greater freedom of lateral expansion than in the center.

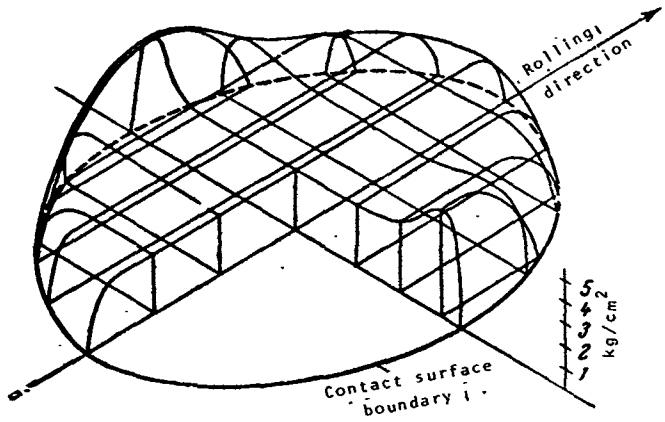

Fig. 79. Pressure Distribution in the Contact Surface of a 7.50-16 Tire with a Rolling Drum.

In addition to contact forces normal to the plane of the road surface there are forces lying in this plane.

Figure 81 shows the nature of distribution of tangential forces over the contact surface of a free-rolling 6.00-16 tire (the load is 450 kg, the internal pressure is 2 kg/cm^2. This figure shows the forces acting on the road surface. The forces acting on the tire have the opposite direction. Figure 81b shows the distribution of the tangential force component in the rolling direction; Figure 81c shows the component perpendicular to the rolling direction [23].

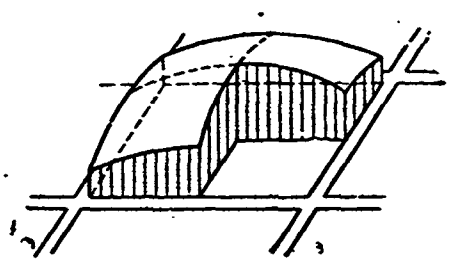

Fig. 80. The Nature of Pressure Distribution in the Limits of One Tread Element.

It can be seen from this figure that the tangential forces acting on the road surface are directed approximately toward the center of the contact surface.

Load Characteristics of a Tire

A basic value characterizing a tire is its pliability, i.e., its tendency to be deformed due to load.

The radial depression of a tire as /104 a function of its load value is called the tire characteristic. The tire characteristic depends on its construction and internal air pressure.

As an example Figure 82 shows the characteristics of a 12.00-18

tire shown with various values of internal pressure (from zero to 3.5 kg/cm^2).

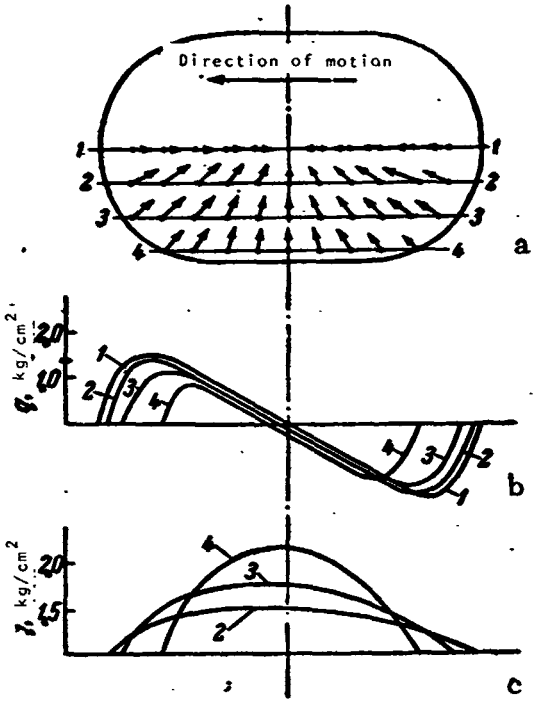

Fig. 81. Distribution of Tangential Forces over the Contact Surface of a Free-Rolling 6.00-16 Tire. Curves 1, 2, 3 and 4 Show the Distribution of Forces over Longitudinal Cross Sections of the Contact Zone (1-1 ...4-4): (a) Direction of the Forces; (b) Longitudinal Component (c) Lateral Component of Tangential Forces.

Each characteristic is a loop whose upper branch was obtained with loading and whose lower branch was obtained with unloading. The difference between these branches is related to the presence of friction, both internal friction in the tire material and external friction on the contact surface.

As the internal pressure p increases the hysteresis loop contracts, and under normal operational pressure for ordinary tires it can be ignored.

We can see from the graphs in Figure 82 that the function relating the depression and the load is nonlinear. As the depression increases the rigidity of the tire increases. As the internal pressure increases the rigidity of the tire also increases, but not in direct proportion. The rigidity of the tire increases more slowly than does the internal pressure. These relationships can also be seen in the compression curves for light 6.00-16 tires shown in Figure 83. /105

In view of the importance of this problem the calculated determination of tire depression has interested a number of investigators. Nonetheless we can show only a few approximate formulas to accomplish this goal. The best known is the Hedecle formula [3].

This formula is based on two hypotheses. It assumes first that except for the contact surface the tire is not deformed, and second, that the mean specific pressure on the contact surface is equal to the internal air pressure.

The second hypothesis may be formulated another way: the work of tire compression is completely expended on compressing the air in the tire. The first of these hypotheses allows us to establish the dimensions of the contact surface in a purely geometric way (Fig. 84).

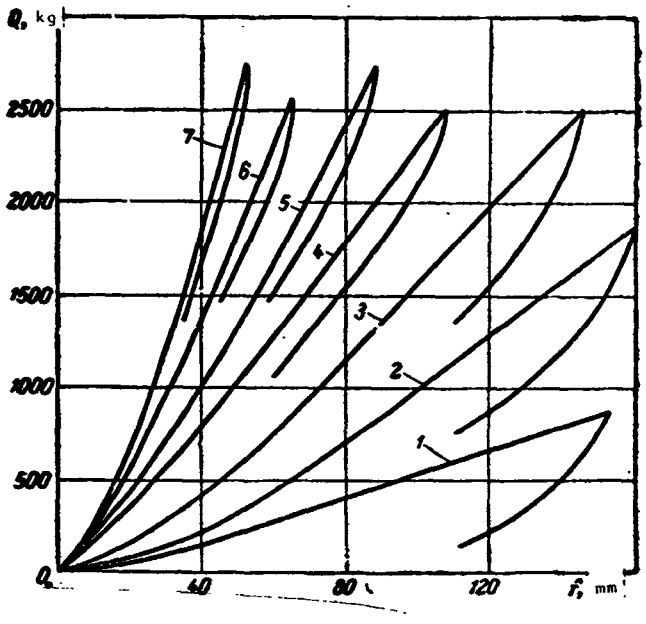

Fig. 82. The Load Characteristics of a 12.00-18 Tire with Various Values of Internal Pressure p (in kg/cm^2): (1) 0; (2) 0.2; (3) 0.5; (4) 1.0; (5) 1.5; (6) 2.5; (7) 3.5.

Assuming that depressions are small, we can find the semiaxes of the contact ellipse: /106

$$a = \sqrt{Df}; \qquad b = \sqrt{2Rf} \tag{63}$$

where D is the external diameter of the tire; R is the radius of curvature of the tread.

The contact surface is defined as

$$F_{gr.} = \pi ab = \pi f \sqrt{2RD}. \tag{64}$$

According to the second hypothesis, the load on the tire Q is defined as the product of the contact surface and the internal pressure:

$$Q = pF_{gr.} = pf\pi\sqrt{2RD}. \tag{65}$$

Thus according to the Hedecle formula, the load on the tire is directly proportional to the depression and to the internal pressure.

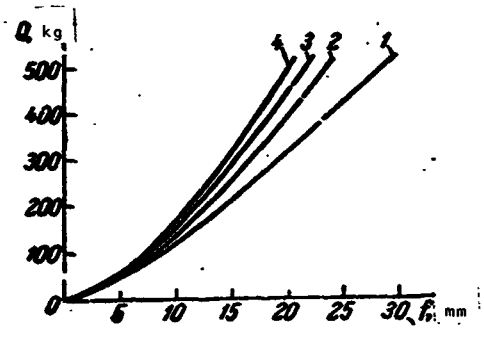

Fig. 83. The Load Characteristics of a 6.00-16 Tire: Model I-77; D (in kg/cm^2): (1) 1.5; (2) 2.0; (3) 2.5; (4) 3.0.

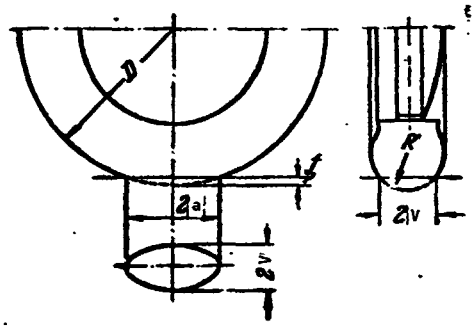

Fig. 84. Determining the Dimensions of the Contact Surface According to Hedecle.

However, as we have seen above, the experimental data indicate that the relationships between the load and both the depression and the pressure are nonlinear.

The imprecision of the Hedecle formula is a consequence of the

hypotheses used. In reality the tire is deformed not only in the contact surface but also outside the contact surface. The hypothesis that the work of compression is completely expended on air compression is also inaccurate.

To clarify the relationship between the total work of deforming the tire and the portion of this work expended on air compression, we conducted a special experiment. We compressed a tire and measured the change in volume ΔV of its internal cavity.

To do this the internal cavity of the tire was filled with water (Fig. 85). The water in the tire (1) and the reservoir attached to it (2) was maintained by constant air pressure in tank (3). The change in volume of the internal cavity of the tire with compression was determined according to the measurement of the water level in the water measuring tube (4). /107

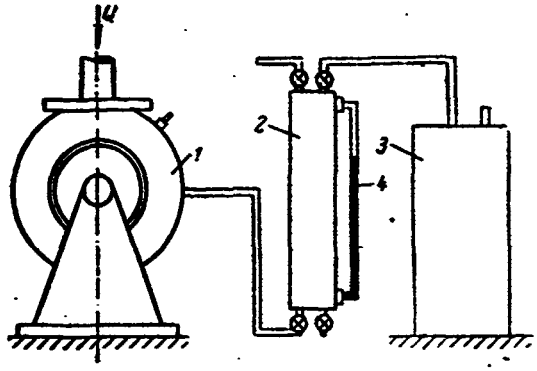

Fig. 85. Diagram of Our Set-Up for Measuring the Volume of the Internal Cavity of a Tire with Compression: (1) Experimental Tire; (2) Measuring Reservoir; (3) Tank; (4) Water Measuring Tube.

Figure 86 shows graphs for the change in volume of the internal cavity of a 9.00-20 tire (8 ply viscose cord) as a function of depression with various values of the internal pressure. It is clear from the figure that as the internal pressure increases the change in the volume decreases. Apparently, this can be explained by two factors. First, as the pressure increases the tread compression deformation increases and a smaller part of the total deformation is absorbed by the carcass. Second, as the pressure increases the configuration of the compressed tire approaches its equilibrium configuration which corresponds to the maximum volume. /108

The work of air compression with tire depression f is defined as

$$A_a = p\Delta V$$

where p is the excess internal pressure[13] and ΔV is the measured change in volume.

The total work expended on tire compression is equal to:

[13] The value of pressure in the tire when it is compressed varies insignificantly (for automobile tires within 1-2% of the initial pressure); therefore the process may be assumed to be isobaric.

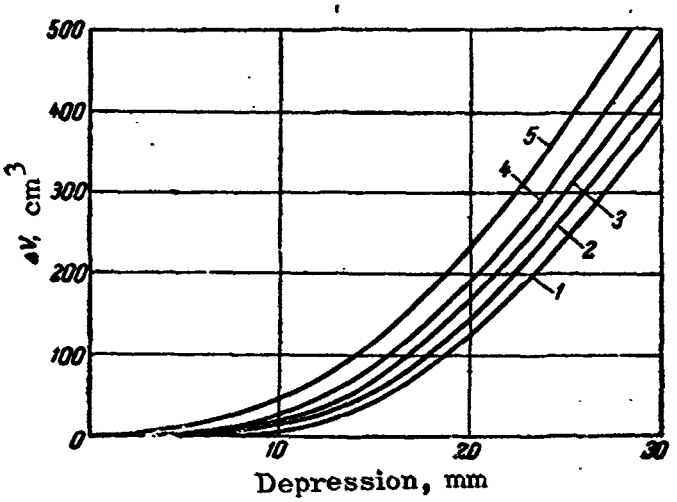

Fig. 86. Change in Volume of the Internal Cavity of a 9.00-20 Tire As a Function of Depression: 13V Cord, 8 Plies; the Internal Pressure (in kg/cm^2) Was: (1) 5; (2) 4; (3) 3; (4) 2; (5) 1.

$$A=\int_0^f Q\,df.$$

The difference between the total work and the work of air compression is the work expended on deformation of the tire material:

$$A_m=A-A_a.$$

Figure 87 shows the change in the values A, A_a and A_m as a function of the depression of a 9.00 tire under an internal pressure of 4 kg/cm^2. Figure 88 shows the relationship between the work of air compression and the total work of compression in percent. As can be seen from the graph, with normal depression (f = 27 mm) the work of air compression is about 60% of the total work of compressing the tire. The remaining 40% is expended on deformation of the tire material. A significant portion of this work (on the order of 1/3)is expended on compressing the tread rubber. /109

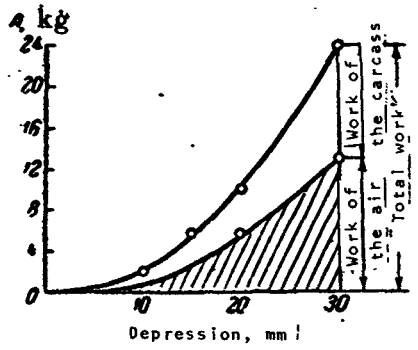

Fig. 87. The Total Work of Compressing a 9.00-20 Tire and the Work of Compressing the Air in Its Internal Cavity as a Function of Depression (p = 4.0 kg/cm^2).

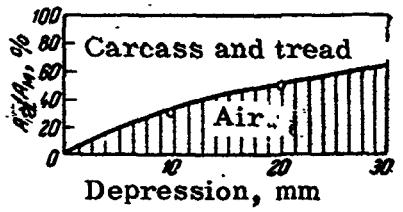

Fig. 88. The Relationship Between the Work Expended on Air Compression and the Total Work of Compressing the Tire as a Function of Radial Depression.

Under a given internal pressure, as the depression decreases the portion of work expended on air compression decreases.

Examining the distribution of the work of tire compression allows us to determine that a basic aspect of rigidity is air compression; however, the formation of the carcass and tread are also significant.

The interaction of the tire carcass and tread under the action of radial load may be represented schematically (Fig. 89).

Elastic elements 1 and 2 refer to the elasticity of air and the elasticity of the tire carcass itself; elastic element 3 corresponds to the elasticity of the tread.

It is easy to see that the total depression of the tire f is the sum of depressions referring to a compression of the tread f_t and the depression f_c caused by carcass deformation:

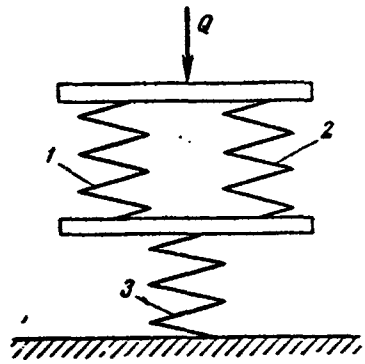

Fig. 89. Schematic of the Interaction between the Tire Carcass and Tread Under the Action of Radial Load: (1, 2) Elastic Elements Corresponding to the Elasticity of Air and the Tire Carcass; (3) Elastic Element Corresponding to the Elasticity of the Tread.

$$f = f_t + f_c .$$

We assume that the work expended on deforming the carcass A_c is proportional to the change ΔV in the internal volume of the tire, as is the work expended on air compression:

$$A_c = p_0 \Delta V$$

where the value p_0 characterizes the rigidity of the carcass with no internal pressure.

Thus the total work expended on air compression and deformation of the carcass is:

$$A_a + A_c = (p + p_0)\Delta V .$$

In order to calculate the value ΔV as a function of depression f_c, it is necessary to know the change in tire configuration with compression. However, we can assume approximately that the actual change in volume is proportional to the corresponding value computed by the Hedecle method; i.e., that ΔV is proportional to the volume of an elliptical segment with semiaxes a and b and to the index f_c (Fig. 84): /110

$$\Delta V = k_1 \frac{1}{2} \pi a b f_c^2$$

where k_1 is the proportionality coefficient.

Substituting the values of a and b according to formula (63) and replacing f by f_c, we find that:

$$\Delta V = k_1 \frac{1}{2} \pi \sqrt{2RD}\, f_c^2 .$$

Thus we obtain a quadratic function relating the change in volume to the depression f_c.

From an examination of Figure 86 we can see that at low internal pressures (p = 1 kg/cm^2) when the tread deformation is very small and $f \approx f_c$, the experimental relationship between ΔV and f is practically a quadratic parabola.

Taking into account the value ΔV we obtain for the work expended on air compression and carcass deformation the expression

$$A_a + A_c = \frac{1}{2C_2}(p + p_0) f_c^2$$

where $C_2 = \frac{1}{k_1 \pi \sqrt{2RD}}$ is a constant for a given tire which is inversely proportional to its linear dimensions.

Considering that

$$A_a + A_c = \int_0^{f_c} Q\, df$$

we find the load value Q corresponding to the carcass depression f_c:

$$Q = \frac{d}{df_c}(A_a + A_c) = \frac{p + p_0}{C_2} f_c$$

from which we obtain

$$f_c = C_2 \frac{Q}{p + p_0}. \qquad (66)$$

Let us now examine the portion of depression f_t caused by tread deformation.

The contact area of the tire with the road surface can be estimated approximately using formula (64):

$$F_{gr} = \pi f \sqrt{2RD}.$$

Then the mean specific pressure in the contact surface is: /111

$$q = \frac{Q}{F_{gr}} = \frac{1}{\pi \sqrt{2RD}} \cdot \frac{Q}{f}.$$

The maximum pressure on the ridges of the tread at the center of the contact surface can be defined as

$$q_{max} = \frac{\psi_1}{\psi} q$$

where ψ is the coefficient of tread saturation, i.e., the ratio of

the area of ridges in the contact to the total contact surface; ψ_1 is a coefficient which takes into account the nonuniform distribution of pressure over the contact surface. With small depressions and high internal pressures the coefficient is great and approaches the number 2; with ordinary pressures the pressure is distributed almost uniformly over the surface and $\psi_1 \approx 1$.

The depression f_t can be found from calculating the tread compression:

$$f_{t1} = \frac{q_{max} h}{\psi_2 E} \tag{67}$$

where h is the tread thickness, E is the elasticity modulus of the tread rubber, ψ_2 is the rigidifying coefficient in connection with the difficulties of lateral rubber deformations. This coefficient decreases and approaches unity as the separation of the tread and the ratio of the depth of the tread to the total thickness of the tread increase. Substituting the value of q_{max} into formula (67), we find that:

$$f_t = C_1 \frac{Q}{f}$$

where $C_1 = \frac{\psi_1}{\psi\psi_2 E} \cdot \frac{h}{\pi\sqrt{2RD}}$ is a coefficient which is constant for a given tire.

The total depression of the tire is the sum of the depressions of the tread and carcass:

$$f = f_{t1} + f_c = C_1 \frac{Q}{f} + C_2 \frac{Q}{p + p_0}. \tag{68}$$

Solving this expression relative to load, we obtain the formula

$$Q = \frac{f}{C_1 + C_2 \frac{f}{p + p_0}}. \tag{69}$$

In this formula C_1, C_2 and p_0 are coefficient which are constant for a given tire. The values of C_1, C_2 and p_0 for a given tire can be determined from the results of three experiments conducted under two different internal pressures. In this case from two experiments conducted at the same pressure p', it is easy to determine the values of C_1 and $\frac{C_2}{p' + p_0}$ and then from an experiment conducted with a different pressure (p''), we can also determine $\frac{C_2}{p'' + p_0}$, after which we can compute the values of C_2 and p_0 individually. /112

This interpretation of the experimental data showed that for

various tires, as a function of the rigidity of the carcass, the value of p_0 lies within the limits 0.1-0.3 kg/cm^2. Therefore when calculating the depressions of ordinary automotive tires this value can be ignored. The value of p_0 must be taken into account only when determining the depressions of tires operating at very low pressures (for example, for tires with variable internal pressure, ground-grip tires and agricultural tires).

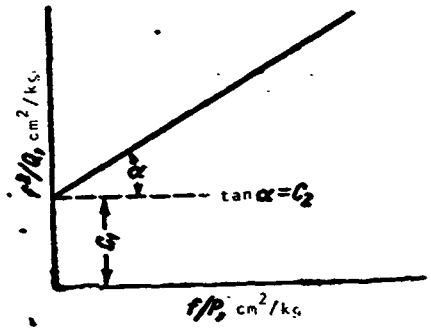

Fig. 90. The Universal Characteristic of a Tire.

Thus in the majority of cases formula (69) can be used in its simplified form:

$$Q=\frac{f^2}{C_1+C_2\frac{f}{p}} \qquad (70)$$

In this case, ignoring the value of p_0 can be to a certain degree compensated for by a certain decrease in C_2.

Let us now examine the experimental data referring to the determination of the constants C_1 and C_2 included in formula (70).

In order to determine the constants C_1 and C_2 according to the data of a statistical sampling of a tire, we can present (70) in the form

$$\frac{f^2}{Q}=C_1+C_2\frac{f}{p}.$$

Thus, if our initial premises are valid, then in the coordinates $\frac{f}{p}$, $\frac{f^2}{Q}$ (Fig. 90) the tire characteristic can be expressed as a straight line which we will call the universal characteristic of a tire. The segment intersecting this line on the $\frac{f^2}{Q}$ axis is equal to C_1 and the tangent of the angle of inclination is equal to C_2.

Figure 91 shows the obtained experimental curves for the compression of 7.50-16, 7.50-20 and 260-20 tires with various internal pressures, and Figure 92 shows the corresponding curves in the coordinates $\frac{f}{p}$, $\frac{f^2}{Q}$ for these tires and for a 6.00-16 tire. For each point in the coordinates $\frac{f}{p}$, $\frac{f}{Q}$ all points independent of pressure and load lie on one line with a satisfactory degree of accuracy. This substantiates the validity of formula (70). /113

At low internal pressures and correspondingly high depressions, as we have already shown, we must take into account these values of p_0. For example, this is clear in Figure 93, which shows in coor-

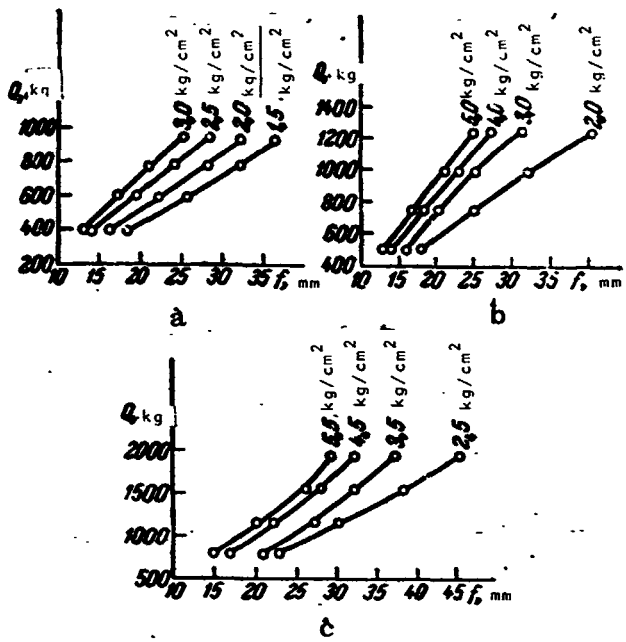

Fig. 91. The Load Characteristics of Tires: (a) 7.50-16; (b) 7.50-20; (c) 260-20.

dinates $\frac{f}{p}$, $\frac{f^2}{Q}$ the results of compressing a 12.00-18 tire. In this case, points corresponding to low internal pressures are far to the right of the straight line constructed according to the points corresponding to a pressure of 3.5 kg/cm^2. But if we plot along the abscissa $\frac{f}{p + p_0}$ instead of $\frac{f}{p}$, assuming that p_0 = 0.3 kg/cm^2, all points (they are shown in Fig. 93 by a slash drawn through the point) again fall on one line. Even the points obtained with compression of an uninflated tire (p = 0) lie near this line.

Thus we may assume that the obtained formula (69), which yields the relationships between the tire depression, load and internal pressure, agrees with the experimental data. In the majority of cases we can use the simpler formula (70), which includes only two parameters (C_1 and C_2) characterizing the tire.

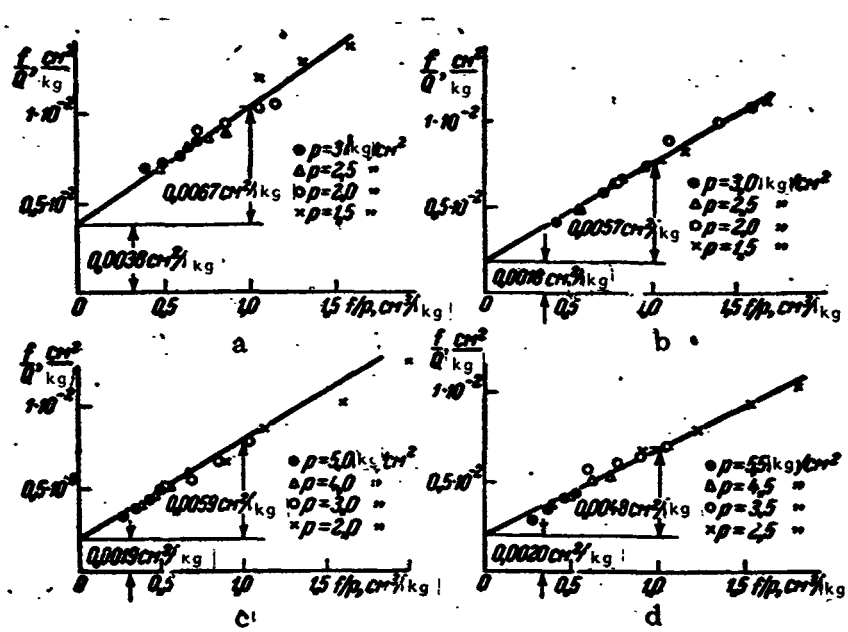

Fig. 92. The Universal Characteristics of Tires: (a) 6.00-6; (b) 7.50-6; (c) 7.50-20; (d) 260-20.

/114

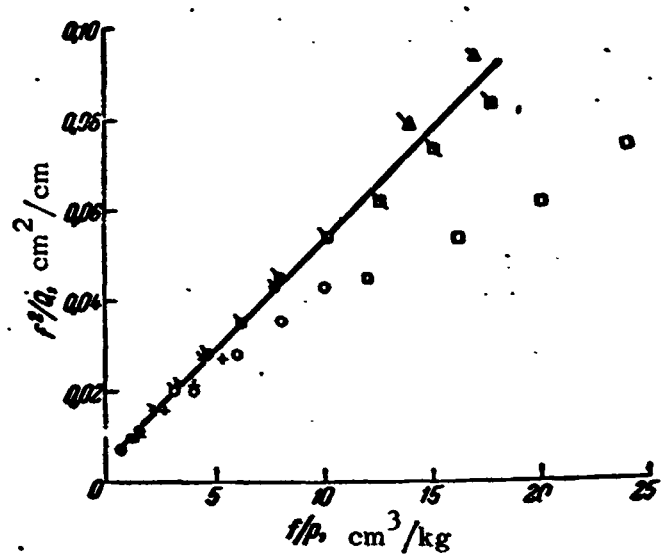

Fig. 93. The Universal Characteristic of a 12.00-18 Tire (for the Points with a Slash through Them We Have Plotted along the Abscissa the Ratio $\frac{1}{p + 0.3}$). The Internal Pressure (kg/cm^2): ● = 3.5; + = 1.5; o = 1.0; □ = 0.5; Δ = 0.

From (70) it is easy to obtain the formula for depression: /115

$$f = \frac{C_2 Q}{2p} + \sqrt{\left(\frac{C_2 Q}{2p}\right)^2 + C_1 Q}$$

and for pressure

$$p = \frac{C_2 Q f}{f^2 - C_1 Q}.$$

Thus when calculating the suspension of an automobile we need to know the rigidity of the tire at a given load; i.e., the derivative $\frac{dQ}{df}$. This value is determined by the formula

$$\frac{dQ}{df} = \frac{Q}{f}\left(2 - C_2 \frac{Q}{pf}\right)$$

into which we substitute the values Q, f and p corresponding to the given regime.

Of great interest is the determination of the values of C_1, C_2 and p_0. As we have already shown, these values may be determined according to the results of tire compression in three regimes. In most cases, when there is no need to take into account p_0, two experiments are sufficient. However, when projecting (when the tire is not yet finished) we must have an opportunity to give a preliminary estimate of the values of C_1, C_2 and p_0.

The values of C_1, C_2 and p_0 used in deriving our formulas contain a number of unknown coefficients and therefore cannot be directly used for calculation. However, they are useful for investigating the qualitative functions of these values.

Thus the value of C_2 is determined by the formula

$$C_2 = \frac{1}{k_1 \pi \sqrt{2RD}}$$

where k_1 is the ratio of the change in tire volume to the volume of the elliptical segment obtained with contact between the tire and a surface. It is obvious that this coefficient varies mainly with the relative thickness of the tire walls, characterized (for a given

type of cord) by the ratio $\frac{n}{B}$ of the number of cord plies to the width of the tire profile. The greater this ratio, the more the volume of the tire will vary with a given depression (k_1 will be greater) and the greater the energy of carcass deformation will be (p_0 will be greater). /116

Thus with a constant external tire geometry (i.e., for tires produced in one mold) the coefficient C_2 must decrease somewhat as the number of plies increases.

In addition, for geometrically similar tires with identical $\frac{n}{B}$ ratios, the value of C_2 must vary in inverse proportion to $\sqrt{2RD}$; i.e., in inverse proportion to the linear dimensions of the tire.

As experiments show, for most light and heavy-duty tires of unusual designation we can assume that

$$k_1 = 0{,}7 - 1 \text{ and } C_2 = \frac{1 - 1{,}4}{\pi\sqrt{2RD}}$$

It is advisable to use this approximate formula only in the absence of experimental data for tires close to the projected construction. If there are such data, we should determine C_2 by scaling. For example, let the value of C_2' be determined experimentally for a tire having dimensions R' and D' close to the projected configuration in terms of construction. Then for the projected tire we may assume

$$C_2 = C_2' \sqrt{\frac{R'D'}{RD}}$$

The coefficient C_1 in the above will be determined by the formula

$$C_1 = \frac{\psi_1}{\psi\psi_2 E} \cdot \frac{h}{\pi\sqrt{2RD}}$$

where ψ, ψ_1 and ψ_2 are dimensionless coefficients which are basically functions of the tread type and h is the tread thickness.

It is clear from this formula that for geometrically similar tires, for which the ratios $\frac{h}{\sqrt{RD}}$ are identical, the value of C_1 is not a function of the absolute dimensions of the tire. For a given type of tire this value varies within comparatively narrow limits. Thus for heavy-duty road tires it lies within the limits 0.001-0.002 cm^2/kg, while lower values correspond to tires with narrowly spaced treads, i.e., tires mounted on wide rims. For high roadability tires the coefficient C_1 is higher than for road tires and reaches values of up to 0.003-0.0035 cm^2/kg.

For four-ply light tires we can assume that C_1 = 0.0035-0.004

cm^2/kg and for six-ply tires $C_1 = 0.002$ cm^2/kg. With regard to the value of p_0 which characterizes the intrinsic rigidity of a tire in the absence of internal pressure, naturally it is primarily a function of the relative tire wall thickness and the rigidity of the materials. On the average for tires with variable internal pressure this value is approximately $p_0 = 0.3$ kg/cm^2. /117

For tires with particularly thin walls (for example four-ply 11.00-18 tires) the value of p_0 is about 0.15 kg/cm^2.

Stresses and Deformations Arising in Elements of a Rolling Tire

Due to the absence of sufficiently reliable methods for calculating the forces and deformations arising in elements of a rolling tire, an experimental investigation of these deformations is of great practical value.

The results of such an investigation allow us to establish the actual operating regimes of tire materials and consequently to determine the requirements which these materials must meet. They are also useful for choosing the testing regimes of materials and the laboratory test regimes of tires.

Investigations of the deformations of tire elements can also be used for comparisons of tires of various construction.

The study of the deformations of tire elements is accompanied by significant difficulties since the standard measuring equipment used to measure deformations of metallic components cannot be used. Rubber deformations in tires are relatively great, up to several tens percent, which precludes the possibility of the indirect use of wire resistance sensors.

Nor can the various types of lever measuring devices be used since these devices, which have a significant intrinsic rigidity and weight, introduce distortions into our initial distribution of deformations in the tire.

In the Scientific Research Institute of the tire industry experimental research on the deformation of tire elements has been conducted since 1950. Various types of deformation sensors were tested and measurements were made of the deformation of tire elements as a function of construction and usage factors.

A large portion of the results was obtained using two types of sensors.

Figure 94 shows a tensiometer which is a bracket made of a thin steel band. Wire resistance sensors are cemented on the horizontal plate of the bracket on both sides. These sensors are included in

adjacent arms of the bridge system. Needles with rubberized disks vulcanized to them are attached to the bracket to locate and hold the tensiometer. Two tubes are also attached to the bracket. In the apertures of these tubes special hooks are placed to hold the tensiometer in the outer cover. /118

A change in the distance between needles of the tensiometer causes the bracket to bend and a corresponding change in the resistance of the sensors which is recorded by the apparatus. Sensors of this construction have significant intrinsic mass which prevents us from using them for measuring a tire rolling at high velocity. In addition, the base of these tensiometers must be very small so that a change in the curvature of the tire wall will not exert an influence on them (in practice we used sensors with a base of 10 - 15 mm).

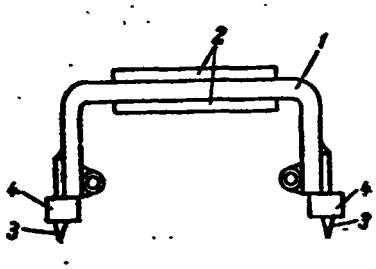

Fig. 94. A Tensiometer with Wire Sensors for Measuring Large Deformations: (1) Bracket; (2) Sensor; (3) Locating Needle; (4) Rubberized Disk.

The small base of the tensiometer increases the difficulty of orienting it in the proper directions with accuracy.

V. A. Pugin developed rubber wire sensors to measure large deformations which do not have the enumerated deficiencies [20].

The sensor (Fig. 95) is a rubber fiber with a thickness on the order of 1 mm to which a constantan wire is mounted. The wire is mounted on a prestretched fiber. When the fiber is relaxed its lateral dimensions increase and the wire becomes taut. This sensor is cemented onto the outer cover in the direction of the measured deformation and is deformed along with the material of the outer cover. The tension on the wire and consequently its electrical resistance varies. Using a measuring circuit the change in the resistance of the sensor is recorded on an oscillograph. Deformations can be measured both with static pressurization of the tire and when it is rolling. In the latter case the sensors are inserted through a collector.

As we know, to make a full determination of the deformed state at a point on the surface of the shell, we must know the linear deformations in any three directions. It is advisable to use for these directions the meridian, the circumference and the cord fiber direction.

To measure the deformations in a tire we usually orient the sensors in these directions. /119

They are cemented both on the external and internal plies of the outer cover carcass. In the latter case, the tire is mounted without a tube.

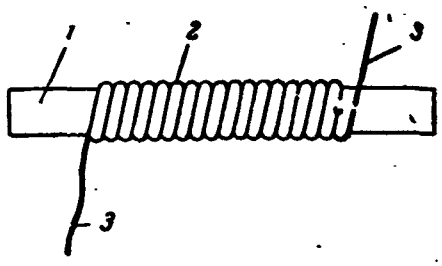

Fig. 95. A Rubber Wire Sensor for Measuring Large Deformations: (1) Rubberized Fiber; (2) Constantan Wire; (3) Leadout.

Reference [21] discusses in detail the results of measurements of deformations in tires of various constructions and under different conditions of inflation. Here we will discuss only briefly the overall character of the change in deformations of tire elements of ordinary construction with slow rolling along an even surface.

Typical examples are the curves of the change in deformations of 9.00-20 tires (8 plies of 13V cord; load of 1560 kg; internal pressure of 4.5 kg/cm^2) shown in Figure 96. Deformations were measured at 5 points along the tire profile (Fig. 97) while at each point three sensors were located, respectively, in meridian and circumferential directions along the cord fibers. The horizontal axis in Figure 96 shows the angle of rotation of the tire. The origin of the coordinates corresponds to the position of the sensor in the plane of symmetry passing through the midpoint of the contact surface.

The zone of noticeable deformations extended roughly 60° in each direction from the midpoint of the contact surface, which corresponds to a distance along the circumference equal to twice the width of the tire profile.

It is clear from Figure 96 that the curves for the change in meridian and circumferential deformations both in the internal and external plies of the outer cover have a characteristic shape with three extrema.

These extrema correspond to the position of the examined point in the vertical plane of symmetry and also in the planes forming angles of 20-25° with this plane and passing somewhat above the contact surface.

The deformation curves at the corresponding points on the internal (solid lines) and external (dotted lines) plies of the tire basically correspond to one another. An exception is the deformations at the edges of the contact surface.

Thus at the center of the contact surface the fibers of the internal ply expand by about 0.5% and the fibers of the external ply contract by about 3%. These values represent additional deformations undergone by the fibers when the outer cover is rolling. The initial fiber deformation caused by internal pressure, according to special

measurements, was about 2.2% (± 0.2%) for an 8-ply outer cover made of 13V cord. Thus the total deformation of the cord fibers at the midpoint of the contact surface is 2.7% in the internal ply (stretch) and 0.3% on the external ply (compression).

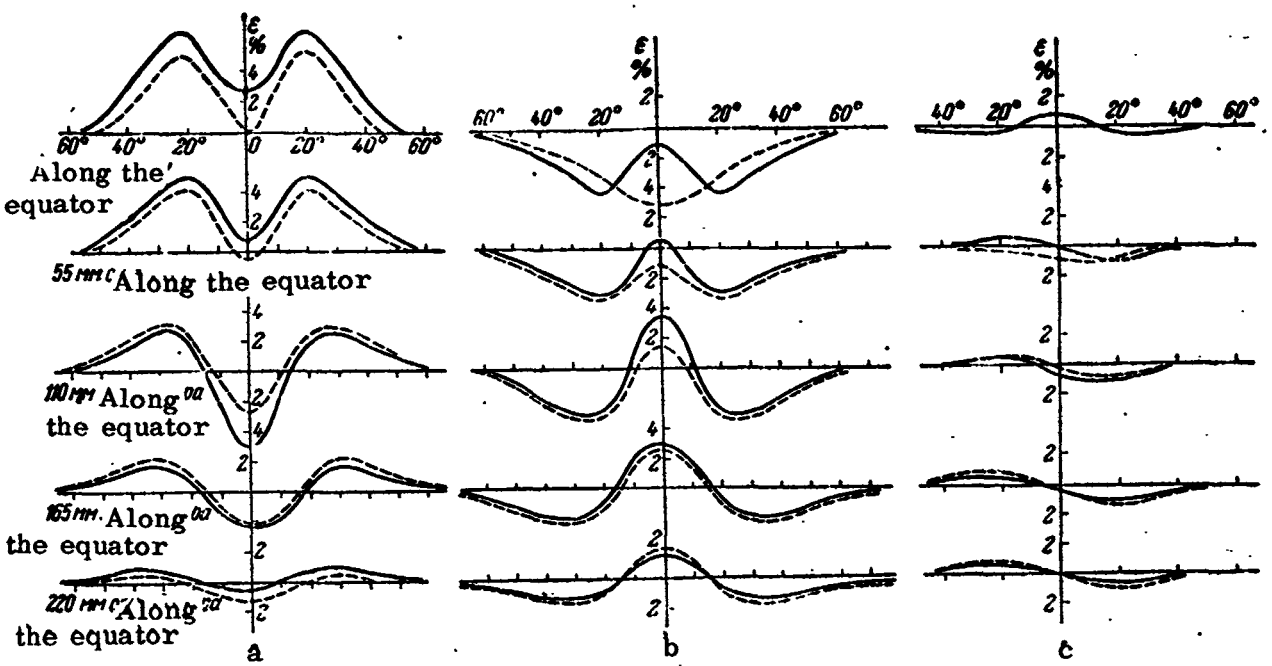

Fig. 96. Deformations of the Internal and External Plies of a 9.00-20 Tire in the Meridian (a), Circumferential (b) Directions and in the Directions of the Cord Fibers (c) as a Function of the Angle of Rotation of the Tire. /120

The difference between the deformation values in the internal and external plies is caused by a bend in the outer cover carcass. This bend plays a significant role in the zone of contact surface /121 ard its vicinity. Outside of this zone we can assume roughly that the deformations of the external and internal plies are identical.

A comparison between deformations in the circumferential and meridian directions shows that these deformations have different signs at all points.

An expansion in the meridian direction corresponds to a contraction in the circumferential direction and vice versa.

Thus, if we can imagine a rhombus formed by the fibers of adjacent cord plies, then an expansion of one of the diagonals of the rhombus corresponds to a contraction of the other diagonal.

Deformations of this type can take place, generally speaking, without a change in the length of the cord fibers if the following

relationship holds between the circumferential (ε_t) and meridian (ε_m) deformations [cf. equ. (14), p. 48]:

$$\varepsilon_t = -\varepsilon_m \cot^2 \beta$$

where β is the angle formed at a given point by the cord fiber and the meridian.

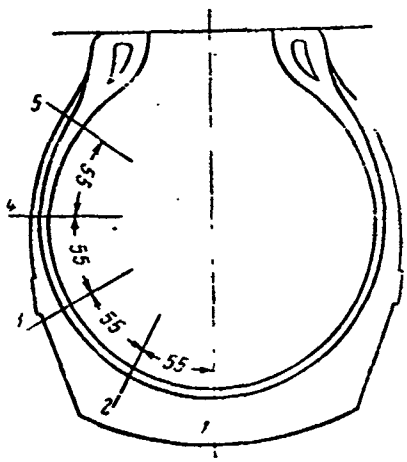

Fig. 97. The Position of the Points at Which the Sensors Were Located on the Tire Profile.

In outer covers with dimensions 9.00-20 the cord fiber angle varies roughly from 52° along the equator to 30-33° along the bead.

In conjunction with this if the cord fibers do not vary in length, then the ratio $\frac{\varepsilon_t}{\varepsilon_m}$ equals 0.7 along the equator, and at distances of 55, 110, 165 and 220 mm from the equator the ratio equals, respectively, 0.81, 1.15, 1.9 and 2.4. The actual ratios, which can be obtained from the graphs in Figure 96, are close to these values. Thus the values of the circumferential and meridian deformations indicate that the expansion of the fibers is insignificant. These data are substantiated by the results of the direct measurements of fiber deformation. As can be seen from Figure 96b, fiber expansions of a rolling outer cover along a plane are at all points less than 1% (2.2% above the initial expansion caused by internal pressure.)

Using the measured values of fiber deformation we can determine /122 the forces which arise in them.

To do this we should use the curves of cord fiber stretch (cf. Fig. 73, p. 80).

There is also the possibility, if we use the results shown on p. 51, to compute the value of rubber deformations in a ply. Since the base of the sensor covers several fibers, the circumferential and meridian deformations measured by the sensor are the average deformations of the ply. If we assume that the cord fibers are practically not deformed at all in comparison to the rubber, then the entire measured deformation value is obtained due to the change in dimensions of the rubber section between the fibers.

By relating the measured deformation to the dimension of the sections we can find the rubber deformation.

In this case the mean shift in direction of the fibers is

$$\gamma^* = (\varepsilon_m - \varepsilon_t)\sin 2\beta$$

and the maximum shift of the rubber between the fibers is

$$\gamma_{max} = \gamma^* \frac{t}{t-d}.$$

For 13V cord the caliber is d = 0.88 mm, and its step is t = 1.25 mm (80 fibers per 100 mm along the equator). Consequently the factor $\frac{t}{t-d}$ is equal to $\frac{1.25}{1.25 - 0.88} = 3.4$

Thus, for example, at the point on the equator at an angle of 20° to the vertical plane where the mean deformations in the internal ply constitute ε_m = 6.6% and ε_t = -4.6% and the cord fiber angle is β = 52°, the shift deformation in the rubber will be

$$\gamma_{max} = (6{,}6 + 4{,}6)\sin 104° \cdot 3{,}4 = 37\%.$$

The corresponding shift angle equals arc tan 0.37 = 20°.

In relation to the change in carcass fiber stretch in the deformation zone of the outer cover, the force transferred by the fibers to the bead rings in the lower parts of the outer cover also varies.

As can be seen from Figure 96c, deformations in the cord fibers in the sidewall zone vary asymmetrically relative to the plane passing through the midpoint of the contact surface. On one side of this plane deformations are very small (low additional stretch); on the other side the fibers undergo substantial contractions. This pattern is also true for plies of one direction (for example, odd). For criss-crossed plies (for example, even) the deformation pattern is a mirror image of the pattern shown in Figure 96c.

The change in the forces in the cord fibers transferred to the bead rings is shown schematically in Figure 98. Figure 98a shows the initial uniform stretch of a ring by two force systems in cord plies $N_1 = N_2$. In Figure 98b the forces in the cord fibers vary in relation to the action of radial load on the tire. In this case the force system N is unstable and equilibrium of the ring is maintained by pressure on the rim q. Due to this pressure the radial load is transferred to the rim. The transfer from the loads of Figure 98a to the load of Figure 98b can be seen as an addition to the ring of supplementary forces shown in Figure 98c and taking into account the action of radial load. It is easy to see that the supplementary forces cause additional tension in the lower part of the ring. Direct experiments measuring the stresses in the ring when the tire is rolling substantiate our statements. /123

When the tire is rolling deformations arise not only in the

plies of the outer cover but also in the rubber interlayers. The appearance of these shift deformations is caused by a difference between the work of various plies in the outer cover. Schematically, the appearance of these shift deformations can be explained by examining a radial cross section of an outer cover (Fig. 99a). When the outer cover is compressed the curvature of the carcass decreases in the contact surface. In conjunction with this, the inner plies are stretched much more intensively than the external plies (Fig. 99b).

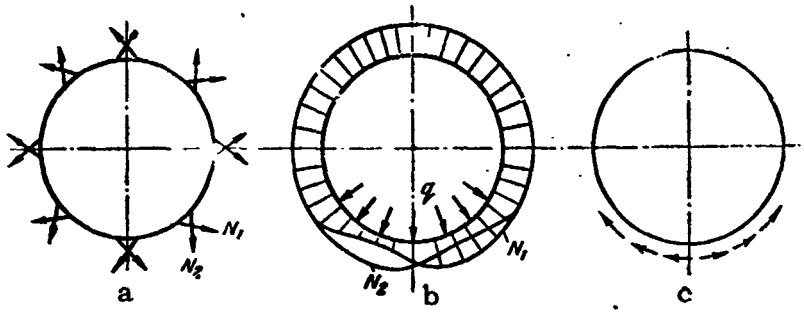

Fig. 98. Supplementary Load on the Bead Ring With Radial Compression of the Tire.

On the other hand, in the sidewall zone the external plies are stretched more intensely in relation to the increase in curvature. After examining the cross section (Fig. 99c) we can establish that the equilibrium of the internal and external plies individually is possible only in the presence of tangential stresses in the rubber interlayer which equalize the difference between the normal stresses along the equator and along the sidewall.

The problem of measuring shift deformations in the rubber interlayer of the tire as a whole has not yet been adequately solved. /124 Approximately, the change in shift deformations throughout the thickness of the carcass wall and along the profile can be obtained using sensors with a base of 3 mm located in the cross section of the outer cover. This cross section was established in a special piece of equipment which allowed us to maintain an internal pressure and to cause radial deformation. As can be seen in Figure 100a which shows the distribution of shift deformations throughout the thickness of the wall of a 210-20 outer cover, at the edges of the rolling part of the tire the maximum shift deformations arise in the breaker zone; on the sidewalls the greatest shifts are transferred to the central layers of the carcass

Figure 100b shows the distribution of shift deformations in the breaker along the profile of a 210-20 outer cover with a radial compression of 25 mm. It is clear from the graph that there is no shift in the center of the contact surface. They reach a maximum at the point lying opposite the boundary of the contact surface and

decrease again toward the sidewall of the outer cover. With an increase in the load on the tire, the shift maximum is transferred to the edge of the rolling part according to the increase in the dimensions of the contact surface. There is a simultaneous increase in the maximum shift deformations.

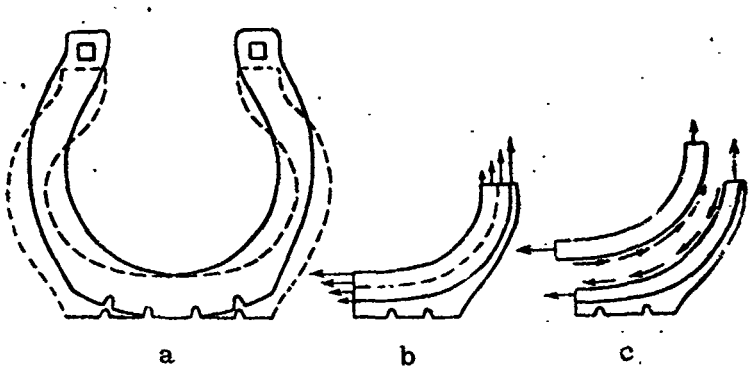

Fig. 99. Diagram of Shift Deformation in the Rubber Interlayer.

As can be seen from Figure 100b the maximum shift deformations in the breaker when the tire is compressed on the surface reach values on the order of 20%.

Of course, results obtained from the cross section rather than the tire as a whole can be examined only qualitatively.

We must note that this mechanism causing a shift deformation in relation to tire wall curvature is not unique. Significant shift deformations also arise due to the lateral effect when the tread is compressed in the contact zone. The tread section which is compressed by contact pressure tends to increase its dimensions in a lateral direction, but this is prevented by the more rigid breaker and carcass. Shifts of this type are maximum in the tread base ply, at the boundary between the tread and the breaker and in the breaker zone. /125

These shifts are especially significant when the tire is used on poor roads, when the tread undergoes very great local compression with concentrated loads. By action of shift deformations, separation of the tread or local separation of the cord fibers in the breaker from the rubber may arise, ultimately causing blowout.

We should examine individually the work of the checks and the tread base layer in the rubber tread.

The tread checks located at the edges of the contact surface between tire and the road are under normal contact pressure. In addition, shift forces arise in the contact surface. With a free rolling wheel these shift forces are small. They increase as the trac- /126

tion and b[illegible] forces exerted on the wheel increase. The maximum value of these forces does not exceed normal pressure multiplied by the coefficient of friction between the tread rubber and the road.

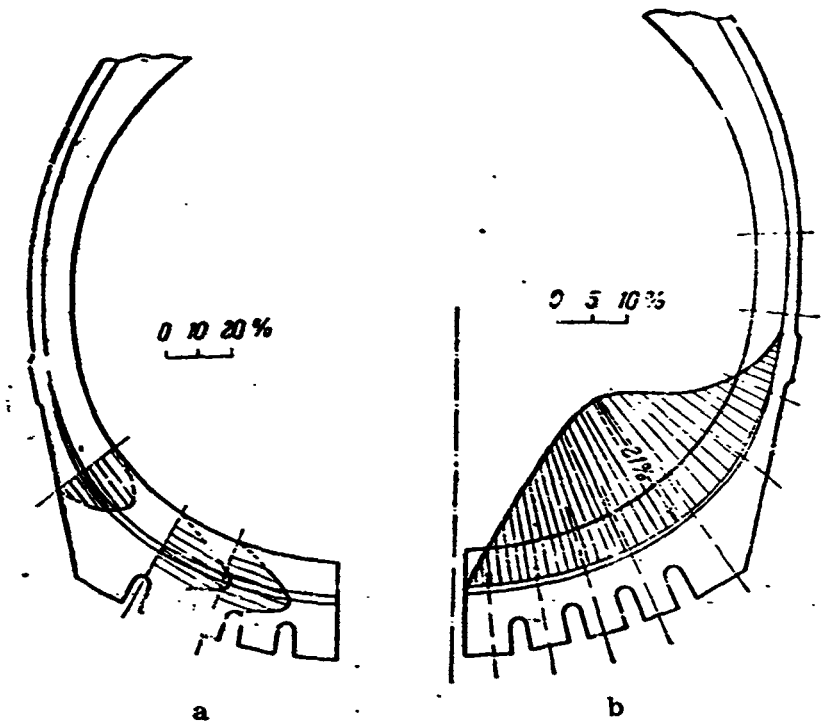

Fig. 100. Shift Deformations During Compression of a Cross Section of a 210-20 Tire: (a) The Distribution of Deformations over the Thickness of the Wall; (b) Change in Shift Deformations in the Breaker Zone Along the Profile.

The tread base ply is deformed as is the carcass of the outer covering and also undergoes forces transferred to it from the tread checks.

With transfer from the tread checks to the tread base ply, a significant deformation concentration arises at the curvature of the grooves.

The distribution of meridian deformations throughout the thickness of the tread is shown in Figure 101 (data were obtained by compression of a cross section). We can see from the graph that the meridian deformation at the bottom of the grooves is approximately four times greater than the deformation at the base of the checks.

Note the distribution of deformations over the height of the checks. At the base of the checks (at the tread base ply) there is a contraction in a meridian direction (in connection with the curva-

ture of the carcass). The extension in this direction near the contact surface with the road is explained by lateral deformation in relation to normal pressure on the check.

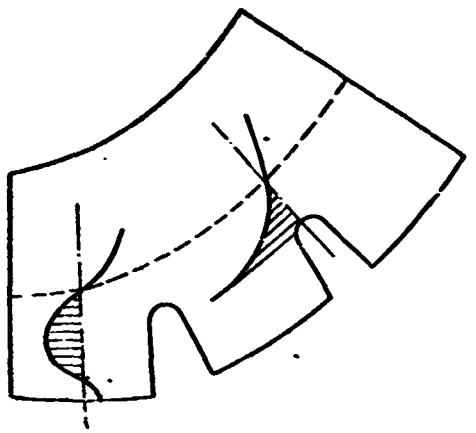

Fig. 101. Distribution of Meridian Deformation Throughout the Thickness of the Tread in the Contact Zone.

These data concerning the change in deformations in the plies of the outer cover when the tire is rolling along a surface show that deformations and stresses in the cord and rubber vary cyclically. The duration of the cycle corresponds to one revolution of the wheel.

Figure 102a shows characteristic curves for the change in the deformations of the cord. The characteristic curves of rubber deformation are given in Figure 102b.

The number of deformation cycles sustained by the material during the lifetime of the outer cover is very great. Thus, for example, the lifetime of a 260-20 tire must be about 80 thousand kilometers, and the rolling radius is R_{rl} = 0.485 m.

Thus, during its lifetime the tire makes

$$n = \frac{80 \cdot 10^3}{2\pi \cdot 0{,}485} = 2{,}6 \cdot 10^7 \text{ revolutions.}$$

Full deformation cycles are repeated the same number of times in elements of an outer cover. /127

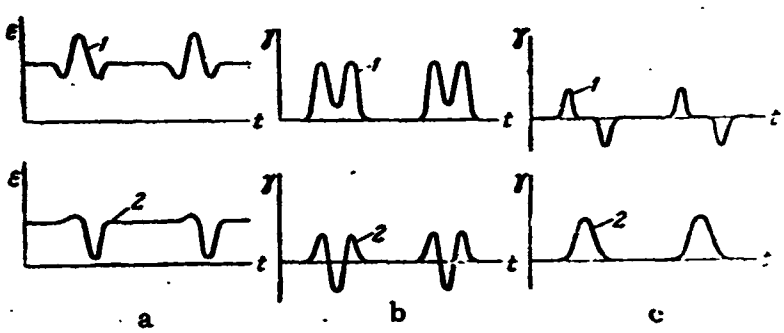

Fig. 102. Characteristic Deformation Cycles: (a) Fiber Deformation; (b) Shift Deformations of the Rubber in a Ply; (c) Shift Deformations of the Rubber Interlayer. (1) Along the Equator; (2) Along the Angle of the Rolling Part ε is the Deformation; t is Time.

These data concerning the deformation values of different elements refer to heavy-duty tires. Deformations undergone by elements of passenger automobile tires vary along curves of the same type during rolling.

The basic difference is that the cord fibers of light tires under normal operating regimes undergo substantial compression deformations in the sidewall zone. This is explained by the fact that for light tires the relative depression is greater than for heavy-duty tires.

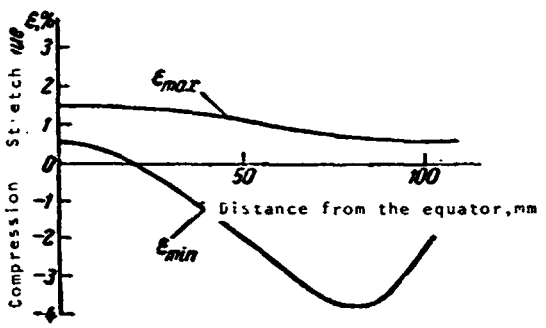

Fig. 103. Maximum and Minimum Deformations Undergone by the Fibers of the Profile. (For a 6.70-15 Tire, the Load is 480 kg, the Pressure 1.8 kg/cm^2).

As an example Figure 103 shows the graphs of change in the maximum and minimum deformations in the cord fibers of a 6.70-15 tire with a load of 480 kg and an internal pressure of 1.8 kg/cm^2. /128

Another difference is that shift deformations in the rubber interlayer and breaker of light tires are substantially less than in heavy-duty tires. This is explained by the smaller number of plies and lower internal pressure in light tires.

If the tire is moving along a rough road and hitting obstacles, significantly greater deformations and stresses arise in its element than if the tire were rolling on a smooth surface. In this case under these operating conditions the deformation cycles are different with each revolution of the wheel.

Fig. 104. Oscillograms of Deformations of Fibers When the Tire is Rolling Along Cobblestones (the Recordings Corresponding to Points of the Fibers on the Sidewalls and on the Equator Are Given Alternately; the Latter Are Indicated by the Letter *K*).

As an example Figure 104 shows oscillograms of cord fiber deformations along the equator and sidewall of a tire moving along cobblestone.

In this oscillogram the recordings of the sensors cemented on the equator and on the sidewall are given alternately; the cycles relating to the equator are marked by the letter *K*. The difference in deformation value with each cycle is determined by the shape and

value of the irregularities in the road, which are random.

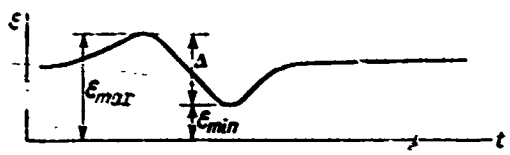

Fig. 105. The Cycle of Deformation Variation.

To evaluate the intensity of deformations on various roads under various conditions of usage we must use a statistical treatment of the experimental results.

The matter is complicated by the fact that no deformation cycle in the general case can be characterized by one particular value. Each cycle (Fig. 105) must be characterized by at least three values: the minimum and the maximum deformations ε_{min} and ε_{max}, and also the deformation range $\Delta = \varepsilon_{max} - \varepsilon_{min}$.

It is obvious that while it is not completely clear what influence each of these values has on the durability of these materials, /129 we must characterize the work of the material under these or other conditions by distribution (frequency) curves of all three parameters. Only at certain points where the deformation cycles are unidirectional (for example, the cord fiber along the sidewall), can we limit ourselves to one index of deformation intensities.

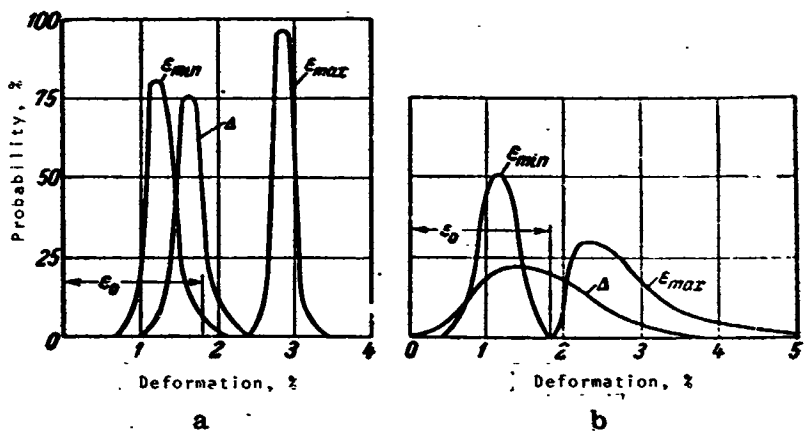

Fig. 106. Distribution Curves of Maximum Deformations (ε_{max}), Minimum Deformations (ε_{min}) and the Deformation Range (Δ) of the Cord Fibers of the First Ply Along the Equator of a 260-20 Tire on an Automobile Moving at a Velocity of 30 km/hr: (a) Along Asphalt Pavement; (b) Along Cobblestones.

Figure 106 shows distribution curves of maximum and minimum deformations of the cord fiber of the first ply along the equator of a 260-20 tire moving along asphalt and cobblestones at a velocity of 30 km/hr.

In our treatment of experimental data, all deformations were divided into groups of 0.35%. By probability we mean the ratio of

the number of cycles with deformations of ε_{min} or ε_{max}, lying within the limits of a given group, to the total number of cycles subject to interpretation.

It is clear from the graph in Figure 106 that under normal operating conditions (pressure of 4.5 kg/cm^2, load of 1560 kg) the cord fibers in the center of the rolling part of the tire remain in the stretch range with motion both along asphalt and along cobblestone. The distribution curves corresponding to asphalt pavement are very narrow. Practically speaking, all measured cycles lie within the limits of one group (1/3%). In this case the maximum fiber deformation reaches 3% stretch, the minimum reaches about 1% stretch.

The distribution curves corresponding to rolling along cobblestone pavement are "blurred". In addition to the significant number of cycles which are safer than those with motion along asphalt pavement, there are also cycles with very high maximum deformations of up to 5-5.5%. It is clear from these curves that the operating conditions of cord fibers along the equator with motion along cobblestones are significantly less favorable than with motion along asphalt. However, in order to evaluate these or other conditions on the basis of these distribution curves, the results of investigations of the fatigue strength of the material with routine pressurization must be available. /130

As we have already shown, the cord fiber on the sidewall undergoes only unidirectional deformations when rolling. Additional compression deformations are added to the initial stretch due to internal pressure ($\varepsilon \approx 1.5\%$). In this case with all cycles $\varepsilon_{max} = 1.5\%$. Figure 107 shows distribution curves for minimum deformations in the fibers.

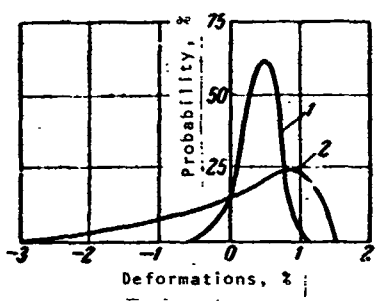

Fig. 107. Distribution Curves of Minimum Cord Fiber Deformations Along the Sidewall of a 260-20 Tire on an Automobile Moving at a Velocity of 30 km/hr Along Asphalt (1) and Cobblestone (2) Pavement ($\varepsilon_{max} = 1.5\%$).

The distribution curve shows that on an asphalt road the cord fibers along the sidewall remain in the stretch region only in 5% of the cycles, unloaded to zero.

On cobblestone in 20% of the cycles, the cord fibers undergo compression. The maximum compression deformation reaches 3%.

In the cord plies the rubber which fills the space between fibers undergoes shift deformations and stretch deformations in a direction perpendicular to the cord fibers (cf. p. 107).

The value of shift deformations in the rubber is related to the mean deformations of a ply in the circumferential

and meridian directions by the equation

$$\gamma = (\varepsilon_m - \varepsilon_t) \sin 2\beta \frac{t}{t-d}$$

In our road tests in order to get direct measurements of the value of $\varepsilon_m - \varepsilon_t$ we cemented onto the outer cover two sensors: one in a circumferential, the other in a meridian direction. These sensors were inserted into adjacent arms of the measuring bridge, and the responses of the measuring instrument were proportional to the difference $\varepsilon_m - \varepsilon_t$.

The curves for the change in the difference $\varepsilon_m - \varepsilon_t$ along the equator when the wheel is rolling have the characteristic form shown in Figure 108. Each cycle can be characterized by one value of maximum shift. /131

Fig. 108. An Oscillogram of Shift Deformations in a Ply Along the Equator.

Figure 109 shows distribution curves for the probability of maximum shifts of rubber in a ply along the equator when the automobile is moving at a velocity of 25 km/hr along asphalt and cobblestone roads.

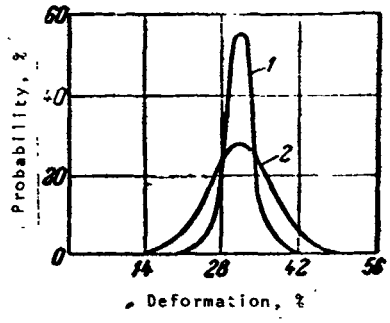

Fig. 109. Distribution Curves for the Probability of Maximum Shift Deformations of Rubber in a Ply Along the Equator When the Automobile is Moving Along Asphalt (1) and Cobblestone (2) Pavement.

For our calculations all deformations were divided into groups $\Delta\gamma = 3.5\%$. As can be seen from Figure 109 the influence of the road type on rubber deformations in a ply are less significant than the influence on cord fiber deformations.

The data obtained from our investigations made under road conditions concerning the deformations of tire elements must be taken into account when determining the technological requirements for materials and when developing laboratory methods for testing tires and tire materials.

Rolling Losses

Tire materials (cord and rubber) are not perfectly elastic. When they are deformed some of the work is irreversibly expended, i.e., transformed into heat. Therefore free rolling of a tire, during which its material undergoes cyclical deformations,

is accompanied by irreversible energy expense. This is manifested in the fact that a tire rolling along the surface at velocity v, with a vertical load force Q, must undergo an additional horizontal force P_f (Fig. 110). P_f is called the rolling resistance force.

It is clear from the conditions of wheel equilibrium that the resultant of the tangential forces in the contact surface is also equal to P_f and that the resultant of normal pressures, equal to Q, /132 is shifted relative to the center of the contact surface by a value a, so that

$$Qa = P_f R_c$$

The dimension a is called the radial reaction drift.

The ratio of the rolling resistance force P_f to the load on the wheel Q is called the rolling resistance coefficient χ.

$$\chi = \frac{P_f}{Q}$$

Sometimes as a characteristic of tire rolling losses, we introduce the value A_f (the work expended on one revolution of the wheel):

$$A_f = P_f \cdot 2\pi R_{rl}$$

where R_{rl} is the rolling radius of the wheel.

The value of rolling losses is a very significant tire characteristic, both from the point of view of the influence of a tire on the dynamics and economy of an automobile and from the point of view of the durability of the tire itself.

The power expended to overcome rolling resistance is a significant fraction of the total power of the automobile's engine. This power is totally transformed into heat, which leads to heating of the tire. Under unfavorable conditions the temperature in certain zones of the tire exceeds 100°C.

An increase in temperature in turn leads to a decrease in the durability of the rubber and cord and the strength of the seal between them. Therefore, the constructor must strive to decrease the rolling losses of the tire.

Since rolling losses are related basically to losses to internal friction in the rubber and cord[14], their value is a function of

---

[14] With motion along a smooth hard surface, losses to internal friction in the contact surface do not exceed 10% of the total losses.

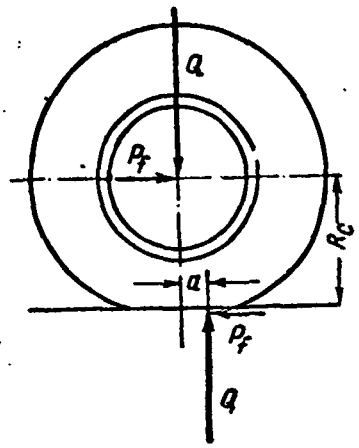

Fig. 110. The Forces Acting on a Wheel With Free Rolling.

the properties of these materials, their quantity and of the value of the deformations which they undergo.

Experiments show that up to half of /133 all losses take place on part of the tread. Therefore the hysteresis characteristics of the tread rubber are of primary importance.

Thus, reference [22] shows that for a 34 X 7 tire made completely of natural rubber, the coefficient of rolling resistance is $\chi = 0.008$ (velocity is 30 km/hr, established heat regime, the load is Q = 1200 kg, the initial internal pressure is $p = 5.75$ kg/cm^2). For the same tire but with a tread and carcass based on synthetic butadiene rubber, the coefficient of rolling resistance is increased to 0.014.

An increase in the load on the tire in connection with an increase in the deformations of these elements causes an increase in the absolute value of its rolling losses. However, the coefficient χ varies very little with load.

As the internal pressure in the tire decreases, its deformations and rolling losses increase. This is specifically demonstrated in Figure 111, which shows a function relating the rolling resistance force of a 9.00-20 tire and the initial internal pressure (with a load of 1560 kg, at a velocity of 50 km/hr).

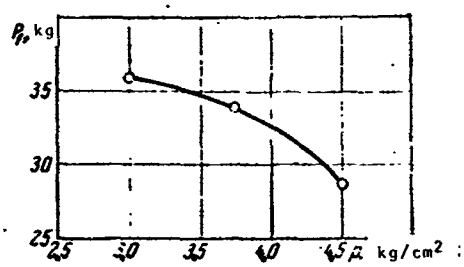

Fig. 111. The Rolling Resistance Forces of a 9.00-20 Tire as a Function of the Initial Internal Pressure.

If we determine the losses at a given tire temperature, as the rolling velocity increases the losses increase somewhat. However, if we conduct tests with an established temperature regime[15], then we can prove that as the velocity increases within known limits, the losses decrease somewhat. This is explained by the fact that as the velocity increases the tire temperature increases with an established regime, and as the temperature increases the hysteresis losses in the rubber and cord decrease.

With a subsequent increase in the rolling velocity above a certain particular value the losses again begin to increase sharply, which is related to the dynamic effects arising at high rolling velocities. These effects will be examined

[15]The temperature regime of the tire is determined every 1.5-2 hours of testing.

in detail below (cf. p. 127).

These data concerning losses refer to a tire rolling along a hard smooth surface. When the tire is moving along dirt we must add to the energy expended on internal friction in the tire material, the energy of deformation of the dirt and the formation of ruts. This energy is a function of the properties of the dirt, its state and the loads transferred to it by the tire. Thus, specifically, a decrease in internal pressure in the tire leads to a decrease in the pressure on the tire, a decrease in its deformation and, finally, /134
to a reduction in the energy expended on rolling (cf. Ch. V).

THE EFFECTS OF TRACTION, BRAKING, AND LATERAL FORCES ON A TIRE

Traction and Braking Forces

With the action of a drive moment M and the corresponding traction force [illegible] the wheel (Fig. 112), the operating conditions of the tire vary in comparison to free rolling.

Primarily this change affects the distribution of forces in the contact surface [23]. With free rolling (cf. Fig. 81, p. 94) the tangential forces in the contact surface are distributed almost symmetrically relative to the center of the contact surface and their resultant, equal to the rolling resistance force, is small in comparison to the radial force. With the action of a drive moment the distribution of tangential forces becomes asymmetrical and their resultant is equal to the traction force P. In this case in the median part of the contact surface the tangential forces increase, and in the trailing part they decrease; the zone of the contact surface in which the longitudinal tangential forces exerted on the tire act in the direction of motion is expanded. As the traction force in the leading part of the contact surface increases, the zone of slippage widens. At a certain maximum value of traction force, the slippage covers the entire contact zone and skidding occurs.

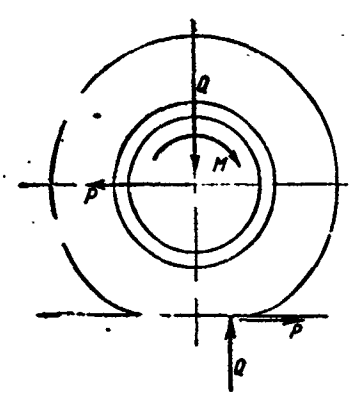

Fig. 112. The Forces Acting on a Drive Wheel.

The relationship between the rolling radius and the value of the traction force has the form shown in Figure 113. The small decrease in rolling radius, which is proportional to the traction force, in segment AB is explained by the increase in compression in a circumferential direction of the tread elements which comprise the contact surface (cf. Eq. (61), p. 91]. The sharp decrease in rolling radius in segment BC is due to skidding.

In certain cases, depending on the character of the road surface, segment BC of function R_{rl} (P) can be unstable (the dotted line in Fig. 113), since the incipient skidding leads to a decrease in traction.

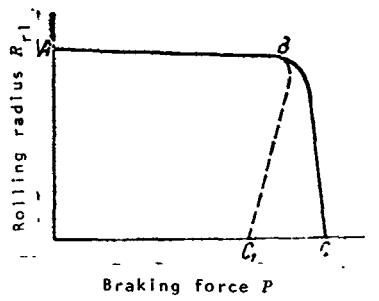

Fig. 113. The Rolling Radius as a Function of the Value of Traction Force.

The stresses and deformations in tire elements arising from the transfer of traction force have not been studied thoroughly enough. However, we can show that the additional forces in the cord fibers, caused by traction force, are small in comparison to the forces caused by internal pressure and radial force. The order of magnitude of these forces can be determined by dividing the traction force by the total number of cord fibers passing through the contact surface. The tangential forces in the tread and tread base zones, related to the transfer of traction force, are also small on a smooth road since their value is limited with motion at low transfers by traction with the road, and with motion at high transfers by the power of the engine. These forces may be very significant with motion along an uneven hard road, where concentrated normal and tangential forces arise. In a number of cases (in particular with motions along rocky ground) the concentrated tangential forces cause elements of the tread to strip away. An increase in the slippage of the tread elements in the contact zone with the action of traction force leads to accelerated (in comparison to free rolling) tread wear. /135

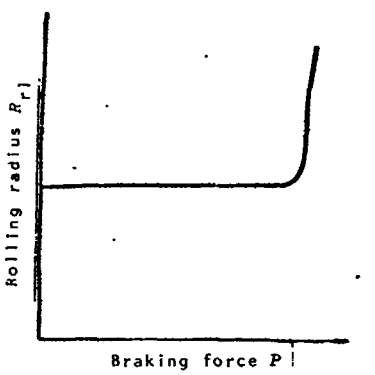

Fig. 114. The Rolling Radius as a Function of the Braking Force.

The phenomena which arise with the action of a braking moment and braking force on the wheel are similar to the phenomena which take place with the transfer of traction force. In this case, as the braking moment increases the tangential forces increase in the trailing part of the contact surface and that section of the contact surface widens in which longitudinal tangential forces exerted on the tire act in a direction opposite to motion. At the maximum value of braking moment, slipping covers the entire contact surface: a lock-skid occurs. As the braking force increases the rolling radius increases, and when a lock-skid occurs the rolling radius becomes indeterminate (Fig. 114).

Just as the traction force, braking force also leads to an increase in tread wear. In this case, with complete braking and lock-

skidding local wear occurs.

A significant characteristic of a tire is its circumferential pliability. For an experimental determination of the circumferential pliability of a tire, we add a torque M to the axle mounted on the bearings of a wheel loaded with a radial force Q. Thus the angle of rotation of the disk ϕ is recorded. Within a certain range of variation in M, before slippage begins, the function $M(\phi)$ is almost linear (Fig. 115). /136

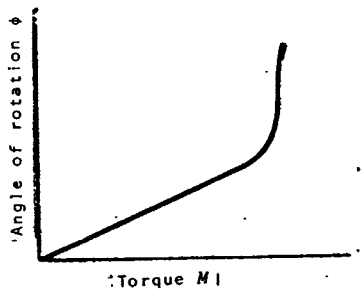

Fig. 115. The Curve of the Function Relating the Angle of Rotation of a Wheel and the Torque.

As a characteristic of circumferential pliability of the tire we use the ratio $\frac{\phi}{M}$ on the rectilinear section of the function $M(\phi)$.

Lateral Force

With the action of lateral force P_{lat} on a fixed wheel with radial force (Fig. 116a) the plane of the wheel shifts due to tire deformation on a certain segment f_{lat}. While the force P_{lat} is small and there is no slippage in the contact surface, the shift f_{lat} is directly proportional to the force P_{lat}. The ratio

$$\frac{f}{P_{lat}} = \lambda_{lat}$$

is called the lateral pliability (or lateral elasticity) of the tire. The contact surface of the tire varies in shape somewhat with the action of lateral force but remains symmetrical with respect to the lateral axis AA (Fig. 116b). In this case additional lateral tangential forces arise which are also symmetrical relative to axis AA. The resultant of these forces is equal to the lateral force P_{lat}.

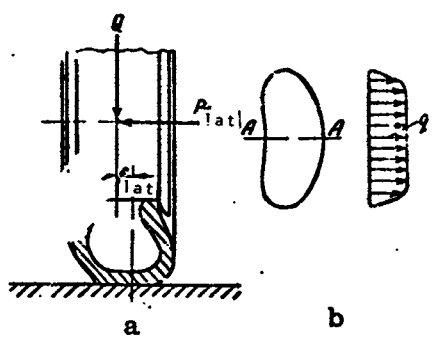

Fig. 116. The Action of a Lateral Force on a Fixed Wheel; (a) Character of Tire Deformation; (b) Contact Surface and the Distribution of Lateral Contact Forces

The matter is totally different with lateral force exerted on a rolling wheel. In this case, since the tread elements included in the contact surface are undeformed in a lateral direction, the intensity of the lateral tangential forces upon entry to the contact surface is equal to zero. These forces gradually increase as the lateral deformations increase when the element leaves the contact surface. /137

Thus the distribution of lateral contact forces remains asymmetrical relative to axis AA (Fig. 117). Tire deformations and the shape of the contact surface also remain asymmetrical. If, as shown in the figure, the lateral force acts on the

wheel from the right to the left, then with rolling each new tread element enters the contact surface more to the left than the corresponding preceding elements. As a result, the direction of motion of the wheel does not coincide with its plane of rotation and forms with it a certain angle θ (Fig. 117).

This phenomenon is called sideslip of a wheel and the angle θ is the angle of sideslip.

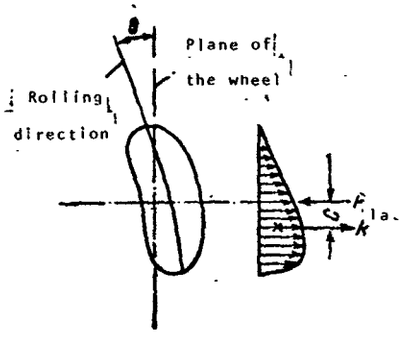

Fig. 117. The Contact Surface and the Distribution of Lateral Contact Forces with a Rolling Wheel Undergoing Lateral Force.

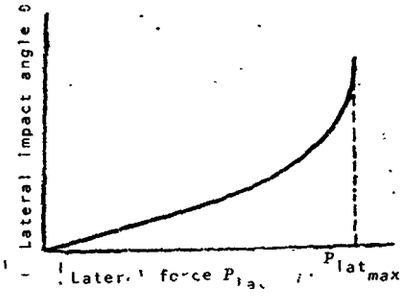

Fig. 118. The Sideslip Angle of the Wheel as a Function of the Lateral Force.

The sideslip of the wheels influences the handling and stability of a moving automobile to a great extent [24-26].

With the action of lateral force, slippage in the lateral direction takes place in the trailing part of the contact surface where the maximum tangential forces arise. As the lateral force P_l increases the zone of slippage widens, and at a certain maximum value $P_{lat_{max}}$, there is a lateral skid, i.e., the tire ceases to "hold the road". Figure 118 shows the characteristic curve of the function relating the angle of sideslip to the value of the lateral force.

Since the lateral contact forces in the trailing section of the contact surface are greater than in the leading section, the resultant of these forces R which is equal to P_{lat} (cf. Fig. 117), shifts backward relative to the midpoint of the contact surface. The moment $M_{st} = P_{lat}c$ which arises in this case tends to turn the plane of the wheel along the direction of motion; this moment is called the stabilizing moment. The relationship between the stabilizing moment and the angle of wheel slip has the form shown in Figure 119. A decrease in the stabilizing moment with large slip angles is accompanied by a widening of the slip zone and a corresponding decrease in the branch c of the lateral reaction. /138

These phenomena refer to a constant sideslip of the wheel when both the slip angle θ and the lateral force P_{lat} are constant over time.

In questions of handling and stability of the automobile, of great importance is the behavior of the tire with an unsteady regime of motion. Let us assume, for example, that the plane of the disk

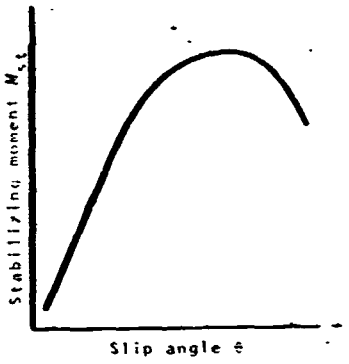

Fig. 119. The Stabilizing Moment as a Function of the Slip Angle.

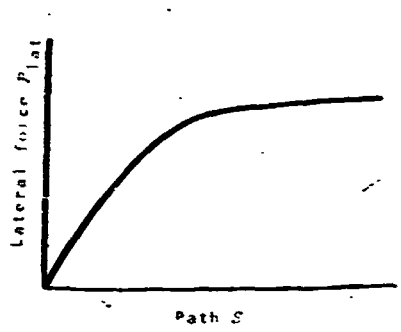

Fig. 120. The Lateral Force as a Function of the Path Traversed After Instantaneous Turn of the Wheel.

of a wheel rolling along a straight line is instantaneously turned by an angle θ. It is clear that in this case the corresponding lateral reaction P_{lat} does not arise immediately but only after a certain amount of time necessary to accomplish the lateral deformation of the tires. Figure 120 shows the function relating P_{lat} and the path S traversed by the wheel after an instantaneous turn of its plane.

Thus, for example, the force which causes the automobile to turn is generated only gradually after the steering wheel is turned. The question of unsteady regimes of rolling wheels with lateral forces has not yet been studied sufficiently.

The slippage which is generated with sideslip in the contact zone of the tire leads to accelerated tread wear. Therefore, to provide longevity of tires it is very important to decrease the lateral forces arising during usage. A decrease in these forces is possible when the automobile is operated properly, i.e., turns are made at /139 low velocities. Of great importance also is the proper alignment of the front wheels. With too high a degree of convergence the front wheels always move with a forced sideslip and the tires undergo intense wear.

From what we have said it follows that the resistance of the tire to lateral forces is of great importance for the motion of the automobile and also for the lifetime of the tire itself. It follows from the very nature of sideslip caused by the asymmetry of tire deformation that the greater the pliability of the rolling part of the tire, the greater the sideslip. The disintegration of the tread, an increase in its caliber and a decrease in the rigidity of the rubber lead to an increase in the sideslip.

The influence of the rigidity of the tire carcass on sideslip is very complex. Even with high lateral pliability of the carcass the slip angle can be small, since it is not the absolute value of the lateral depression of the tire which is important, but rather the difference in depressions upon entering the contact surface and leaving it.

If the tread base part of the carcass is sufficiently rigid (a strong breaker), then even with very pliable sidewalls (for example, type R tires) the slip will be small. In addition, an increase in the pliability of the carcass (due to low internal pressure or special construction) always leads to a less steady rolling regime with sideslip and, correspondingly, to a certain decrease in the quality of handling of the automobile ("heavy handling").

OPERATING CHARACTERISTICS OF TIRES AT HIGH ROLLING VELOCITIES

Stresses in Tire Elements Caused by Centrifugal Forces

When the tire is rotating rapidly, on each of its elements with mass dm there is exerted a radially directed centrifugal force equal to

$$dQ = dm\omega^2 r$$

where r is the distance of the element from the axis of rotation, ω is the angular rotational velocity of the tire.

Centrifugal forces cause a change in the shape of the tire profile. The external diameter increases and the profile width decreases, as is shown in Figure 121.

A calculation of the change in tire dimensions due to the action of centrifugal force is examined in [27]. This calculation, based on various methods for solving the equilibrium equations of a rubberized cord shell, is rather complex. We can assume approximately that an increase in the tire radius due to the action of centrifugal forces is proportional to their intensity and is equal to: /140

$$\Delta R = k\frac{q_0\omega^2 R}{p}B \qquad (71)$$

where q_0 is the mass/cm^2 of the rolling part; R is the external radius of the tire; B is its profile width; p is the internal pressure. The coefficient k varies with the relationship between the tire dimensions and with the mass distribution along its profile. It decreases with the rim width; the cord fiber angle along the equator and the cord rigidity increase. Experiments yield values within the limits of $0.1 < k < 0.2$ for various tires. Formula (71) can be used up to the value $\frac{q_0\omega^2 R}{p} \leq 0.5$; with large values of this number the increase ΔR decelerates.

We will now discuss those forces which arise in the tire carcass due to centrifugal forces. We will compile the sum of the projections on the axis of rotation of the tire of all forces acting on that part of the tire cut into cylindrical and conical cross sections (Fig. 122). It is easy to see that the centrifugal forces Q are not included in the equilibrium equations since they are perpendicular to the indicated axis. Therefore the equilibrium equation has the same form as for a nonrotating tire [f. Eq. (42), p. 63], and the intensity of the forces T_m is:

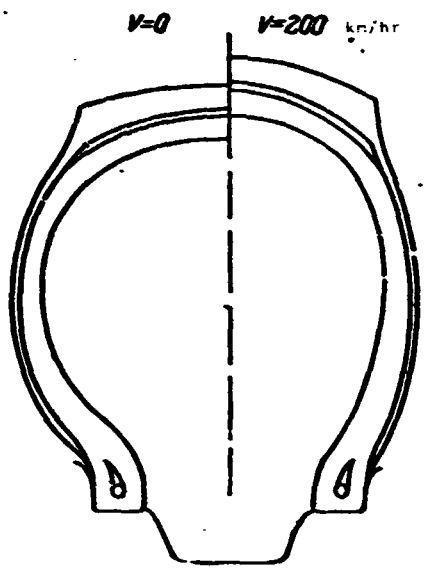

Fig. 121. The Equilibrium Profile of a 7.50-16 Tire at Zero Velocity and at a Velocity of 200 km/hr.

$$T_m = p\frac{r^2 - r_0^{*2}}{2r\cos\varphi^*}$$

where tne zero radius r_0^* and the angle ϕ^* between the normal and the axis of symmetry of the profile are taken for a tire deformed by centrifugal forces.

The force in the cord fiber N is:

$$N = \frac{T_m}{ni^*\cos^2\beta^*} = p\frac{r^2 - r_0^{*2}}{2rni^*\cos\varphi^*\cos^2\beta^*} \qquad /141$$

In particular for forces along the equator ($\phi^* = 0$, $r = R^*$, $\beta = \beta_c^*$, we obtain:

$$N_c = p\frac{R^{*2} - r_0^{*2}}{2R^* ni^*\cos^2\beta_c^*}$$

This formula differs from (53), which determines the forces in the cord fibers along the equator without rotation, only in that it includes the values R and r_0, as well as i_c and β_c, for a tire deformed by centrifugal forces.

Calculations show that in the majority of cases the value of the force in the cord fiber along the equator of tire varies only slightly with the action of centrifugal forces. In addition, centrifugal forces exert a great influence on the value of the forces in the cord fiber in the bead section of the tire and on the value of the forces in the bead rings.

However, since the initial forces due to internal pressure are significantly greater along the equator than in the bead section, at moderate rolling velocities the force in the cord fibers near the bead remains smaller than along the equator, and only at very high velocities does this force exceed the value of the force along the equator due to the addition of inertia.

Substantial difficulties [27] arise when determining the forces in the bead rings. However, we can estimate these values approximately based on the following arguments.

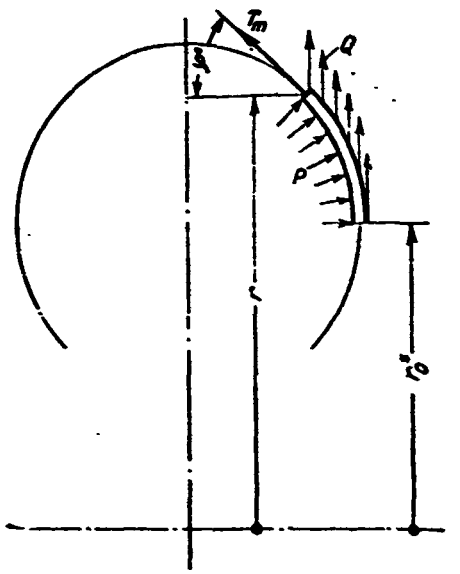

Fig. 122. Determining the Forces in the Cord Fibers Taking Centrifugal Forces into Account.

Let us examine the equilibrium of half the tire along the diameter (Fig. 123), taking into account only the additional inertial forces which arise when the tire is rotating and ignoring the change in the cross sectional area of the tire when it is deformed. Projecting all these forces on the normal to the cross section we find:

$$4P_i + 2\int_s T_t^i ds = \int\int_F r\omega^2 \sin\theta \, dm$$

where P_i is the inertial force in the bead; T_t^i is the intensity of the circumferential inertial force in the carcass; $r\omega^2 dm$ is the inertial force exerted on an element dm of mass of the tire. /142

Replacing $dm = qrd\theta ds$, where q is the mass/cm^2 of the tire wall, and integrating over θ from zero to π, we obtain:

$$4P_{i1} + 2\int_s T_t^i ds = 2\omega^2 \int_s qr^2 ds$$

where we integrate along the tire profile.

If in this formula we ignore the inertial forces in the cord fibers in comparison to the forces in the bead rings[16], we obtain:

$$P_{i1} = \frac{\omega^2}{2}\int_s qr^2 ds \qquad (72)$$

To compute the integral we may use any numerical or graphic method. Thus, if we assume that the specific weight of the cord plies is equal to the specific weight of the rubber γ, then

$$q = \frac{\gamma}{g} t$$

[16] As we have already shown, the inertial forces in the fibers of the rolling part are insignificant; ignoring these forces in the remaining part of the carcass leads to an exaggeration of the forces in the rings and thus provides a safety factor.

where t is the thickness of the tire wall at a given point; g is the acceleration of the force of gravity. Then

$$\int_s qr^2 ds = \frac{\dot{\gamma}}{g} I_0$$

where $I_0 = \int_s r^2 t ds$ is the moment of inertia of the cross sectional area of the tire relative to the axis of rotation, which can be computed by subdividing the cross section into simple figures.

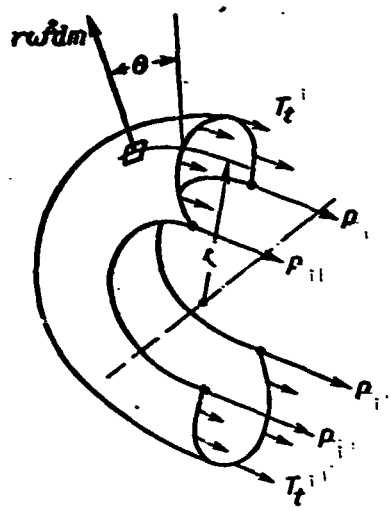

Fig. 123. The Inertial Forces Acting on Half a Tire.

We can also use the equation

$$\int_s qr^2 ds = \frac{m}{4} R_{cg}$$

where m is the total mass of the tire, R_{cg} is the distance from the axis of rotation to the center of gravity of half the tire.

Roughly[17]

$$R_{cg} = \frac{2}{\pi} R_{lat} \frac{1 + \frac{2}{3}\frac{q_2}{q_1}\cdot\frac{R_{lat}^2 - r_{rim}^2}{R_{lat}^2}}{1 + \frac{q_2}{q_1}\cdot\frac{R_{lat}^2 - r_{rim}^2}{R_{lat}^2}} \qquad /143$$

The dimensions included in this formula are shown in Figure 124; q_1 and q_2 are the mean mass of a unit area of the rolling part in sidewalls of the tire, respectively. With similar densities of the cord plies and the rubber the ratio q_2/q_1 can be replaced by the ratio of the average thickness of the sidewall and the rolling part of the tire. Other formulas can also be used to compute R_{cg}.

The value of the inertial force on the ring P_i must be added to the force caused by internal pressure and the tightness of the seal.

If we know P_i we can also estimate approximately the additional inertial forces in the cord fibers in the rim zone $N_{i\ rim}$. Actually, intensity of the meridian force T_m^i is related to the force in the ring P_i and with $N_{i\ rim}$ by the following expression:

$$T_{mi} = N_{i\,rim}(ni)_{rim}\cos^2\beta_{rim} = \frac{P_{i\,i}}{r_{rim}}$$

[17] To derive this formula one should replace the outer cover contour with a rectangle.

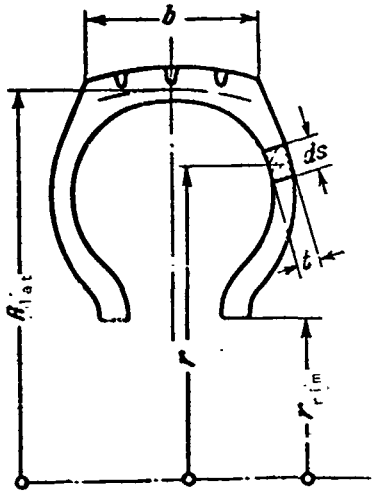

Fig. 124. Determining the Inertial Forces in the Bead Rings.

and thus

$$N_{i|\,rim} = \frac{P_{i|}}{r_{rim}\,(mi)_{rim}\cos^2\beta_{rim}}$$

Critical Rolling Velocity of a Tire

As the rolling velocity of a pneumatic tire increases to a certain limit its rolling conditions vary. Rolling losses sharply increase and waves arise on its surface which are fixed in space but move with the rolling velocity relative to the tire material.

The velocity at which a sharp change in the rolling conditions of the tire takes place is called the critical velocity.

A very thorough experimental study of critical velocity was made. As an example, Figure 125 shows photographs of a 7.50-16 tire rolling along the drum of a test assembly at velocities of 50, 150, 200 and 250 km/hr. We can see from the figure that at a velocity of 150 km/hr a wave arises on the surface of the tire after leaving the contact surface. As the velocity increases further the amplitude of the vibrations and the number of different waves increases and the wavelength also increases.

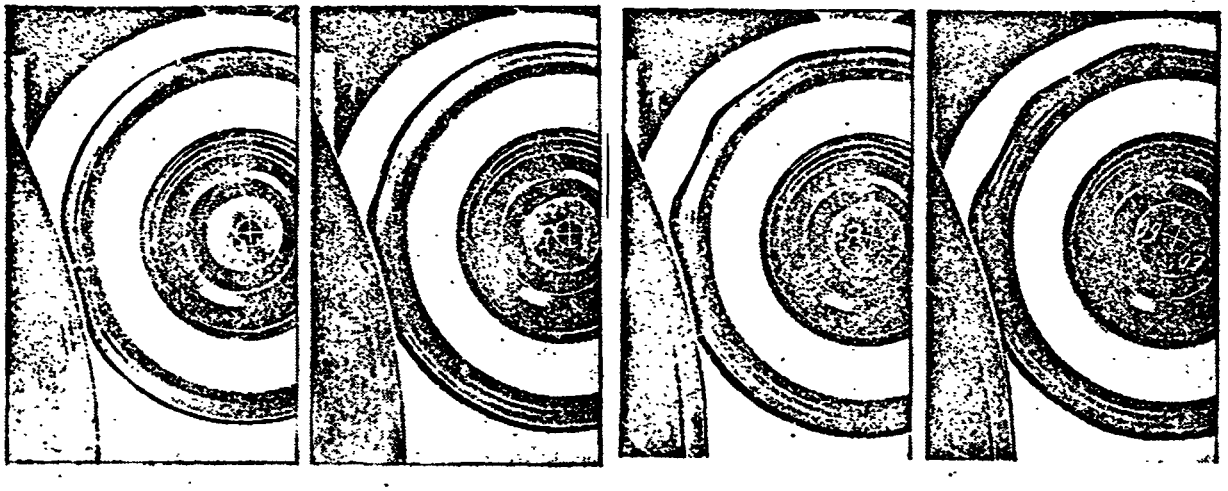

a b c d

/144

Fig. 125. A 7.50-16 Tire Rolling Along a Rolling Drum at Velocities (in km/hr): (a) 50; (b) 150; (c) 200; (d) 250 km/hr (The Load is 720 kg, Pressure 1.5 kg/cm^2).

Figure 126 shows the change in rolling losses of the same tire /145
[22]. At low rolling velocities the coefficient of rolling resistance varies very little with velocity, but beginning from a certain velocity, these losses increase very quickly and by many factors.

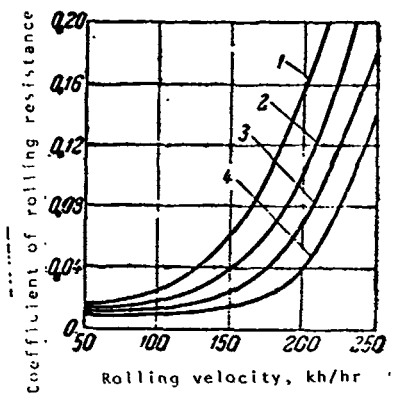

Fig. 126. Rolling Losses of a 7.50-16 Tire as a Function of Velocity: the Internal Pressure p (in kg/cm^2) Is: (1) 1.5; (2) 2.5; (3) 3.5; (4) 5.

The value of the velocities at which the rapid increase in losses begins becomes greater as the internal pressure in the tire becomes greater. As this velocity increases the distribution of force in the contact zone and deformation of tire /146
elements vary. Figure 127 shows the pressure curves in the contact surface of a 7.50-16 tire at various rolling velocities. A comparison of the curves shows that as the rolling velocity increases, the length of the contact surface increases. The pressure as the tire element enters the contact surface increases and decreases as the tire element leaves the contact surface. At a velocity of 180 km/hr there is a sharp pressure peak when the tire element enters the contact surface, and the pressure curve drops completely when the tire element leaves the contact surface.

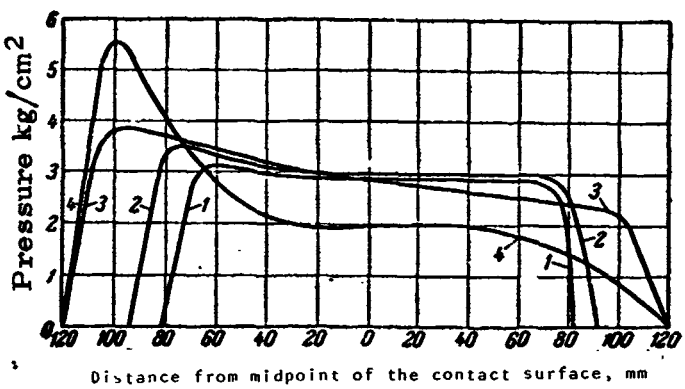

Fig. 127. The Pressure Distribution Along the Longitudinal Axis of Symmetry of the Contact Surface of a 7.50-16 Tire at Various Rolling Velocities (the Load is 785 kg, Pressure Is 2.5 kg/cm^2). The Rolling Velocity (in km/hr) Is (1) 25; (2) 100; (3) 150; (4) 180.

The curve of the change in the deformation of tire elements as a function of the rolling velocity can be seen for example in Figure 128. This figure shows oscillograms of the meridian deformation of the external ply of a 7.50-16 tire at 50 mm from the equator taken at various rolling velocities. At low velocities (up to 100 km/hr) deformations are practically invariable with rolling velocity. With an increase in velocity above 140 km/hr the amplitude of the deformation sharply increases and the shape of the curve varies; i.e., as tire elements leave the contact surface there are additional vibrations. At these same velocities the wave on the surface of the rolling tire becomes discernable.

In general, with an increase in rolling velocity the lifetime of the tire decreases, which at moderate velocities is mainly related

to an increase in the tire temperature and the corresponding decrease in the strength of the tire material. As the rolling velocity approaches critical level, the decrease in lifetime becomes especially sharp and in the presence of waves the lifetime of the tire is usually measured in minutes. The decrease in the lifetime, in this case, /147

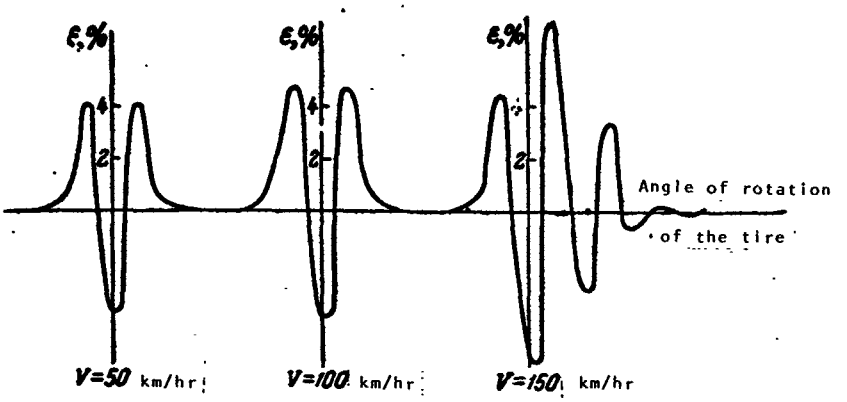

Fig. 128. Meridian Deformations of the External Ply of a 7.50-16 Tire (50 mm from Equator) at Various Rolling Velocities (Load 400 kg; Pressure 1.5 kg/cm^2).

is explained by the sharp increase in amplitude of tire element deformation. A basic reason for the destruction of the tire at high velocities is the separation of the tread layer.

The phenomena which arise at a critical velocity limit the opportunity to use tires at high velocities. Therefore for racing cars and planes it is necessary to develop special tires with as high a critical velocity as possible.

It was established in [14] that the critical velocity of a tire is the velocity at which deformations are propogated along its circumference.

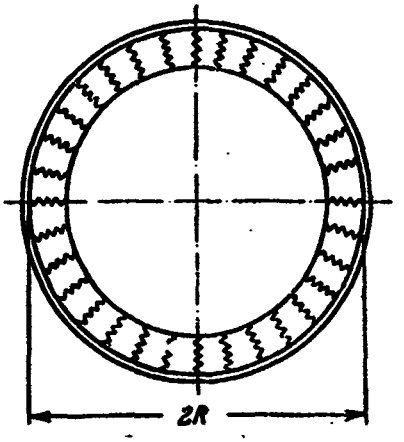

Fig. 129. Dynamic Model of a Tire.

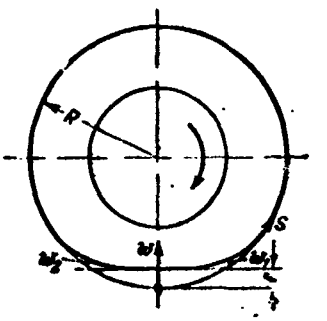

Fig. 130. The s, w Coordinate System.

In view of the complexities involved in theoretical investigation of the rolling of a real tire, to determine the basic characteristics of its behavior at high velocities it is expedient to examine its simplest model.

We can use as such a model (Fig. 129) an elastic elongated ring with distributed mass, lying on a solid elastic base [8]. The ring represents the rolling part of the tire and the elastic base replaces the sidewalls of the tire. We assume also that radial shift in the ring is related to damping.

Such a ring is a very simple mechanical system and its behavior when rolling can be computed in full.

If we relate to this ring a progressively moving coordinate system (Fig. 130) taking arc s from the midpoint of the contact surface and taking the positive direction as toward the rolling part of the tire then we can show [28] that depressions w in the ring can be described by the differential equation /148

$$(T-\mu v^2)\frac{d^2w}{ds^2}+k_1\frac{dw}{ds}-kw=-q \qquad (73)$$

where T is the stretching force in the ring, μ is the mass per unit length, v is the rolling velocity; the coefficient k_1 characterizes the damping, k characterizes the rigidity of the elastic base. The intensity of the external force q is nonzero only within the limits of the contact surface; outside this zone $q = 0$.

Therefore, everywhere except the contact zone, depression of the model can be determined by the uniform equation

$$(T-\mu v)^2\frac{d^2w}{ds^2}+k_1\frac{dw}{ds}-kw=0 \qquad (74)$$

A partial solution to this equation can be given in the form

$$w=e^{cs}$$

Substituting this expression in the equation and cancelling e^{cs}, we obtain a quadratic equation for determining the coefficient c

$$(T-\mu v^2)c^2+k_1c-k=0$$

from which we find two values for c:

$$c_1=-\frac{\sqrt{k_1^2+4k(T-\mu v^2)}+k_1}{2(T-\mu v^2)}$$

$$c_2=\frac{\sqrt{k_1^2+4k(T-\mu v^2)}-k_1}{2(T-\mu v^2)}$$

While the rolling velocity v is small the value of c_1 is negative and the value of c_2 is positive; consequently equation (74) has two solutions, decreasing as the arc s increases:

$$w_1 = Ae^{c_1 s}$$

and increasing as it increases:

$$w_2 = Be^{c_2 s}$$

A and B are constants which can be determined from the condition of the contingency of the free part of the model and the contact zone.

To describe deformations we need only the solutions which decrease with distance from the contact zone. Therefore deformations in the rolling part (before entering the contact zone), where $s > 0$, are determined by the expressions w_1 and after leaving the contact zone, where $s < 0$ are determined by the expression w_2. As the rolling velocity v increases the value of $T - \mu v^2$ decreases and the values c_1 and c_2 increase in absolute value. With $v > \sqrt{\frac{T}{\mu}}$ both coefficients become positive. In this case (74) does not have solutions which decrease as s increases which can be used to describe ring deformations before entering the contact zone. /149

The absence of the solution indicates that the rolling part of the ring with $v > \sqrt{\frac{T}{\mu}}$ remains undeformed. The velocity

$$v_{cr} = \sqrt{\frac{T}{\mu}} \qquad (75)$$

is the velocity at which waves are propagated around the ring (this velocity of wave propagation is measured along a string stretched with force T with a mass per unit length μ).

If the rolling velocity is greater than v_{cr} then the material of the ring will move more rapidly than deformation caused by force exerted in the contact zone can be propagated through it.

For just this reason in this case the ring before entering the contact zone remains undeformed.

With a small increase in velocity above the critical level, both coefficients c_1 and c_2 become complex with positive real components:

$$c_{1,2} = \alpha \pm \beta\sqrt{-1}$$

where

$$\alpha = \frac{k_1}{2(\mu v^2 - T)}; \qquad \beta = \frac{\sqrt{4k(\mu v^2 - T) - k_1^2}}{2(\mu v^2 - T)}$$

In this case (74) has the solution

$$w = e^{\alpha s}(A\cos\beta s + B\sin\beta s)$$

describing the damping waves after leaving the contact zone.

An importa t rolling characteristic of the ring at a velocity above the critical level is the presence of a concentrated shock force P_j upon entering the contact surface (Fig. 131a). This force arises as a result of a drastic change in the direction of motion of the material upon entering the contact surface.

It is easy to determine the value of the force P_j by examining the change in momentum of a small part of the ring upon entering the contact zone (Fig. 131b). During time dt this section shifts its position, as shown by the dotted line, in relation to which the vertical components of its momentum de-reases by a value $\mu v dt \sin\phi$. The vertical projection of the impuls_ of the forces exerted on the section during the same time is

$$(P_j + T\sin\varphi)dt$$

Equating the change in momentum to the impulse of the force, we find /150

$$P_j = (\mu v^2 - T)\sin\varphi$$

and finally, expressing $\sin\phi$ in terms of the depression f and the external radius of the model R ($\sin\phi \approx \sqrt{\frac{2f}{R}}$), we obtain:

$$P_j = T\left(\frac{v^2}{v_{cr}^2} - 1\right)\sqrt{2\frac{f}{R}}$$

The shock force P_j yields relative to the axis of the model the moment:

$$M_j = P_j a \approx T\left(\frac{v^2}{v_{cr}^2} - 1\right)2f$$

This moment, which prevents the rolling of the model, increases quickly as the velocity above critical increases.

The solution to differential equation (73) taking into account boundary conditions (given depression in the contact zone) allows us to find the change in shape of the model of the specific pressures in the contact zone and the rolling resistance [28].

This calculation was made with the following data: R = 40 cm,

T = 720 kg; k = 14.7 kg/cm^2, k_1 = 18 kg/cm, μ = 40·10^{-6} kg·sec^2/cm^2.

These values were chosen so that at low velocity the model with a depression f = 23 mm would undergo a load of 780 kg with a contact

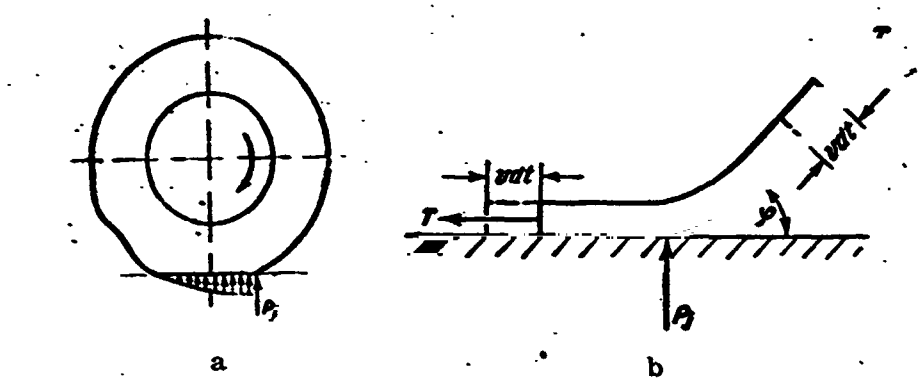

Fig. 131. Shock Reaction P_j Upon Entering the Contact Surface (a); Computing the Shock Reaction (b).

zone of length 165 mm and a coefficient of rolling resistance χ = 0.01. These numbers correspond to a rolling 7.50-16 tire with an internal pressure of 2.5 kg/cm^2. The value of μ was assumed equal to the real mass of the material of this tire within the limits of 1 cm of length of the rolling part. With these data the critical velocity is:

$$v_{cr} = \sqrt{\frac{T}{cr}} = 4.24 \cdot 10^3 \text{ cm/sec} = 152.5 \text{ km/hr}$$

The calculated configuration of the model with zero velocity and with velocity v = 175 km/hr which exceeds the critical velocity by 15% is shown in Figure 132. Figure 133 shows the calculated function relating the coefficient of rolling resistance to velocity. The rapid increase in this coefficient at velocities exceeding critical velocity is explained mainly by the presence of shock force upon entering the contact surface[18]. /151

The close correlation in the shape of the curves for the coefficient of rolling resistance and also the shapes of the waves when rolling at supercritical velocities for the model and for a real tire leave no doubt that in both cases the nature of the critical velocity is the same. The critical velocity is that velocity at which free vibrations are propagated along the circumference of the tire.

---

[18] It is interesting to note that losses related to the shock force do not depend at all on the internal friction in the material. They have a purely inertial character. The energy expended on overcoming the shock force is thus diffused with free vibrations of the elements after leaving the contact surface.

The model of a tire in the form of an elastically supported ring is very convenient to clarify the qualitative picture of those phenomena which take place at critical velocity. It can also be used for an approximate calculation of the critical velocity of a tire. To do this we should only calculate the force which stretches the ring of the rolling part of the tire, the mass of 1 cm of length and base our calculations on formula (75).

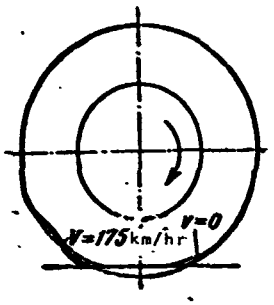

Fig. 132. Computed Configurations of a Model with v = 0 and with v = 175 km/hr.

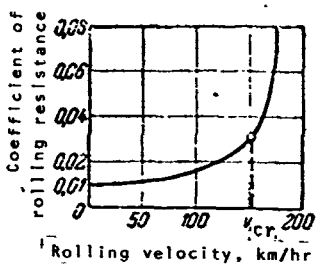

Fig. 133. The Coefficient of Rolling Resistance as a Function of Rolling Velocity for the Model.

The intensity of the meridian force T_m at any point in the tire is determined by formula (50)

$$T_m = \frac{p(R^2 - r_0^2)\cos\beta_c}{2r\cos\beta}$$

The intensity of circumferential force T_t is related to T_m by formula (43): /152

$$T_t = T_m \tan^2\beta = \frac{p(R^2 - r_0^2)\cos\beta\tan^2\beta}{2r\cos\beta}$$

T_t is the force exerted on a unit length of a lateral cross section of the carcass. The total force exerted on the part of the carcass beneath the rolling part of the tire is:

$$T = \int_b T_t ds$$

where the integral is taken along the width of the rolling part.

Since the values of r and β vary very little along the rolling part, we can replace T_t by its value on the equator ($r = R$, $\beta = \beta_c$):

$$T_{tc} = \frac{p(R^2 - r_0^2)}{2R}\tan^2\beta_c$$

and the value of the force T is

$$T = T_{tc}b = \frac{p(R^2 - r_0^2)}{2R}\tan^2\beta_c b$$

The mass per unit length of the rolling parts in turn can be calculated according to the formula

$$\mu = q_{ave} b$$

where q_{ave} is the average mass pertaining to 1 cm^2 of the surface of the rolling part. Thus the critical velocity[19] is:

$$v_{cr} = \sqrt{\frac{T}{\mu}} = \sqrt{\frac{p(R^2 - r_0^2)}{2Rq_{ave}}} \tan \beta_c \qquad (76)$$

Approximate formula (76) shows that the critical velocity is directly proportional to the square root of the ratio of the internal pressure in a tire to the specific mass of the rolling part and is proportional to the tangent of the cord fiber angle along the equator and the square root of the linear tire dimension.

In (76) we assumed that the elasticity of the tire is caused only by the presence of its internal pressure, and we did not take into account the rigidity of the rubber. Therefore, the formula is sufficiently accurate only for tires with high internal pressure. For tires with low internal pressure we must take into account the rigidity of the rubber and the rigidity of the walls during the curvature. Methods for an approximate calculation of these factors are examined in detail in references [29, 30]. /153

The final computed formula can be given in the form

$$v_{cr} = \sqrt{\frac{p(R^2 - r_0^2)}{2Rq_{ave}} (\tan^2 \beta_c + 2\sqrt{ac})} \qquad (77)$$

where

$$a = 2 \tan^2 \beta_c + \frac{4Gh_{red}}{pR} (1 + \tan^4 \beta_c - \tan^2 \beta_c)$$

$$c = \frac{A}{\rho R^3} \cot^4 \beta_c$$

$$\rho = \frac{R^2 - r_0^2}{2R}$$

G is the dynamic shift modulus of the rubber, h_{red} is the reduced thickness of the tire wall determined as a function of the actual thickness of the wall[20] along the equator h, the number of cord plies n and the cord caliber d according to formula (19)

$$h_{red} = h + nd(K - 1)$$

where K is found from the graph in Figure 51 for formula (17). The

---

[19] It is interesting to note that the obtained formula in the particular case of small tire curvature (r_0 differs very little from R) and the absence of fastening on the rim coincides with the precise formula which determines the rate of wave propagation along a straight, rubberized cord sleeve [29].

[20] Thickness h is measured without taking into account the ridges of the tread.

value of A characterizes wall rigidity during curvature. If the wall has n cord plies then assuming that the neutral axis during curvature passes through the center of the cord plies, we find:

$$A = E_c \Sigma i y^2 \sin^4 \beta + \frac{4}{3} G (h_1^3 + h_2^3)$$

where i is the cord fiber frequency, E_c is the dynamic elasticity modulus of the fibers (in kg/fiber), $\Sigma i y^2$ is the summation of the products of fiber frequency and the square of the distances of all cord plies from the neutral ply, h_1 and h_2 are the distances of the neutral ply from the external and internal surfaces of the wall.

Let us examine now an example of calculation based on our formulas for the critical velocity of a 6.00-16 racing tire with an internal pressure of 2.5 kg/cm^2.

The equilibrium configuration of this tire is characterized by an equator radius along the first ply of the carcass R = 348 mm and a zero radius r_0 = 280 mm. The cord fiber angle along the equator β_c = 54°. The tire carcass has four plies of kapron cord with a fiber frequency along the equator of 12.9 fibers/cm. The breaker is two-ply with a frequency of 9.4 fibers/cm. The thickness of the cord fibers is d = 0.6 mm. The static elasticity modulus of the fiber, i.e., the ratio of the force increment to the deformation increment near the initial static force N = 1 kg is E_c^{st} = kg/fiber. The dynamic modulus is estimated at

$$E_c = 1.25 E_c^{st} = 75 \text{ kg/fiber}.$$

The static shift modulus for rubber G^{st} = 20 kg/cm^2. We will use as a dynamic modulus G = 1.25 G^{st} = 25 kg/cm^2. We can find the mass per unit area of the rolling part of the tire starting from an average thickness of the rolling part of 10 mm and a specific weight of the material $\gamma = 1.15 \cdot 10^{-3}$ kg/cm^2: /154

$$q_{ave} = \frac{1 \cdot 1.15 \cdot 10^{-3}}{981} = 1.17 \cdot 10^{-6} \text{ kg} \cdot \text{sec}^2/\text{cm}^3.$$

We can find the reduced thickness of the tire wall as follows:

$$h_{red} = h + n_1 d (K_1 - 1) + n_2 d (K_2 - 1) =$$
$$= 0.7 + 4 \cdot 0.06 (2.9 - 1) + 2 \cdot 0.06 (1.8 - 1) = 1.26 \text{ cm}$$

where h = 0.7 cm is the actual average wall thickness along the rolling part (without taking into account the ridges of the tread); n_2 = 4 is the total number of basic cord plies, n = 2 is the number of breaker plies; d = 0.06 cm is the thickness of a cord fiber, K_1 = 2.9 is a coefficient determined according to the graph in Figure 51 (cf. p. 51), as a function of the ratio of fiber thickness to fiber

step in the basic plies

$$\frac{d}{t} = di = 0{,}06 \cdot 12{,}9 = 0{,}77$$

K_2 = 1.8 is the same for the breaker plies ($\frac{d}{t}$ = 0.06·9.4 = 0.56). Assuming that the neutral axis passes at the level of the third carcass ply, we can find the distance of the cord plies from this axis (Fig. 134):

$$y_1 = 0{,}16 \text{ cm} \quad y_2 = 0{,}08 \text{ cm} \quad y_3 = 0$$
$$|y_4| = 0{,}08 \text{ cm} \quad |y_5| = 0{,}18 \text{ cm} \quad |y_6| = 0{,}26 \text{ cm}$$

where distances y_5 and y_6 refer to the breaker.

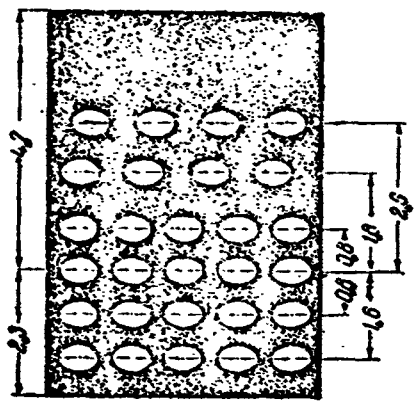

Fig. 134. The Position of Cord Plies.

Let us determine the value of $\Sigma i y^2$:

$$\Sigma i y^2 = 12{,}9\,(0{,}16^2 + 0{,}08^2 + 0{,}08^2) + 9{,}4\,(0{,}18^2 + 0{,}26^2) = 1{,}43$$

and compute the value of A:

$$A = E_c \Sigma i y^2 \sin^4 \beta + \frac{4}{3} G\,(h_1^2 + h_2^2) = 75 \cdot 1{,}43 \sin^4 54° +$$
$$+ \frac{4}{3} \cdot 25\,(0{,}23^2 + 0{,}47^2) = 55 \text{ kg/cm}$$

We can now find the values of ρ, a and c:

$$\rho = \frac{R^2 - r_0^2}{2R} = \frac{34{,}8^2 - 28{,}0^2}{2 \cdot 34{,}8} = 6{,}1 \text{ cm}$$

$$a = 2 \tan^2 \beta_c + \frac{4Gh_{red}}{p_i^2}\,(1 + \tan^4 \beta_c - \tan^2 \beta_c) = 2 \tan^2 54° + \qquad /155$$
$$+ \frac{4 \cdot 25 \cdot 1{,}26}{2{,}5 \cdot 6{,}1}\,(1 + \tan^4 54° - \tan^2 54°) = 25{,}8$$

$$c = \frac{A}{p_i^3} \cot^4 \beta_{cl} = \frac{55}{2{,}5 \cdot 6{,}1^3} \cot^4 54° = 0{,}0267$$

We can find according to formula (77) the critical velocity

$$v_{cr} = \sqrt{\frac{2.5\,(34{,}8^2 - 28{,}0^2)}{2 \cdot 34{,}8 \cdot 1{,}17 \cdot 10^{-6}}\left(\tan^2 54° + 2\sqrt{25{,}8 \cdot 0{,}0267}\right)} =$$
$$= 6{,}82 \cdot 10^3 \text{ cm/sec} = 245 \text{ km/hr}$$

Calculations according to the simpler formula in (76) would yield in this case a value for the critical velocity almost 30% less (v^*_{cr} = 178 km/hr).

According to the experimental data for the tire under examination the critical velocity is about 270 km/hr. Thus the calculation using (77) understated the critical velocity by approximately 10%.

The obtained formulas allow us to investigate the relationship between critical rolling velocity of a tire and the specific mass of the rolling part, internal pressure, the cord fiber angle, the rubber rigidity.

Figure 135 shows the corresponding calculated graphs for a 7.50-16 tire. We can see from these graphs that in order to increase the critical velocity, along with an increase in the internal pressure and a decrease in the tire mass it is advisable to increase the cord fiber angle and to increase the rigidity of the rubber. An increase in the rim width also leads to an increase in the critical velocity since in this case the radius r_0 decreases and the value of ρ increases as follows:

$$\rho = \frac{R^2 - r_0^2}{2R}.$$

We should note that if we take the above-mentioned measure to increase the critical velocity we must use high strength materials. Actually, an increase in internal pressure, an increase in cord fiber angle and rim width leads to an increase in the forces in the cord fibers. To eliminate the need to increase the number of plies in the tire and consequently its mass, it is necessary to use high strength cord. A decrease in the mass of a tire by means of decreasing the tread caliber requires the use of rubber having high wear resistance.

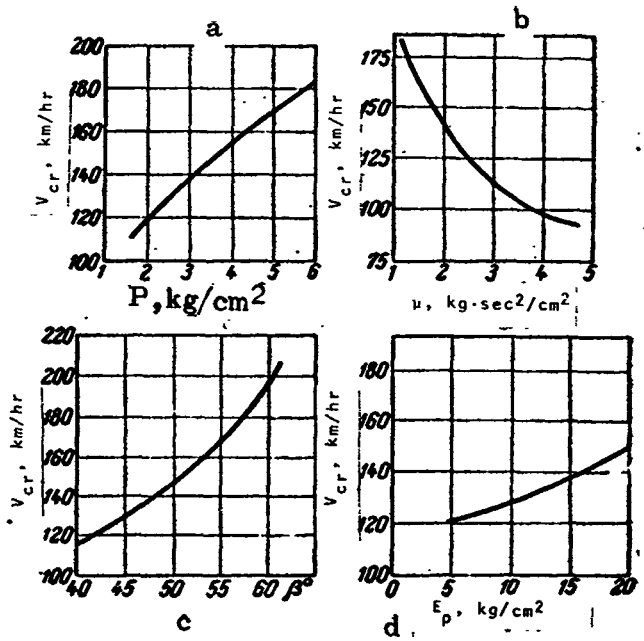

Fig. 135. The Relationship Between the Critical Velocity and: (a) Internal Pressure; (b) the Mass of the Rolling Part; (c) the Cord Fiber Angle; (d) the Elasticity Modulus of the Rubber.

Since the influence of the dynamic processes on the operation of the tire begins to appear at a velocity significantly lower than critical, the permissible operating velocity must be determined as /156

$$v_{max} = \eta v_{cr},$$

where η is a coefficient less than unity.

The value of the coefficient η can be defined as a function of tire pressurization and required mileage at a velocity of v_{max}. At the present time it is difficult to assign concrete numerical values to the coefficient η.

Deformation Regimes of Tire Materials

A machine builder who is designing a piece of equipment chooses for his production one or another grade of steel, depending on the values of the stresses and deformations undergone by the piece of equipment.

Replacing one grade of steel with another does not entail changes in the stresses or elastic deformations of the piece of equipment but changes only its strength. This is related to the fact that all grades of steel have practically identical elasticity moduli $E = 2 \cdot 10^6$ kg/cm^2. A tire constructor is in a more favorable and at the same time more complex position. Replacing one grade of rubber or cord with another which differs in terms of strength he can and must vary not only the strength of the material but also its operating conditions, i.e., the value of the stresses and deformations which arise, the value of hysteresis losses, and consequently the temperature conditions. We can distinguish the following basic /157
operating regimes of the material: the regime of given stresses, the regime of given deformations and the regime of a given deformation energy.

With the regime of given stresses the value of the stresses undergone by the material remains constant regardless of its rigidity and the corresponding value of deformation varies in inverse proportion to the elasticity modulus of the material. As an example of the regime of given stresses let us examine, in particular, the compression of tread elements in the contact surface of the tire. In this case the value of the compression stresses is equal to the contact pressure and varies very little with the properties of the material. In this case the lower the elasticity modulus of the material, the higher the deformations undergone by the material. A graphic representation of the regime of given stresses is shown in Figure 136a. The stress σ_0 is given. The material whose characteristic is shown by ray 1 undergoes deformation $\varepsilon_1 = \frac{\sigma_0}{E_1}$, and the softer material with elasticity modulus E_2 undergoes more deformations $\varepsilon_2 = \frac{\sigma_0}{E_2}$.

Deformation energies shown by the shaded areas in Figure 136a and equal, respectively, to $A_1 = \frac{\sigma_0^2}{2E_1}$ and $A_2 = \frac{\sigma_0^2}{2E_2}$, vary in this case also in inverse proportions to the elasticity modulus.

Thus, with the regime of given stresses rigid material is, gen- /158
erally speaking, in a more favorable condition than pliable material.

The regime of given deformations differs in that the value of the deformations is not a function of the properties of the material, and the stresses which arise are directly proportional to the elasticity modulus. As may be seen in Figure 136b the deformation

work equal to $A = \frac{E\varepsilon_0^2}{2}$ is also directly proportional to the elasticity modulus.

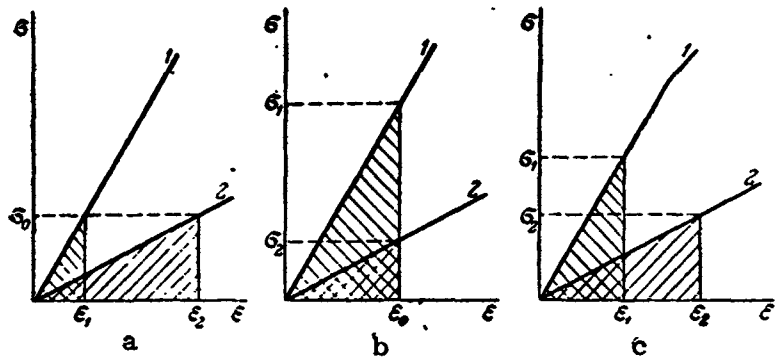

Fig. 136. A Graphic Representation of the Various Operating Regimes of the Material: (a) Regime of Given Stresses; (b) Regime of Given Deformations; (c) Regime of Given Deformation Energy. (1) Material with High Elasticity Modulus; (2) Material with Low Elasticity Modulus.

With the regime of given deformations the material with the lowest elasticity modulus is best suited.

The regime of given deformations is realized, for example, when samples are tested on an MRS-2 machine when the motion of the movable clamp of the machine is given and the stress arising in the sample is a function of its properties.

The regime of given deformation energy is an intermediate stage between the regimes of given stresses and given deformations. With this regime, regardless of the elastic properties of the material the deformation energy remains constant and the stresses and deformations vary so that $\frac{\sigma\varepsilon}{2} = A = \text{const}$. It follows from this that with the regime of given deformation energy, the stress is directly proportional to the square root of the elasticity modulus of the material and the deformation is inversely proportional to the same root.

Figure 136c compares the stresses and deformations for two materials of different rigidity with given deformation energy. Regimes are possible and very often encountered which are intermediate between these three basic ones.

From what we have said above, it is clear that a knowledge of the operating regime of the material in one or another part of the tire is of great importance. If we know the character of this regime we can justifiably proceed to the choice of material having the optimal properties. If we know only the operating regime of the material during operation we can correctly establish a series of physical-

mechanical tests which reflect the operating quality of the material. In the opposite case, errors are always possible since with a difference between the operating regime and the regime of the laboratory tests, the rubber which showed the best results in the laboratory might be the worst in the finished product.

Unfortunately the construction and operating conditions of pneumatic tires are so complicated that the operating regimes of the material in its various parts are difficult to attribute precisely to one or another type. However, the investigations we have made allow us in most cases to establish the type of the dominant regime.

We have stated above that elements (ridges) of the tread undergo given stresses when they pass through the contact area. For the tread base ply, the operating regime is even more complex. The tread base ply transfers the given load from the tread ridges to the /159
carcass and, together with the carcass, takes part in the overall deformation of the carcass. The latter varies very little with the elastic properties of the tread base ply; i.e., it is given. Which of these regimes is most important? Clearly, the answer to this question must be different for different types of tires. Thus, in high pressure tires, the load transferred from the tread ridges is as great as the contact pressure, and the carcass deformation is relatively small. In low pressure tires (variable pressure tires, passenger tires), the contact pressures are significantly less and carcass deformations are greater. Thus we may assume that in heavy duty tires the dominant regime for the tread base ply is the regime of given stresses; for extra low pressure tires and passenger tires the regime is closer to the regime of given deformations.

The rubber which fills the spaces between the fibers in each cord ply undergoes deformations accompanied by distortions of the elementary rhombi formed by the cord fibers. These deformations are not a function of the rigidity of the rubber, and therefore are given.

The most complicated problem is that of the regime of deformations of the interlayer and breaker rubber.

The interlayer rubber is deformed simultaneously with the plies in its plane and also undergoes shift deformations related to the mutual shifting of the adjacent plies; the latter deformations have special importance. The problem of the relationships between the amplitude of shift deformations in the interlayer rubber and its properties was discussed earlier in the general form (cf. p. 55). Formula (39) obtained with a number of cord plies $n > 4$ can be presented in the form

$$\gamma = \frac{\gamma_0}{1 + 2{,}5 \frac{G t^2}{E_c n i h (k - nd)}} \qquad (78)$$

where $\gamma_0 = \frac{A\pi}{l}\sin\frac{\pi s}{l}$ is a value fully determined by the shape of the curved surface and is not a function of the properties of the rubber; G is the shift modulus of the rubber; E_c is the modulus of the cord fibers, n is the number of plies; i is the fiber frequency; h is the thickness of the carcass; l is the dimension of the zone in which the change in curvature of the wall has the same sign (l varies along the cord fibers); d is the fiber caliber.

Formula (78) shows that depending on the relationships between the rigidity of the rubber and the rigidity of the cord and between the length of the deformation zone and the thickness of the wall, the rubber deformation regime can vary from the regime of given deformations to the regime of given stresses.

Thus, if the cord is very rigid (metal cord) and E_c is large, /160
then the second term in the denominator of (78) is small in comparison to unity and $\gamma \approx \gamma_0$, i.e., is not a function of the shift modulus of the rubber G. In this case the deformation regime of the interlayer rubber is close to the regime of given deformations. On the other hand, if the second term in the denominator of (78) is large in comparison to unity (for example, for tires with a small number of plies made of textile cord) the regime is close to the regime of given stresses.

We can also establish that if the second term in the denominator is equal to unity, then with small changes in the shift modulus of the rubber G the shift γ varies so that the deformation work $\frac{G\gamma^2}{2}$ is maintained as an almost constant value. In this case the regime is close to the regime of given deformation energy. As we saw above (cf. p. 59), for an 8-ply heavy duty tire with a length l = 10 cm the second term in the denominator of (78) is equal to 0.85, i.e., near unity. From this we can draw the conclusion that the deformation regime of the interlayer rubber of this tire is close to the regime of given deformation energy.

The interlayer rubber in the breaker zone, except for shifts related to the curvature of the tire wall, also undergoes given stresses related to the transfer of contact pressure. Therefore, the regime characteristic of this rubber is close to the regime of given stresses.

For heavy duty tires of greater dimensions having 12 or more cord plies with curvature with the same half-wavelength l = 10 cm, the deformation regime of the interlayer rubber will be close to the regime of given deformation, since in this case the value of $\frac{2.5Gl^2}{E_c nih(h-nd)}$ will be significantly less than unity. On the other hand, for tires with few plies (for example, passenger tires) the deformation regime of the interlayer rubber will be close to the regime of given stresses.

We can draw a number of practical conclusions from this. Thus, in particular, we can establish that for multi-ply tires used on rough road surfaces, rubber with a low modulus is preferred in the carcass.

We cannot, however, substantiate that for tires with few plies high modulus rubber has an advantage. Although when using these rubbers, shift deformations are somewhat less, in thin-walled tires these deformations are generally small and do not determine the strength of the construction.

It is inadvisable to use low modulus breaker rubber (especially above the breaker) since this type of rubber will undergo significant deformations connected with the transfer of contact pressure.

In four-ply tires made of metal cord the interlayer rubber operates in the regime of given deformation; here it is advisable to use low modulus rubber. This conclusion does not pertain to two- /161
ply tires made of metal cord since in that case there are no plies with parallel fibers and shift deformations between the plies are insignificant.

Of great interest is the problem of the deformation regime of the cord fibers.

We should bear in mind that cord fiber deformations are the sum of two types of deformations: membrane deformations, which are identical for all plies; and curvature deformations, which have opposite signs in the internal and external plies.

The forces which arise in cord fibers with membrane deformations are the sum of the initial forces of the inflated tire and the auxiliary forces which arise when it is rolling. In first approximation, the membrane forces are not functions of the elastic properties of the cord. For a given tire their value increases as the internal pressure increases (with constant buckling) and as buckling increases (with constant internal pressure).

As we have shown (p. 58), curvature deformations are functions of the elastic properties of the cord. Formula (40), which determines cord fiber expansion with curvature, can now be presented in the form

$$\varepsilon = \frac{\varepsilon_0}{1 + \frac{E_c n i h (h - nd)}{2,5 G^n}} \qquad (79)$$

where all the notations are the same as in (78), $\varepsilon_0 = \frac{\chi h}{2}$ where h is the carcass thickness, χ is the change in its curvature.

It is clear from formula (79) that an increase in the elasticity modulus of the cord leads to a decrease in the fiber deformations

with curvature. In addition, the corresponding force in the fibers is equal to

$$N' = E_c \varepsilon = \frac{\varepsilon_0}{\frac{1}{E_c} + \frac{nih(h-nd)}{2{,}5Gl^2}}$$

increases as the modulus increases.

Thus the operating regime of the fibers with curvature of the wall is between regimes of given deformations and the given stress. The greater the second term in the denominator of (79), i.e., the more rigid the cord and the softer the rubber, the more this regime will approach the regime of given stresses.

Since in the tire the cord undergoes simultaneous membrane and curvature deformations, the actual operating regime of the cord depends on the relationship between the values of the deformations. It is obvious that the role of curvature becomes greater as the thickness of the tire wall becomes greater and as its curvature with deformation varies.

In connection with this, the results of an experimental investigation of the relationships between cord fiber deformations and the rigidity is very interesting. The Scientific Research Institute for the Tire Industry conducted research[21] on the cord fiber deformations of a 260-20 tire constructed of cord made of kapron wire and standard wire. Both types of cord had similar fiber diameters, /162

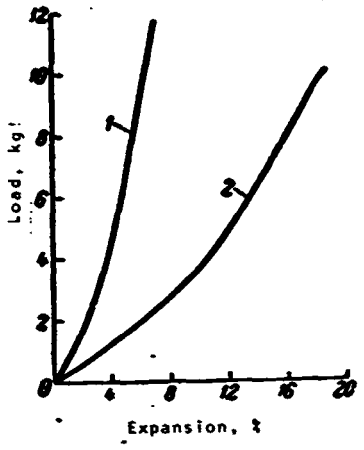

Fig. 137. Diagrams of Tire Cord Stretch: (1) Standard Cord; (2) Kapron Cord.

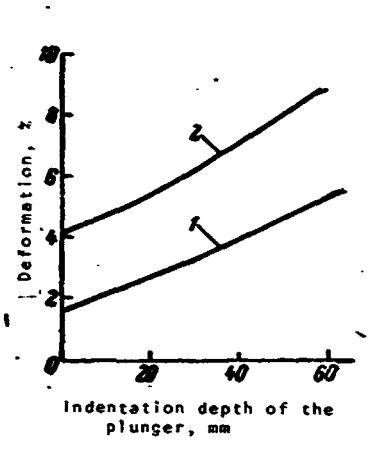

Fig. 138. The Relationship between Cord Fiber Expansion and Plunger Identification Depth: (1) Standard Cord; (2) Kapron Cord.

[21] The work was conducted by engineer V.A. Pugin.

identical blowout strength (14.3 kg/fiber) but sharply different expansions with blowout (9% for the standard cord, 25% for the kapron cord). The density of both cords was identical.

As can be seen from the fiber stress characteristics shown in Fig. 137, the standard cord is approximately twice as rigid as the kapron cord.

The investigation of deformations was conducted by inserting a conical plunger with a circular apex radius of 20 mm into the tire. Under these conditions, curvature deformations played an important role.

Figure 138 shows the experimentally obtained functions relating cord fiber expansion of the internal ply of the tire to plunger indentation depth. It is clear from the graph that both the initial deformations caused by internal pressure and the additional deformations caused by inserting the plunger are greater for the more pliable kapron cord than for the standard cord. Using the stretch characteristic of the cords, we can determine the forces in fibers with one or another plunger indentation depth. The corresponding graph is shown in Figure 139. Comparing the graphs in Figures 138 and 139 we can determine that the initial forces in cord fibers are not a function of their rigidity and the supplementary forces with plunger indentation increase as the rigidity increases and the corresponding deformations decrease.

Since the blowout strength of both cords is the same, in this case the rigid standard cord is less suitable. /163

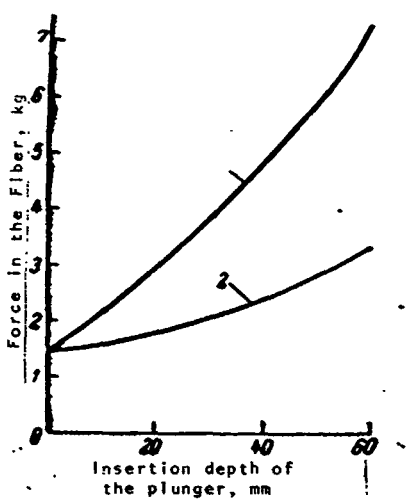

Fig. 139. Relationship Between the Forces in the Cord Fibers and the Insertion Depth of the Plunger: (1) Standard Cord; (2) Kapron Cord.

Actually, the experiment showed that tires made of this cord blow out when the plunger is inserted to a depth of 136 mm, while tires made of kapron blow out at a depth of 163 mm (at an internal pressure of 6 kg/cm^2).

Thus, the additional deformations in this case correspond to a regime between the regime of given stresses and given deformations close to the regime of given deformation energy. This is valid for multi-ply tires. It is obvious that in two-ply tires where the role of curvature is small, the deformation regime of the cord is close to the regime of given stresses.

When the problem of choosing the optimal rigidity of the rubber or cord is solved, in addition to their deformation regimes, one must first consider the static and fatigue strength of the material.

One should bear in mind that a change in rigidity of one or another tire element leads to a change in stresses and deformations not only in that element but also in other elements. Thus, for an example, an increase in the rigidity of interlayer rubber leads to an increase in stresses in the cord fibers, and an increase in the rigidity of the cord fibers leads to an increase in the stresses in the rubber.

Similarity Relationships and the Choice of Basic Tire Dimensions

Conditions have not yet been created under which it is possible to choose the basic parameters of tires for a given operating regime based on calculations for the strength, starting from the required lifetime of the tire and the characteristics of the material used.

The relationships between the stresses and deformations in tire elements and the construction and operating conditions of the tire have not been studied in sufficient detail. There is not yet sufficient knowledge concerning the fatigue strength of tire material.

Therefore, when choosing basic tire dimensions one should rely /164
in most cases on experimental data. One of the methods for using experimental data is the use of various types of norms (All Union State Standard, norms used in various countries).

However, these materials contain norms of load and internal pressures only for standard tires, and extrapolation of the normative functions is not always possible. In addition, as tire materials improve new types of cords and new rubbers are introduced; requirements for tire lifetime change; the norms periodically undergo revision. Therefore, for a tire manufacturer it is most important to have methods for computing the norms of load and pressure for tires.

In engineering a number of approximate formulas are used to calculate the norms of load on the tire. Thus, for example, the Hull formulas introduced in foreign literature [3] have the following form:

for light tires

$$Q = 0{,}113 p^{0{,}585} B_1^{1{,}39} (a + B_1)$$

for heavy duty tires

$$Q = 0{,}099 p^{0{,}585} B_1^{1{,}39} (d + B_1)$$

Included in these formulas are Q (kg), i.e., the permissible load p in kg/cm^2, the internal pressure; d (cm), the nominal rim

diameter; B (cm), the relative width of the tire profile which is function of the actual profile width B and the rim with C according to the formula

$$B_1 = 1{,}4B - 0{,}645C$$

The Hull formula is purely empirical and has several significant problems. It is assumed in these formulas that the actual width of the rim on which the tire is mounted does not influence its load-carrying capacity. The impression is also created that by increasing internal pressure we can increase the load-carrying capacity of the tire without limit. This does not correspond at all to reality; as we know, an increase in internal pressure cannot compensate for overloading the tire. Therefore, the Hull formulas are not recommended for practical use.

A number of references proposed computing the load beginning from a particular ratio of load to internal tire volume which is determined by calculations or even experimentally by filling the tire with water. This method is also unjustified since a change in /165
internal volume of the tire (for example, due to a change in the rim construction) is in no way related to a change in its load-carrying capacity.

A method for calculating the norms of load and internal pressure for pneumatic tires based on the methods of similarity theory is examined in reference [31].

An analysis of the uniformities shows that the operating regimes of tire materials are basically determined by the following dimensionless parameters:

$$\frac{H}{B}, \frac{D}{B}, \frac{C}{B}, \frac{h}{B}, \beta_c, \frac{niE_c}{Gh}, \frac{p}{G}, \frac{Q}{GB^2}, \frac{f}{B}$$

The first parameters ($\frac{H}{B}$, $\frac{D}{B}$, $\frac{C}{B}$, $\frac{h}{B}$, β_c) characterize tire geometry (cf. Fig. 140) and the cord fiber angles in the tire; the parameter $\frac{niE_c}{Gh}$ determines the ratio of the rigidity of the cord plies to the rigidity of the rubber. Finally, the parameters $\frac{p}{G}$, $\frac{f}{B}$, and $\frac{Q}{GB^2}$ determine the ratio of internal pressure to the elasticity modulus of the rubber, the ratio of tire buckling to the profile width and the ratio of the radial load to the product of the elasticity modulus of the rubber and the square of the profile width.

Naturally, not all these parameters are independent. Thus, for a tire with given dimensions and made of particular materials, the load, internal pressure and buckling are inter-related. Therefore, we can write for example:

$$\frac{Q}{GB^2} = \varphi\left(\frac{f}{B}, \frac{p}{B}, \frac{H}{B}, \frac{D}{B}, \frac{C}{B}, \frac{h}{B}, \beta_c, \frac{niE_c}{Gh}\right) \qquad (80)$$

The precise form of function (80) cannot be determined, however, using the approximate formula (69) /166

$$Q = \frac{f^n}{C_1 + C_2 \frac{f}{p + p_0}}.$$

This function may be presented in the form

$$\frac{Q}{GB^2} = \frac{\left(\frac{f}{B}\right)^n}{C_1 G + BC_2 \frac{f/B}{p/G + p_0/G}} \qquad (81)$$

where the parameter $\frac{Q}{GB2}$ in the explicit form is expressed in terms of the parameters $\frac{f}{B}$ and $\frac{p}{G}$ and the influence of other dimensionless

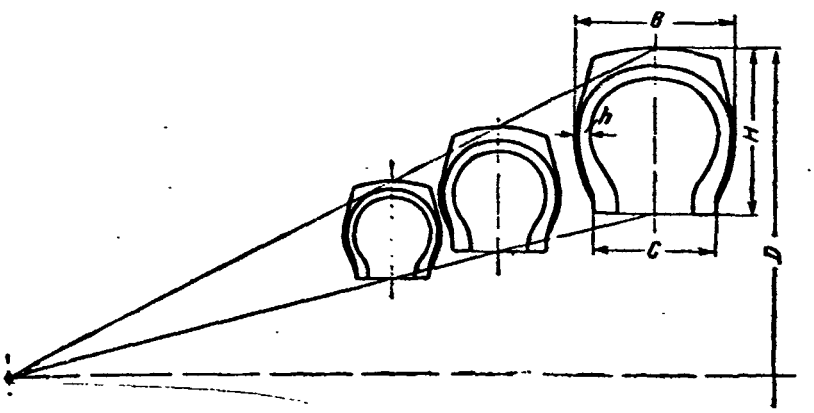

Fig. 140. A Series of Geometrically Similar Tires.

parameters is reflected in the values of C_1G, BC_2, $\frac{p_0}{G}$.

Let us now examine a series of geometrically similar tires made of identical materials (Fig. 140). For these tires, all ratios of geometric dimensions and also β_c and the ratio $\frac{niE_c}{Gh}$ are identical. The shift modulus of the rubber G is also the same.

It follows from this that for geometrically similar tires, identical deformation regimes are realized with identical internal pressures, identical relative bucklings and with load which is directly proportional to the square of the profile width.

Thus, in all similar tires the internal pressure must be the same p = const, and the load on the tire must be determined by the formula

$$Q = kB^2 \qquad (82)$$

where k is a coefficient which is constant for a given tire series, usually called the load capacity coefficient.

The conclusion which we have drawn based on an analysis of uniformities can be obtained by another method [31]. Thus, we find from (53) that identical forces in the cord fibers of similar tires arise with an identical internal pressure value, and (69) shows that in this case the constant value of relative buckling takes place with a load determined according to (82).

An analysis of the constructions of standard tires for heavy duty vehicles shows that the profile shapes of these tires basically satisfies the similarity conditions. The ratios $\frac{H}{B}$, $\frac{B}{C}$, $\frac{h}{B}$ vary within comparatively narrow limits, and only the value $\frac{D}{B}$ decreases systematically as the tire dimensions increase, since standard tires (independent of profile width) are computed for a 20 inch rim.

Thus, tires of standard construction with identical profile geometries, cord fiber angles along the equator and made of identical materials are not similar with regard to the ratio $\frac{D}{B}$, which is different for tires of different dimensions. /167

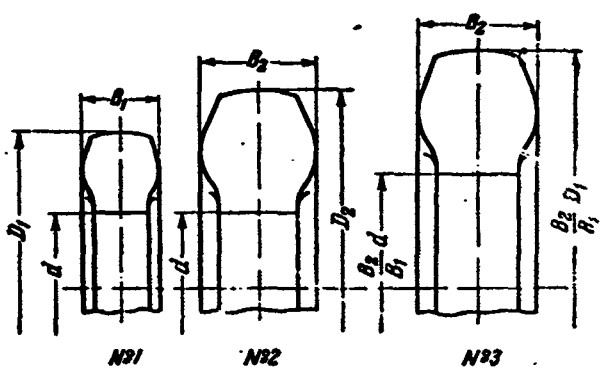

Fig. 141. Determining Norms of Load and Pressure for Tires with Different Profile Widths but Identical Rim Diameters.

It is obvious that in tires which do not satisfy a condition of geometric similarity, identical conditions of deformation, strictly speaking, cannot be attained; however, an approximation to them is possible.

Let us now examine how the internal pressure and load must vary in tires of different dimensions mounted on a rim of a single diameter.

Let the internal pressure p_1 and load Q_1 which provide normal operation of tire No. 1 with profile width B_1 (Fig. 141) be known; we must determine the load and pressure for tire No. 2 with profile width B_2. As a preliminary we will determine the load Q_3 and pressure p_3 for tire No. 3, which is similar to tire No. 1 and has the profile width B_2.

According to the similarity conditions with pressure $P_3 = P_1$

and load $Q_3 = Q_1 \frac{B_2^2}{B_1^2}$ the operating conditions of tire No. 3 will be the same as those of tire No. 1. Obviously, if we assume a load Q_3 on tire No. 2 with pressure p_3, then this tire will be in a worse situation than tire No. 3 (No. 1), since its dimensions are smaller. We may assume that the operating conditions of the material in tire No. 2 when rolling will be close to the operating conditions of the material in tires No. 1 and 3 if the relative buckling $\frac{f}{B}$ for all tires is the same. To do this it is necessary either to decrease the load on tire No. 2 in relation to tire No. 3 or to increase correspondingly its internal pressure. /168

Under the given norms (All Union State Standard, the American TRA norms) for heavy duty tires of various dimensions with the same rim diameter, the ratio $\frac{Q}{B^2}$ is held constant, while for tires of greater dimensions a greater value of the internal pressure is used, so that all tires have identical relative buckling.

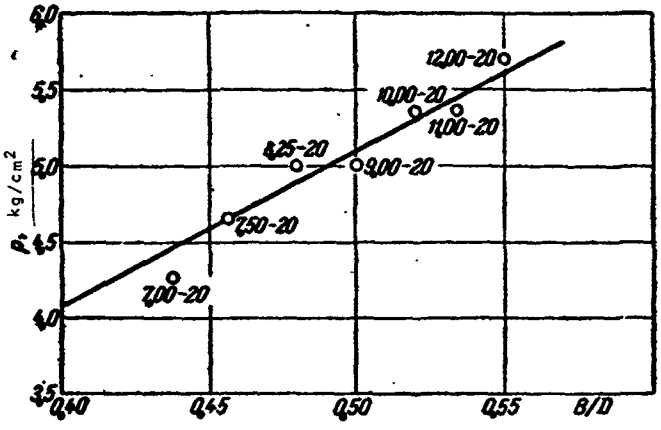

Fig. 142. The Relationship Between the Normal Internal Pressure in Heavy Duty Tires Mounted on Rims with a Diameter of 20 Inches and the Ratio $\frac{B}{D}$ (the Points Show the TRA Norms, the Line Shows the Equation $p = 10.2\frac{B}{D}$.)

It is natural that in this case tires of greater dimension are somewhat more pressurized due to the greater forces in the cord fibers and the greater specific pressure in the contact area. Therefore, in the preparation of tires of greater dimensions, as a rule the highest quality materials are used.

To determine the necessary internal pressure in the tire we can use (69) into which we should substitute the given values of $\frac{Q}{B^2}$, $\frac{f}{B}$ and also the value of p_0, C_1 and $C_2 = \frac{1-1.4}{\sqrt{RD}}$ which are characteristic of a given type of tire. As calculations show [31], the pressure in this case must vary in direct proportion to the ratio $\frac{B}{D}$ for the tire. Figure 142 shows the relationship between the internal pressure recommended for heavy duty tires by the TRA norms, and the ratio $\frac{B}{D}$. It can be seen from the graph that the actual function is almost linear. /169

For light tires the normal internal pressure is determined mainly by conditions of comfort and is taken, as a rule, to be identical

for tires of a given type mounted on a rim of a given diameter. Thus, to obtain identical relative buckling $\frac{f}{B}$, for tires of greater dimension the ratio $\frac{Q}{B^2}$ is somewhat decreased. In this case, for calculations we can use formula (69).

Tube Deformations in Pneumatic Tires

For tube tires the tube is an important part which significantly affects the reliability and lifetime of the tire as a whole. Tube puncture during operation often leads to the destruction of the outer cover and, in certain cases, can cause an automobile accident.

In addition to punctures and other mechanical hazards, the most important form of tube failure during operation is a rupture of the belt or a wearing down due to the formation of wrinkles; both these types of failure are caused by the state of tube tension in the outer cover. Excessive stretching forces in the tube material eventually lead to its rupture. The failure of the tube under the action of stretching forces is accelerated by the influence of rim heating from the brake drum and the heat formation when the tire is rolling.

The presence of compression forces in the tube when it is inflated in the outer cover or subsequently when the tire is in operation leads to the formation of wrinkles, due to the small thickness of the tube walls.

To prevent the appearance of these defects, when designing the tubes we should take into account the stresses and deformations arising when it is inflated. The problem of a theoretical determination of these deformations and stress was solved in reference [32]. Let us now introduce the basic conclusions from this reference.

(1) The distribution of meridian deformations ε_m along the contour of the tube have the character shown in Figure 143. The maximum deformations arise in the rim zone; the minimum arise along the equator.

(2) Nonuniform distribution of meridian deformations ε_m along the contour becomes greater as the ratio $\frac{D}{d}$ increases for the tire.

(3) The value of meridian deformations ε_m varies very little with the profile shape of the tire (for example, with the ratios $\frac{H}{B}$), and for ordinary configurations of light and heavy duty tires it is determined only by the value of the mean stretch ε_{m_0} along the contour, the value of circumferential deformation in the rim zone $\varepsilon_{t\ \text{rim}} = -\frac{2h}{d}$ and the ratio $\frac{D}{d}$. The average stretch along the profile is found by formula /170

$$\varepsilon_{m0}=\frac{S-S_0}{S_0}$$

where S is the internal perimeter of the profile of the inflated outer cover; S_0 is the profile length of an undeformed tube.

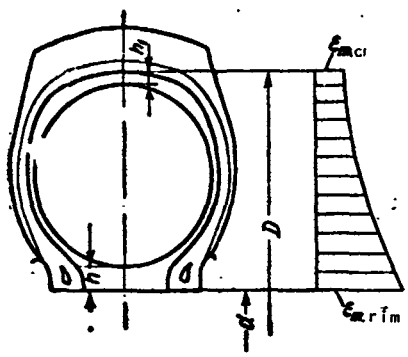

Fig. 143. The Position of an Inflated Tube in the Outer Cover and the Distribution of Meridian Deformation Along the Tube Contour.

(4) The values of the meridian deformation of the tube in the rim zone $\varepsilon_{m\ rim}$ and along the equator ε_{mc} can be calculated approximately according to the formulas:

$$\varepsilon_{m\,rim}=\varepsilon_{m0}+K_1\left[(1+\varepsilon_{m0})\left(\varepsilon_{m0}+\frac{2h}{d}\right)\right]$$
$$\varepsilon_{mc}=\varepsilon_{m0}-K_2(1+\varepsilon_{m0})\left(\varepsilon_{m0}+\frac{2h}{d}\right).$$

where the coefficients K_1 and K_2 are determined as a function of the ratio $\frac{D}{d}$ according to the graphs of Figure 144.

(5) Circumferential deformations in the rim zone and along the equator are determined by the formulas:

$$\varepsilon_{t\,rim}=-\frac{2h}{d}$$
$$\varepsilon_{tc}=\frac{2h_1}{D}$$

(6) Stresses in circumferential and meridian directions are equal, respectively, to:

$$\sigma_t=4G(\varepsilon_t+0{,}5\varepsilon_m)$$
$$\sigma_m=4G(\varepsilon_m+0{,}5\varepsilon_t)$$

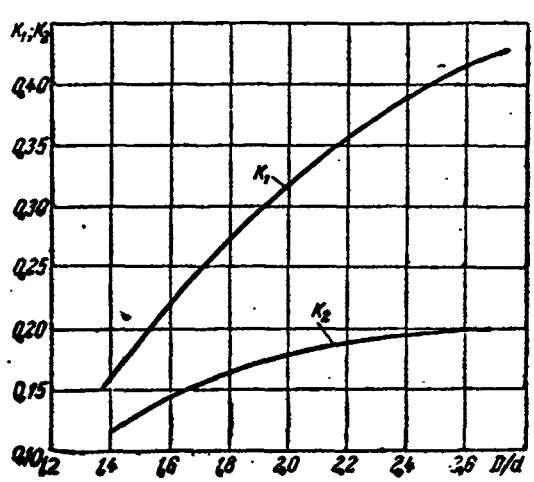

Fig. 144. The Coefficients K_1 and K_2 as a Function of the Ratio $\frac{D}{d}$.

To prevent the formation of wrinkles the stresses both in the rim zone and along the equator must be positive (stretching).

(7) An increase in the thickness of the tube wall in the rim zone does not lead to a decrease in deformations in that zone; with high internal pressure, deformations of the thicker section of the tire even increase. When it is necessary to decrease tube deformations in the rim zone, reinforcing cord strips can be used. /171

CHAPTER VI

METHODS OF TESTING TIRES

Types of Tire Tests

Tire tests are conducted with a two-fold purpose. On the one /291
hand, tires are tested to determine the tire characteristics on which the operational quality of the vehicle depends. These characteristics are static characteristics which determine the pliability of the tire at various radial, lateral and circumferential loads, the traction indices of the tires, side slip, rolling losses. On the other hand, we determine the indices characterizing the reliability of the tire during operation, i.e., its wear resistance, fatigue strength and resistance to concentrated loads, etc.

Tires are tested both by laboratory methods and by special experiments under road conditions; the lifetime of the tire is determined under normal operational conditions and with accelerated road tests.

Laboratory tests investigated the properties of tires as components of an automobile and determined certain indices on which the lifetime of the tire depends. These tests allow us also to check the uniformity of the quality of the tires produced.

Tests of automotive tires under laboratory conditions on special equipment allow us to obtain results quickly and to guarantee that the test conditions remain constant [40].

However laboratory tests of tires at the present time do not yield sufficient data for predicting the lifetime of the tire during operation and extensive appraisals of their operational properties. Therefore the best tire samples after laboratory tests undergo road and operational tests.

Road tests consist in obtaining indices which characterize the operational qualities of the tire by means of experiments on automobiles or on dynomometric trollies.

Road tests approximate actual conditions. There is also an opportunity to obtain the characteristics of the operational qualities for various operating conditions of automobiles by setting

up various experiments. The problems associated with road tests in /292
comparison to laboratory tests consist in the difficulty of reproducing their conditions.

In road tests, tire estimates (basically of their lifetime) are made under normal operating conditions in automobile factories. Operational tests provide the possibility of obtaining a more reliable value for the shock absorbing range of the tire. The difficulty of this type of testing is the fact that it is very time-consuming, and one can obtain in most cases only one index of the operational qualities of the tire, i.e., their lifetime. Other operational qualities in these tests can be determined only approximately, i.e., by observations, questioning drivers, etc.

Since operational tests are time-consuming, tires undergo accelerated road tests for a more rapid determination of their operational reliability. In this case tires are tested on automobiles weighted with ballast which move along a particular direction for a long average daily distance (up to 800 km). With accelerated tests the lifetime of the tires is significantly lower than during normal usage; therefore, these tests are of a relative nature.

Determining the Operating Characteristics of Tires

The Pliability of a Tire and the Contact Surface

The radial pliability determines the properties of the tire as an absorber of dynamic loads on the automobile.

For each new tire construction there is a function relating radial depression and the load on the tire (the load characteristic) to certain values of the internal pressure.

An experiment (the so-called "tire compression") is conducted on special equipment which allows us to record both the value of the load and the value of depression.

The technique for interpreting the experimental data by constructing universal load characteristics of the tire was described in Chapter II (p. 112).

Figure 235 shows a schematic of an OPSh-30 universal press for testing tires. This press was developed in the Scientific Research Institute for the Tire Industry based on a UIMCh-30 serial machine which is used to test the breaking point of metal samples.

Attached to the moveable cross-arm (1) is a hydraulic cylinder (2) with a plunger (3) and pull rods (4) on which the tire (5) is attached. A hoisting mechanism (6) for mounting and unmounting the tire is also located on this cross-arm. A frame consisting of an immovable cross-arm (7), a pull rod (8) and a compression platform (9) lies on the operating plunger of the cylinder.

When the pump (13) feeds fluid to the power cylinder, the cross-arm (7), the pull rods (8) and the platform (9) shift upwards and the platform comes in contact with the tire. To regulate the initial distance from the tire to the platform when testing tires of different dimensions, pull rods (4), on which the tire is attached, can be shifted in a vertical direction using a worm mechanism. /293

The load on the tire is measured by a pendulum force-measuring device which reacts to the value of the oil pressure in the operating cylinder. The force-measuring instrument (10) shows the load. The pen (11) of the recording device shifts in proportion to the load. The drum (12) of this device rotates in proportion to the shift of the platform (9). Thus the recording instrument yields a load curve (deformation in rectangular coordinates).

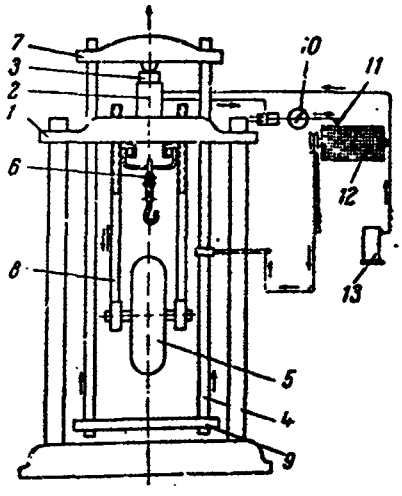

Fig. 235. Schematic of the OPSh-30 Universal Press for Testing Tires: (1) Immovable Cross-Arm; (2) Hydraulic Cylinder: (3) Plunger; (4) Pull Rods; (5) Tire; (6) Hoisting Mechanism; (7) Immovable Cross-Arm; (8) Immovable Pull Rods; (9) Compression Platform; (10) Force-Measuring Instrument; (11,12) Pen and Drum of Recording Device; (13) Pump.

The OPSh-30 press allows us to test tires with diameters from a 300 - 2000 mm with a profile width up to 600 mm. The maximum load on the tire is 30,000 kg. The accuracy of the load measurement is ± 1%.

Tire depressions with various radial loads can be measured even without special equipment. To do this one usually uses load devices of tire rolling equipment (cf. p. 310). During the experiment a flat plate is placed between the tire and the platform.

When the tire is compressed, imprints of the contact are recorded allowing us to determine the contact surface of the tire.

To do this dye (carbon black dissolved in machine oil) is placed on the tread section over an area somewhat exceeding the contact surface, and the flat plate of the press is covered with paper. After the tire is compressed a sharp imprint remains on the paper, showing the tread design on the contact surface.

From the obtained imprint we can measure its width, length, total area and area of the tread ridges.

In addition to radial pliability of the tire, we also determine

its circumferential and lateral pliability. To determine these characteristics we apply to a tire loaded with radial load an additional torque or lateral force and measure the corresponding shifts. We determine the circumferential and lateral pliability from equipment designed to study traction with the road surface (cf. below, Figs. 238, 239). /294

Pressure in the Contact Surface

The mean pressure in the contact surface or the mean pressure on the surface of the ridges is determined by dividing the radial load by the surface of the entire contact imprint or by the contact imprint of the ridges.

To determine the true pressure on a hard surface we used special pressure sensors mounted on the surface of a road with a hard surface or on the rolling surface of a drum.

The proper construction of the tensiometric sensor is described in reference [19]. The sensor (Fig. 236) is a rod (1) held by four elastic cross-arms (2) upon which wire tensiometers (3) are cemented. Depending on the way the tensiometers are inserted into the measuring circuit the sensor records normal pressure in the contact surface, lateral or longitudinal tangential forces. The value of the pressure arising when the tire hits the sensor is recorded by an oscillograph.

One of the approximate methods for determining the curve of pressure distribution over the contact surface of the tire consists of placing under the tire a rubber mat with conical ridges. The ridges are covered with dye and a mat is placed on paper lying on a flat plate. The uninflated tire is placed on the mat and held in place in the position corresponding to the necessary radial load. The tire is inflated and the ridges of the mat are deformed according to the amount of pressure. Then the air is let out of the tire and the tire is removed. This leaves imprints of the deformed ridges of the mat on the paper (Fig. 237). Pressure is determined according to the value of these imprints. For this purpose a preliminary calibration is made, i.e., determining the diameter of the cone imprint as a function of the value of pressure. /295

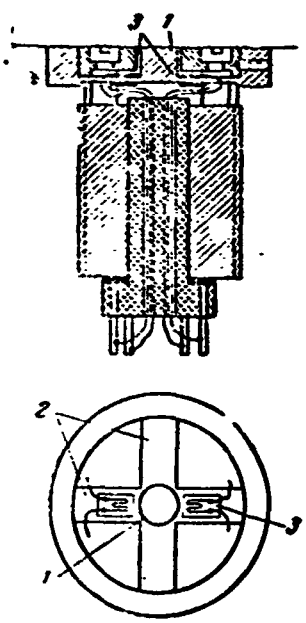

Fig. 236. A Sensor for Measuring Pressure and Lateral Forces in the Contact Surface: (1) Rod; (2) Elastic Cross-Arms; (3) Wire Tensiometers.

Traction

Traction is one of the most important qualities of automotive tires since it exerts a great influence on the tractive and braking characteristics of the automobile, its stability and safety.

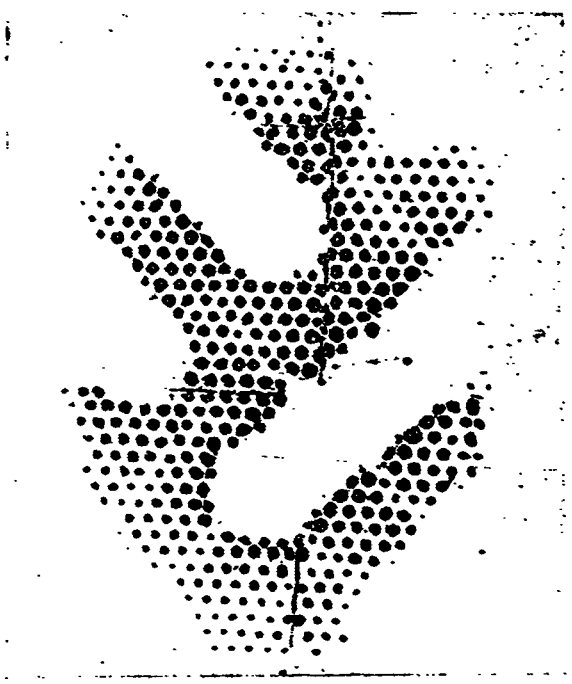

Fig. 237. Imprints of Conical Ridges of the Rubber Mat Which Characterize the Pressure Distribution in the Contact Surface.

Traction is usually determined by coefficients which describe tire traction in longitudinal and lateral directions.

The coefficient of longitudinal traction is computed as the ratio of the tractive force to the normal load when the wheels are skidding or as the ratio of the braking force to the normal load on braking wheels. The coefficient of lateral traction is the ratio of the lateral force to the normal load on wheels which are slipping sideways. The coefficient of traction is determined for an individual wheel or for the automobile as a whole. /296

For an individual wheel the coefficient of traction equals:

$$\varphi = \frac{P_w}{Q_w}$$

For the automobile as a whole:

$$\varphi = \frac{P_a}{Q_a}$$

where ϕ is the coefficient of traction with the road, P_w is the force of traction of the wheel, P_a is the traction force of the automobile with the road, Q_w is the load on the wheel, Q_a is the load on the automobile.

The coefficient of traction is determined by laboratory or road tests [41]. Obtaining comparative values for the coefficient of traction under laboratory conditions is difficult, due to the fact that the conditions of interaction between the tire and the road cannot be reproduced completely, and the fact that the surface of the sample of the road (especially during skidding) varies during the tests; with road tests there are analogous difficulties connected with the heterogeneity of the road surface.

The coefficient of longitudinal traction is determined under laboratory conditions on equipment which provides gradual addition of torque to a wheel under normal load. One of these devices is shown in Figure 238. The wheel (3) with the tire being tested is joined to a ratchet wheel (12) using a universal shaft (11). A sector (16) with a catch (13) is freely established on the axle of the latter. Using a screw (15) and a cable, sector (16) is rotated and the universal shaft (11) turns through the ratchet mechanism placing a torque on the wheel. The normal load on the wheel is created by a movable weight (2) which transfers pressure to the wheel through the spring (9) and a cross-arm (4) attached to the axle of the stand (10). The weight (6) is designed to weigh the wheel using the screw (7); thus the arm (1) attached to a joint (8) begins in the zero position.

The value of the torque which causes the tire to skid on section (5) of the road surface is computed according to the force necessary to rotate sector (16); the force is recorded by a dynamometer (14).

The coefficient of lateral traction is determined on the equipment schematically shown in Figure 239. A wheel with the tire being tested (5) attached to a tube (3) which sits freely on an axle (2) can be shifted sideways by a weight (10) hanging on a cable (6). The axle (2) is tightly fixed in the base (1) which rotates on axle (8). Normal load on the tire is created by a weight (11) located on the frame (4).

Preliminary weighing of the equipment is accomplished with a counter weight (9). The coefficient of lateral traction is found according to the value of the weight (10) which causes lateral slip /297 of the tire with a particular value of normal load.

Together with determining the coefficient of traction we can also measure the lateral deformation. For this we use a recording device (7).

Laboratory tests of tires in motion along soft dirt are made on equipment with dirt channels, in which we measure the interaction of the tire with the dirt under various regimes of motion.

Road tests for traction are made on dynamometric trolleys and on the automobiles themselves. In dynamometric trolley tests, the coefficient of longitudinal traction is determined by the braking of the wheel. Certain trolley constructions provide the possibility of setting the wheel at an angle to the direction of motion. When the tire is rolling, lateral forces arise and the tire slips sideways. The conditions of such a test are somewhat different from the conditions of lateral slip of a tire in operation on a vehicle, where the sidewards motion of the wheel usually begins at rather high velocities.

The most reliable data on traction are obtained by testing tires on the automobile themselves. The coefficient of longitudinal traction is determined on automobiles by the skid method and the braking method.

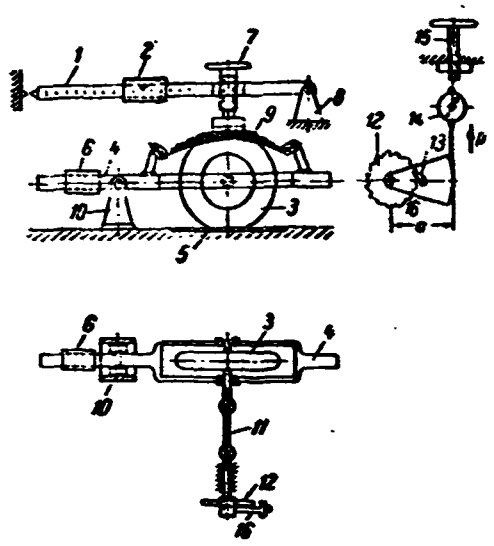

Fig. 238. Equipment for Determining the Coefficient of Longitudinal Traction of the Tire: (1) Arm; (2) Movable Weight; (3) Wheel with the Tire Being Tested; (4) Cross-Arm; (5) Section of the Road Surface; (6) Weight for Weighing the Wheel; (7) Screw; (8) Hinge; (9) Spring; (10) Base; (11) Universal Shaft; (12) Ratchet Wheel; (13) Catch; (14) Dynamometer; (15) Screw; (16) Sector.

With skidding we can measure /298 the values of the coefficient of longitudinal traction for wheels skidding in place or skidding partially during motion, and also for wheels completely locked (lock skid) or partially braked.

To determine the coefficient of traction by skidding, the automobile on the tires being tested, with uniform motion at low velocities (3-5 km/hr), is braked by a trailer (Fig. 240). The differential mechanism of the automobile is locked to obtain equal circumferential velocities of both the drive wheels.

The braking force is recorded by a dynamometer. To determine the regime of motion we install counters to count the revolutions of the wheel. By comparing the readings of the counters and the distance traversed by the automobile we can determine the percentage of wheel skid with a given braking force.

The coefficient of traction of the braked wheels is determined by a tow car. The regime of motion

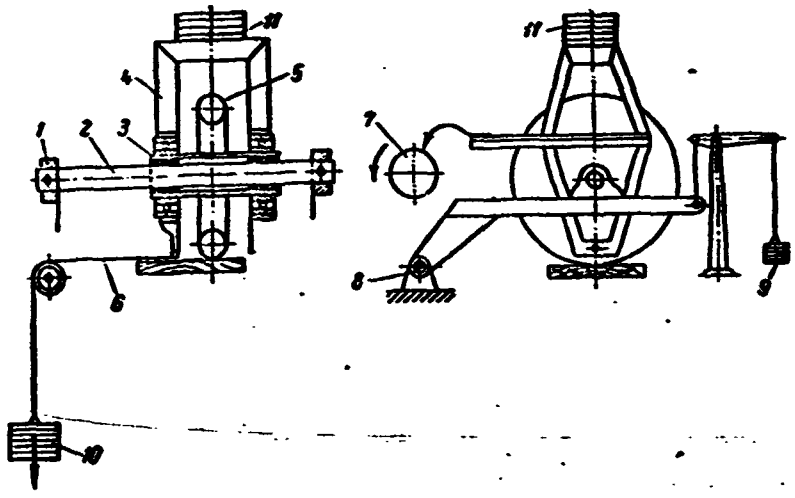

Fig. 239. The Setup for Determining the Lateral Traction of an Automotive Tire: (1) Base; (2) Axle; (3) Movable Tube; (4)Frame; (5) Wheel with Tire; (6) Cable; (7) Recording Device; (8) Axle of the Base; (9) Counterweight; (10,11) Weights.

of the wheels and the braking force are determined analogously. /299

The coefficient of longitudinal traction ϕ can be determined according to the data of tests with complete skidding of the rear drive wheels by the formula:

$$\varphi = \frac{P_{d1}}{Q_r}$$

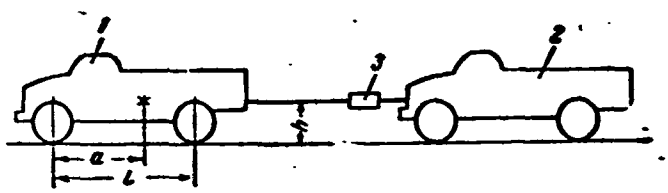

Fig. 240. A Schematic for Determining the Coefficient of Traction by Road Tests: (1) Vehicle with the Test Tires Mounted on the Drive Wheels; (2) Braking Trailer; (3) Dynamometer.

where P_d is the reading of the dynamometer; Q_r is the load on the rear wheels, determined in turn as

$$Q_3 = \frac{Ga + P_d h}{L}$$

where G is the weight of the automobile; a is the distance along the horizontal from the midpoint of the contact surface of the front wheels to the projection of the center of gravity of the automobile on the horizontal (cf. Fig. 235); h is the height at which the tow-line is attached; L is the wheel base of the automobile.

With partial skidding we must also take into account the force of rolling resistance of the front wheels P_{f_1}. In this case

$$\varphi = \frac{P_{d1} - P_{f1}}{Q_{r1}}.$$

With complete or incomplete braking of the rear wheels the same formula holds, but the load on the rear wheels is determined according to the formula

$$Q_3 = \frac{Ga - P_d h}{L}$$

The force of rolling resistance of the front wheels can be determined by skidding the vehicle when the rear wheels are detached from the differential axles. The force of rolling resistance of the front wheels can be determined as that fraction of the obtained tractive force proportional to the load on these wheels.

The coefficient of longitudinal fraction is also determined by driving the automobile in reverse and then sharply braking to a complete stop.

For a test on the horizontal section of the road at low velocities the coefficient of longitudinal traction for an automobile with 4-wheel brakes is determined according to the formula /300

$$\varphi = \frac{v^2}{2gS}$$

where v is the initial velocity (with a lock skid), S is the braking distance (with a lock skid) and g is the coefficient of gravitational acceleration.

Determining the lateral traction on automobiles is rather difficult. We can recommend one of the simple means for comparing tires according to lateral traction. This method consists in moving an automobile on the tires being tested at increasing velocity along a circle with a given radius. When the rear wheels skid (which usually happens rather sharply), the velocity is recorded. The tires are compared according to the obtained values of the velocities. We can also make tentative calculations of the value of the coefficient of lateral traction according to the formula

$$\varphi = \frac{v^2}{Rg}$$

where R is the radius of the periphery, v is the velocity with skid.

Traction depends on tire construction, the shape and condition of the road and the regime of motion of the tire. The tread is of almost no importance on dry hard surfaces but has great importance for motion along wet or ice-covered surfaces and also on soft dirt. The internal pressure in the tire is a very decisive factor especially under conditions of motion along soft ground with a low carrying capacity.

The coefficient of traction varies under various road conditions within a wide range from 0.01:0.03 (ice) to 0.8:1.0 (asphalt, concrete).

Sideslip

The tendency of tires to sideslip influences the ease of handling and maneuverability of the automobile. Sideslip is determined under laboratory and road conditions.

Sideslip is measured on laboratory equipment by adding a lateral force to the normally loaded wheel. Such tests are conducted on equipment of various kinds. Figure 239 shows the device which is best for studying stationary sideslip. The tire rolls along a drum which is rotated by an electric motor. At the beginning of the test there are no lateral forces exerted on the wheel, then lateral forces are exerted and the wheel under the action of lateral forces, rotates in a spiral. In this way conditions are created which are analogous to a lateral skid when the wheel of the automobile is rolling. The lateral shift of the wheel is measured as a function of distance traveled by the tire. /301

A simpler system is that used to study sideslip with a stationary regime. The axle of the wheel is set at a certain angle (slip angle) to the axle of the drum and the lateral force which acts on the wheel during rolling is measured.

With rectilinear motion the tests are conducted on a road with a constant lateral slant or an automobile with wings attached at an angle to the axle of the automobile. The lateral force which arises in one or the other case causes sideslip and changes the direction of motion. To guarantee rectilinear motion of the automobiles the front wheels must rotate at a certain angle recorded according to the revolutions of a pin using a special lever device[1].

The slip angle of the rear wheels is determined according to the trails left by the front and rear wheels when they cross chalk marks drawn across the road. According to the displacement of these trails and the wheelbase of the automobile we can find the angle between its longitudinal axis and the direction of motion which is equal to the slip angle of the rear wheels.

The slip angle of the front (maneuvering) wheels is determined from the expression

$$\tan(\theta - \delta_A) + \tan\delta_B = 0$$

where θ is the angle of revolution of the front wheels; δ_A is the slip angle of the front wheels; δ_B is the slip angle of the rear wheels.

The slip angle of the wheels when they are turning can be determined by various methods. The most widely used are methods for determining the slip angles of the wheels according to the trails of the wheels using a theodolite or projection instrument and with the help of a "fifth-wheel". In the first method an automobile moves at a particular velocity along the rear radius of gyration (not less than 10-15 m). The tire is constantly covered with water and leaves trails on the road. During the tests we record the angle of rotation of the front wheels of the automobile (according to the rotations of a pin). A schematic is shown in Figure 241.

According to these trails, we measured the difference between the radii of rotation of the front and rear wheels.

The slip angle of the rear wheels δ_B is determined from the the expression: /302

$$\sin\delta_B = \frac{L^2 + p^2 - 2Rp}{2(R-p)L}$$

---

[1] Measurement of the angle of rotation of the wheels according to the angle of rotation of the steering wheel is not accurate due to the presence of slack in the drive train.

where L is the wheelbase of the automobile; p is the distance between trails of the front and rear inner wheels (the difference between the radii of rotation); R is the actual radius of rotation according to the inner front wheels.

The slip angle of the front wheel δ_A is determined from the expression

$$\cos(\theta - \delta_A) = \frac{(R-p)\cos\delta B}{R}$$

Determining the slip angle of the wheels using a theodolite or a projection instrument attached to the automobile is also made when the automobile is moving in a circle. In the center of the circle we placed a stake with a marker whose image is recorded on the scales of the instruments. By measuring the displacement of the image we can determine the lateral inclination of the longitudinal axis of the automobile which corresponds to the slip of the rear wheels. Using this value and the value of the measured angle of rotation of the front wheels according to the expression determined earlier, we can determine the slip angle of the front wheel. The set up for determining the slip angles of the wheel using the "fifth wheel" (Fig. 242), consists of this wheel, a hinge connected to the rear bridge of the automobile and a counterweight.

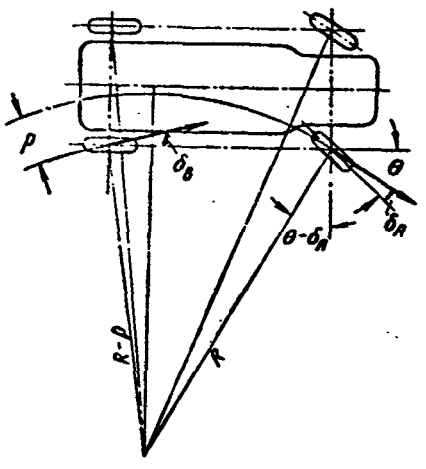

Fig. 241. A Schematic of the Motion of the Automobile Along a Circle for Determining Sideslip.

With motion along a circle the automobile turns due to the slip of the wheels and the trajectory of the "fifth wheel" remains constant due to the presence of a counterweight which counterbalances the centrifugal force. The displacement angle of the rear axle of the automobile according to its ratio to the lever connected to the fifth wheel is recorded by a special device according to the slip angle of the rear wheels.

Determining the slip angle of an individual wheel is usually done under road conditions on dynamometric trolleys, whose constructions provide for the possibility of setting a wheel at an angle to the direction of motion and measuring the lateral force which arises.

Rolling Resistance

The coefficient of rolling resistance (cf. Ch. II, p. 118) is determined by laboratory and road tests with uniform or decelerated motion of the wheel. /303

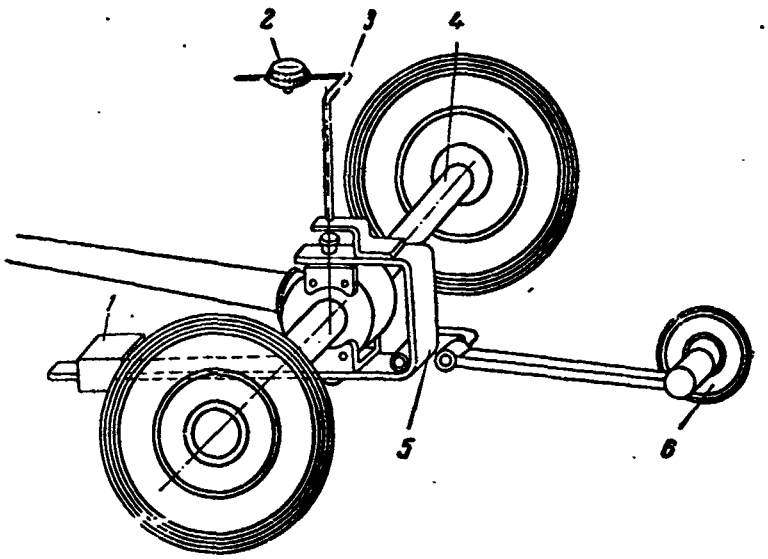

Fig. 242. A Schematic of the "Fifth Wheel" Setup for Determining Sideslip: (1) Counterweight; (2) Index; (3) Lever; (4) Rear Axle; (5) Hinge; (6) Fifth Wheel.

With laboratory tests for determining rolling resistance we use equipment of various constructions: with a wheel rolling along a cylindrical surface of a drum or along a horizontal rolling disk.

Under road conditions rolling resistance is determined on electric cars or trolleys, on automobiles or on dynamometric trolleys.

Figure 243 shows the principal system for determining rolling resistance with constant velocity. The power lost to rolling resistance of the wheel and ventilation losses are registered as the difference in the powers of the electric motor and the generator. The ventilation losses are determined by an individual rotation of the wheel and the rolling drum with the velocities used during the test.

The power expended on rolling is defined as the difference between the powers of the electric motor and the generator minus the value of the ventilation losses. The coefficient of rolling resistance f can be found according to the formula /304

$$f = \frac{N}{Qv}$$

where N is the power expended on rolling along the drum, in kg·m/sec; Q is the load on the wheel in kg; v is the circumferential velocity in m/sec.

On a setup with a horizontal rolling disk (Fig. 244) the wheel with the tire being tested is set in motion by a balancing electric motor (1) and loaded by a frame (2) with a weight. The torque transferred to the rolling disk from the wheel is absorbed by a mechanical brake (3). The tractive force on the wheel P_w is measured by a hydraulic dynamometer (4) with a mercury manometer (5).

The coefficient of rolling resistance can be determined according to the formula

$$f = \frac{M - P_w r_w}{Q r_w}$$

where M is the torque on the wheel, P_w is the tractive force; r_w is the rolling radius of the wheel, Q is the load on the wheel. /305

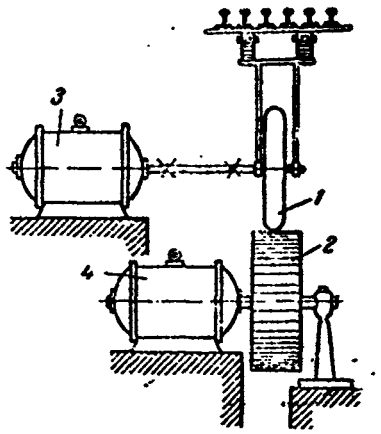

Fig. 243. A Schematic of the Dynamometric Setup for Determining Rolling Resistance; (1) Tire; (2) Rolling Drum; (3) Motor; (4) Generator.

The rolling radius of the wheel can be found according to the formula

$$r_w = \frac{\omega_d}{\omega_w} R$$

where ω_d is the angular velocity of the rolling disk, ω_w is the angular velocity of the wheel, R is the distance from the axis of the rolling disk to the midplane of the wheel.

On the setup shown in Figure 245, rolling losses are determined with free decelerated rolling of a wheel with the tire being tested along a drum. We measure the time during which the rolling velocity of the wheel along the drum decreases by 5 or 10 km/hr from a given value. The precision starting and stopping of the clock is guaranteed by an automatic device which reacts to the rotation rate of the drum. When determining the coefficient of rolling resistance of tires on this setup we should use the following formula which takes into account approximately the losses to friction in the bearings of the rolling drum:

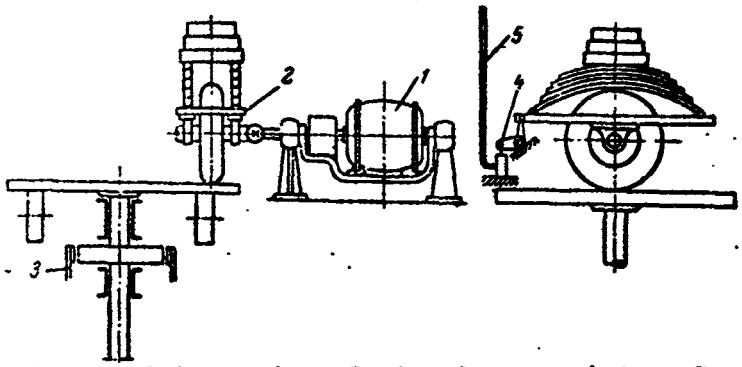

Fig. 244. Schematic of the Setup with a Rolling Disk: (1) Motor; (2) Frame; (3) Brake; (4) Hydraulic Dynamometer; (5) Mercury Manometer.

$$f = \frac{\Delta v}{3{,}6 t_t r_d^2}\left(I_0 \frac{t - t_t}{t} + I_w i^2\right)$$

where Δv is the interval of velocity decrease, in km/hr; t_t is the time of the rotation deceleration of the rolling drum with the tire (in seconds); t is the time of deceleration of the rotation of the rolling drum without the tire (in seconds); I_d is the moment of in-

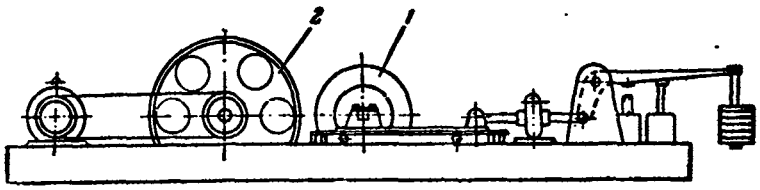

Fig. 245. The Machine with an IPS-1 Rolling Drum for Determining Rolling Resistance with Decelerated Motion: (1) Tire; (2) Rolling Drum.

ertia of the drum (in kg·m/sec^2); I_t is the moment of inertia of the wheel with the tire (in kg·m/sec^2); R_d is the radius of the rolling surface of the drum (in m); $i = \frac{r_d}{r_{rl}}$; r_{rl} is the rolling radius of the tire (in m).

Determining the rolling resistance of tires in these setups has a common problem; i.e., the fact that the rolling conditions do not coincide completely with the conditions of the motion of the vehicles.

In setups with drums whose rolling surfaces have a sufficiently high degree of curvature (usually the diameter of the drums do not exceed 2-2.5 m), the deformation of the tire is greater than the deformation of the tire under road conditions, therefore the obtained value of the coefficient of rolling resistance exceeds the actual one.

When testing on setups with a horizontal rolling disk, the deformation of the tire is normal, but when a wheel is rolling along a circle, sideslip of tread elements takes place. Therefore the coefficient of rolling resistance obtained under these conditions will also be higher than the real one. /306

When determining rolling resistance on these setups it is difficult to take into account, with a sufficient degree of accuracy, friction losses in the bearings and air resistance.

Determining the coefficient of rolling resistance under road conditions on electric cars and trolleys takes place by measuring with instruments the power expended on uniform motion along a

horizontal road at low velocities when we can ignore the force of air resistance.

This power is decreased by the value of the losses in the transmission which was measured by rotating the weighted drive wheels at the same velocity as in the tests[2].

The calculated formula is as follows:

$$f = \frac{N}{Q_a v}$$

where N is the power expended on rolling in kg·m/sec; Q_a is the weight of the electric car (trolley) in kg; v is the velocity in m/sec.

This method for determining rolling resistance does not take into account friction losses in the bearings of the rear wheels or air resistance.

The coefficient of rolling resistance is determined by different methods for an automobile: by skidding with decelerated motion ("coasting") and by motion along a road slanted at various angles.

In the first method the automobile on the tires being tested skids with a constant velocity of up to 10-15 km/hr (so that losses due to overcoming air resistance are insignificant). In the linking device between the tow car and the skidding car a dynamograph is placed which records the value of the force necessary for the wheels to roll on the tires being tested. The coefficient of rolling resistance (defined as the ratio of the tractive force to the weight of the automobile) will differ somewhat from the actual value, since the actual value will include friction in the transmission and in the wheel bearings and will also refer to the rolling of all the drive wheels at that time when with independent motion of the automobile, torque is transmitted through the drive wheels. To exclude /307 the influence of friction in the transmission we detach the transmission by detaching the wheels from the semiaxles.

When determining the coefficient of rolling resistance on an automobile by the remaining methods and when conducting other road tests, in a number of cases we record the time, distance and velocity. To measure these values we use various instruments, one of the most popular of which is the "distance-velocity-time" instrument, which is activated by the "fifth-wheel", i.e., a wheel with a pneumatic tire, usually of small dimensions, which is attached to the chassis or the frame of the automobile and rolls along the road

---

[2] The losses measured in this way in the transmission, which transfer almost no moment, differ from the friction losses in the loaded transmission during the tests.

along with the automobile. The instrument records the change in velocity as a function of the distance traveled by the automobile and also records segments of this distance traveled during various time intervals.

Sometimes a simpler "distance-time" instrument is used. We can calculate the velocity according to the readings of these instruments.

In the absence of "distance-velocity-time" or "distance-time" instruments we can calculate the time by a clock, and mark off the road using a device which ejects dye under pressure. By successive measurements of sections of the road between the marks we can determine the values of velocity and deceleration (at low velocity). The necessary motion parameters of the automobile can also be obtained by calculating time of passage past columns set up along the road.

Deceleration (negative acceleration) at various points along the path of the automobile can also be recorded by inertial type instruments (decelerometers).

The coefficient of rolling resistance at low velocities can be determined by the decrease in velocity within a given range of values or up to a complete stop of the automobile.

In the first case the coefficient of rolling resistance is found from the expression

$$f = \frac{v_1^2 - v_2^2}{2gS}$$

where v_1 is the velocity at the beginning of motion, v_2 is the final velocity, S is the distance over which deceleration occurs.

This formula does not take into account air resistance. If we measure using a decelerometer the initial (j_1) and final (j_2) deceleration we can exclude air resistance using the formula

$$f = \frac{j_2 v_1^2 - j_1 v_2^2}{g(v_1^2 - v_2^2)}$$

When the vehicle comes to a complete stop the coefficient of rolling resistance is determined by the formula /308

$$f = \frac{v^2}{2gS}$$

where v is the initial velocity and S is the distance traveled by the vehicle.

Since in the last formula losses due to overcoming air resistance are not taken into account, the velocity v must be small (10-15 km/hr).

These formulas do not take into account the friction losses in the transmission and wheel bearings. Nor do they take into account the kinetic energy of wheel rotation in comparison to the energy of the forward motion of the automobile.

The influence of friction in the transmission can be eliminated by disconnecting the drive wheels from the transmission. However, this complicates the tests.

To ignore friction losses in the transmission and in the drive wheel bearings we must suspend the wheels and run the engine at a velocity equal to the initial velocity in the road test. Then we disengage the gears and measure the time it takes for the velocity of rotation to decrease to the value of the final velocity in the road test.

The value which takes into account the influence of losses in the transmission on the coefficient of rolling resistance can be expressed approximately by the formula

$$\rho = \frac{zI(v_1 - v_2)}{Q_a r_{r1}^2 t}$$

where z is the number of suspended drive wheels; I is the moment of inertia of the wheels in kg·cm/sec^2; Q_a is the weight of the automobile in kg; r_{r1} rolling radius of the wheel in m; t is the time of rotation of the suspended drive wheels in sec.

The coefficient of rolling resistance taking into account the influence of these losses will be:

$$f_1 = f - \rho$$

The determination of the coefficient of rolling resistance when the automobile is moving along the road with a constant slope is based on the fact that the automobile under these conditions reaches a certain velocity which remains stable, since that component of the weight of the automobile parallel to the road P_h equals the motion resistance comprised of rolling resistance and air resistance:

$$P_h = P_f + P_w$$

where P_f is the force of rolling resistance, P_w is the force of air /309 resistance.

In this type of test the coefficient of rolling resistance is determined from the formula

$$f = \tan\alpha - \frac{kFv^2}{Q_a}$$

where α is the slope of the road, k is the coefficient of air resistance, F is forward surface of the automobile in m^2, v is the velocity of uniform motion of the automobile, in m/sec.

The value of k is found by placing a model of the automobile in a wind tunnel. For the basic types of automobiles this coefficient is given in the manuals.

When making tests on small slopes where the velocity of the automobile is small, we can assume that the coefficient of rolling resistance is equal to the slope on which motion of the automobile is uniform.

We should note that use of the above-mentioned method is complicated by the need to have a rather large section of the road with a constant slope. It is easy to produce these conditions by conducting the test on a racetrack.

We can propose a more convenient method for determining the coefficient of rolling resistance under road conditions which provides an opportunity to use practically any section of road with a small slope for our experiment.

From a prescribed location the automobile moves from a stationary position, without engaging the engine, and after it descends and coasts it stops according to inertia. This method can also be used successfully since it does not require measuring the parameters of motion of the automobile (velocity, acceleration), which eliminates the need to use instruments and increases the accuracy of the experiment.

In this case the coefficient of rolling resistance can be determined according to the formula:

$$f = \frac{\sum_{1}^{n} S_i \sin \alpha_i}{\sum_{1}^{n} S_i \cos \alpha_i}$$

where S_i is the extension of the road sections; α_i are the slope angles of the road sections to the horizontal.

Using this expression we can determine the value of the coefficient of rolling resistance with any set of slopes and dimensions of the road sections. The slopes need not be significant (to eliminate the influence of air resistance), the velocity of the automobile need not exceed 10-15 km/hr.

Rolling resistance of tires under road conditions can also be determined on dynamometric trollies. We can also use dynamometric /310

trollies, skidded by an automobile, and also self-propelled trollies on which we measure the forces arising with various rolling regimes of the wheels. The coefficient of rolling resistance, as in previous methods for testing, is defined as the ratio of the force necessary for the wheel to roll to the normal load.

The advantage of tests on dynamometric trollies in comparison to tests on automobiles consists of the possibility of more precise measurements and creating the most diverse test conditions.

Investigation of the Characteristics which Determine the Lifetime of a Tire

The lifetime of a tire during operation depends on a whole series of factors and for different tires is determined by different properties.

A large number of tires become useless due to tread wear; however, carcass blowout or separation of the tread also take place.

Such defects as a break in the tire bead or a break in the wire rings are encountered much less often: with improper construction of the tire or improper usage.

Included in the series of laboratory tests designed to evaluate the lifetime of tires are such tests as rolling the tire on stands up to the blowout point, determining the durability of the carcass under concentrated loads, determining the wear resistance of the tread. Under laboratory conditions we also determined the operating temperatures of the tire under various kinds of conditions which influence the durability of the materials. However, as we have already pointed out, it is impossible to completely evaluate quality of automobile tires under laboratory conditions.

A complete evaluation of the lifetime of one or another set of tires can be obtained only as a result of operational tests.

Bench Rolling Tests

Bench rolling tests are conducted basically to obtain data which allow us to determine the fatigue strength of the tire. Figure 246 shows a schematic of an IPZ-type bench rolling machine used by domestic industry to test tires. The rolling drum (1) is set in motion by an electric motor. The tires being tested (3) are placed on two carriages (4) which are shifted on rollers along the frame. One tire is placed on each carriage. Load is placed on the tire by the weight (6) using a lever (5). The bench allows us to test tires with a diameter up to 1400 mm under a load up to 4500 kg at rolling /311 velocities from 25 to 150 km/hr with an even regulated velocity. Similar benches are used for rolling tires in the factories of the Firestone Company (USA). Figure 247 shows a schematic of the bench

rolling machines used in certain factories of the Dunlop Company (England). The wheel with the tire being tested (3) is mounted on a lever (2). The lever pivots at point (1) on the frame of the bench. By action of the weight (4) the tire is pressed onto the rolling drum (6). As the screw (5) is rotated the weight moves along the lever and thus can exert a prescribed radial load on a given tire.

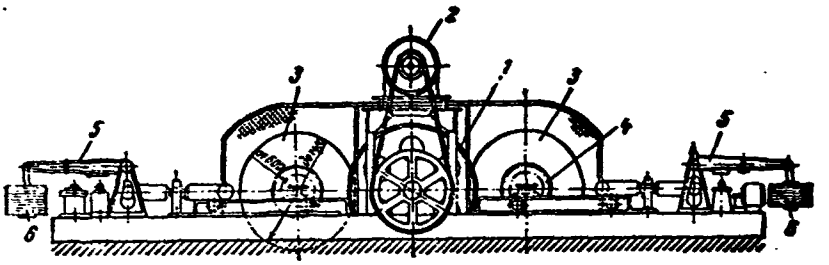

Fig. 246. An IPZ Bench Rolling Machine: (1) Rolling Drum; (2) Motor; (3) Tire; (4) Carriage; (5) Lever; (6) Weight.

Figure 248 shows a schematic of a bench rolling machine for testing 12 light tires simultaneously. This machine was installed in a tire factory of the Goodyear Company. The bench consists of a metallic drum with a diameter of 6 m, fixed in a vertical position, and a shaft. On this shaft inside the drum in four parallel planes 12 outer covers are installed which roll along the internal surface of the drum. The radial load on the tire is exerted by a pneumatic system. Air is fed through the hollow shaft of the motor and the rods on which the tires are attached. The rolling velocity is about 50 km/hr.

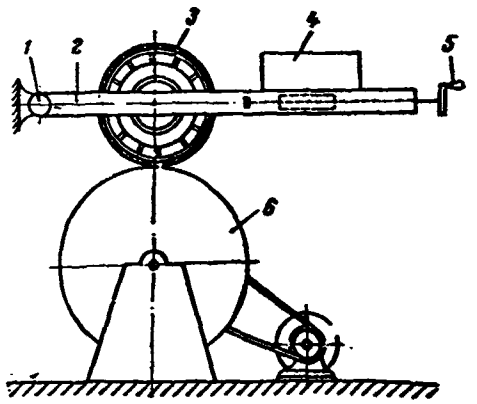

Fig. 247. A Bench Rolling Machine with a Movable Weight: (1) Pivot Point; (2) Lever; (3) Tire; (4) Weight; (5) Load Screw; (6) Rolling Drum.

Figure 249 shows a schematic of /312 the bench rolling machine used in the tire testing laboratories of the U.S. Rubber Company. The bench machine consists of a massive metal ring-drum (2) resting on two wide rollers (4) with flanges. In the upper portion the ring passes through a guide (1) which prevents the rings from lateral shifts. The radial load on the tire is exerted using a vertical shift of a plate (5). The electric motor (3) rotates the tire which moves the ring.

Usually the surface of the drum of a bench rolling machine is covered with a certain number of cleats. Cleats cover the entire width of the rolling part and are set at various angles to the

generating line of the drum. Cleats of various heights (from 10-40 mm) are used.

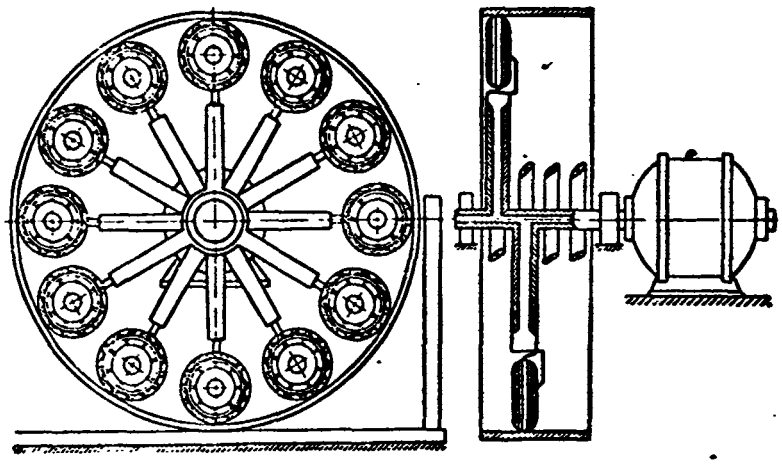

Fig. 248. A Machine for the Simultaneous Rolling of 12 Tires Along the Internal Surface of the Drum.

The way in which the tire fails on the machine depends on the construction of the tire and the test regime. /313

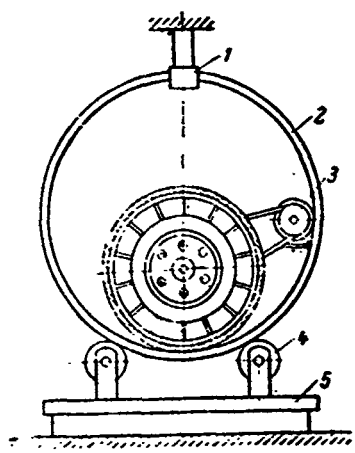

Fig. 249. Machine for Rolling Tires Along the Internal Surface of a Ring-Shaped Drum: (1) Guide; (2) Ring; (3) Electric Motor; (4) Roller; (5) Loading Plate.

So that the test results on the machine provide a representation of the operational reliability of the tire, it is necessary that form of tire failure corresponds to total destruction during usage. Thus it is also necessary that the operating temperature of the tire on the machine not differ substantially from the operational temperature.

It is very difficult to satisfy these requirements and at the same time provide a rather short duration for the test.

Therefore, as a rule, bench tests are conducted with particular types of regimes, and their results are used mainly for comparison of various models of tires.

A typical test regime for tires on bench machines is usually determined in the following way.

The internal pressure in the tire and the radial load at the beginning of the

tests are set equal to the normal operational values. The choice of rolling velocity of the tire is guided mainly by those temperatures which the tire attains when rolling. The temperature of the tire when rolling on machines must not exceed its maximum operational temperature by more than 15-20° C. Otherwise, the tires when rolling on the machine might fail due to the higher temperatures and in operation might be sufficiently efficient. In most cases the rolling velocity of the tire decreases as the number of carcass plies increases (or as the tire dimensions increase).

As an example let us present the values of rolling velocity for one of the regimes for testing heavy duty tires used in the National Research Institute of the Tire Industry:

Number of Cord Plies in a Carcass	Rolling Velocity km/hr
6-8	50
10-12	40
14 or more	30

To accelerate the tests and obtain a certain particular mileage, the load on the tire is increased. Thus a rolling regime is usually used in which the load is increased by 25% of the initial value every thousand km over 5000. Thus the load is reduced to a factor of 2 and there is no subsequent increase. We should note that similar methods of test intensification are not valid. Apparently, when necessary it is advisable to designate a more rigorous initial test regime.

Along with a typical regime of bench tests, special regimes are also used to obtain a particular form of tire failure. Thus, for /314 example, when testing tires at low pressure separation of the carcass plies takes place; with high internal pressures and velocities, the tread can be stripped off, etc.

It is very difficult to develop a test regime which provides an identical form of failure for all tires being compared. However, tests under these regimes are of great interest since they allow us to compare tires according to a particular index (the strength of the seal between plies, carcass durability, etc.).

The operating temperature is usually measured during bench rolling.

The temperature is measured by a needle thermocouple usually in the highest temperature range, i.e., in the breaker, carcass, and in the various zones of the outer cover profile. The characteristic zones of measurement are along the equator, in the shoulder zone, and in the side section.

To obtain average data measurements are usually made in cross sections, at "light" and "heavy" points on the tire or in cross

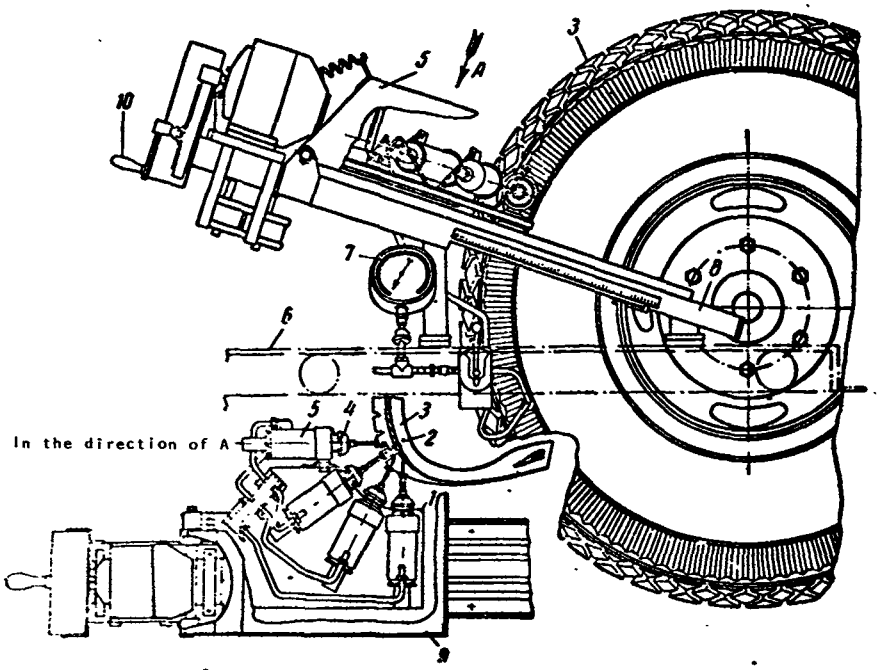

Fig. 250. A Device for Simultaneously Measuring the Temperature at Five Points on a Tire: (1) Corner Plate; (2) Thermocouple Needle; (3) Outer Cover; (4) Thermocouple Mount; (5) Pneumatic Cylinder; (6) Carriage; (7) Manometer; (8) Angle Bracket; (9) Carriage; (10) Screw Handle.

sections located equidistant from these points. To determine the temperature of the tread surface we used a ribbon thermocouple. /315

The problems of this method of measurement are the need to interrupt the test for a rather long period of time (1-3 minutes), during which the temperature in the tire is redistributed, and also the expenditure of large physical force on inserting the thermocouple needle into the outer cover.

These problems are eliminated to a certain degree under laboratory conditions by using a device (Fig. 250) which consists of a carriage with several thermocouples. The carriage is moved into position by rotating a screw using an electric motor (or manually). The thermocouple needles are inserted into the outer cover using a pneumatic drive; the needles are restored to their initial position using springs. When using this device, the time required to measure the temperature (at 5 points), is decreased to 30-40 sec.

To eliminate completely the need to interrupt the test, tempera-

ture measurements are made by miniature thermocouples embedded in the outer cover. A comutator with a series of insulated contact rings (Fig. 251) is used to connect the current.

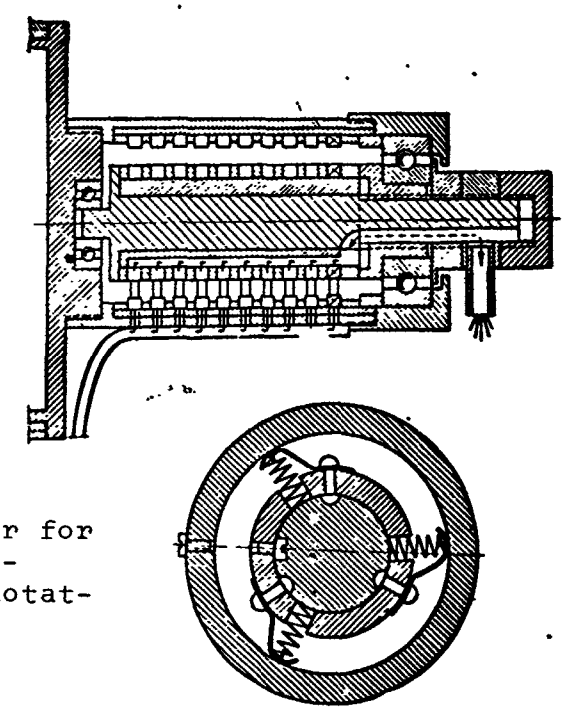

Fig. 251. A Collector for Connecting the Thermocouple Located in a Rotating Tire.

The maximum temperature of the tire is usually reached within 1-2 hours. The temperature and time of maximum heating depend on tire construction and the test conditions (velocity, internal pressure of the tire). /316

The temperature distribution over the cross section of the tire varies with its construction, materials and operating conditions. Usually the carcass or breaker in the shoulder zone and along the equator are heated to the highest temperature. As the internal pressure decreases, the maximum temperature may be generated in the sidewalls of the tire.

Evaluation of Carcass Resistance to Concentrated Stresses

When the vehicle is in operation the tires usually come in contact with the various road obstacles. In most cases when the tire hits these obstacles it undergoes high concentrated forces which can lead to tire blowout if the strength of the rubberized cord carcass is not sufficiently great.

To evaluate the ability of the tire to resist the action of high concentrated stresses, the tires undergo tests for carcass strength which simulate the interaction between a tire and an obstacle under road conditions. These tests were conducted by static

compression of the tire on a press by puncturing the tire with a plunger or by passing it over obstacles located on the drum of a bench rolling machine. Sometimes these tests are conducted under road conditions.

For road tests a metal plate with detachable obstacles was located and attached on the road flush with the outer cover. The obstacles were made of several conical disks and a round conical tip. This allows us to regulate the height of the obstacle by using various numbers of disks. The left front wheel of the vehicle was driven over the obstacle (Fig. 252). This allows us to obtain a function relating the height of an obstacle necessary to cause blowout and the internal pressure and the velocity of a vehicle [42]. As obstacles we used cones made of a number of disks, 10 mm in height (Fig. 253). The greatest height of the obstacles was 150 mm, the angles at the apexes of the cones were 30 and 70°, and the radii of curvature of the apexes were, respectively, 0 and 7.5 mm. When the tire was driven across the obstacles at velocities of 30-40 km/hr the tire tread remained intact and the carcass was usually detected by a slight leak at the impact point or by misalignment of the tread checks. When the tire was unmounted after the test, inside the outer cover we discovered a break in all the carcass plies. At higher velocities we observed local destruction of the tread along with a break in the carcass.

Puncture tests under road conditions are not popular due to /317
their complexity and danger. Therefore it was necessary to develop a way to simulate a tire hitting an obstacle under laboratory conditions. To do this we used a bench rolling machine equipped with an obstacle which moves on the rolling part of the drum for repeated contact with the tire.

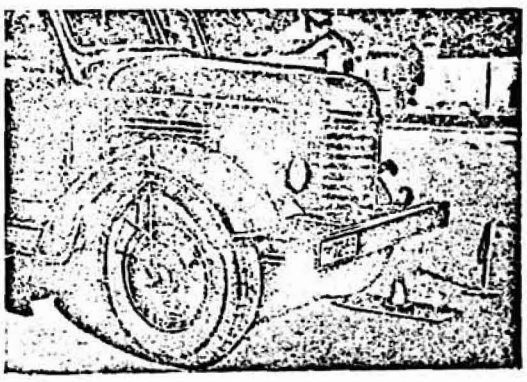

Fig. 252. A Vehicle Hitting an Obstacle During a Test.

The corresponding device (Fig. 254) consists of a mechanism for shifting the carriage and a directional mechanism. The carriage (2) is shifted along the tracks of the frame (1). The obstacle is screwed onto a pin on the carriage, is easy to remove and can be replaced by one which differs in shape or height. To hold the carriage in the lowest position and in the middle of the rolling part of the drum a roller (3) with two cams (the cams which hold the car- /318
riage cannot be seen in Fig. 254) and a lever (4) are located in the frame.

When the lever (4) is in a vertical position, the carriage, due to the tension of the cables (5), is held in place by a tooth on one

of the cams of the shaft (3). When the lever (4) is rotated and consequently the cams free the tooth of the carriage, and by action of the tension of the cables, the carriage is allowed to shift along the generating line of the drum. The frame (1) is attached to the rim of the drum of the bench rolling machine. The tension of the cables is maintained by centrifugal forces of weights attached to the lever, which is in turn attached to the rolling drum, and also by action of a spring (not shown in Fig. 254), which holds the lever in the lowest position when the drum is stationary.

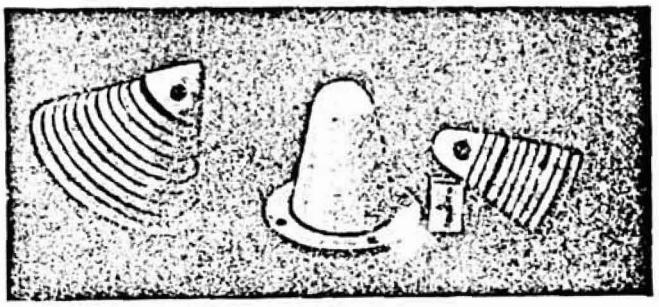

Fig. 253. Types of Obstacles Used for Determining Carcass Strength During Road Tests.

The directional mechanism of the device is attached to the frame of the machine and consists of a solenoid with a lever, a return spring and a peg. When the solenoid is engaged, the peg moves forward. When the solenoid is disengaged the spring returns the peg to the initial position. The solenoid is inserted at a distance from the control panel.

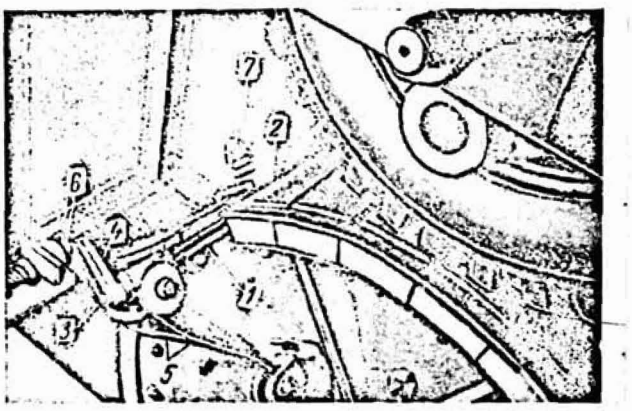

Fig. 254. The Drum of a Bench Rolling Machine with a Device for Shifting the Obstacles: (1) Frame; (2) Carriage; (3) Shaft; (4) Shaft Lever; (5) Cables; (6) Solenoid Peg; (7) Obstacle.

Before the test begins, the carriage with the obstacle is set in the lowest position and held in place by the shaft cam. When the tire is rolling, at a particular moment the solenoid is engaged and the peg (6) moves forward toward the drum. The lever (4) of the shaft (3) when it hits the peg rotates together with the shaft and its cams. The end cam releases the carriage, and the carriage together with the obstacle begins to move along the generating line of the drum due to the tension of /319 the cables. After the lever (4) hits the peg of the solenoid, the return spring restores the shaft to its initial position, and therefore the carriage and obstacle do not slip through to the opposite side of the drum but hit the middle cam and are held in the center of the rolling part and the tire hits the obstacle only once. When the lever (4) hits the solenoid peg again, the shaft rotates and the carriage is retracted from the rolling surface of the drum.

To determine the zone of the tire which comes in contact with the obstacle, before each impact on the obstacle the apex of the latter is marked with a colored wax crayon which leaves a mark on the tire. Tests begin at the lowest obstacle height. After the tire hits the obstacle twice, the height is increased by 5 mm until the blowout point is reached. The blowout height of the obstacle is defined as the average of the test results in a tire in 2-3 zones. The tire strength of a given group of tires is evaluated according to the test results of 2-3 tires. Tire tests involving contact with obstacles provide the operational characteristic of the carcass strength of the tire. These tests are most convenient for comparing the strength of tires of various dimensions or the tire strength of tires with various operational regimes. To make a comparative estimate of the strength of tires of a particular type such complex tests are not necessary. In this case, simpler tests are conducted on plungers or presses.

Drop hammer tests are made by dropping the mounted inflated tire on an obstacle set on a plate (Fig. 255), or dropping a weighted obstacle from a particular height onto a stationary tire (Fig. 256).

To prevent the plate from bouncing several times after the drop, the drop hammer (Fig. 256) is equipped with a device which, after the frame and obstacle recoil from the tire, automatically holds it in the most vertical position.

Figure 257 shows a schematic of a pendulum drop hammer developed at the Institute for Scientific Research of the Tire Industry.

During drop hammer tests the work expended on tire blowouts is determined. To do this the height of the drop or the weight of the weights is gradually increased to the point where impact causes the tire carcass to blow out. Before each drop the tire is rotated so that impact does not take place twice at the same point. For each tire dimension a strength norm is set; i.e., a value for the blowout energy.

Sometimes a different test method is used: with a constant, rather high drop height, the height of the obstacle is varied. These obstacles consist of a number of conical disks and the height of the obstacle necessary to cause tire blowout is measured.

Both test methods give identical comparative characteristics of tire strength and either is acceptable.

The most popular method for testing the carcass strength of tires is the press method. In these tests a pin of a particular shape is slowly pressed into the tire. The values of the force and deformation at the blowout points are determined. One can also determine the work expended on tire blowouts.

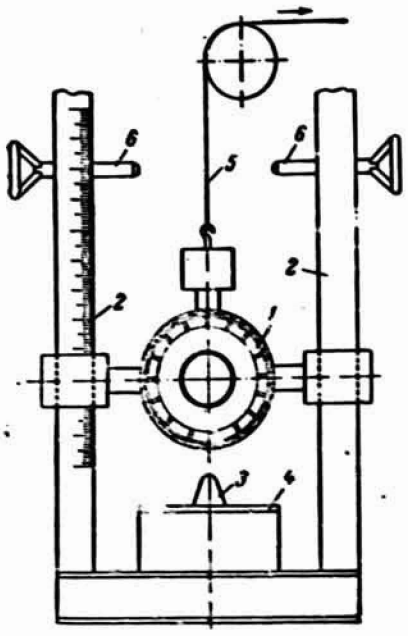

Fig. 255. A Schematic of a Drop Hammer for Testing Tires by Dropping a Frame with a Tire; (1) [illegible]; (2) Track; (3) Pin; (4) Plate; (5) Cable; (6) Catch.

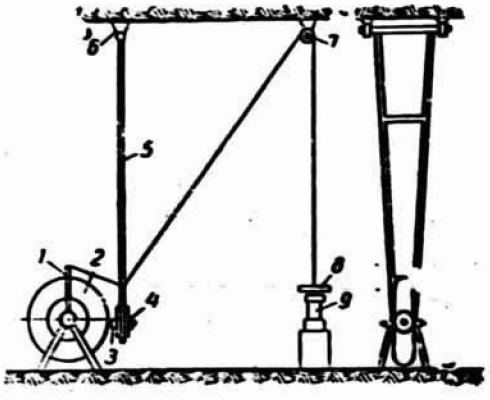

Fig. 257. A Schematic of a Pendulum Drop Hammer: (1) Frame; (2) Tire; (3) Pin; (4) Detachable Weight; (5) Pendulum; (6) Bearings; (7) Pulley for the Braking Cable; (8) Braking Weight; (9) Pneumatic Lift for the Braking Weight.

/320

Fig. 256. A Drop Hammer for Testing Tires by Dropping a Pin.

The tire is usually pressed /321
by one constant cylindrical or conical pin at 4-6 points on the tire. The tire strength is defined as the average of the obtained readings.

Figure 258 shows an overall view and Figure 259 shows a schematic of a small press for tire pressing developed at the Scientific Research Institute of the Tire Industry.

On the upper part of the welded rectangular frame at a height of 2 m are a cylinder (6) with a plunger (7), a grease pump (2) and an electric motor (1). The plunger is moved downward by grease pressure in the cylinder (6), and its free return upward is accomplished by special weights (9) located in the vertical columns of the frame.

The mounted tire is placed so that the pin (8) of the plunger lightly touches the tire tread (10). Afterwards the overflow valves are shut (15) and the motor (1) of the grease pump (2) is engaged.

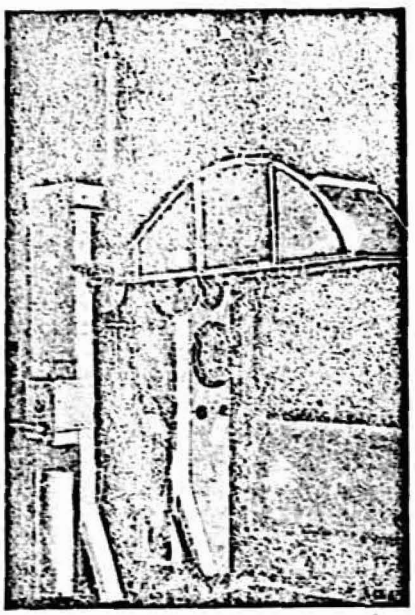

Fig. 258. A Press for Press Testing Tires.

The grease flows from the tank (17) under pressure to the operating cavity of the cylinder (6) and causes the plunger (7) to move. The weights (9) move upward. When outer cover blowout takes place, the grease pressure in the cylinder falls drastically and the contact manometer (14) disconnects the electric circuit and the motor of the grease pump is shut off. Then the valves (15) are opened and during the free ascent of the plunger the grease flows back into the tank (17). The instrument (13) for measuring the value of the force of the pin in the tire is a cylindrical shaft on whose axis an arrow is drawn. The plunger is connected by a flexible cable through a system of rollers with the instrument shaft, whose dial is marked off in mm. The change in the force on the tire, in proportion to the pressing strength, is determined according to the change in the grease pressure in the operating cavity of the overflow cylinder; it is automatically registered by a recording manometer (12). /322

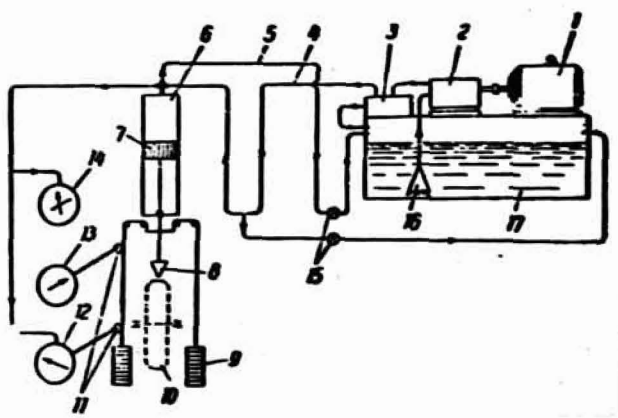

Fig. 259. A Schematic of a Small Press for Tire Pressing: (1) Electric Motor; (2) Grease Pump; (3) Valve Box; (4) Pressure Line; (5) Overflow Line; (6) Cylinder; (7) Plunger; (8) Pin; (9) Weights; (10) Tire; (11) Cable Rollers; (12) Recording Manometer; (13) Instrument for Measuring Tire Deformation; (14) Contact Manometer; (15) Valves; (16) Grease Filter; (17) Grease Tank.

Figure 260 shows the characteristic functions relating tire deformation to load on the pins obtained by pressing a 9.00-20 tire. We can see from the graphs that the force can be assumed to be directly proportional to tire deformation. Thus the work necessary to cause tire blowout is defined by the expression

$$A = \tfrac{1}{2}PS = \tfrac{1}{2}pFS$$

where P is the blowout force, S is the blowout deformation, p is the grease pressure in the cylinder (after deducting the pressure of the free ascent), F is the area of the plunger.

The experiments showed that a relative estimate of carcass strength is not a function of pin shape. Therefore, to estimate carcass strength we can take a press pin of a single shape. The Scientific Research Institute of the Tire Industry in their tests on heavy-duty tires used a pin with a conical angle of 30° and a radius of curvature of the apex of 40 mm, and for light tires the pin had a radius of curvature of 7.5 mm. /323

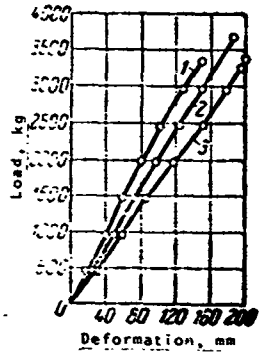

Fig. 260. Deformation of a 9.00-20 Tire as a Function of the Load on the Pins with Internal Pressures of: (1) 5.5 kg/cm^2; (2) 4.5 kg/cm^2; (3) 3 kg/cm^2.

The OPSh-30 press (cf. Fig. 235, p.258) is also used for press tests. In this case an obstacle of the same shape as in a small press is placed on its plate.

Parallel tests for carcass strength on drop hammers and presses of a large number of tires of varying strength which were conducted in the Scientific Research Institute of the Tire Industry showed that the blowout work of tires during tests on drop hammers and the blowout work of tires during press tests are roughly equal. These tests also showed that the values of the blowout deformation during tests on drop hammers and presses are also equal.

Thus the experiments showed that methods for testing the carcass strength of tires on a drop hammer do not have significant advantage over static methods. The press method for testing tires, since it is the most simple and precise, is the most convenient for practical use in factory tests. The blowout energy of a tire of a given dimension can be used under factory conditions as one of the indices of production quality.

Estimate of the Wear Resistance of Tires

Tread wear is a major cause of tire failure when operating under normal road conditions. At the present time, up to 80-90% of tires become useless after complete wear of the tread.

The wear resistance of a tire is determined by the value of the specific wear of the tread equal to the wear of those sections of the tread referring to a unit distance (usually 1000 km) under particular road conditions and by the coefficient of the uniformity of wear which is equal to the ratio of the maximum specific wear and its average value for the tire as a whole. Wear is frequently measured in mm (the value of the decrease in the height of the tread ridges). In this case measurements are made by calipers or by a mechanical gauge. The problems with this method are its low degree of measuring accuracy (roughly ± 0.5 mm when the total height of the

tread is 10-15 mm), which is explained by rubber deformation by the measuring instrument and also by the difficulty of making measurements precisely at one place.

Sometimes wear is determined by the weight of the entire worn section of the tread relative to the mileage of the tire. However, this method yields only an average value for wear and is accompanied by difficulties in the precise weighing of a heavy wheel and the need for a very careful cleaning with each measurement.

Tires are tested for wear under laboratory and road conditions. /324 Laboratory tests consist in rolling the tire along the surface of a road surface attached to the drums of a bench rolling machine or on plane rolling disks of the carousel type.

Bench tests are sometimes made by transferring torque from the tire through the wheel. According to certain data, when the torque is increased from 5 kg·m to 10 kg·m the wear intensity when the tire is rolling along a drum with riffled steel surface increases by a factor of 4.5.

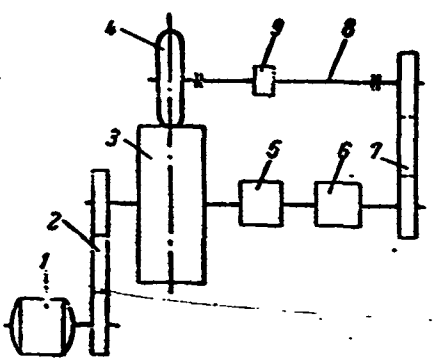

Fig. 261. Schematic of a Machine for Rolling Tires by Transferring Torque or Braking Moment: (1) Electric Motor; (2) Belt Drive; (3) Rolling Drum; (4) Tire; (5) Transmission; (6) Electromagnetic Clutch; (7) Chain Drive; (8) Cardan Shaft; (9) Diameter for Measuring Torque.

Machines are used which provide for a rolling wheel with torque transferred by a braking device (dynamo, hydraulic brake, etc.). In certain machines torque or a braking moment is exerted on the tire by using a closed kinematic system which provides power circulation. A schematic of one of these machines is shown in Figure 261. The electric motor operates and transfers torque to the closed system consisting of machine drive, a rolling drum, a reducer, an electromagnetic clutch, a chain drive, a Cardan shaft, and an instrument to register the value of the torque and a wheel with the tire being tested.

Since the tire is rotated simultaneously by the drum and by the drive, it is possible by varying the transmission ratios in the latter, to conduct tests with the transfer to the tire of either torque or braking moment.

The test conditions on these machines differ from road conditions since the nature of tire contact with the road surface varies. Great difficulties also arise because of the rapid change in the state of the rolling surfaces of the machines (lubrication, wear), and therefore the results of these tests are not comparable.

Road tests for wear have been widely employed. These tests are conducted in a number of accelerated tests by loading the automobile with ballast. In this case the mean daily path reaches 600-800 km/day. During the tests the wheels are rotated as they would be in operation. Wear is measured and designated at points on the tread usually every 1000 km. /325

Wear tests are also made under conditions of normal automobile operation in automobile factories [43]. This provides an opportunity to obtain the most reliable data on wear. However, these tests take a long time.

To obtain the data on the wear resistance of tires quickly, test methods are used based on recording the wear of a thin surface layer of the tread. Included in the number of accelerated methods for determining the intensity and character of wear in the tire is wear measurement using radioactive substances and dye covering the treads.

One of these methods based on using radioactive substances consists in measuring the activity of the tire trail on the road. Into the upper tread ply (4 mm) during preparation of the outer cover triphenolphosphate is injected which contains radioactive phosphorus P^{32}. Measurement is made with a geiger counter mounted on a dolly which follows at a distance of 1 m from the rear "active" wheel.

One problem with this method is its insufficient accuracy since the radioactivity of the trail is approximately equal to the level of the background radiation. In addition, triphenolphosphate is unevenly distributed in the upper ply of the tread, penetrates the rubber toward its surface and the radioactive particles may be only slightly dispersed. For small distances (several tens or hundreds of meters), this method allows us to clarify the qualitative influence of various factors on wear, but does not allow us quantitatively to estimate the wear resistance of tires.

According to a method developed in Czechoslovakia, the tire is given additional radioactivity by a benzene solution of radioactive sulfur S^{35} which is injected into the finished outer cover by swelling. The use of this method is limited by the same reasons as the previous one since the radioactive sulfur quickly permeates the rubber and the radioactivity of the trail varies.

We have some data concerning another method using radioactive sulfur S^{35}. The latter is injected under the tread and wear is determined according to the change in intensity of the radiation on the tire surface.

The Scientific Research Institute of the Tire Industry employs a method using radioactive substances. This method consists of injecting at various places on the tread of the outer cover before the test radioactive point sources prepared using radioactive thallium Tl^{204}.

Sources of length 0.3-0.5 mm and diameter 0.2-0.5 mm are injected using a hyperdermic needle and a plunger (Fig. 262) at various places on the tread to a depth of no more than 1.5 mm. The radioactivity of the sources is then measured. /326

During the tests the prepared tires undergo a series of measurements of the radioactivity of the sources, according to the change in which the wear is determined for a section of the tread located under the source. New sources to replace the old ones are introduced in proportion to the wear.

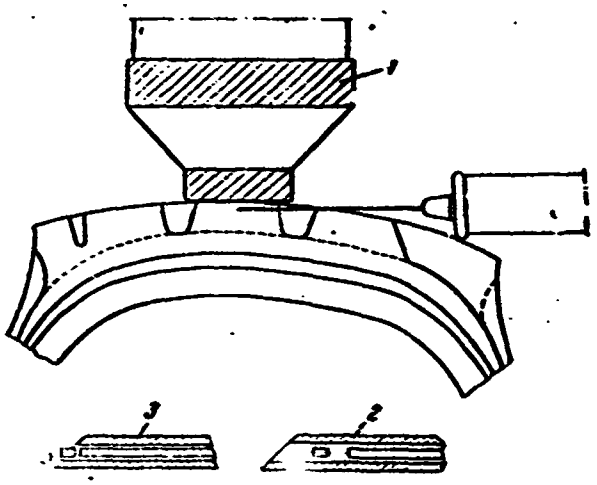

Fig. 262. Injection of Radioactive Sources into the Tire Tread: (1) An MAI Instrument Sensor (Marked Atom Intensiometer); (2) Position of the Source and the Plunger in the Canal of the Needle During Injection; (3) Position of the Source and the Plunger at the Moment of Injection.

To obtain sufficient data concerning tire wear it is necessary to test 4 tires; 8 sources should be injected into each tire. The distance traveled by the tire to estimate wear resistance of the tread with an accuracy of no less than ± 10%, according to the data of the authors, must be 1600 km. The preliminary distance before testing must be no less than 500 km.

The advantage of this method over the previous one is the possibility of estimating wear resistance of both a new tire and of one that has already been in use, since the radioactive substance is injected into the outer cover directly before the test. This method eliminates the necessity to produce tires with radioactive substances and also reduces the danger of contaminating the operator, the equipment and the road during tests.

A more simple technique, but one which gives less precise results, for an accelerated determination of the intensity and nature of tire wear under road conditions consists in recording the wear of dye which has been previously applied to the tread.

To obtain data which is independent of the influence of disbalance, the tread is painted at 2 diametrically opposed sections which are equally distant from the "heavy" and "light" points. A thin layer of colored dye is applied to a section somewhat larger than the contact zone. The wear resistance of the layer of dye after it dries is checked using a simple device which records the time it takes the dye to wear off by a sample of the road surface on which the road tests are conducted. /327

A vehicle riding on these tires moves at a prescribed velocity until the dye has completely worn off. The total distance traveled characterizes the intensity of wear as a function of the tire construction. The influence of the properties of the tread rubber is not apparent.

Operational Tire Tests

Tire tests conducted under conditions of normal usage yield the most reliable data concerning their lifetime.

Since the distance a tire can travel depends to a large extent on the road condition, tire tests are usually conducted on particular groups of roads.

As a function of their influence on the mileage of tires, we can divide roads into three groups: A, B, C (cf. Chap. VII, p. 199).

An objective evaluation of the condition of a road is obtained using a special instrument; i.e., an impact measuring device of the Kharkhov Highway Institute system. This instrument records the total (for 1 km) shift in the rear axle relative to the body of the automobile. An impact measuring device installed in an M-20 automobile ("Pobeda"), for roads of Group A yields the reading 250-300 cm/km, and on roads of Groups B and C, respectively, 700-900 cm/km and 1200-1500 cm/km.

To obtain reliable data about the distance traveled by a tire before failure, certain necessary conditions must be satisfied. The first and most important of these conditions is a sufficient number of tires whose operation has been observed.

Due to the natural heterogeneity of the quality of tires and mainly due to the heterogeneity of operation conditions there is a significant divergence in the values of the lifetimes of tires.

Under these conditions to determine the average distance traveled during the lifetime of a tire with a particular degree of accuracy, it is necessary to test at least a certain number of tires.

The results of testing a group of n tires is characterized by an average lifetime before tire failure of S. If the difference between the lifetime of each given tire S_i and the average lifetime of the group S can be given in terms of $S_i - S$ (deviation), then the discrepancy in the values for the lifetime can be characterized by the mean square deviation:

$$s = \sqrt{\frac{\Sigma (S_i - S)^2}{n}}$$

The relative characteristic of divergence is the so-called variation coefficient: /328

$$v = \frac{\sigma}{S} .$$

Probability theory allows us to determine the number of tires undergoing tests necessary so that their average lifetime characterizes within a certain margin of error the average lifetime of all the tires of the given group (total number of tires in a group is assumed to be very great). The corresponding formula has the form

$$n = \frac{t^2 v^2}{\Delta^2}$$

where Δ is the permissible relative difference between the average mileage of the tires tested and the average mileage of the entire tire group, v is the variation coefficient; the coefficient t is chosen depending on the necessary reliabilities of determination of the average mileage.

With $t = 2$ the reliability of the result is 0.954, i.e., in 95 cases out of 100 the average lifetime of all tires will differ from the average lifetime of the tested tires by no more than the given value Δ. With $t = 3$ the reliability is 0.99.

An interpretation of the results of numerous tire tests showed that when testing tires on roads of one group, the variation coefficient v lies within the limits $v = 0.35$-0.4.

Thus taking $t = 2$ and limiting ourselves to determination of the average lifetime of tires with an accuracy of up to 5% ($\Delta = 0.05$), we obtain the required number of tires:

$$n = \frac{t^2 v^2}{\Delta^2} = 190 - 250 .$$

A decrease in the number of tires tested inevitably leads to a less reliable determination of the average lifetime. Depending on the uses of the tires, they are tested on roads of one or another group or on roads of all groups. Thus the indicated number of tires must be tested on roads of each group.

In order to exclude the influence on the test results of random factors not related to the tire quality, when conducting operational tests an additional observation should also be made of the technical state of the automobile (the state of the rim, brake, steering, alignment and fatigue in the wheels, etc.). The rules for operating a tire should be followed precisely (cf. Chap. VII, p.193).

The tires to be tested should be systematically inspected to determine their condition.

Tires which fail should be carefully analyzed to ascertain the reasons for failure and the lifetime of a tire should be precisely recorded.

The final conclusion concerning the average lifetime of tires, /329 whose operation has been observed, may be made only after all or almost all of the tires had failed.

In view of this, the operational tests are very time-consuming and continue, as a rule, no less than 2 years, which complicates the use of the test results for improving the construction or technology of tires.

We can determine that long before the tests are completed a significant number of tires will have failed but the "remnant" tires which are operated at a lower intensity do not allow us to draw a conclusion about the average mileage of all the tires.

Therefore of great practical value is the method of estimating the results of uncompleted operational tests of tires [44]. This method allows us to decrease the influence of the "remnant" tires on the results and allows us to evaluate the average mileage of tires when only 25-30% of the tested tires have failed.

The basic concept of this method consists in accounting for the lifetime of tires at particular intervals of distance traveled (0-5000 km, 5000-10,000, 10,000-15,000 km, etc.). The number of tires which have failed in a given interval refers not to the total number of tires but to the number of tires which have been actually tested in a given interval. Thus we take into account that due to failure of tires in the earlier intervals, the number of tires tested during each interval beyond the first is lower than the total number of tires per group.

Data concerning the distance traveled by each tire before the time of preliminary interpretation of the test results are recorded on special cards (Table 14). The distance traveled by the tire is noted (with an accuracy up to 5,000 km) in the corresponding column of the card. If the tire has not failed a dot is placed in the column; if it has failed a symbol designating the reason for failure is placed in the column.

Then we add up in each column the number of tires which have passed the given interval (a), which remain in that interval (d) and which have failed in that interval (b). The tires which have failed are classified also as to reasons for failure. The total data on all cards compiled on the tires of a given group are totaled and tabulated which provides a basis for subsequent calculations.

Let us now examine the determinations of the percentage of tires which failed before a given distance interval.

TABLE 14.

Card for Measuring the Lifetime of Tire No. _____ Designation _____

Starting Date of Test _____ Dimensions _____

Number of Tires in Group _____

No.	Serial Number	Distance Traveled, Thousand km												
		0–5	5–10	10–15	15–20	20–25	25–30	30–35	35–40	40–45	45–50	50–55	55–60	60–65
1		—	—	●										
2		—	—	●										
3		—	—	—	—	—	TB							
4		—	—	—	—	—	●							
5		—	—	—	—	—	—	TW						
6		—	—	—	—	—	●							
7		—	—	—	—	—	—	—	●					
8		—	—	—	—	—	—	—	●					
9		—	—	—	—	—	—	—	●					
10		—	—	—	—	—	—	—	●					
No. of Tires Passed, Interval (*a*)		10	10	8	8	8	5	4	—					
No. Tires Remaining, Interval (*d*)				2	—	—	2	—	4					
No. of Tires Failed, Interval (*b*)							1	1						
Due to Blowout							1							
Due to Wear							—	1						
Due to Separation of Plies							—							

TB - Tube Blowout; TW - Tread Wear

In the interval 0-5000 km let b_5 tires fail; the total number of tires tested in this interval is equal to the sum of the tires which have passed the interval (a_5) and the number of tires which have failed in that interval (b_5). Thus the percentage of tires which have failed in the interval 0-5000 km is determined by the formula

$$n_5 = \frac{b_5}{a_5 + b_5} \cdot 100$$

Since, with the final tests, all tires are tested in the first interval, the value n_5 is the percentage of tires which failed both according to the ratio to the tires tested in the given interval and to the entire group. In the same way we can determine the percentage of tires which have failed in the interval 5000-10,000 km in relation to the number of tires tested in this interval: /331

$$\Delta n'_{10} = \frac{b_{10}}{a_{10} + b_{10}} \cdot 100$$

Since not all the tires of the group were tested but only part of the group, equal to $\frac{100 - n_5}{100}$, then the percentage of tires which fail in this interval in relation to the entire group is

$$\Delta n_{10} = \frac{b_{10}}{a_{10} + b_{10}} (100 - n_5)$$

The total percentage of tires which have failed up to 10,000 km is:

$$n_{10} = n_5 + \frac{b_{10}}{a_{10} + b_{10}} (100 - n_5)$$

Thus we can determine the percentage of tires which have failed up to 15,000, 20,000, etc. km:

$$n_{15} = n_{10} + \frac{b_{15}}{a_{15} + b_{15}} (100 - n_{10})$$

$$n_{20} = n_{15} + \frac{b_{20}}{a_{20} + b_{20}} (100 - n_{15})$$

e .

These calculations provide sufficiently reliable results as long as the number of tires tested in the last interval is sufficiently great to define the quality of the tires of the entire group.

The number of tires tested in the last interval of number i is $a_i + b_i$ and corresponding size of the group is

$$N_i = (a_i + b_i)\frac{100}{100 - n_{i-1}}$$

To ensure reliability, the number N_i must be sufficiently large either in absolute terms (for example, $N_i > 50$) or in relation to the actual group a_0 (for example $\frac{N_2}{a_0} > 0.5$).

These limitations determine the possibility of continuing the calculation up to one or another distance interval.

According to these calculated data graphs are constructed showing the change in the number of tires failed as a function of distance traveled (Fig. 263). This graph allows us to characterize the lifetime of tires. The graph shows the number of tires which have failed up to one or another distance interval (in particular up to the limit of the guarantee). /332

The average lifetime of tires before failure is determined by the formula

$$S_{avei} = \frac{1}{100}\int S\,dn$$

where the integral is the shaded area in Fig. 263.

This value can be determined by planimetry or according to the trapezoidal formula:

$$S_{avei} = \frac{1}{100}[n_5 \cdot 2{,}5 + (n_{10} - n_5)\,7{,}5 + (n_{15} - n_{10})\,12{,}5 + \cdots] \text{ thous. km}$$

or

$$S_{avei} = S_i - 2{,}5 - \frac{1}{20}(n_5 + n_{10} + \cdots + n_{i-1}) \text{ thous. km},$$

where S_i is the maximum mileage of the last interval in which tires failed.

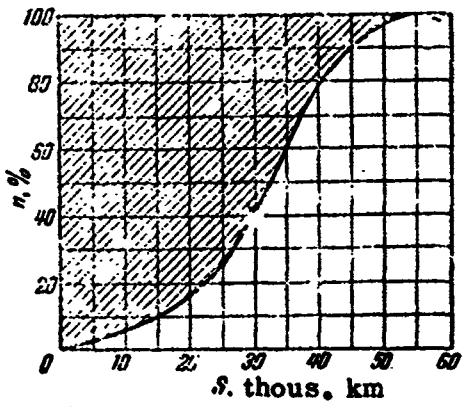

Fig. 263. The Number of Tires Which Failed as a Function of Distance Traveled.

The graph of $n(s)$, constructed according to the proposed method on the basis of the data of incomplete tests, approximates the graph obtained on the data of completed tests and we can make conclusions from it. However, when the interpretation of results is made at an earlier test stage, the curve does not reach the level of 100% and to calculate the average mileage of a group it is necessary to extrapolate the curve.

Since the curves of mileage distribution of tires are almost

symmetrical, the mean lifetime of a group of tires differs very little from that distance interval in which 50% of the tires fail. Therefore instead of extrapolating the curves we can assume approximately that the average lifetime of a group is determined by the point of intersection of the curve on the graph with the level n = 50%.

In 1954-1955, according to the proposed technique the operational test laboratory of the Scientific Research Institute of the Tire Industry analyzed the test data of more than 1700 tires produced at various factories. These tires were at the earliest test stage (9-12 months after they were placed in operation). Then the /333
tests of these tires were completed and it was possible to compare the predictions of the lifetime of the tires which were made according to the data of the incomplete tests with their actual lifetime.

These data are given by groups in Table 15.

TABLE 15. COMPARATIVE RESULTS OF TIRE TESTS

No. of Group	No. of Tires in Group	No. of Tires Which Failed Before Analysis		Average Lifetime of the Group of Tires in Thousands of km		Percentage of Tires Which Failed Before 30,000 km	
		No.	%	According to Prediction	Actual	According to Prediction	Actual
				Group A Roads			
1	72	20	30	50	51,4	5,5	6,7
2	102	33	33	46	44	11,2	11,5
3	72	15	22	36	33,6	35	29
				Group B Roads			
4	101	35	35	44	41	11,3	12,9
5	115	29	25	47	43,2	8	9,4
6	108	35	33	37	33	31	35
7	180	78	43	28	28,8	52	50,3
8	187	41	23	35,5	33,4	26,2	21,8
9	168	49	29	39	32,7	32	29

In all cases the prediction of the lifetime of the tires was made using the intersection of the curve with the level n = 50%.

It can be seen from the tables that an estimate of the average lifetime of a group is sufficiently precise when the number of tires which fail reaches 25-30%.

Using this method not only can we estimate the total lifetime of a group of tires, but we can also construct rising graphs of tire failure for various defects.

Thus if the number of tires which have failed because of a particular defect (for example, carcass blowout) during the interval 0-5000, 5000-10,000, 10,000-15,000 km, etc., is equal to respectively c_5, c_{10}, c_{15}, etc., then the calculated values for the percentage of tires which have failed because of this defect up to a given mileage can be determined according to the formula

$$n_5^p = \frac{c_5}{a_5 + b_5} \cdot 100$$

$$n_{10}^p = n_5^p + \frac{c_{10}}{a_{10} + b_{10}} (100 - n_5)$$

$$n_{15}^p = n_{10}^p + \frac{c_{15}}{a_{15} + b_{15}} (100 - n_{10})$$

etc.

In these formulas n_5, n_{10}, etc. are the total percentage of tires which failed up to a given mileage, computed according to the formulas given above. /334

We should note that with incomplete tests the number of tires which failed because of a particular defect is determined only approximately since at various stages of testing the tires failed for various reasons.

According to the data given in the cards and the tables, in addition to the accepted average lifetime of tires we can compute also other values which characterize the tests.

Thus the average lifetime of an entire group of tires (including those which fail) is determined according to the formula

$$S_{ave} = \frac{1}{a_0} [(b_5 + d_5) \cdot 2{,}5 + (b_{10} + d_{10}) 7{,}5 + \cdots]$$

where a_0 is the size of the entire group of tires.

The average lifetime of tires which remain in operation is equal to:

$$S_{op} = \frac{d_5 \cdot 2{,}5 + d_{10} \cdot 7{,}5 + \cdots}{d_5 + d_{10} + d_{15} + \cdots}$$

The average lifetime of tires which failed is:

$$S_{fl} = \frac{b_5 \cdot 2{,}5 + b_{10} \cdot 7{,}5 + b_{15} \cdot 12{,}5 + \cdots}{b_5 + b_{10} + b_{15} + \cdots}$$

This method for interpreting the results of incomplete operational tests allows us, as a rule, to obtain reliable data concerning the lifetime of tires for a year after the start of the test.

Accelerated Road Tests

Due to the long time required to test tires under the normal operational conditions and the necessity of a large number of tires for these tests, accelerated road tests are conducted for a rapid estimate of the quality of tires of a new construction or tires produced using a new technological process.

In accelerated road tests, the tires are tested on vehicles weighted with ballast, with high daily mileages.

Under these conditions the lifetime of the tire before failure for wear is significantly less than in operation.

Therefore accelerated road tests are always comparative tests. Parallel tests are conducted for several variations in the tire, the qualities of which are then compared. Usually standard tires are used as one of the variations.

The number of tires of each variation which are tested, as a rule, is usually small, i.e., less than 20 tires. /335

Therefore, to obtain reliable results we use special indices to ensure that all tires operate under identical conditions. To do this the vehicles with the tires being tested move along one particular course. To prevent the influence of the individual characteristics of the vehicles and drivers, the tires are periodically transferred from one vehicle to another. The internal pressure in the tires and the technical condition of the automobile are carefully inspected.

CHAPTER VII

THE OPERATION OF AUTOMOBILE TIRES

Basic Reasons for Tire Failure During Operation

The normal operation of tires and their lifetime depends to a large extent on operational conditions. /336

Tires fail due to complete wear of the tread or due to the development of other defects (damage).

Tire failure due to tread wear at rather high mileage is normal. Tires with worn tread can in most cases be repaired by installing new tread.

Other forms of tire failure (carcass blowout, separation of the carcass plies, separation of the tread plies) are either related to poor tire quality or are the result of improper or careless use.

As an example let us present the most typical defects of 260-20 heavy duty tires and the typical frequency of their appearance:

	Frequency of Appearance in %
Tread Wear	73.8
Separation of Tread Ply	0.5
Carcass Blowout	4.9
Separation of the Carcass Plies	0.9
Punctures or Cuts	19.7
Other Defects	0.2

In practice we cannot always determine whether a given defect which led to tire failure was caused by poor quality or improper operation. The frequency of the appearance of clearly operational defects of tires such as punctures depends to a large extent on the strength of the tire carcass. As the strength of the tire carcass increases, even with constant operational conditions the amount of tire damage sharply decreases.

With a given tire quality, lifetime depends to a large extent on the proper choice of an operational regime, the technological condition of the automobile, the skill of the driver, the extent to which the tires are systematically cared for and repaired at the proper times [45].

The proper organization of tire operation leads to a significant decrease in the number of tires which fail at low mileage and to an increase in the average lifetime of tires. In the same way one can economize on means and materials expended on producing tires, and the cost of automotive transport will decrease. /337

The Influence of Road Conditions and Climate on Tire Operation

According to the classification system used in the USSR, roads are divided into 5 categories shown in Table 16.

TABLE 16. CLASSIFICATION OF ROADS

Road Category	Calculated Velocity for Identical Passenger Automobiles (km/hr)	Traffic Intensity (Number of Automobiles per Day)	Maximum Longitudinal Slope (%)	Type of Road Surface
First....	120	more than 5000	4	Improved (Primary Roads)
Second...	100	3000-5000	5	
Third....	80	1000-3000	6	Improved (Secondary Roads), Transitional
Fourth...	60	200-1000	7	Improved (Secondary Roads), Transitional, Inferior
Fifth....	40	less than 200	9	Transitional, Inferior

Note: We have in mind the following types of road surfaces: for primary improved roads: asphalt-concrete, block roads; secondary improved: black road metal and black gravel; transitional: road metal-gravel, cinder, dirt-road metal, dirt, reinforced by cementing materials; inferior: dirt and dirt with admixtures.

The lifetime of tires depends not only on the type of road surface but mainly on its condition. Therefore we can divide roads into three groups depending on their influence on the lifetime of tires: (A) roads of the I and II categories in satisfactory

condition, (B) roads of the III, IV and V categories in satisfactory condition, (C) roads of all categories in unsatisfactory condition.

According to the data of the Scientific Research Institute for the Tire Industry, the lifetime of tires operating on Group B roads is 20-25% lower and on Group C roads is 40-50% lower than when operating on Group A roads.

The amortization mileage on mountain roads is 15-20% lower than /538 on roads in flat country. On such roads with a large number of turns and slopes, tread wear is accelerated.

When operating vehicles in quarries or processing plants the unsatisfactory road surface and mountain terrain is influential. Under these conditions the number of cuts, punctures and carcass blowouts is increased, tread wear is accelerated and the lifetime is decreased by 30-50% in comparison to lifetime on flat roads with hard, even surfaces.

When operating in forest industries, the lifetime is decreased by 15-20% due to increased tread wear and the large number of carcass blowouts.

In addition to road conditions, climatic conditions also exert great influence on the operation of the tires.

Both the temperature of the surrounding air and, to a certain degree, road conditions depend on climate and time of the year. The change in the temperature of the surrounding air leads to a change in the temperature of the tire and corresponding changes in the strength of the tire materials. A typical function relating tire lifetime to air temperature is shown in Figure 264. 100% denotes tire lifetime at a temperature of 22° C.

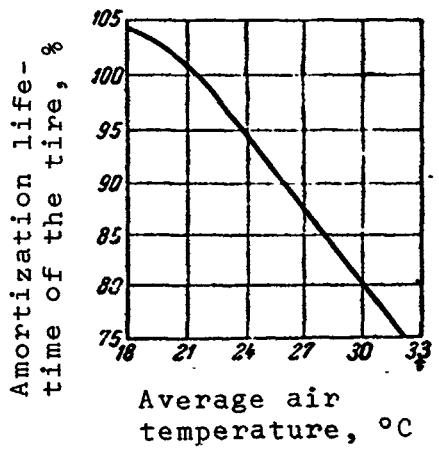

Fig. 264. A Typical Function Relating Tire Lifetime and Air Temperature.

On wet or snow-covered roads the intensity of tread wear decreases.

The decrease of operational velocities under winter conditions are also important. As statistical data show, when operating in autumn or winter, tire lifetime before failure is 25-30% higher than in spring or summer (under the conditions of the temperate zones).

Operating Regime of the Tire

The operating regime of a tire is determined by the value of the radial load, the internal pressure and velocity

of the automobile.

These factors are inter-related; thus with an increase in the operating velocity of the vehicle the permissible weight on the tire should be decreased. On the other hand, at low velocities the weight on the tire can be increased with a simultaneous increase in the internal pressure.

The value of the permissible weight for tires under normal operating conditions is determined by the corresponding All Union State Standards and Norms[1]. An increase in the weight of the tire above the maximum recommended weight leads to a decrease in its lifetime (Fig. 265). /339

The operating velocities are determined by the type and designation of the vehicle. As the velocity of the vehicle increases the lifetime of the tire decreases (Fig. 266).

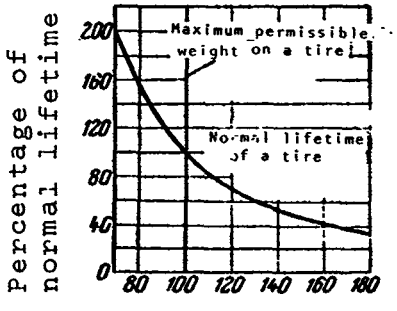

Fig. 265. A Typical Function Relating Tire Lifetime to Weight.

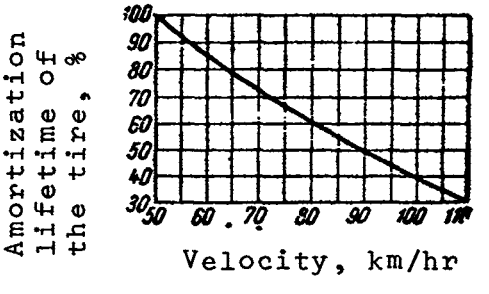

Fig. 266. A Typical Function Relating Tire Lifetime to Operating Velocities.

The most important condition of proper tire operation is the choice and maintenance of the optimum internal pressure.

The optimum internal pressure depends on the operating conditions of a tire. A change in even one of the operating factors sometimes leads to a change in pressure. Thus, when moving at high speeds (for example, racing cars) the internal pressure must be significantly higher than under normal conditions. To increase the permissible weight on a tire when operating at low velocities (on road-building machines) internal pressure should be increased. This choice of internal pressure for each given operating regime creates the most favorable conditions for operating the tire and guarantees the maximum lifetime of its service.

---

[1] The basic criteria used to determine weight norms were examined in Chapter II.

The graph shown in Figure 267 shows that the greatest lifetime of tires under given conditions is reached with a particular value of internal pressure. In practice, tires operate under various conditions; therefore, for a given weight the value of internal pressure is set so that it corresponds to the average operational conditions.

An increase in internal pressure leads to a decrease in the amplitude of change in the stresses, and the value of the maximum stresses increases. If the tire with increased internal pressure hits an obstacle, then carcass blowout is possible since the cord fibers are overstretched. /340

When the internal pressure is decreased, cord fiber deformations become alternating and the amplitude of change in deformation increases. With this operating regime, fatigue failure of the cord fibers quickly appears. At the points of greatest curve deformation on the sidewalls along the internal surface, a dark band is formed along the entire circumference of the outer cover. Subsequently, with continued operation of the tire at low internal pressure, at the location of the dark band, the cord fibers of the inner and then the other carcass plies become separated from the rubber. Then the fibers split and blowout occurs. As a result there is an annular rupture in the sidewall of the carcass.

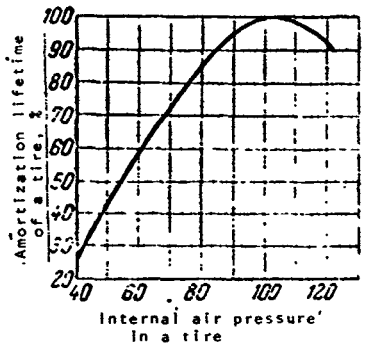

Fig. 267. Typical Function Relating Tire Lifetime to the Value of Internal Pressure.

When the vehicle is moving on tires with decreased internal pressures there is a sharp increase in the heating of the tires (Fig. 268), which has a drastic influence on their lifetime. As the temperature increases the strength of the materials (rubber, cord) and the strength of the seals between the tire elements decrease. The increased stress and additional heating of the tire frequently lead to local separation of the carcass plies.

At the point where the plies separate, temperature increases even more since friction between the cord plies arises. Under these conditions tire blowout often occurs.

We must note that under certain operational conditions an increase in pressure also causes an increase in tire heating. This is due to the increase in pressure on the contact surface and the increase in the dynamic stresses exerted on the tire when the automobile moves along an uneven road.

Both the absolute value of outer cover wear and the nature of the wear depend to a significant degree on the internal pressure. /341

With a significantly decreased internal pressure the so-called "bridge effect" is observed: in the middle part of the tread pressure on the contact surface sharply decreases and the entire weight is shifted to the edges of the rolling part. In this case there is uneven wear on the tread; the edges of the rolling part undergo drastic wear while the middle section remains almost unworn. This nonuniform wear leads to a decrease in the lifetime of the tire. An excess internal pressure also leads to undesirable consequences; i.e., intense wear of the middle part of the tread. In addition, with an increase in the internal pressure cracks sometimes appear in the tread base ply at the edges of the tread ridges.

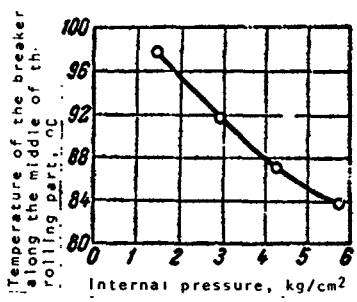

Fig. 268. A Function Relating Temperature in the Breaker Zone of a 34 X 7 Tire and the Internal Pressure (Rolling on a Machine at a Velocity of 40 km/hr, a Weight of 1200 kg).

Thus deviation in the internal pressure of the tire from the optimal values, corresponding to the concrete operational condition, leads to an operating regime with more stresses in the tire elements and therefore to a decrease in its lifetime.

Normal operation of an automobile includes motion on roads with a hard even surface. Under these conditions the internal pressure decided when designing the tire and fixed by the All Union States Standards is optimum. When vehicles are being operated on poor uneven roads, it is advisable to decrease the internal pressure in certain cases. A certain decrease in internal pressure under these conditions provides a decrease in the dynamic stresses. In addition, when moving along soft dirt roads a decrease in internal pressure in the tire increases the roadability of the automobile (cf. Chap. V, p. 65,66).

The recommendation to decrease the internal pressure on poor roads was determined by studying tires with various internal pressures.

The automobiles were mostly operated on roads with hard but uneven surfaces, differing from one another by the condition of the road surfaces: on roads of the III, IV categories (i.e., road metal, cinder, cobblestone and gravel).

The test results showed that a decrease in internal pressure under these road conditions increases the lifetime of the tire within the limits 10-60% (Table 17) for various dimensions in groups of tires which differ both in terms of construction and in the materials used for their production.

By decreasing the internal pressure in tires used on uneven roads, the number of carcass blowouts in the tire was decreased in

a number of groups within the limits of 15%, which in the final analysis increased their lifetime. Operating tires with decreased internal pressure on roads with even surfaces did not yield positive results.

TABLE 17. THE INFLUENCE OF DECREASING INTERNAL PRESSURE ON THE LIFETIME OF TIRES ON POOR ROADS

/342

Tire Designation	Automobile Model	Pressure in the Tires, kg/cm^2		Lifetime of the Tire[2], %
		Front Wheel	Rear Wheel	
260-20	ZIL-150	3.5	4.5 (Normal)	100
		3.0	3.5 (Decreased)	119
		3.5	4.5 (Normal)	100
		3.0	3.5 (Decreased)	125
		3.5	4.5 (Normal)	100
		3.0	3.5 (Decreased)	109
210-20	ZIL-5	4.0	5.0 (Normal)	100
		3.0	4.0 (Decreased)	159
		4.0	5.0 (Normal)	100
		3.0	4.0 (Decreased)	112
12.00-20	YaZ-210Ye	5.0	5.5[3]	100
		4.5	4.5 (Decreased)	120
		3.5	3.5 (Decreased)	139

When operating on tires whose internal pressure has been increased by 10-15% over the norm, their lifetime is decreased. This was particularly noticeable on roads with hard uneven surfaces.

When choosing the internal pressure in a tire one should take into account the influence of this value on the operation of other mechanisms and parts of the automobile.

A decrease in the internal pressure increases the comfort and safety of the automobile when operating on uneven roads, since in this case a decrease in pressure in the tires decreases the dynamic stresses. Under these conditions a decrease in pressure can also cause a decrease in the fuel consumption of the automobile due to a

[2] The lifetime of a tire when operated under normal pressure (according to the All Union State Standard) is used as 100%.

[3] Normal pressure for the front and rear wheel tires is 5.0 kg/cm^2.

decrease in the energy expended on vertical shifts of the automobile when traveling along an uneven surface.

Some increase in internal pressure may be advisable at high velocities on roads with hard even surfaces. In this case the coefficient of rolling resistance is somewhat decreased and the dynamic operation of the vehicle is improved. Under these conditions tire heating may also be somewhat decreased.

Thus when operating vehicles on roads having hard, but uneven surfaces it is advisable to decrease the internal pressure by 10-15% over the norms. At high velocities on roads with hard even surfaces /343
pressure in the tires may be increased by 10-15%. When operating vehicles under conditions of normal roads and at moderate velocities the internal pressure set by the All Union State Standard should be strictly observed.

Tire Servicing

Servicing the tires properly and at the proper time has a great influence on their lifetime.

According to the data of the Scientific Research Institute of the Tire Industry, almost half of the tires which have failed to date have failed because the rules for their usage were not observed.

Tire care basically consists of proper operation, maintenance of the optimum internal air pressure and the control of other factors which influence the operating regime of the tire (proper weight on the tires, proper operation of the automobile, care of the undercarriage of the vehicle).

The proper matching of tires and wheels and the proper completion of the mounting-unmounting operation plays a significant role in conserving the tire. The tire must be mounted on the rim specified by the All Union State Standard.

The use of an improper wheel can cause danger to the beads of the outer cover both during mounting and unmounting and during operation.

When the tire is used on a rim with the incorrect internal diameter, which does not correspond to the tire either in height or rim configuration, the beads may be broken due to a concentration of pressures on the internal points or due to a shift of the bead relative to the rim when the wheel is rolling.

Other undesirable consequences can be caused by the improper matching of tubes and outer covers in terms of their dimensions. If the tube is stretched excessively or if wrinkles form because the tube is not stretched sufficiently, a blowout may occur and the

outer cover may be damaged.

The improper matching of tires on the double rear wheels of trucks (using outer covers having a different tread design [road and high roadability tread] or different wear) leads to nonuniform distribution of weight on tires. In this case the tire with the most weight undergoes accelerated wear. The tire with the least weight is worn unevenly by individual sections of the tread which are stressed during vertical oscillations of the vehicle.

Mounting and unmounting of tires in garages must be done on special equipment. Using hand tools is never advisable considering the possibility of damaging the bead part of the outer cover. A tire mounting and unmounting machine operates on a pneumatic, hydraulic or electric drive. Machines for mounting tires used on one-piece wellbase rims, are used to remove the beads from the bead seats and to lift them over the drop center rim (when unmounting) or to lift them over the drop center rim and inflate the tire (when mounting). Machines for heavy duty tires which are used on collapsible rims, usually complete only the basic operation of unmounting, which consists of removing the bead from the bead seats. /344

An overall view of one such machine for mounting and unmounting passenger car tires is shown in Figure 269.

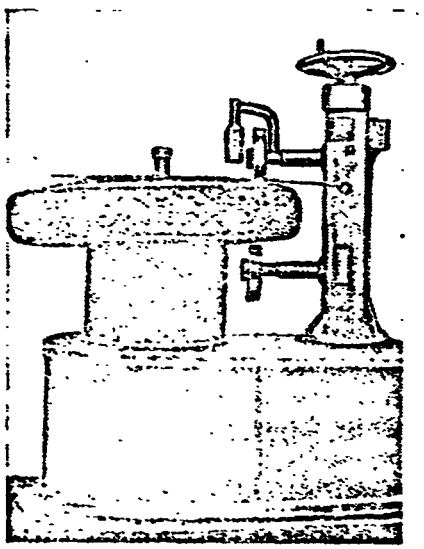

Fig. 269. A Machine for Mounting and Unmounting Passenger Car Tires.

After mounting the passenger car tires it is necessary to balance the wheel assembly. Modern automobiles can operate at rather high velocities, and therefore wheel balance is very important. If the wheel is not balanced properly, when the automobile is in motion the wear on the tires and the undercarriage will increase and the safety of the automobile will decrease due to a decrease in the handling ability of the vehicle.

Outer covers for passenger car tires are balanced in the tire factories, and a "light" point is recorded.

New wheel assemblies are balanced in the automobile factories. In a garage the wheel must be balanced each time the tire is changed.

Special machines are used to balance wheels. These machines operate on either static or dynamic balancing. Some machines accomplish both forms of balancing. In static balancing, the center of gravity of the wheel is aligned with the axis of rotation and thus an unbalanced inertial force acting in the rolling plane is prevented (Fig. 270a).

If the center of gravity of the wheel is shifted from the axis of rotation by e, then the centrifugal force which arises will be $\frac{Pe}{g}\omega^2$, where P is the weight of the wheel and ω is the angular velocity of its rotation. The product Pe is called the wheel disbalance. /345

Dynamic balancing is a more complete operation than static balancing since it may also eliminate the action of the moment of inertial force which tends to rotate the wheel in a direction perpendicular to the rolling plane (Fig. 270b).

The simplest machine for static balancing is a vertical frame on which a horizontal shaft is placed on bearings. The wheel to be balanced is attached to the shaft. The "heavy" point of the wheel is determined by rotating the wheel alternately in both directions and letting it come to a stop. Thus the "heavy" point of the wheel ends at the bottom. By rotating the wheel in different directions, this point is somewhat shifted since the "heavy" point does not reach the low position due to friction with the bearing.

The "heavy" point of the wheel is located midway between the lowest points obtained when rotating the wheel in different directions. Frequently, to decrease the influence of friction, the shaft of the balancing machine is fastened on bearings whose outer rings are rotated by a motor in opposite directions. Using special devices, a balancing machine can allow us not only to determine the position of the "heavy" point but also to determine the degree of disbalance.

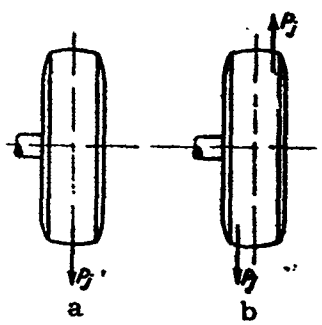

Fig. 270. Inertial Stress Arising: (a) With Static Disbalance; (b) With Dynamic Disbalance of the Wheel.

When necessary a wheel can be statically balanced on the hub of the front wheel of an automobile which has been raised.

After balancing, balancing weights are attached to the rim at the points opposite the heavy points to equilibrate the wheels. The amount of weight is chosen according to readings of the machine and is checked by repeating the balancing operation. Wheel disbalance is measured by the product of the weight of the balancing weight and the distance from the center of the axis of the wheel. For passenger car tires the All Union State Standard permits no disbalance greater than 1 kg·cm.

Dynamic balancing is done on machines with a shaft which rolls in bearings. The wheel attached to the shaft, in the presence of dynamic disequilibrium, tilts relative to the vertical plane when rotated. By recording the angle of inclination and the position of the wheel in the plane of rotation at the moment of inclination we can characterize a value and location of the disbalance.

Observing the Norms of Weight and Internal Pressure

For proper operation of a tire it is necessary to strictly observe the norms of weight on the tire and the internal pressure in the tire. /346

Since overloading the tires leads to a sharp decrease in their lifetime, one should see that the vehicle is not overloaded and that the weight is properly distributed in the body. The internal pressure in the tire must be checked regularly using a sufficiently precise manometer and, when necessary, air should be added to the tire. Pressure should be checked when the tires are cold before the vehicle begins moving. When a vehicle is moving, the tires heat up and their pressure increases. The pressure in a heated tire should not be decreased since the internal pressure norms take into account its increase when moving.

Operating the Automobile

The influence of proper operation of the automobile on the maintenance of all its parts is very significant. As we know, the length of time a vehicle can go between repairs (depending on the qualifications of the driver) can vary by several factors. The lifetime of tires depends to a greater extent on the proper operation of the automobile since all the forces in interaction with the road are exerted on the tires. Among the basic causes for decreased lifetime of the tires, depending directly on the driver, are drastic acceleration, sharp braking, high velocity and sharp turns, careless hitting of obstacles. Drastic acceleration leads to heavy tread wear especially if the wheels spin.

One of the basic causes of uneven and rapid tread wear is sharp braking. With sharp braking, tread is usually worn in spots. In addition to heavy tread wear high shift stresses arise in the breaker and carcass sometimes leading to separation of the tread or separation of the carcass plies. Sharp braking from high velocities can also cause the tire to be pulled off the rim, the valve to be broken or the bead to be broken.

As velocity increases the specific (per unit mileage) tread wear increases, which is explained by the increase in the slip of tire elements in the contact surface at high velocities. In addition, when traveling at high velocities, turning the vehicle creates high lateral inertial forces which cause intense slip in the tread elements and accelerated tread wear. We can see from the graph (cf. Fig. 266, p. 201), that with a two-fold increase in velocity (from 50 to 100 km/hr) the amortization lifetime of a tire will be decreased roughly by a factor of three.

Carelessly driving over an obstacle can lead to carcass blow- /347

out even at low velocities, due to a high concentration of stresses arising in the cord fibers.

Care of the Automobile

Cases frequently arise in practice of damage or rapid wear of automobile tires due to improper care of the components of the automobile.

The greater part of this problem is caused by the improper setting of the front wheels. Improper alignment and wheel wobble cause additional slip of the tread elements of the front tires in the contact surface with the road and accelerated tread wear.

If the norms of the angle of wobble of the front wheels are not observed, one-sided increased tread wear will occur (Fig. 271), and if the alignment is not proper, spot wear will occur. The reason for one-sided wear due to excessive wheel wobble is the concentration of heavy contact pressures in the outer zone of the tread. Spot wear due to deviation from the proper value of alignment is a consequence of the fact that the direction of rolling of the wheel does coincide in this case with the direction of motion of the vehicle. Thus the tread elements slip along the road but due to the elasticity of the tire, this lateral slip alternates with periods when the tire is rolling without slip.

Fig. 271. One-Sided Wear of a Tire Due to Excessive Wobble of the Front Wheels.

Rather common reasons for accelerated spot wear on the tread are wear or improper adjustment of the front wheel bearings, a front wheel which is not tightly attached to the hub, wear or improper adjustment of the connections of the tie-rods. All these problems cause the wheel to wobble and period differences between the rolling direction of the wheels and the direction of motion of the vehicle to arise.

Heavy wear on the brake drum of the automobile also leads to rapid local wear of the tread. This usually causes the drum to become elliptical and prevents even braking of the wheel. Thus the tread is worn intensely in particular places on its circumference. /348

Overheating of the brake drum when the brakes are too tight causes additional heating of the tires and therefore accelerated wear. If the brakes are not properly adjusted or the brake system is defective, sharp braking can occur which leads to lock-skids.

Therefore tread wear will significantly increase.

We should note that the maximum braking force occurs not with total slip (lock-skid of the wheel) but when they are rolling with some slip. According to experimental data, the maximum braking force of a tire rolling along asphalt occurs with 20-25% slip of the wheel.

Rotating the Tires

We know from numerous data that the tires of the drive wheels undergo greater wear than the tires of the wheels (usually the front wheels) which do not undergo tractive force. In addition, the nature of wear of the front and rear wheels, of the right and left wheels of the automobile varies so that they operate under different conditions.

Therefore, to ensure equal wear on tires and to increase the amortization lifetime, the position of the tires on the automobile should be periodically changed. This is done by rotating the tires.

There are different systems for rotating tires with variations in the order of rotation, some including the spare tire in the rotation and others not including the spare tire.

When constructing these systems one takes into account the advisability of completing the rotation cycle for a given amortization lifetime of the tires and carrying out these operations while the automobile is being serviced.

In view of the existing norms of amortization lifetime of the tires and the periodicity of servicing of the automobile, it is reasonable to rotate the tires during the No. 2 (TO-2) servicing operation, i.e., every 6,000-8,000 miles.

Tire Repair

Tire repair is very popular due to the high price of tires and also the possibility of increasing the lifetime of the tire by using simple repair methods.

Various substances are used as repair materials including crude and vulcanized rubber and rubber-fabric materials, which as a rule correspond to the material of the damaged point on the tire: tread rubber, rubberized cord, rubberized chafer strip, etc.

En route and garage repairs differ. /349

Repair en route is limited by conditions and is usually of a temporary nature.

Tube punctures en route are repaired by the "cold" and "hot" methods. The most rapid and simple is the "cold" method. This method of repair is temporary and consists in cementing a patch using nonvulcanized cement. The more reliable method consists in vulcanizing the patches using various instruments: electric sealing rings, hot briquets, etc.

In case of large damage to the outer cover en route, in the absence of a spare tire, temporary repair should be made by cementing patches or sealing rings made of rubberized cord to the point of damage from the inside of the outer cover using nonvulcanized rubber cement.

Punctures in tubeless tires can be repaired en route without unmounting using a special self-vulcanizing cement injected by a syringe (for punctures of up to 2 mm) at the location of the puncture or by rubber plugs for larger punctures (Fig. 272). Cylindrical plugs (solid or hollow) are inserted into the puncture from the tread side and cemented in place by self-vulcanizing cement. This type of repair can be made without unmounting the tire and takes little time.

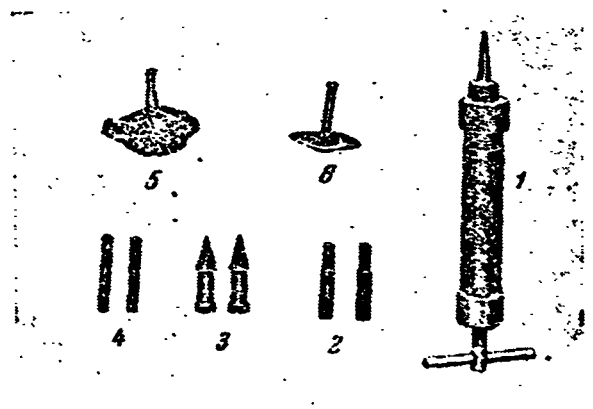

Fig. 272. Tools for Repairing Punctures in Tubeless Tires: (1) Syringe for Injecting Cement; (2, 3, 4) Plugs; (5, 6) Mushroom-Shaped Plugs.

A more reliable method for repairing punctures is that using mushroom-shaped plugs but in this case the tire must be unmounted since the mushroom plugs are introduced from the inside.

Significant damage to tubeless tires en route cannot be eliminated; in the absence of a spare tire the tubeless tire can be repaired with a patch or a sealing ring and the use of a tube.

The technological process of stationary repair of outer covers /350 is discussed in special literature.

Keeping Track of Tire Operation

A record or systematic control of the operation of the tires and the interest of the driver exert a direct influence on the lifetime of tires. Due to precise records and control, defects in tires can be quickly detected and the latter corrected by repair, the tires can be rotated properly thereby providing the proper setting of the tires.

The reward of overfilling the norms of amortization lifetime of tires is facillitated by the proper care of the tires and proper and careful operation of the automobile.

The lifetime of a tire is recorded for each automobile and for each outer cover individually. On the card the lifetime, date of mounting and unmounting, repair, place of origin of the tire are recorded. In addition, a complete record is kept which takes into account all tires of the garage.

References

1. Genin, G. and B. Morrison: Encyclopedie Technologique de l'industrie du Caoutchouc (Technical Encyclopedia of the Rubber Industry). Paris, 1956. /351
2. Marcs, A: Konstrukte pneumatic (Tire Construction). Prague, 1958.
3. Woods, E.: Pneumatic Tyre Design. Cambridge, 1952.
4. Levin, S.L. and S.M. Tsukerberg: Avtomobil'nyye beskamernyye shiny (Automotive Tubeless Tires). Avtotransportizdat, 2nd Edition, 1958.
5. Levin, S.L. and S.M. Tsukerberg: Nekotoryye voprosy razrabotki beskamernykh shin (Certain Problems in the Development of Tubeless Tires). Kauchuk i rezina, No. 11, p. 9, 1957.
6. Tsukerberg, S.M.: K Raschetu beskamernykh shin (Calculations for Tubeless Tires). Kauchuk i rezina, No. 9, p. 20, 1958.
7. Biderman, V.L., A.P. Bogayevskiy and V.F. Shchaveleva: Shiny iz metallokorda (Tires Made of Metal Cord). Kauchuk i rezina, No. 4, p. 19, 1957.
8. Bogayevskiy, A.P., L.V. Desidley and I.P. Bagretsova: Shiny s meridional'nym raspolozheniyem nitey korda v karkase (Tires with the Cord Fibers Running Radially in the Carcass). Kauchuk i rezina, No. 1, p. 6, 1960.
9. Lyubashevskiy, I.Yu., L.T. Margulis and B.Ya. Niselovskiy: Tekhnologiya shinnogo proizvodstva (The Technology of the Tire Industry). Goskhimizdat, 1951.
10. Ragulin, V.V.: Proizvodstvo pnevmaticheskikh shin (The Production of Pneumatic Tires). Goskhimizdat, 1958.
11. Saltykov, A.V.: Osnovy sovremmenoy tekhnologii avtomobil'nykh shin (Fundamentals of the Contemporary Technology of Automotive Tires). Goskhimizdat, 2nd Edition, 1950.
12. Dobratina, M.Yu.: Raschet spetsifikatsii pokryshki (Calculating the Specifications of Outer Covers). Kauchuk i rezina, No. 7, p. 23, 1938.
13. Biderman, V.L.: Raschet formy profilya i napryazheniy v elementakh pnevmaticheskoy shiny, nagruzhennoy vnutrennim davleniyem (Calculation of the Profile Shape and Stresses in the Elements of a Pressurized Pneumatic Tire). Trudy NII shinnoy promyshlennosti (Proceedings of the Scientific Research Institute of the Tire Industry), Goskhimizdat, Collection 3, p. 16, 1957.
14. Ponomarev, S.D., V.L. Biderman, K.K. Likharev, V.M. Makushin, N.N. Malinin and V.I. Feodos'yev: Raschety na prochnost' v mashinostroyenii (Strength Calculations in Machine Construction). Mashgiz, Vols. I, II, III, 1958-1959.
15. Alekseyev, P.I.: Nagruzheniye bortovykh kolets shiny v razlichnykh usloviyakh deformatsii (Stresses on Tire Bead Rings Under Various Deformation Conditions). Kauchuk i rezina, No. 2, p. 2, 1960.
16. Biderman, V.L.: Uravneniya deformatsii rezino-kordnykh obolochek vrashcheniya (The Deformation Equations of Rubberized

Cord Rotation Shells). In "Raschety na prochnost' v mashinostroyenii" (Strength Calculations in Machine Construction). Mashgiz, No. 89, p. 119, 1959.
17. Biderman, V.L. and V.L. Bukhin: Energetichneskiy metod rascheta rezino-kordnykh obolocheck vrashcheniya (The Energy Method For Calculating a Rubberized-Cord Rotation Shell). Izvestiya Akad. Nauk SSSR, Otdel Tekhnicheskikh nauk, Mekhanika i Mashinostroyeniye, No. 6, p. 76, 1959.
18. Biderman, V.L. and B.L. Bukhin: Ravnovesiye rezinokordnoy tsilindricheskoy obolochki (Equilibrium of a Rubberized Cord Cylindrical Shell). Izvestiya Akad. Nauk SSSR, otdel tekhnicheskiky nauk, Mekhanika i mashinostroyeniye, No. 6, p. 156, 1960.
19. Zakharov, S.P. and V.I. Novopol'skiy: Raspredeleniye udel'nogo davleniya shiny na dorogu pri vysokikh skorostyakh (Specific Pressure Distribution of a Tire Moving Along a Road at High Velocities). Trudy NII shinnoy promyshlennosti (Proceedings of the Scientific Research Institute of the Tire Industry). Goskhimizdat, Collection 3, p. 139, 1957.
20. Pugin, V.A.: Elektricheskiye tenzometry dlya izmereniya bol'shikh deformatsiy (Electrical Tensiometers for Measuring High Deformations). Kauchuk i rezina, No. 1, p. 24, 1960.
21. Biderman, V.L. and V.A. Pugin: Eksperimental'noye issledovaniye deformatsiy v avtomobil'nikh shinakh (An Experimental Investigation of Deformations in Automotive Tires). In the Collection: Raschety na prochnost' (Strength Calculations). Mashgiz, No. 6, p. 295, 1960.
22. Novopol'skiy, V.I.: Izmereniye poter' na kacheniya (Measuring Rolling Losses). Trudy NII shinnoy promyshlennosti (Proceedings of the Scientific Research Institute for the Tire Industry). Goskhimizdat, Collection 3, p. 122, 1957. /352
23. Knoroz, V.I.: Rabota avtomobil'nikh shin (The Operation of Automotive Tires). Avtotransportizdat, 1957.
24. Zimelev, G.B.: Teoriya avtomobilya (Automobile Theory). Second Edition, Publication of the Ministry of Defense, 1957.
25. Fal'kevich, B.S. and N.V. Divakov: Ispytaniya avtomobilya (Automotive Testing). Mashgiz, 1952.
26. Yakovlev, N.A.: Teoriya i raschet avtomobilya (Automotive Theory and Calculation). Mashgiz, 1949.
27. Bukhin, B.L.: Raschet napryazheniy i deformatsiy v pnevmaticheskikh shinakh pri ikh vrashcheniya (A Calculation of the Stresses and Deformations of Rotating Pneumatic Tires). In the Collection: Raschety na prochnost' (Strength Calculation). Mashgiz, No. 6, p. 56, 1960.
28. Biderman, V.L.: Kriticheskaya skorost' kacheniya pnevmaticheskoy shiny (The Critical Rolling Velocity of a Pneumatic Tire). In the Collection: Raschety na prochnost' (Strength Calculations). Mashgiz, No. 7, p. 324, 1961.
29. Biderman, V.L.: K raschetu kriticheskoy skorosti kacheniya pnevmaticheskoy shiny (Calculating the Critical Rolling Velocity of a Pneumatic Tire). Trudy NII shinnoy promyshlennosti (Proceedings of the Scientific Research Institute for the Tire Industry). Goskhimizdat, Collection 3, p. 64, 1957.

30. Biderman, V.I. and B.L. Bukhin: Raschet kriticheskoy skorosti kacheniya pnevmaticheskoy shiny (Calculating the Critical Rolling Velocity of a Pneumatic Tire). Izvestiya Akad. Nauk SSSR, Otdel tekhnicheskikh nauk, Mekhanika i mashinostroyeniya, Vol. 52, No. 1, 1961.
31. Biderman, V.L.: Raschet norm nagruzok i davleniy dlya avtomobil'nykh shin (Calculating the Norms of Load and Pressure for Automotive Tires). Trudy NII shinnoy promyshlennosti (Proceedings of the Scientific Research Institute of the Tire Industry). Gaskhimizdat, Collection 3, p. 52, 1957.
32. Biderman, V.L.: Raschet deformatsiy v kamerakh pnevmaticheskikh shin (Calculating Deformations in Tubes for Pneumatic Tires). Trudy NII shinnoy promyshlennosti (Proceedings of the Scientific Research Institute of the Tire Industry). Goskhimizdat, Collection 3, p. 76, 1957.
33. Yevstratov, V.F., T.N. Buyko and L.V. Desidlin: Avtomobil'nyye gruzovyye shiny iz sinteticheskogo kauchuka i puti povysheniya ikh kachestva (Truck Tires Made of Synthetic Rubber and Ways to Improve Their Quality). Khim. nauka i promyshlennost', No. 1, p. 5, 1959.
34. Slyudikov, L.D.: Profil' meridional'nogo secheniya shiny tipa "R" (The Profile of the Meridian Cross Section of Type "R" Tires). Kauchuk i rezina, No. 8, p. 27, 1962.
35. Biderman, V.L.: Shiny s meridional'nym raspolozheniyem nitey korda v karkase (Tires with the Cord Fibers in the Carcass Running in a Radial Direction). Kauchuk i rezina, No. 7, p. 10, 1960.
36. Slyudikov, L.D. and V.L. Biderman: Novyy metod sborki avtopokryshek (A New Method for Assembling Automotive Outer Covers). Kauchuk i rezina, No. 8, p. 45, 1960.
37. Tsukerberg, S.M., S.P. Zakharov, B.V. Nenakhov and E.A. Abramova: Shiny dlya avtomobiley povyshennoy prokhodimosti (Tires for High Roadability Vehicles). Gaskhimizdat, 1960.
38. Tsukerberg, S.M. and B.V. Nenakhov: Shiny s reguliruyemym davleniyem vozdukha (Variable Air Pressure Tires). Avtomobil'nyy transport, No. 10, p. 47, 1959.
39. Zakharov, S.P., S.M. Tsukerberg and B.V. Nenakhov: Shi[illegible]profil'nyye shiny (Wide-Profile Tires). Kauchuk i rezi[illegible]o. 8, p. 20, 1959.
40. Novopol'skiy, V.I., V.F. Yevstratov and S.L. Levin: Kompleksnaya metodika laboratornykh ispytaniy avtomobil'nykh shin (A Complex Technique for Laboratory Tests of Automotive Tires). Trudy NII shinnoy promyshlennosti (Proceedings of the Scientific Research Institute of the Tire Industry). Goskhimizdat, Collection 3, p. 106, 1957.
41. Tsukerberg, S.M.: Stsepleniye shiny s dorogoy (Tire Traction). Trudy vsesoyuznogo zaochnogo politekhnisheskogo instituta (Proceedings of the All-Union Polytechnical Correspondence Institute). 1961.
42. Guslitser, R.L.: Metody otsenki prochnosti karkasa avtomobil'nykh shin (Methods for Evaluating the Carcass Strength of Automotive Tires). Trudy NII shinnoy promyshlennosti

(Proceedings of the Scientific Research Institute of the Tire Industry). Goskhimizdat, Collection 3, p. 169, 1957.
43. Sakhnovskiy, N.L., V.F. Yevstratov, L.A. Smirnova and V.I. Katkov: Otsenka iznosostoykosti protektornikh rezin pri ekspluatatsionnykh ispytaniyakh shin (An Evaluation of the Wear Resistance of Tread Rubber in Operational Tests of Tires). Kauchuk i rezina, No. 1, p. 10, 1960.
44. Biderman, V.L.: Novyy metod obrabotki rezul'tatov nezakonchennykh ekspluatatsionnykh ispytaniy shin (A New Method for Interpreting the Results of Uncompleted Operational Tests of Tires). Trudy NII shinnoy promyshlennosti (Proceedings of the Scientific Research Institute of the Tire Industry). Goskhimizdat, Collection 3, p. 190, 1957.
45. Seleznev, I.I., S.M. Tsukerberg and B.V. Nenakhov: Puti uvelicheniya probega avtomobil'nykh shin (Ways of Increasing the Lifetime of Automobile Tires). Avtotransportizdat, 1960.

Translated for the National Aeronautics and Space Administration by:
Aztec School of Languages, Inc.
Research Translation Division (555)
Maynard, Massachusetts and McLean, Virginia
NASW-1692

APPENDIX

NOMOGRAMS FOR CALCULATING TIRE CONFIGURATIONS /355

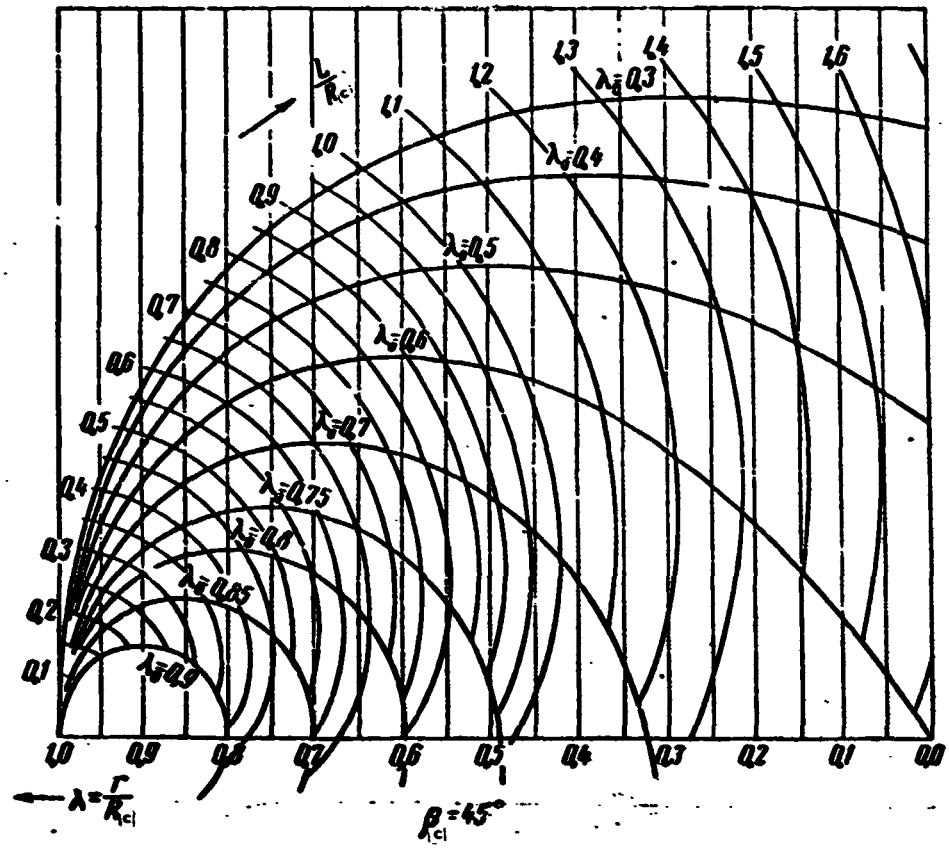

Fig. 1. Equilibrium Configurations of Tires with $\beta_c = 45°$.

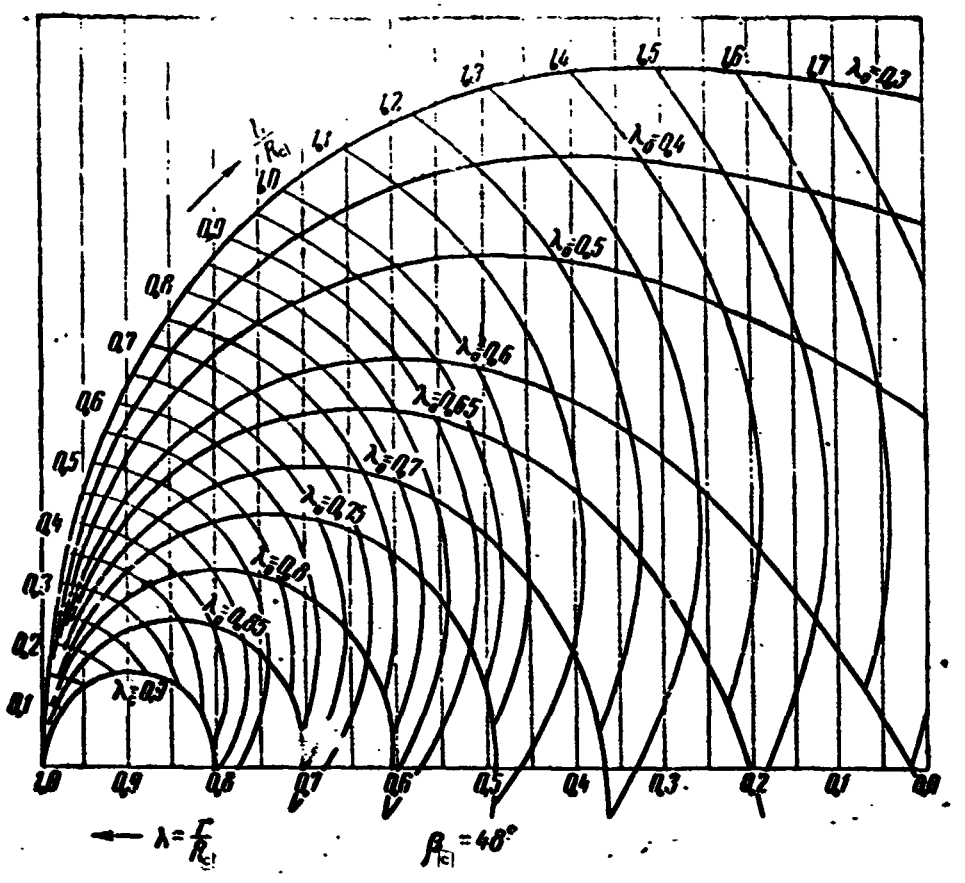

Fig. 2. Equilibrium Configurations of Tires with $\beta_c = 48°$.

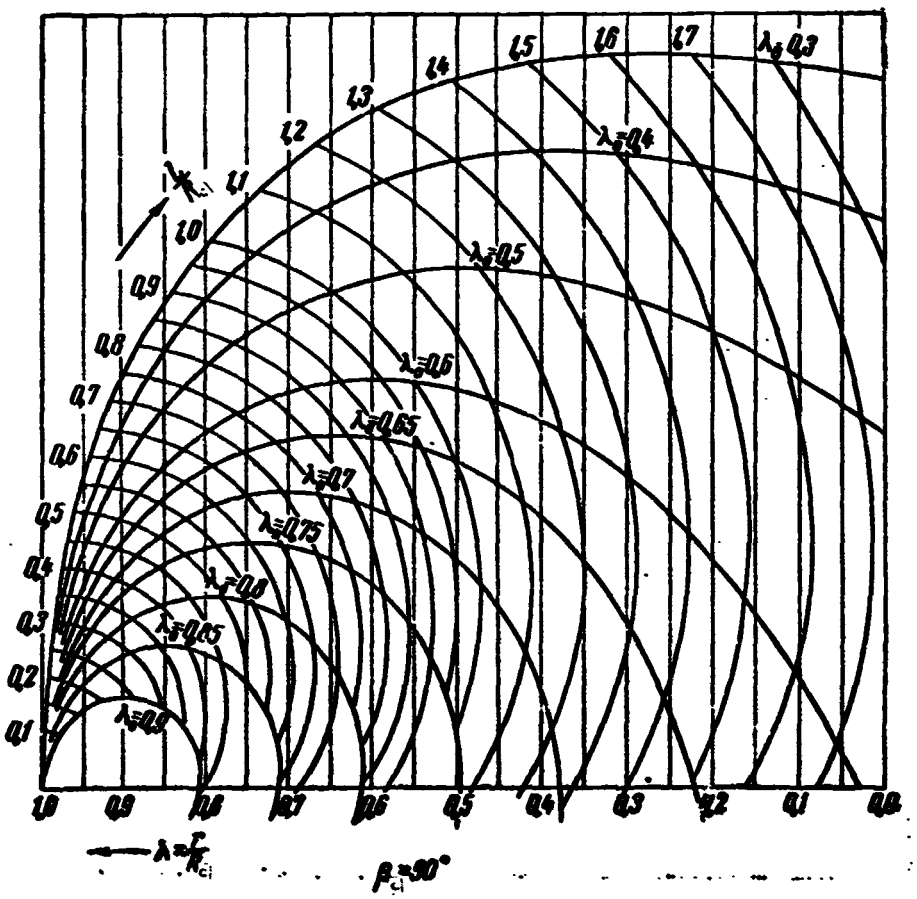

Fig. 3. Equilibrium Configurations of Tires with $\beta_c = 50°$.

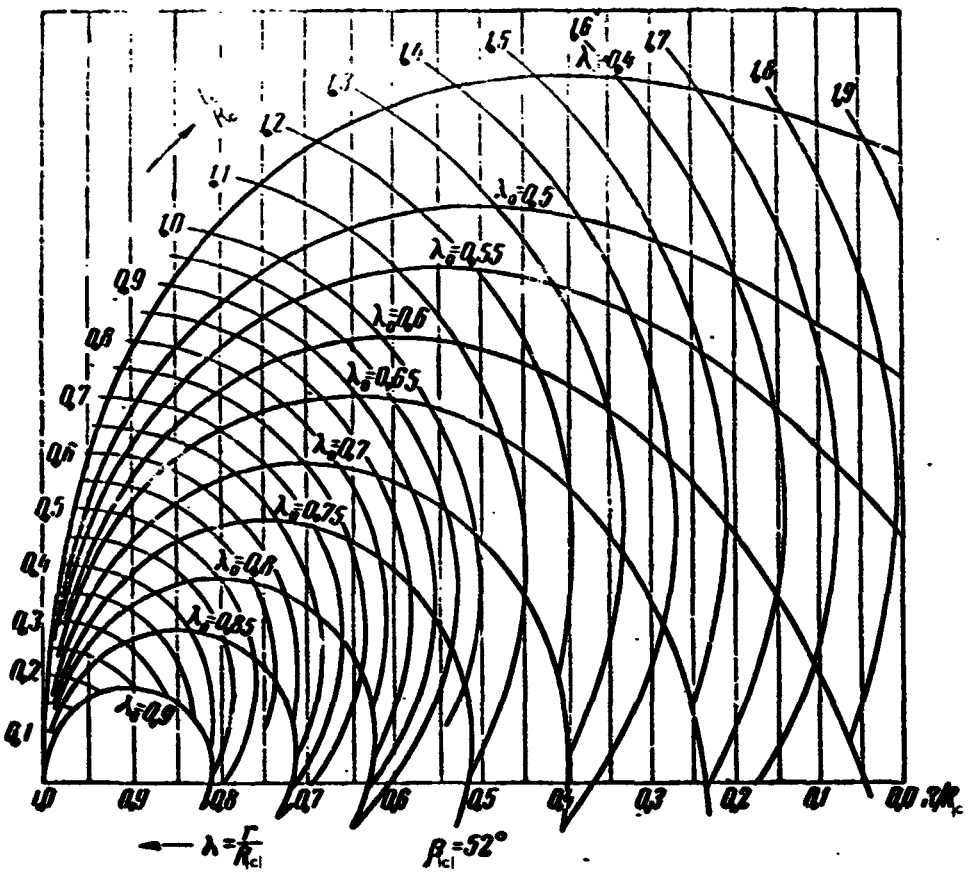

Fig. 4. Equilibrium Configurations of Tires with $\beta_c = 52°$.

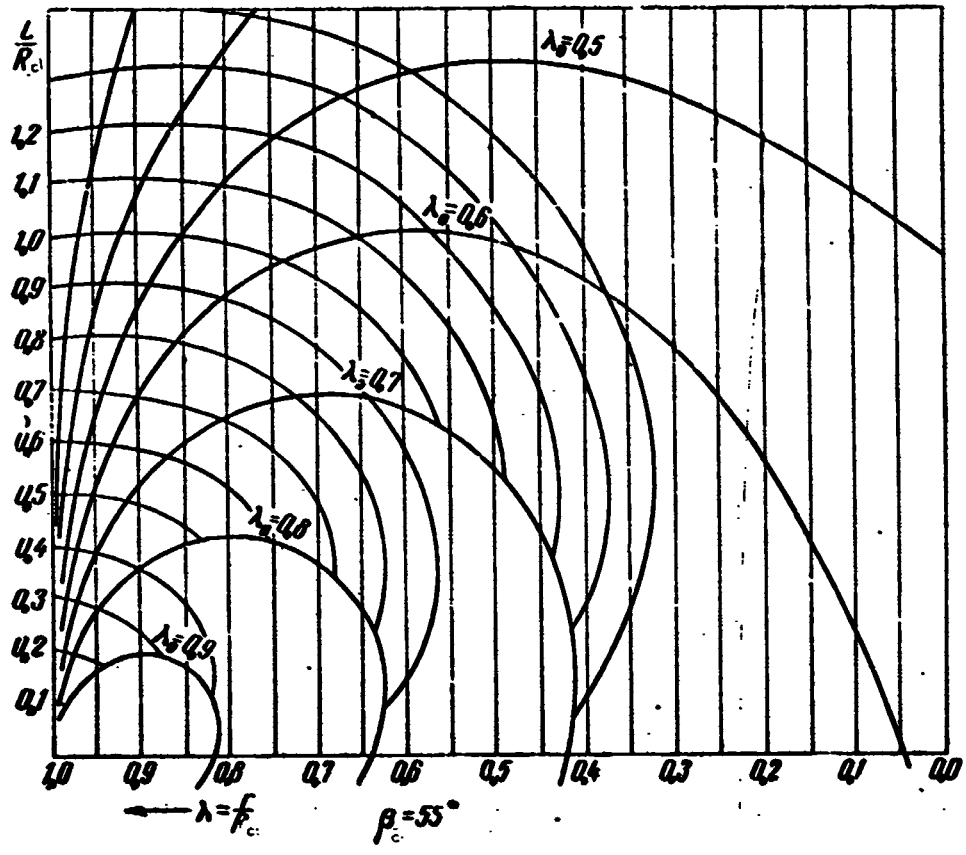

Fig. 5. Equilibrium Configurations of Tires with $\beta_c = 55°$.

/359

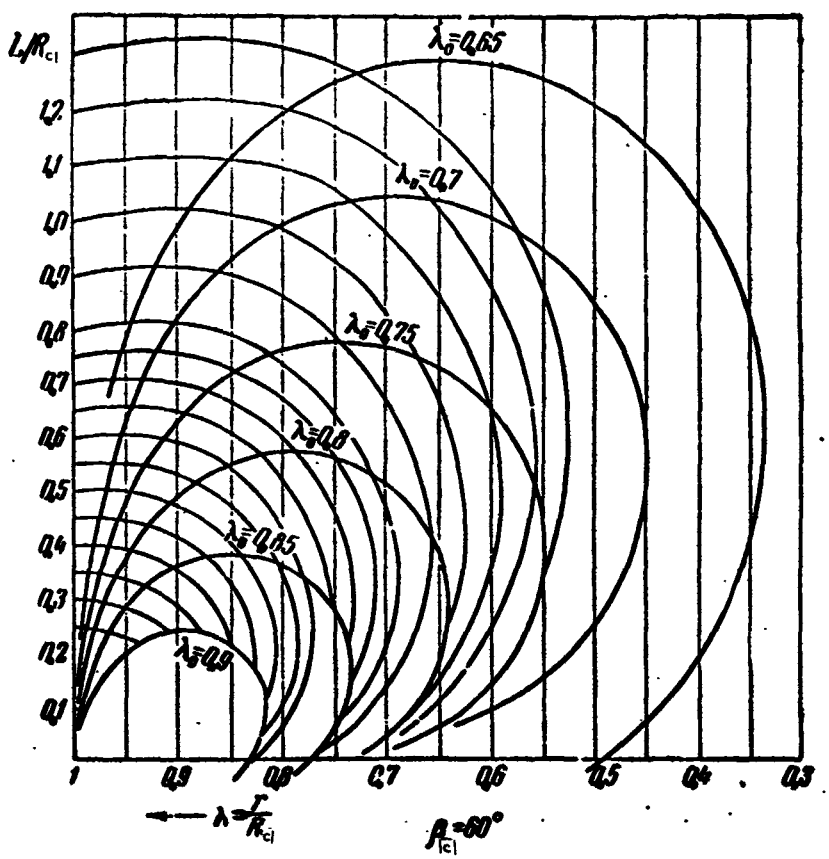

Fig. 6. Equilibrium Configurations of Tires with $\beta_c = 60°$.

/360

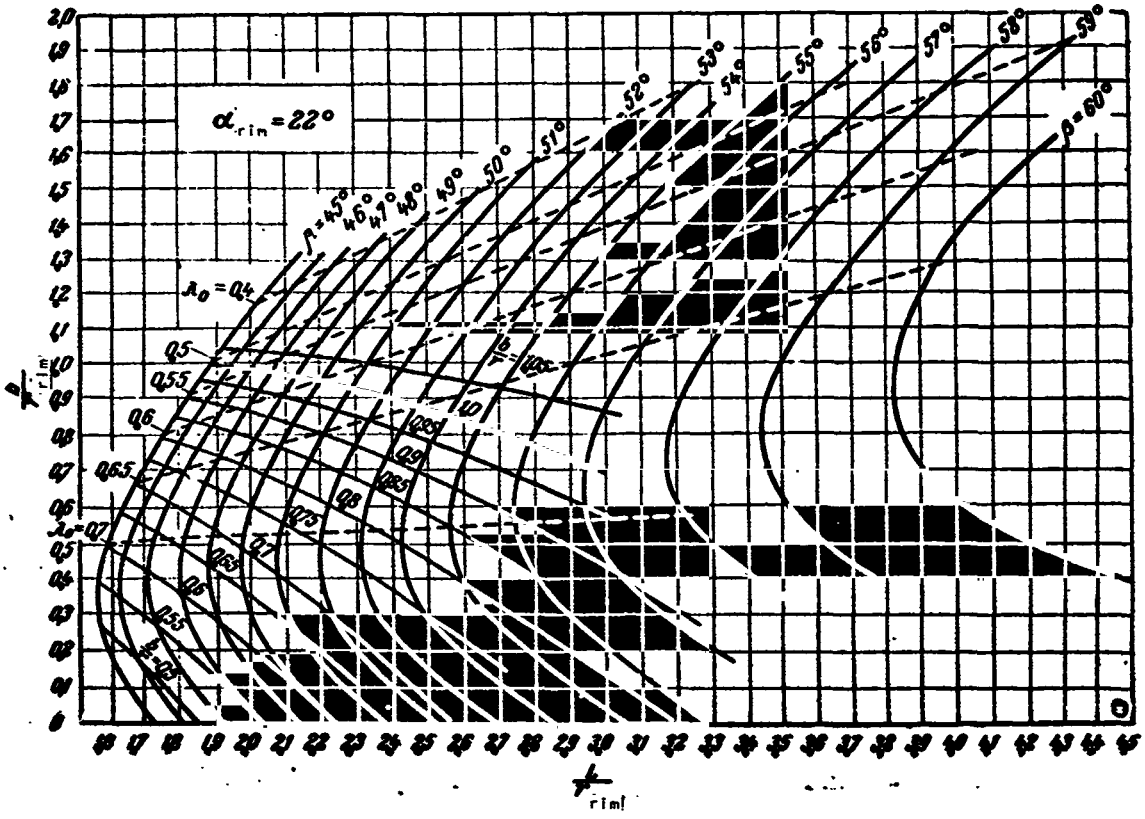

Fig. 7. Calculated Nomogram for α = 22°.

/361

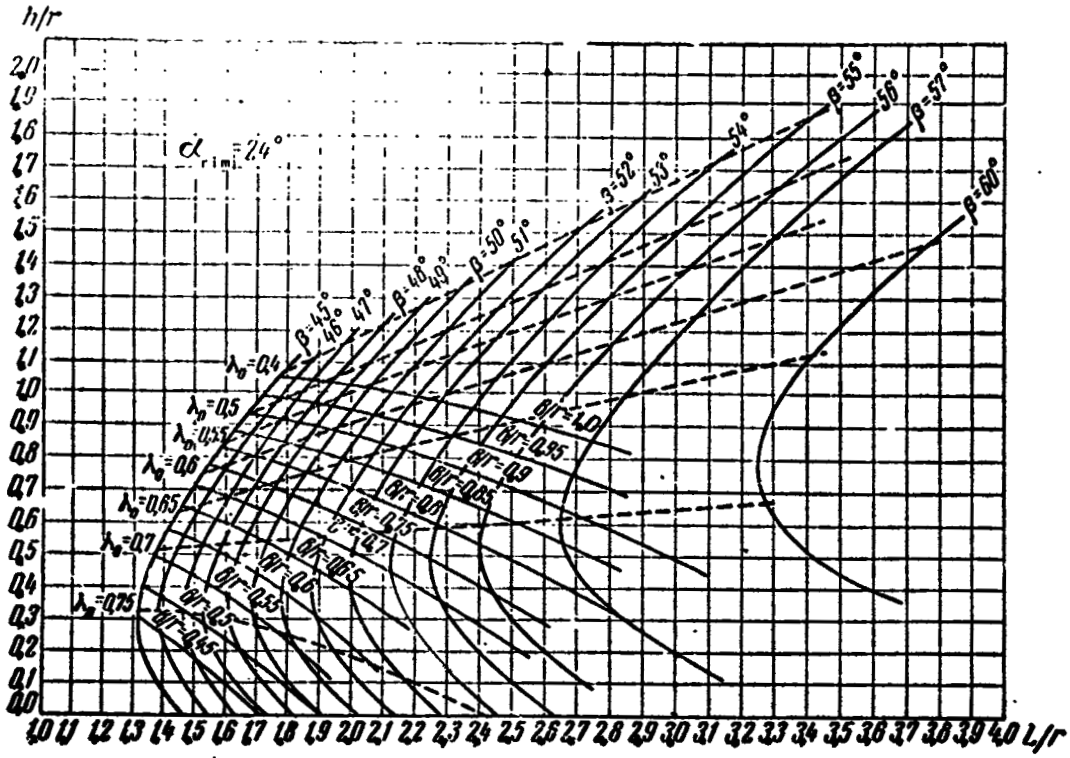

/362

Fig. 8. Calculated Nomogram for α = 24°.

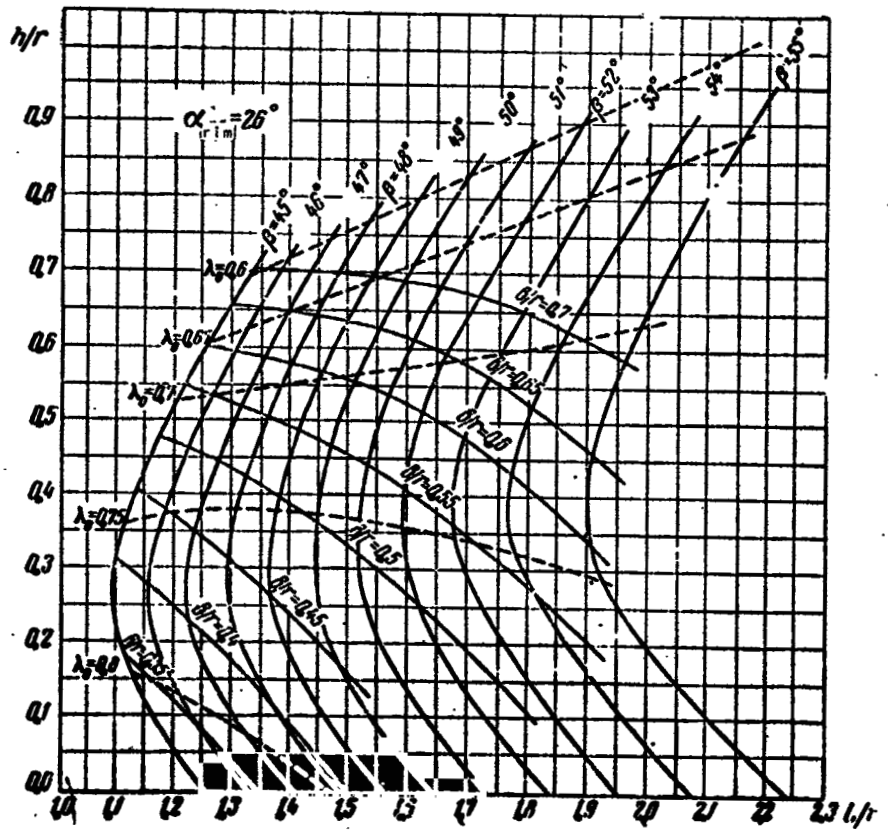

/363

Fig. 9. Calculated Nomogram for α = 26°.

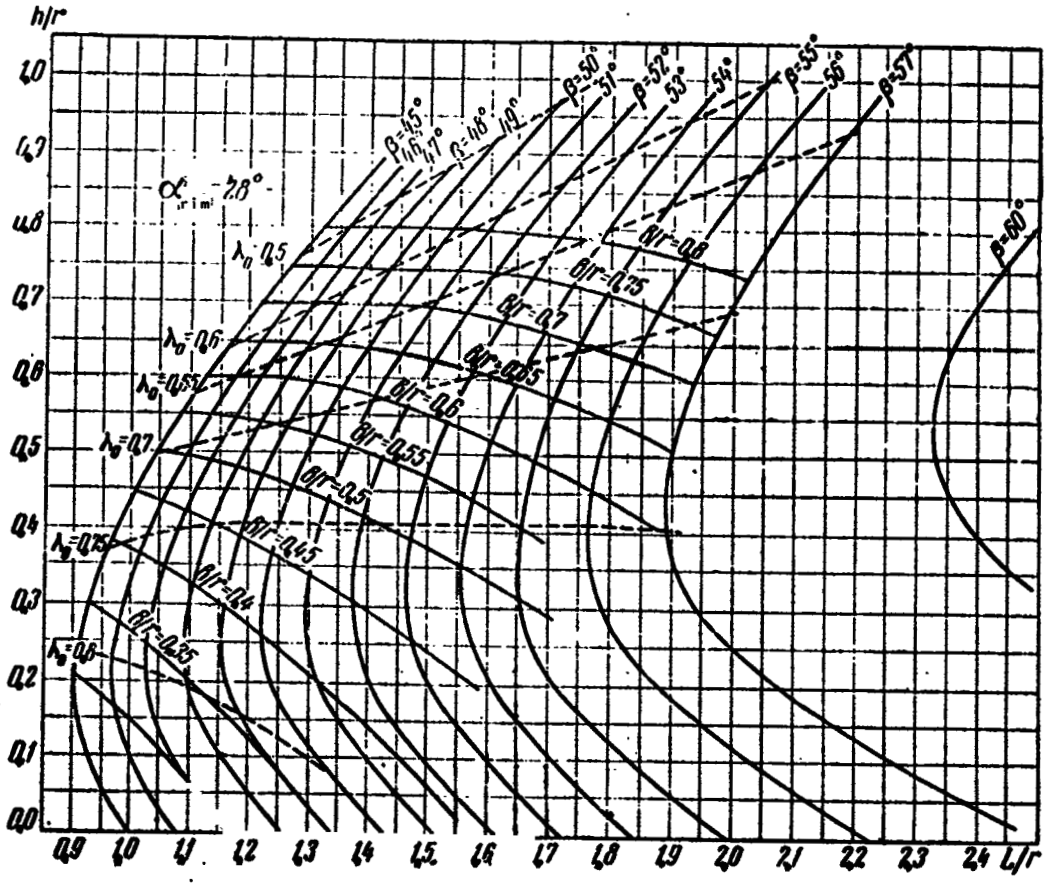

Fig. 10. Calculated Nomogram for α = 28°.

/364

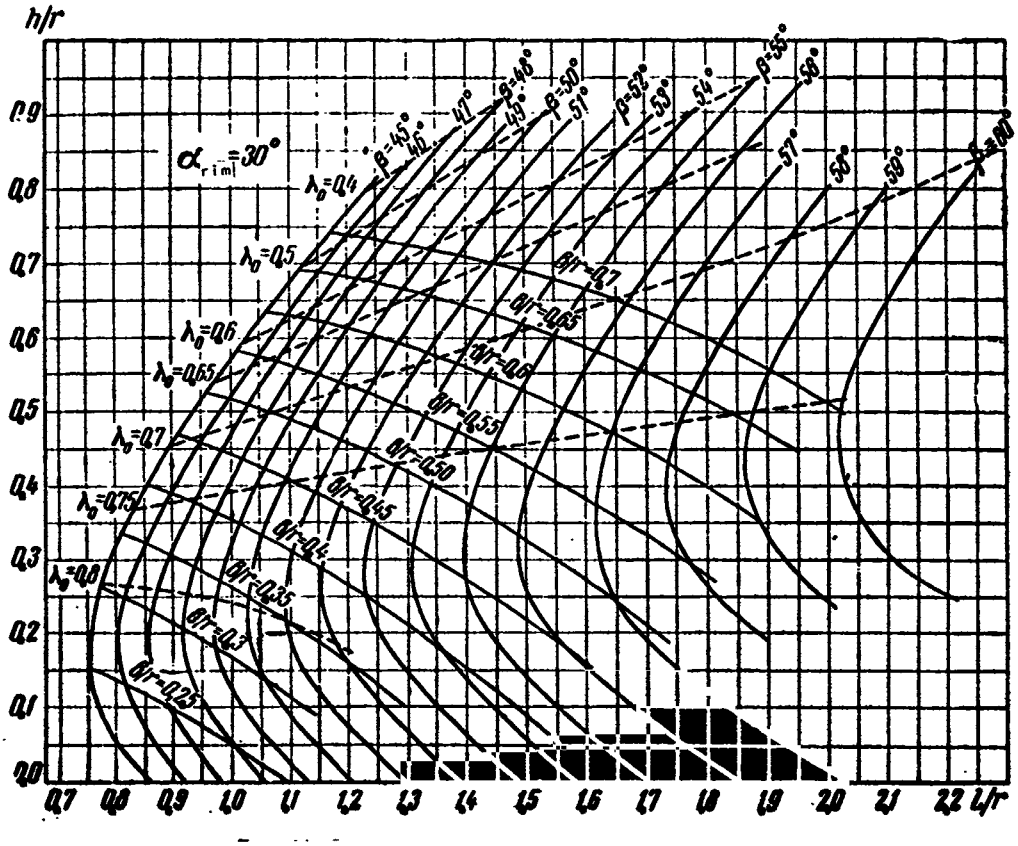

Fig. 11. Calculated Nomogram for $\alpha = 30°$.

/365

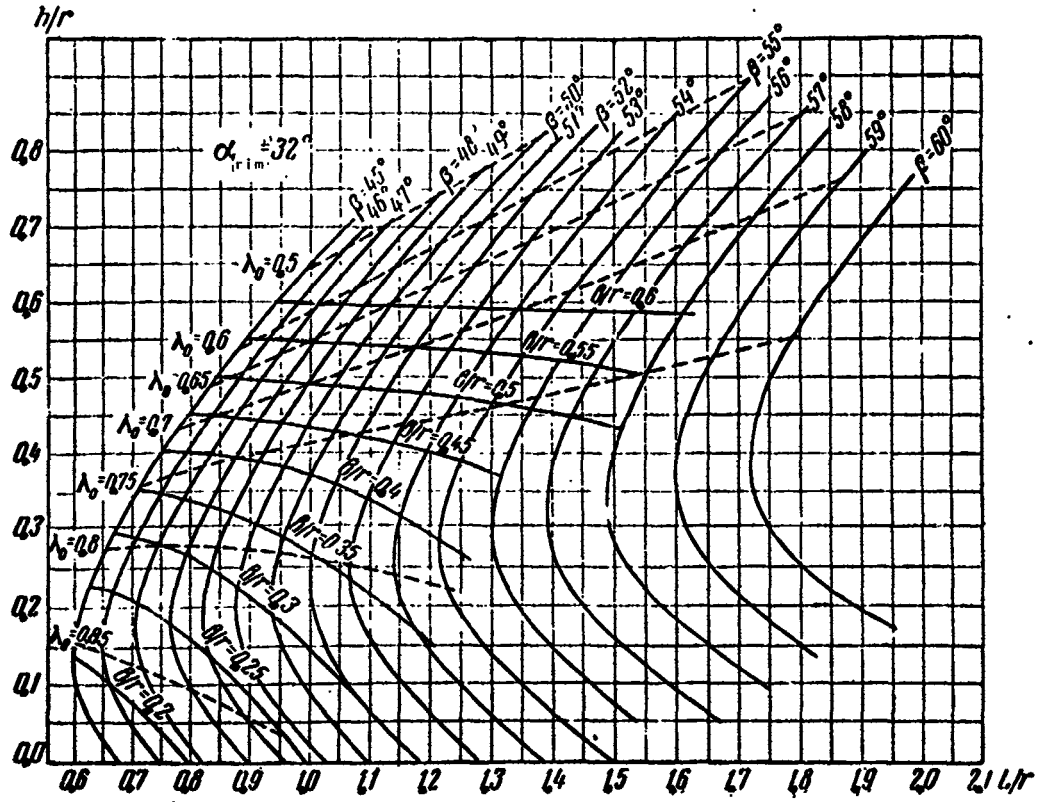

Fig. 12. Calculated Nomogram for α = 32°.

/366

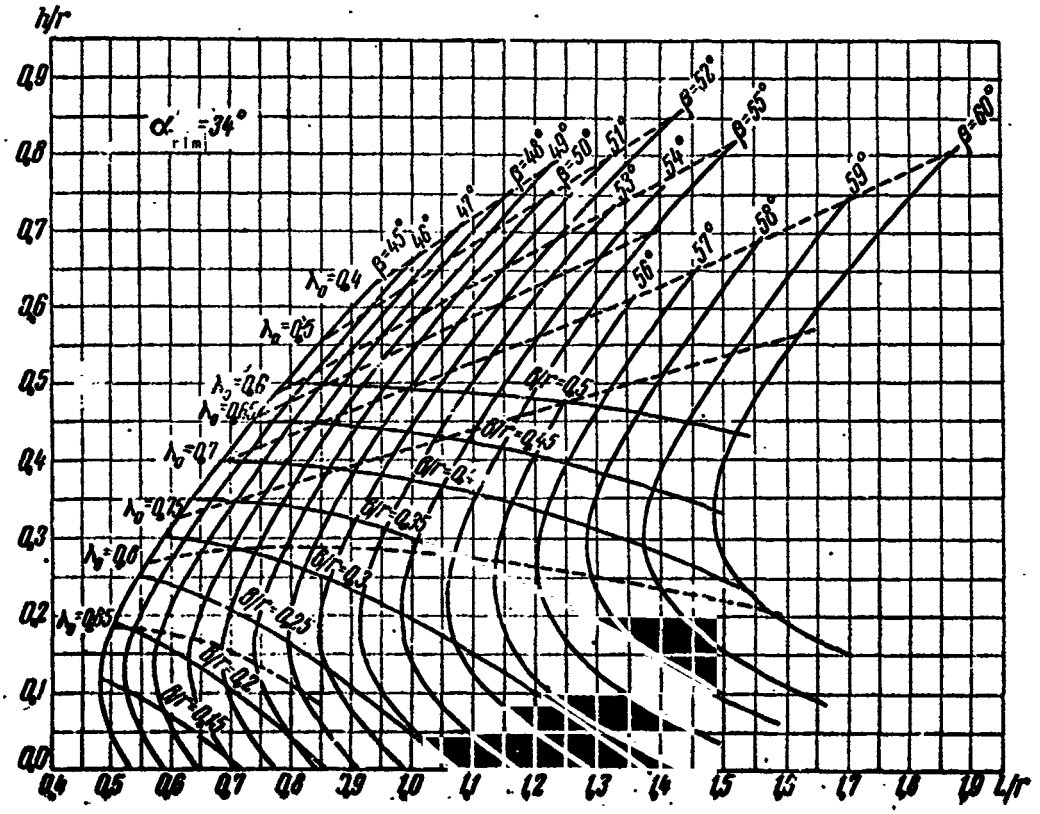

Fig. 13. Calculated Nomogram for α = 34°.

/367

/368

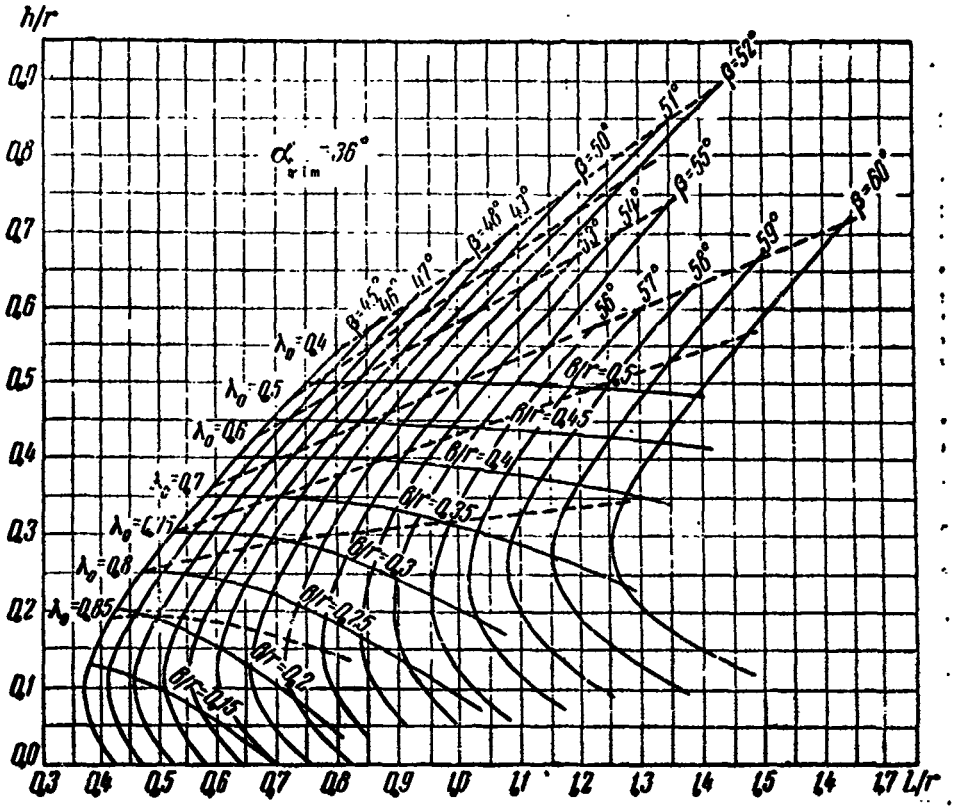

Fig. 14. Calculated Nomogram for α = 36°.

/369

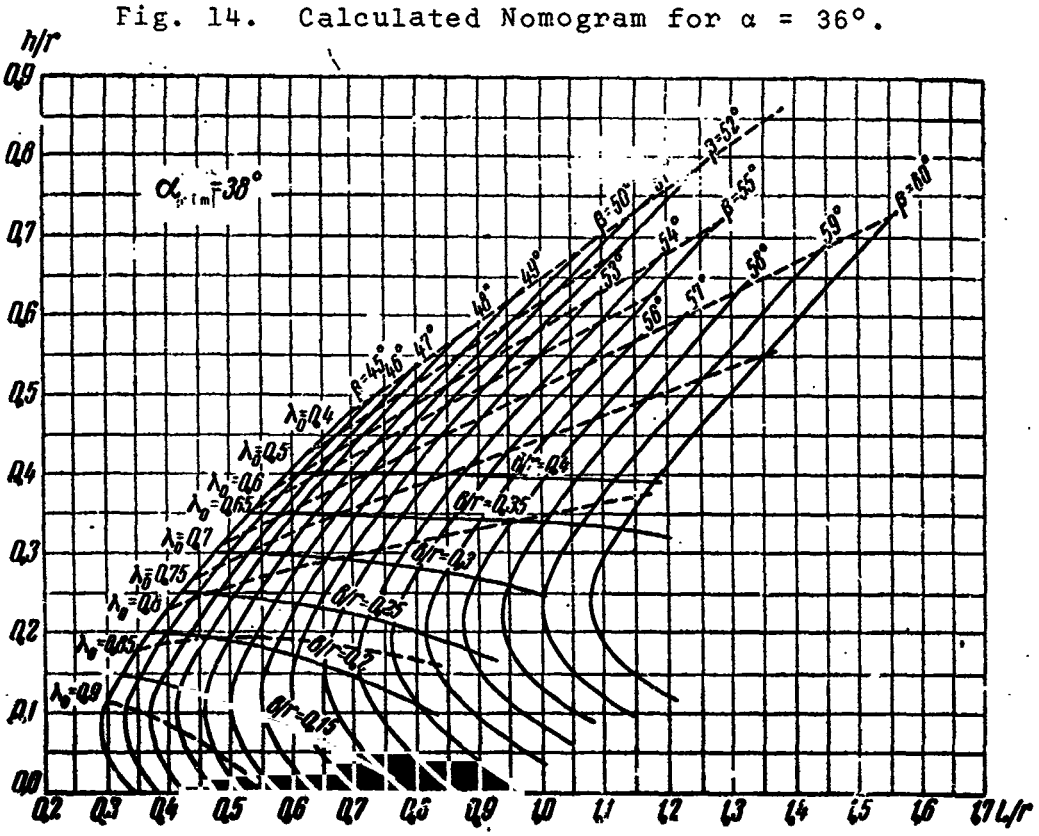

Fig. 15. Calculated Nomogram for α = 38°.

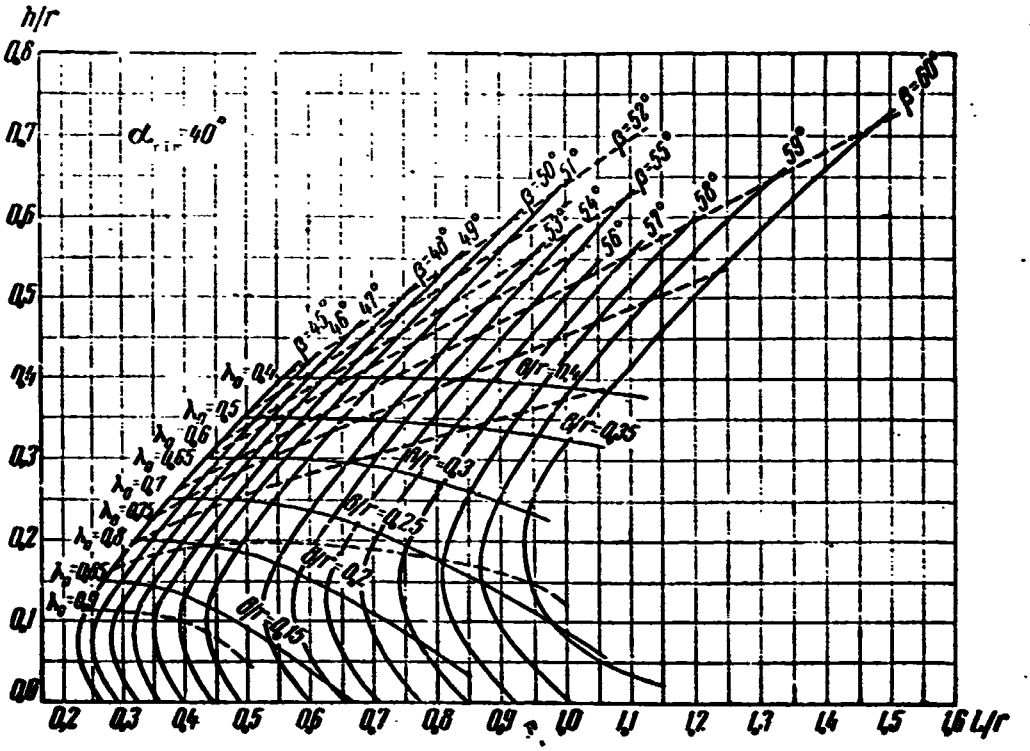

/370

Fig. 16. Calculated Nomogram for α = 40°.

PNEUMATIC TIRES FOR VARIOUS TYPES OF VEHICLES

TABLE 1. PNEUMATIC TIRES FOR TRUCKS, BUSES, TRAILERS AND TROLLEYS

Tire Designation	Number of Plies	Tread Design	Designation of Rim Profile	Wt.* of Standard Tire with Min. No. Plies (kg)	Dimensions of Inflated Tire (mm)				Maximum Recommended Load and Corresponding Internal Pressure		Minimum Recommended Internal Pressure and Corresponding Load	
					External Diameter	Profile Width (Unloaded)	Profile Width (Loaded)	Static Radius (Loaded)	Load (kg)	Pressure (kg/cm^2)	Load (kg)	Pressure (kg/cm^2)
6.50-20	6-8	Road	3.75P	26	860	175	185	406	750	3.5	2.75	500
7.50-20	8-10	"	5.00S	39	923	204	215	436	1000	4.0	2.75	850
7.50-20	8-10	High Roadability	5.00S	40	933	207	217	443	1000	4.0	2.75	850
200-20	8-10	All-Purpose	5.00S	39	937	209	220	445	1000	4.0	2.8	850
210-20	10-12	" "	5.00S	45	960	218	229	456	1200	5.75	4.0	1000
8.25-20	10-12	High Roadability	5.00S	53	971	222	235	463	1300	4.5	2.75	1000
9.00-20	10-12	Road	6.00T	56	1014	250	260	478	1550	4.5	3.25	1250
9.00-20	10-12	High Roadability	6.00T	60	1026	254	263	485	1550	4.5	3.25	1250
260-20	8-12	All-Purpose	6.00T	62	1037	260	270	490	1550	4.5	3.25	1250
9.75-18	12-14	High Roadability	6.00T	65	996	253	264	467	--	--	--	--
10.00-18	12-14	" "	6.00T	67	1018	260	272	484	1700	5.0	3.5	1400
10.00-18	12-14	All-Purpose	6.00T	67	1010	260	272	480	1700	5.0	3.5	1400
10.00-20	12-14	Road	7.33V	72.5	1056	280	290	500	1000	5.0	3.5	1500
11.00-20	12-14	"	7.33V	73.5	1082	285	296	507	2050	5.0	4.25	2100
320-20	14-16	"	8.37V	83	1125	319	331	525	2450	5.25	4.3	2050
12.00-20	14-16	"	8.37V	90	1123	313	324	529	2400	5.5	4.25	2100
12.00-20	14-16	High Roadability	8.37V	95	1130	323	338	535	2400	5.5	4.25	2100

Notes:

*No more than:

1. The geometric dimensions of the tires are given for a narrow rim.
2. 9.75-18; 9.00-20; 7.50-20 and 6.50-20 tires are not recommended for use on the new model automobiles.
3. Tubes and rim bands are matched with outer covers mounted on standard rims; if the tires are mounted on expanded rims, outer covers are matched with tubes and rim bands according to the technological conditions.

TABLE 2. PNEUMATIC TIRES FOR PASSENGER AUTOMOBILES

Tire Designation	Number of Plies	Tread Design	Designation of Rim Profile	Wt. of Standard Tire with Min. No. Plies (kg) No More Than:		Dimensions of Inflated Tire (mm)				Maximum Recommended Load and Corresponding Internal Pressure		Minimum Recommended Internal Pressure and Corresponding Load	
				Tube	Tubeless	External Diameter	Internal Rim Diameter	Profile Width (Unloaded)	Static Radius (Loaded)	Load (kg)	Pressure (kg/cm^2)	Load (kg)	Pressure (kg/cm^2)
5.20—13	4	Road	4J	—	8.5	595	329.4	136	282	275	1.7	1.4	235
5.60—13	4	High Roadability	4J	—	10.5	613	329.4	138	294	225	1.4	1.2	200
5.60—15	4	Road	4½K	10.0	9.5	670	380.2	150	312	330	1.7	1.4	290
6.40—15	4—6	High Roadability	4½K	13.5	13.5	698	380.2	160	331	360	1.7	1.4	340
6.70—15	4—6	Road	5K	13.5	13.5	718	380.2	175	335	505	1.3	1.4	435
7.00—15	6	"	6L	18.7	—	745	380.2	196	352	605	2.5	1.4	425
8.20—15	4—6	"	6L	—	16	760	380.2	205	355	700	2.0	1.4	575
8.40—15	4—6	All-Purpose	6L	—	19	775	380.2	215	360	750	2.0	1.4	600
8.90—15	6	Road	6½L	—	22	796	380.2	226	370	820	2.0	1.4	665
5.00—16	4	"	3.00D	10.6	—	670	405.6	130	312	320	2.1	1.5	255
6.00—16	4—6	"	4.00E	14.7	13.5	728	405.6	160	343	460	2.2	1.5	340
6.50—16	6—8	High Roadability	4.50E	21.0	—	762	405.6	172	357	550	2.5	1.5	390
7.00—16	4	Road	4.50E	18.0	—	760	405.6	182	354	520	1.75	1.5	445
7.50—16	6	"	5.00F	25.0	—	795	405.6	200	375	785	2.5	1.5	500

Note: 5.00-16; 6.00-16; 7.00-16 and 7.50-16 tires are not recommended for the new model automobiles. When using the tires shown in the table for trucks with a small load capacity, the internal pressure in the tires must be increased by 0.35 kg/cm^2 for 4-ply tires and by 0.45 kg/cm^2 for 6-ply tires without increasing the load on the tires.

TABLE 3. VARIABLE PRESSURE TIRES

Tire Designation	Number of Plies	Tread Design	Tire Weight (kg)	Designation of Rim Profile	Dimensions of Inflated Tire (mm)				Max. Recommended Load and Corresponding Internal Pressure		Min. Recommended Int. Pressure (for Short Operating Periods) and Corr. Load		Tread Depth (Along the Center of the Rolling Part in mm)	Tread Thickness (Along the Center of the Rolling Part in mm)	Tread Saturation (%)
					External Diameter	Profile Width (Unloaded)	Profile Width (Loaded)	Static Radius under Maximum Load	Load (kg)	Pressure (kg/cm²)	Load (kg)	Pressure (kg/cm²)			
9.00—16	4	High Road-ability	32	6.50CS	886	244	245	410	700	2.5	0.5	700	15	20	48.6
11.00—16	8	"	—	8.00CV	962	283	—	442	1000	1.8	0.7	1000	25	32	—
11.00—18	10	"	62	8.00CV	1045	305	315	485	1650	3.5	0.7	1650	15	20	42.5
12.00—18	8	"	72	9.0	1090	327	340	507	1580	3.0	0.5	1580	15	21	40.5
12.00—20	8	"	75	9.0	1145	305	—	—	1702	3.0	0.5	1702	25	34	39.7
13.00—18	8	"	73	9.0	1144	350	368	530	1590	2.5	0.5	1508	16	22.5	40
13.00—20	8	"	76.5	9.0	1190	348	379	387	1850	2.5	0.5	1850	17	24	44
14.00—18	8	"	85	10.0	1215	390	410	563	1580	2.0	0.7	1580	17	24	39.6
14.00—20	10	"	140	10.0	1272	385	392	587	2500	3.2	0.7	2500	28	35	40
16.00—20	8	"	130	11.5	1390	438	457	635	1900	2.0	0.5	1900	30	40	36.4
16.00—24	12	"	160	11.5	1457	443	483	635	3000	2.0	0.7	3000	17	24	43.6
18.00—24	10	"	250	13.0	1600	555	574	690	3500	1.5	0.7	3500	20	28	43.7
18.00—24	16	"	270	13.0	1594	503	574	717	5500	2.8	0.7	5500	20	28	43.7
18.00—25	16	"	—	13.0	1620	500	—	750.9	5500	2.8	0.7	5500	30	30	48
21.00—28	14	"	—	17.0	1744	603	—	—	6500	2.5	0.8	6500	18	27	44

/373

TABLE 4. GROUND-GRIP TIRES

Tire Designation	Number of Plies	Tread Design	Weight of the Tires (kg) No More Than:	Dimensions of Inflated Tire (mm)			Max. Recommended Load & Corresponding Internal Pressure	
				External Diameter	Profile Width (Unloaded)	Static Radius (Loaded)	Load (kg)	Pressure (kg/cm^2)
600×340	4	High Roadability	17,85	615	340	273	250	0,8
760×315	4	" "	31	760	325	352	620	0,7
900×450	4	" "	51	930	450	424	900	0,9
1000×600	6	" "	73	1040	600	478	2000	1,4
1060×600	8	" "	95	1075	600	489	2400	1,8
100×650	6	" "	70	1035	650	442	2000	1,4
1140×700	8	" "	114	1162	720	465	3000	1,4
1300×750	8	" "	177	1298	750	572	5000	2,0
1500×840	8	" "	145	1578	840	783	1600	0,5

TABLE 5. PNEUMATIC TIRES FOR AGRICULTURAL MACHINES

Tire Designation		Number of Plies	Tread Design	Designation of Rim Profile		Tire Weight (kg) No More Than:	Dimensions of Inflated Tire (mm)			Maximum Recommended Load & Corresponding Internal Pressure		Minimum Recommended Internal Pressure and Corresponding Load		Valve Type
				Metric	Inches		External Diameter	Profile Width (Unloaded)	Static Radius (Loaded)	Load (kg)	Pressure kg/cm²	Pressure kg/cm²	Load (kg)	
Tires on Drive Wheels														
150—406	550—16	4	High Road-ability	102E	4,00E	15,5	710	148	337	200	1,25	0,9	155	R
210—508	8—20	6	" "	W178	W7	—	950	210	—	680	1,9	0,8	410	-
240—508	9—20	6	" "	W203	W8	43	970	240	445	805	1,8	0,8	500	V
420—508	15—20	8	" "	DW356	DW14	85	1158	398	518	2040	1,5	1,0	1760	V
300—610	11—24	8	" "	W229	W9	78,5	1164	285	545	1425	2,3	0,85	805	DM-95
363—610	14—24	8	" "	W229	W9	115,0	1335	365	615	2200	2,5	1,0	1290	DM-95
400—610	15—24	8	" "	W305	W12	130,0	1345	400	600	2500	2,5	1,0	1455	DM-95
450—610	18,4—24	8—10	" "	DW406	DW16	125,0	1380	445	635	1900	1,0	1,1	1890	V
600—660	23,1—26	12	" "	DW508	DW20	—	1630	585	735	4500	1,7	1,1	2950	V
270—711	10—28	6	" "	W229	W9	65	1210	267	567	845	1,1	0,8	690	V
360—762	13—30	6	" "	DW305	DW12	90	1408	360	650	1550	1,3	1,0	1360	V
420—762	15—30	6	" "	DW356	DW14	116	1523	426	685	2420	1,4	1,1	2100	V
210—813	8—32	4	" "	W178	W7	37,5	1166	200	542	680	1,2	0,8	535	V

TABLE 5. (Cont.)

Tire Designation	Number of Plies	Tread Design	Designation of Rim Profile		Tire Weight (kg) No More Than:	Dimensions of Inflated Tire (mm)			Maximum Recommended Load & Corresponding Internal Pressure		Minimum Recommended Internal Pressure and Corresponding Load		Valve Type
			Metric	Inches		External Diameter	Profile Width (Unloaded)	Static Radius (Loaded)	Load (kg)	Pressure kg/cm²	Pressure kg/cm²	Load (kg)	
300—965 11—38	6	" "	DW254	DW10	90	1522	305	710	1410	1,5	0,8	975	V
330—965 12—38	6	" "	DW279	DW11	98	1575	332	742	1570	1,4	0,8	1130	V
210—1016 8,25—40	6	" "	152S	6,00S	61	1455	206	685	1360	2,3	1,2	1200	V
240—1067 9—42	6—8	" "	DW203	DW8	68	1512	238	723	1180	2,0	0,8	695	V
Maneuvering Wheels													
115—406 4,00—16	4	Maneuvering Ribs	76D	3,00D	9,0	655	115	308	230	2,0	1,4	185	R
150—406 5,50—16	6	"	102E	4,00E	15,5	715	150	335	420	2,5	1,4	300	R
170—406 6,00—16	6	"	102E	4,00E	16,5	716	166	347	550	2,5	1,4	390	R
180—406 6,50—16	6	"	114E	4,50E	22,5	765	180	355	900	3,5	1,4	525	R
240—403 9,00—16	6	"	152F	6,00F	36,0	887	243	395	1100	2,5	1,4	780	DM-95
190—508 6,50—20	6	"	140F	5,50F	26,0	883	186	420	660	2,7	1,4	450	R
210—508 8—20	6	"	140F	5,50F	35	920	210	430	925	2,5	1,4	680	R

TABLE 5. (cont.)

Tire Designation	Number of Plies	Tread Design	Designation of Rim Profile		Tire Weight (kg) No More Than:	Dimensions of Inflated Tire (mm)			Maximum Recommended Load & Corresponding Internal Pressure		Minimum Recommended Internal Pressure and Corresponding Load		Valve Type
			Metric	Inches		External Diameter	Profile Width (Unloaded)	Static Radius (Loaded)	Load (kg)	Pressure kg/cm^2	Pressure kg/cm^2	Load (kg)	
Tires on Supporting Wheels													
200×60 —	Cordless	Without Tread Design	Special	—	0,7	200	60	94	25	Atmospheric	—	—	Valveless
300×100 —	"	"	Special	—	2,8	296	100	133	50	"	—	—	"
400×100 —	"	High Roadability	Special	—	3,0	390	100	180	60	"	—	—	"
130—230 4,50—9	4	All-Purpose	89D	3,50D	4,2	470	129	220	245	2,8	—	—	R
135—254 5,0—10	4	"	102E	4,00E	6,6	510	135	241	330	3,0	1,4	220	R
215—381 8,25—15	8	Road	127S	5,00S	32,0	834	216	384	1350	3,5	1,4	790	DM-105
230—406 230—16	10	Longitudinal Ribs	152F	6,00F	43	885	247	405	1450	3,4	1,4	840	DM-95
310—406 12—16	8	"	W254H	W10H	48	935	288	—	2100	3,0	1,4	1340	DM-95
980×390—406 —	8	"	W305	W12	70	980	390	433	3200	3,0	—	—	--
980×390—457 —	8	"	W305	W12	60	980	390	442	3200	3,0	—	—	--

/377

TABLE 6. FLAT BASE RIMS FOR HEAVY DUTY TIRES

Dimension \ rim	3,75P	4,33R	5,00S	6,00T	7,33V	8,37V	10,00W
A, mm	95,25±2,3	109,98±2,3	127,0±2,3	152,4±2,3	186,18±3,2	212,60±3,58	254,0±4,75
B, mm	31,75	36,65	42,34	50,8	62,05	70,87	70,87
C, mm	25,40	28,57	33,32	38,10	44,45	44,45	50,80
D,* mm	17,45	19,84	19,84	23,80	28,57	28,37	30,18
a, mm	15,87	15,67	15,67	17,02	17,02	17,02	17,02
R_1, mm	15,87	18,25	18,25	22,22	26,97	26,97	28,57
R_2, mm	6,35	6,35	6,35	7,94	7,94	7,94	7,94

* Minimum permissible dimension

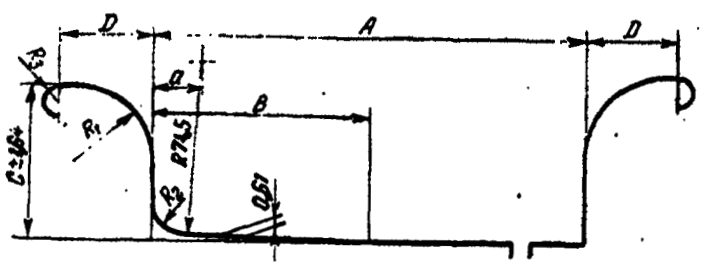

TABLE 7. RIMS WITH CONICAL BEAD SEATS FOR HEAVY DUTY TIRES

Dimension \ rim	5,0 A	5,5 A	6,0 B	6,5 B	7,0	7,5 C	8,0 C	8,5 C	9,0 D	10,0 D
A, mm	127	140	152	165	178	190	203	216	228	254
B, mm	28	28	33	33	38	43	43	43	48	48
*a**, mm	16	16	18	18	21	23	23	23	26	25
R_1, mm	14	14	16,5	16,5	19	22	22	22	24	24
R_2, mm	6,5	6,5	6,5	6,5	8	8	8	8	8	8
d, mm	508	432; 457;	432; 457;	432; 457;	457;	457; 508;	457; 508;	457; 508;	457; 508;	
	381	508; 381	508	508	508	559; 610	559; 610	559; 610	610	508

* Minimum permissible dimension

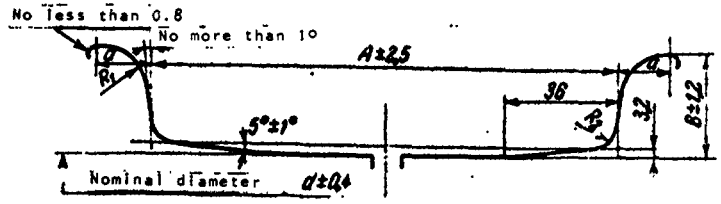

TABLE 8. WELL-BASE RIMS FOR TUBELESS HEAVY DUTY TIRES

Dimension / Rim	A, mm	B, mm	H, mm	D, mm	E, mm	R, mm	a, mm	b, mm	c, mm
17.5 x 5.25	128	27	25	33	26	10	13	23	8
22.5 x 7.50	179	51.5	26	47	41	6	12	19	11

/380

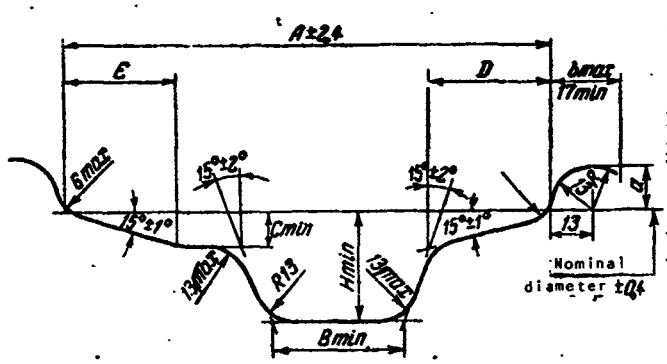

TABLE 9. RIMS FOR PASSENGER CAR TIRES

Rim \ Dimensions	A, mm	C, mm	D, mm	E*, mm	F, mm	H**, mm	b, mm	c, mm	d, mm	f, mm	e, mm	R_6, mm	R_7, mm
$4^1/_2K$	114,3	23,11	19,81	25,40	25,40	355,17	13,00	10,31	19,56	16,08	1,38	10,67	6,35
5K	127,0	26,12	19,81	25,40	25,40	355,17	13,00	10,31	19,56	16,08	1,98	10,67	6,35
6L	152,4	47,73	25,4	31,75	28,58	348,82	13,34	10,97	21,59	15,70	3,96	11,89	7,00
$6^1/_2L$	165,1	60,81	25,4	31,75	28,58	348,82	13,34	10,97	21,59	15,70	3,96	11,89	7,00

* Minimum permissible dimension
** Maximum permissible dimension

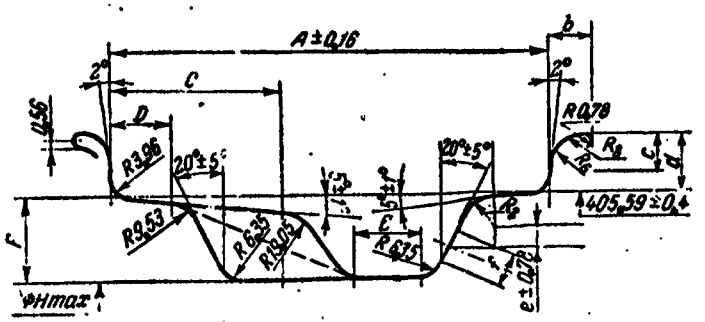

TABLE 10. RIMS FOR THE DRIVE WHEELS OF AGRICULTURAL TIRES

Rim Profile Designation / Dimension	W5	W6	W7	W8 DW8	W9 DW9	W10 DW10	W11 DW11	W12 DW12	DW14	DW16	DW20	W8H	W10H
A, mm.	127	152	178	203	229	254	279	305	356	405	508	203	254
B, mm	22	22	22	22	25,5	25,5	25,5	25,5	28,5	28,5	28,5	25,5	25,5
a, mm	10,5	10,5	10,5	10,5	12	12	12	12	12	12	12	12	12
R_1, mm	9,5	9,5	9,5	9,5	11	11	11	11	11	11	11	11	11
R_2 mm	8	8	8	8	13	13	13	13	13	13	13	13	13
h, mm	—	—	—	—	—	—	28	28	30	30	30	—	—
$\alpha°$	—	—	—	20	20	20	20	20	20	20	20	—	—
b_1, mm	24	24	24	24	27	27	27	27	37	37	37	33	33

Note: The letter W denotes rim profiles shown in (1); the letters DW denote rim profiles shown in (2) and (3); the letter H denotes an expanded width of the conical bead seats of the rim as shown in (1) and (3).

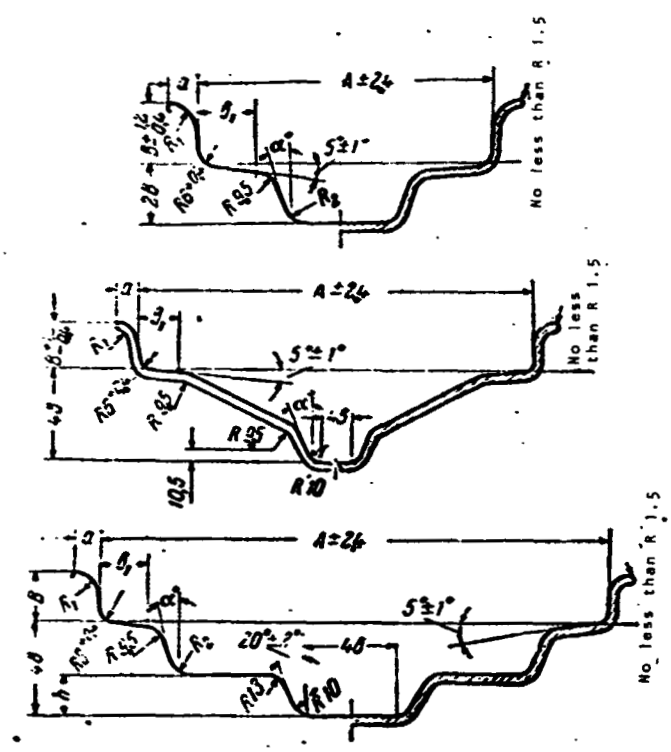

TABLE 11. RIMS FOR THE MANEUVERING WHEELS OF AGRICULTURAL TIRES

Dimension \ Rim Profile Designation	3,00D	4,00E	4,50E	5,50P	6,00F
A, mm	76	102	114	140	152
B, mm	17,5	20	20	22	22
R_1, mm	8	8,5	8,5	10	10
R_2, mm	13	14	14	15,5	15,5
R_3, mm	6,5	9,5	9,5	19	9,5
R_4, mm	5,0	6,5	6,5	6,5	6,5
h_1, mm	19	25	25	28,5	28,5
h_2, mm	12,5	13,5	13,5	14,5	14,5
α°	—	15	15	20	20
b_1, mm	16	18,5	18,5	24	24
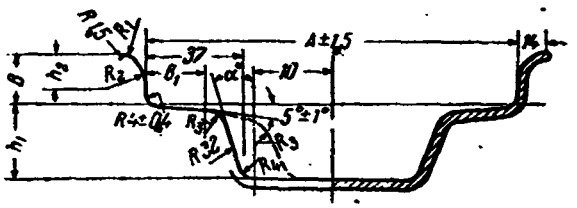
Note: The conventional notation of a rim profile includes: a number corresponding to the rim width (in inches); a letter which determines the profile configuration of the bead rims (a set of dimensions h_1, R_1, R_2, R_4); a number corresponding to the conventional rim diameter.